STEADY-STATE AND TIME-DEPENDENT BEHAVIOR OF
FUSION-FISSION HYBRID SYSTEMS

By

WILLIAM G. VERNETSON

A DISSERTATION PRESENTED TO THE GRADUATE COUNCIL OF
THE UNIVERSITY OF FLORIDA
IN PARTIAL FULFILLMENT OF THE REQUIREMENTS FOR THE
DEGREE OF DOCTOR OF PHILOSOPHY

UNIVERSITY OF FLORIDA

1979

Dedicated to

Theresa

without whom this work

would have been impossible.

ACKNOWLEDGMENTS

The author would like to express his appreciation to his graduate committee for their assistance during the course of this research. Special thanks are extended to Dr. H. D. Campbell, chairman of the author's supervisory committee for providing guidance and encouragement throughout the course of this work. Dr. Campbell's many helpful comments and suggestions have greatly aided the completion of this work. Thanks are also extended to Dr. E. E. Carroll, Dr. R. T. Schneider, and Dr. T. L. Bailey who have also served on the author's supervisory committee.

Special thanks are extended to Dr. M. J. Ohanian for the research and teaching assistantship opportunities presented which enabled the author to pursue the doctorate.

The author's studies at the University of Florida have been supported, in part, by a National Science Foundation Traineeship and also by a one-year Fellowship from the University of Florida and this support is gratefully acknowledged.

A large portion of the funds for the computer analysis were furnished by the Northeast Regional Data Center on the University of Florida campus through the College of Engineering. This help, though at times meager and difficult to obtain, is also acknowledged.

Special thanks are due to Dr. N. J. Diaz without whose efforts and encouragement this study might never have been completed.

Special thanks are also due to Dr. E. T. Dugan whose knowledge of computer analysis and nuclear reactor physics was of great assistance during much of this work. In addition, thanks are extended to Mr. I. Maya for his aid with some of the plasma calculations and their implications. Thanks are also extended to Mr. B. G. Schnitzler for a number of helpful consultations.

Finally, the author would like to extend his deepest appreciation to his wife whose support and encouragement made it possible to complete this work.

TABLE OF CONTENTS

LIST OF TABLES

ix

LIST OF FIGURES

xi

Abstract of Dissertation Presented to the Graduate Council
of the University of Florida in Partial Fulfillment of the Requirements
for the Degree of Doctor of Philosophy

STEADY-STATE AND TIME-DEPENDENT BEHAVIOR OF
FUSION-FISSION HYBRID SYSTEMS

By

William G. Vernetson

June 1979

Chairman: Hugh D. Campbell
Major Department: Nuclear Engineering Sciences

This study examined stability analysis of point-model systems repre-
senting pure fusioning plasmas as well as coupled fusion-fission systems.
The stability criteria for these systems were derived for constant plasma
confinement conditions based on engineering perturbations of the system
feedrate. The results of linearized point-model plasma stability analysis
of the thermal instability were shown to be applicable to hybrid plasmas
and to be attainable from considerations of engineering-related per-
turbations in the extrinsic plasma feedrate variable.

A Tokamak fusion-fission hybrid design was selected for further,
more specific analysis. The modeled hybrid system in linearized form was
found to be stable provided certain hybrid plasma temperature and con-
finement time limits are met. However, for realistic installations,
absolute stability is not sufficient; nor is it guaranteed by linearized
analysis. Therefore, hybrid plasma behavior was examined under transient
and overpower conditions.

Time-dependent analysis of a low reactivity hybrid plasma (8 keV,
9.56×10^{13} ions/cm^3) subjected to various parameter perturbations showed
the resultant transients to be less quickly developing than those associated

with perturbations to pure fusion plasmas with high plasma reactivity. In addition, the predictions of plasma stability ranges were verified for various confinement times. The slowly developing hybrid plasma transients following $\pm$ 5% temperature or feedrate perturbations were found to be significant for the control of the power-producing hybrid.

Neutrons and their associated energy are multiplied in hybrid blankets; therefore, the global equation in use to relate the blanket energy deposition per fusion neutron to the blanket effective neutron multiplication factor was investigated. Results were obtained which indicate the global approach supplies a poor estimate of blanket energy multiplication for a fusion neutron source and an even poorer estimate for fission energy neutrons.

Although results showed the blanket energy deposition per fusion neutron to be some 60% below point-model predictions, the selected blanket is still a significant multiplier, by a factor of 25 or more, of the neutron energy entering the blanket via fusion neutrons. The documentation of the reduced worth of fusion neutrons, entering the blanket through a convertor region, may be a significant factor in redesigning vacuum walls of hybrid reactors despite the advantages of reduced 14 MeV wall loadings.

Diffusion theory and discrete ordinates transport theory analysis were both applied to establish the relative importance of the inner convertor region for power generation. The results of the S_n transport calculation were used to determine the source size required by volume equivalence with the Tokamak geometry to produce 6500 MWth in the blanket. The source value was used to establish the steady-state requirements on plasma temperature and density from geometric considerations of the

Tokamak hybrid plasma volume involved. In addition, the S_n calculation was used to show that only about 6% of the 14 MeV fusion neutrons reach the thermal fission lattice without a collision. These transmission results indicate graphically why the blanket is less effective at energy multiplication than expected from previous reports.

Finally, space-time kinetics calculations were performed on the blanket to demonstrate the fast response of the blanket in keeping with its millisecond prompt neutron lifetimes and subcriticality. Although no time-dependent feedback effects were examined, the speed of response of the system was determined for typical transients and some character-istics for hybrid operational controllability were established.

CHAPTER 1

INTRODUCTION

Preliminary Concepts for Fusion-Fission Reactors

The fusion-fission hybrid reactor concept is a combination of a sub-Lawson fusion reactor and a subcritical fission reactor in a single power-producing system. Fission reactors are "power rich" but "neutron poor," while anticipated D-T fusion reactors will be "neutron rich" but "power poor." Hence, the essential hybrid feature is the combination of these two systems to use excess fusion neutrons to breed fissile fuel while simultaneously sustaining and driving the system for useful power using fission energy multiplication of the fusion neutron source energy.[1]

Limited studies, concentrating on blanket neutronics, have been done on hybrid systems in parallel with pure fusion blanket work; however, no system dynamics or stability investigations have been reported for hybrids. Some research effort has been devoted to global stability analysis of the plasma in pure fusion devices. The present research extends such pure fusion time-dependent studies into the area of hybrid systems. This continued development of the hybrid in parallel with the fast breeder reactor is supported by the hybrid's potential as an alternate and attainable energy and fuel producing concept.[2] In fact, some researchers suggest replacing the breeder reactor with the hybrid concept.[3]

Much research effort and capital investment have been committed to the realization of a mixed burner-breeder nuclear reactor economy planned for the end of this century. This effort is justified by expected continued growth of energy needs, and by a marked shift from direct consumption of fossil fuels to secondary consumption of electrical energy within the past few decades.[4]

With the growth in nuclear generating capacity, limited fissile fuel reserves have caused the thrust of research and development in the nuclear industry to shift to the fast breeder reactor (LMFBR). Even with the projected impact of the commercial LMFBR sometime after 1990, considerable additional enriching capacity and capital investment will be required for fueling burner reactors.

Current emphasis on the safety and the environmental impact of nuclear generating facilities as well as certain technological and political objections[5] make it increasingly unlikely that high gain breeder reactors will make a significant impact prior to the mid-1990's or later. Even if the breeder is introduced sooner, the relatively long doubling times under consideration (15 years or more) may not be adequate for generation of sufficient additional fuel to support an existing burner reactor economy.[6] With so much effort and capital investment committed to the realization of the mixed burner-breeder economy planned for the 1990's, the availability of an effective alternate concept to produce fissile fuel could be important.

One candidate for producing fissile fuel is the controlled thermonuclear reactor utilizing the D-T cycle. Deuterium resources are virtually unlimited (enough for 10^9 years).[7] Since tritium can be bred from lithium at rates resulting in less than one month doubling times,[7,8]

fusion neutrons can be used to breed fissile material. By diverting neutrons from tritium production, the tritium supply can be maintained at a reasonable level while fertile materials (^{238}U and ^{232}Th) are converted to fissile reactor fuel. Unfortunately the realization of pure fusion power is too far removed and uncertain to be counted upon to produce fissile fuel in the near term.

The alternative concept currently receiving renewed attention is the coupled fusion-fission hybrid system combining a less than self-sustaining (energy) fusion reactor with a subcritical but power producing fission reactor. Although achievement of pure fusion power is not yet possible, recent advances indicate the plasma requirements for hybrids will be reached while the fission power component of the electrical economy is still increasing.[9] Then, as an alternative to the LMFBR for fissile fuel and power production, the hybrid can be very useful.

The hybrid concept has many potential advantages over the LMFBR for providing power and fissile fuel in the latter part of this century. First, the hybrid reactor possesses great potential as a breeder of fissile fuel. With its abundant supply of neutrons, the hybrid should be able to produce fissile material more rapidly than any of the current breeder reactor concepts to keep pace with power requirements.[2,3]

Second, the hybrid makes an alternative fuel cycle available for existing burner reactors. Reliance on the ^{238}U-^{239}Pu fuel cycle with its weapons grade plutonium can be reduced in favor of the ^{232}Th-^{233}U fuel cycle.

Third, hybrid development allows early introduction of fusion reactors while protecting the large capital investment represented in operating thermal reactors. By using fission blanket power to drive the

hybrid system, current advanced reactor technology would require only
modest extensions to produce a hybrid system as a natural link in the
development leading from pure fission to pure fusion power.[1,3,4]

Finally, the hybrid concept using subcritical blankets is attractive
from a safety standpoint since it would diminish the need for critical
nuclear reactors.[1,3,4,10] The current concern over reactor safety and
core meltdown could be essentially eliminated.[11]

Past studies of the hybrid concept have been restrictive. Typical
hybrid analyses are limited to steady-state evaluation of the technical
characteristics of a concept with emphasis on the neutron economy of the
conceptual blanket.[1-3,12-14] Important features in such hybrid studies
parallel ordinary fusion reactor blanket studies and include:

1. Tritium conversion ratio and doubling time.

2. Fissile breeding ratio and doubling time.

3. Energy production and multiplication in the blanket

4. Constraints on the fusion plasma due to neutronics.

5. Vacuum wall loading and neutron energy transport.

The neutron economy and energy multiplication of the hybrid blanket
have been of primary interest in these initial studies; both are enhanced
by fission events. Little consideration has been given the fusioning
plasma in these hybrid designs beyond setting plasma characteristics
necessary to achieve the assumed blanket power performance. Basic fusion
reactor blanket studies and hybrid blanket work to date are reviewed in
the next section; the similarity of the two is remarkable despite the
increased importance of energy production in hybrid blankets.

Although some hybrid safety considerations have been made based on
the subcriticality of the blanket (effective neutron multiplication

factor, k_{eff}, less than unity) as well as the heat generation rates in the blanket, no time-dependent analysis has been considered; dynamic behavior and associated safety of the hybrid fusion-fission system have been ignored. The effects of perturbations on the coupled system have also been ignored.

Some studies on safety and control analysis of pure fusion reactors have been reported.[15-24] Mills[15-17] described the stability requirements on a steady-state, point model, fusioning plasma, and found the steady-state (equilibrium) plasma unstable against various parameter fluctuations below a critical ion temperature. The effects of artificial feedback were simulated at lower temperatures to control this thermal instability and maintain equilibrium operation below the critical temperature. The work of Mills is a benchmark work in fusioning plasma global dynamics and control.

The work on stability by Ohta et al.[18] is one of the most complete thermal stability studies of point model thermonuclear plasmas. Stability criteria were established using linear analysis of coupled particle and energy balance plasma equations. The thermal instability was evaluated and suitable feedback control was implemented to allow stable operation below the critical plasma temperature set by the stability criteria. Stacey[22] as well as Usher and Campbell[23,24] have reported extensions of this work to more sophisticated plasma models. Yamato et al.[19,20] have extended such stability studies to simple inhomogeneous plasmas with comparable results.

Since such time-dependent analysis was neglected in previous hybrid studies, this research analyzes some dynamic characteristics of a fusion-fission coupled system along with certain steady-state characteristics

of fusion energy blanket multiplication not previously considered. The much larger hybrid blanket energy multiplication demands a coupled time-dependent analysis. The establishment of specific safety and operating characteristics for a coupled hybrid system is necessary for the continued development of the concept into a viable energy alternative.

The effect of thermal instabilities in the fusioning plasma on the fissioning blanket are analyzed in this work to establish hybrid system interactions, safety, and ease of control. This work eliminates a major deficiency in existing studies of hybrid systems so that a decision can be made on its place in the power industry of this country in the last decades of this century.

Review of Fusion Blanket Studies

The Fusion Process

Since hybrids depend on fusion neutrons to breed fissile fuel, at least two fusion reactions have potential for use in a hybrid reactor. These are the deuterium-tritium and the deuterium-deuterium reactions which have the following balances:[25]

$$\text{}^{2}_{1}D + \text{}^{3}_{1}T \longrightarrow \text{}^{4}_{2}He \ (3.52) + \text{}^{1}_{0}n \ (14.06) \tag{1}$$

$$\text{}^{2}_{1}D + \text{}^{3}_{1}D \quad \begin{cases} \longrightarrow \text{}^{3}_{2}He \ (0.82) + \text{}^{1}_{0}n \ (2.45) \tag{2a} \\ \\ \longrightarrow \text{}^{3}_{1}T \ (1.01) + \text{}^{1}_{1}p \ (3.03) \tag{2b} \end{cases}$$
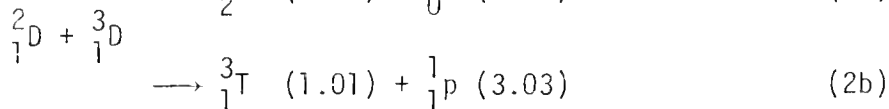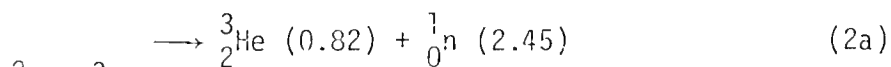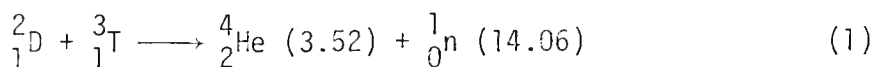
where the two D-D branches have nearly equal probabilities at energies of interest. The numbers listed in parentheses are the energies (MeV) with which the fusion reaction products emerge.

The properties of the D-T fusion reaction are far superior to those of the D-D reaction. For energies below 200 keV the D-T reaction cross section with its broad resonance at 110 keV is nearly two orders of magnitude above the D-D cross sections. The probability for a fusion reaction occurring is characterized by the reactivity or rate coefficient, $<\sigma v>$, which is an average of the product of the cross section, σ, for the fusion reaction in question and the relative speed, v, of the reactants. The reactivity can usually be approximated using a Maxwellian distribution of particle speeds. With a broad resonance around 65 keV, the D-T reaction rate coefficient is also much greater than the D-D reaction rate coefficient below 100 keV.

Finally, the energy released per fusion reaction, Q_F, is significantly higher for D-T fusion events. These comparative values are summarized in Table 1-I[25] and indicate why near term fusion reactors and hence hybrids are limited to the D-T fuel cycle.

Table 1-I

Fusion Reaction Parameters

Reaction	σ (barns) at 100 keV	$<\sigma v>$ (cm^3/sec) at 65 keV	Q_F (MeV)
D-D	0.46	8×10^{-16}	3.65
D-T	5.0	9×10^{-15}	17.6

As noted in Eq. (1), the 17.6 MeV per D-T fusion reaction is divided between the resultant neutron and alpha particle. The alpha particle ultimately is expected to impart most of its energy to the fusioning

plasma, but the 14.06 MeV of neutron energy must be recovered in surrounding blanket regions.

Fusion Reactor Blanket Studies

Since only limited quantities of tritium occur in nature, sufficient tritium must be generated through nuclear reactions to refuel operating fusion devices. The 14.06 MeV fusion neutrons are used for this purpose in two lithium reactions:[7,8]

$$_{3}^{6}Li + _{0}^{1}n \text{ (slow)} \longrightarrow _{2}^{4}He + _{1}^{3}T + 4.8 \text{ MeV} \tag{3}$$

$$_{3}^{7}Li + _{0}^{1}n \text{ (fast)} \longrightarrow _{2}^{4}He + _{1}^{3}T + _{0}^{1}n - 2.82 \text{ MeV} \tag{4}$$
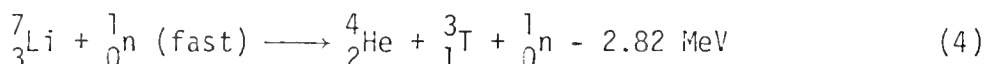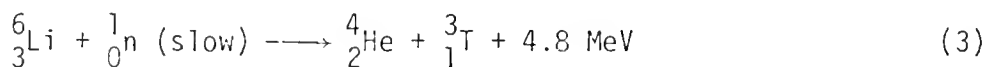
where natural lithium has the composition: 7.56% $_{}^{6}Li$ and 92.44% $_{}^{7}Li$. The exothermic reaction has a 2.9 b resonance at 0.25 MeV while the endothermic reaction, with its threshold at 2.8 MeV, has a 450 mb resonance at 8.0 MeV.[26]

For the usual toroidal fusion reactor using superconducting coils for the magnetic confinement, the position of the blanket used for heat recovery and tritium generation is illustrated in Fig. 1. This configuration conforms to the Tokamak designs most often considered for economic, power-producing fusion machines.[27-33] Refractory metals such as vanadium, molybdenum, and niobium are usually postulated as the vacuum wall and structural material due to the high heat and stress load as well as the need for (n,2n) reactions to enhance tritium breeding.[8] Graphite is the usual outer moderator/reflector material and the shield region is usually of lead and steel composition.[8,31,33] While heat recovery and
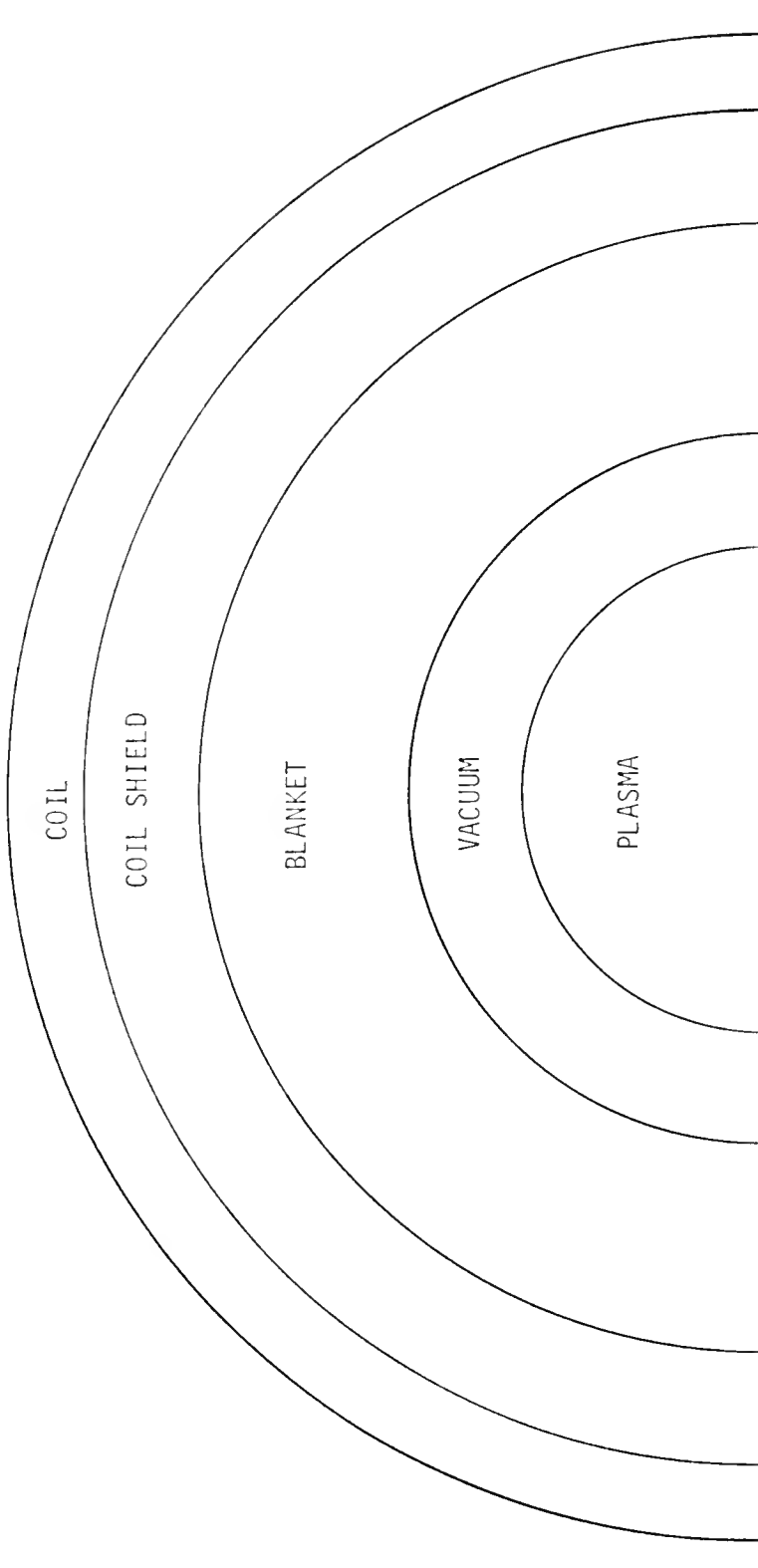
Figure 1. The essential components of a Tokamak fusion reactor.

tritium breeding are confined to the inner reflector/moderator regions of the overall blanket, the outer regions shield the low temperature superconducting magnets from the deposition of energy by high energy particles generated within the fusioning plasma and inner blanket region. A typical thickness for the total heat recovery and shielding regions of the blanket is about two (2) meters with actual heat recovery and tritium production confined to the first meter.[33]

Many early studies were conducted to evaluate tritium breeding and heat generation in idealized fusion blankets. These initial studies indicated that adequate tritium generation was possible but with severe heat transfer requirements on the vacuum wall. This problem was partly due to the fact that only the exothermic lithium reaction was known and used in the earliest studies.[8]

Myers et al.[34] used diffusion theory to examine homogeneous cylindrical blankets of varying thicknesses from 9 to 96 cm. Materials tested included a lithium beryllium-fluoride salt ($LiF + BeF_2$) called "flibe," natural lithium metal and ^6Li metal. All but ^6Li provided adequate tritium breeding ratios above 1.45; the value of only 0.976 for ^6Li demonstrated the potential significance of ^7Li breeding reactions.

Impink[35] and Homeyer[36] also examined the effects of blanket composition on tritium breeding and on spatial heating rates, respectively. Graphite was used as the neutron moderator with molybdenum as the vacuum wall material because of its neutronic and refractory characteristics. The flibe coolant and tritium generation medium was selected to avoid electromagnetic resistance to coolant circulation. For variations in vacuum wall thickness, ^6Li enrichment and flibe-Be composition, Impink obtained tritium breeding ratios, T/n, as high as 1.55.

Since nuclear heating rate calculations showed extreme peaking near the first wall based on 14 MeV neutron energy flux of only 1 MW/m^2 on the vacuum wall, Homeyer concluded that cooling of the vacuum wall would be the most severe heat removal problem in the blanket. The recoverable blanket energy was calculated to be 17.4 MeV per entering 14-MeV neutron.

Bell[37] used multigroup transport calculations to analyze an infinite annular blanket and concluded that pure lithium is an attractive breeding material but requires a thicker blanket than one containing beryllium. Unfortunately beryllium is probably too expensive to justify its large volume usage in systems of the size of power-producing fusion devices.

Realistic blanket designs required more detailed neutronics studies to consider structural and heat generation requirements as well as the tradeoff between tritium breeding and energy generation as shown in more recent, detailed calculations.[8,27,38-43]

Lee[38] used Monte Carlo theory to calculate neutronics results for a three zone spherical annular blanket with outer radii of 101, 202, and 302 cm for a 100 cm radius plasma. Structural effects were simulated by homogeneous volume fractions of niobium chosen for its refractory, fabricating, and welding characteristics; excellent results were obtained for a structureless lithium blanket. More realistic blankets were simulated by making Zone 2 (1 cm) all niobium and diluting the lithium in Zones 3 and 4 with increasing volume fractions of niobium structure. Lee's results are summarized in Table 1-II where the increase in energy generation per fusion event is due to Nb(n,γ) reactions. Since ^{6}Li enrichment was found to be ineffective and only 5 to 6% niobium is necessary for real blanket structure, Lee concluded the simplest blanket containing lithium and structure can meet tritium breeding requirements.

Electromagnetic resistance to lithium flow may be excessive near the vacuum wall where high coolant velocities are needed. Induced currents in the lithium act to retard lithium flow across magnetic field lines; but such resistance is greatly reduced in the outer blanket regions where heating rates and hence flow rates are reduced.

Table 1-II

Dependence of Tritium Breeding Ratios and Energy Deposition
Rates for Lee's Fusion Blankets

Nb (Volume Per Cent)	T/n	Q_β (MeV)
0	2.10	17.14
5	1.77	18.63
10	1.38	19.60
15	1.16	20.20
20	1.00	20.50

Steiner[8,39] analyzed the neutronic behavior of two designs based on the ORNL standard blanket configuration containing niobium structure, coolant, and graphite reflector. These two blankets reflected an optimistic (Design 1) and a conservative (Design 2) outlook on the problem of cooling the vacuum wall. Design 1 contained lithium throughout the blanket; Design 2 assumed that flibe must be used to cool the vacuum wall with lithium elsewhere. Steiner rejected flibe coolant throughout the blanket since it produced an inadequate (T/n = 0.95) tritium breeding ratio. Neutron activation problems were also first revealed by Steiner.[8]

Niobium was selected over molybdenum as the vacuum wall and structural material because of superior fabrication and welding characteristics

as well as lower sputtering ratio despite molybdenum's demonstrated superiority for tritium breeding.[8] Graphite was employed as the moderator/reflector in both designs. Summary descriptions of these two blankets with 6% niobium structure are presented in Table 1-III to indicate typical blanket models.

Table 1-III

Summary Descriptions of ORNL Optimistic (1) and Conservative (2)
Blanket Designs

Region Number	Description of Region	Thickness by Region (cm)	Volume Composition by Region	
			Design 1	Design 2
1	First wall	0.5	Nb	Nb
2	Coolant + Structure	3.0	94% Li / 6% Nb	94% Flibe / 6% Nb
3	Second wall	0.5	Nb	Nb
4	Coolant + Structure	60.0	94% Li / 6% Nb	94% Li / 6% Nb
5	Moderator-reflector	30.0	Graphite	Graphite
6	Coolant + Structure	6.0	94% Li / 6% Nb	94% Li / 6% Nb

The basic 100 cm Design 1 blanket with first wall at 200 cm radius was adopted as the standard blanket model at the Neutronics Session of the Working Sessions on Fusion Reactor Technology held at Oak Ridge

National Laboratory (ORNL) in June 1971.[44] This blanket has been frequently used to check neutronics calculations.

Transport theory was applied in slab geometry to obtain the tritium breeding results listed in Table 1-IV where the breeding ratio of 1.35 in Design 1 is some 10% above the 1.23 value for Design 2. Slab geometry is adequate due to the large plasma radii (1-5 meters) for steady-state fusion reactors.[33,45]

Table 1-IV

Summary of Steiner's Tritium Breeding Calculations per Incident
14 MeV Neutron

Design	T/n	Neutron Leakage
1	1.35	0.023
2	1.22	0.020

If hypothesized low levels of tritium holdup[46,47] are realized, then breeding ratios only slightly above unity ($\sim$ 1.01) will be sufficient for seven year doubling times. Therefore, Steiner's relatively low 1.3 breeding ratio is sufficient to obtain the one month doubling time to establish initial tritium inventories.

Steiner's results for spatially dependent, nuclear-heating rates were based on a standard first wall energy transport of 10 MW/m^2 due to the 14 MeV neutron flux. Extreme peaking of nuclear-heating rates was found in the first wall regions as shown in Fig. 2; Design 1 yielded heating rates up to 180 W/cm^3 while Design 2 with flibe first wall coolant was less but still over 120 W/cm^3. Due to plasma radiation, the usual
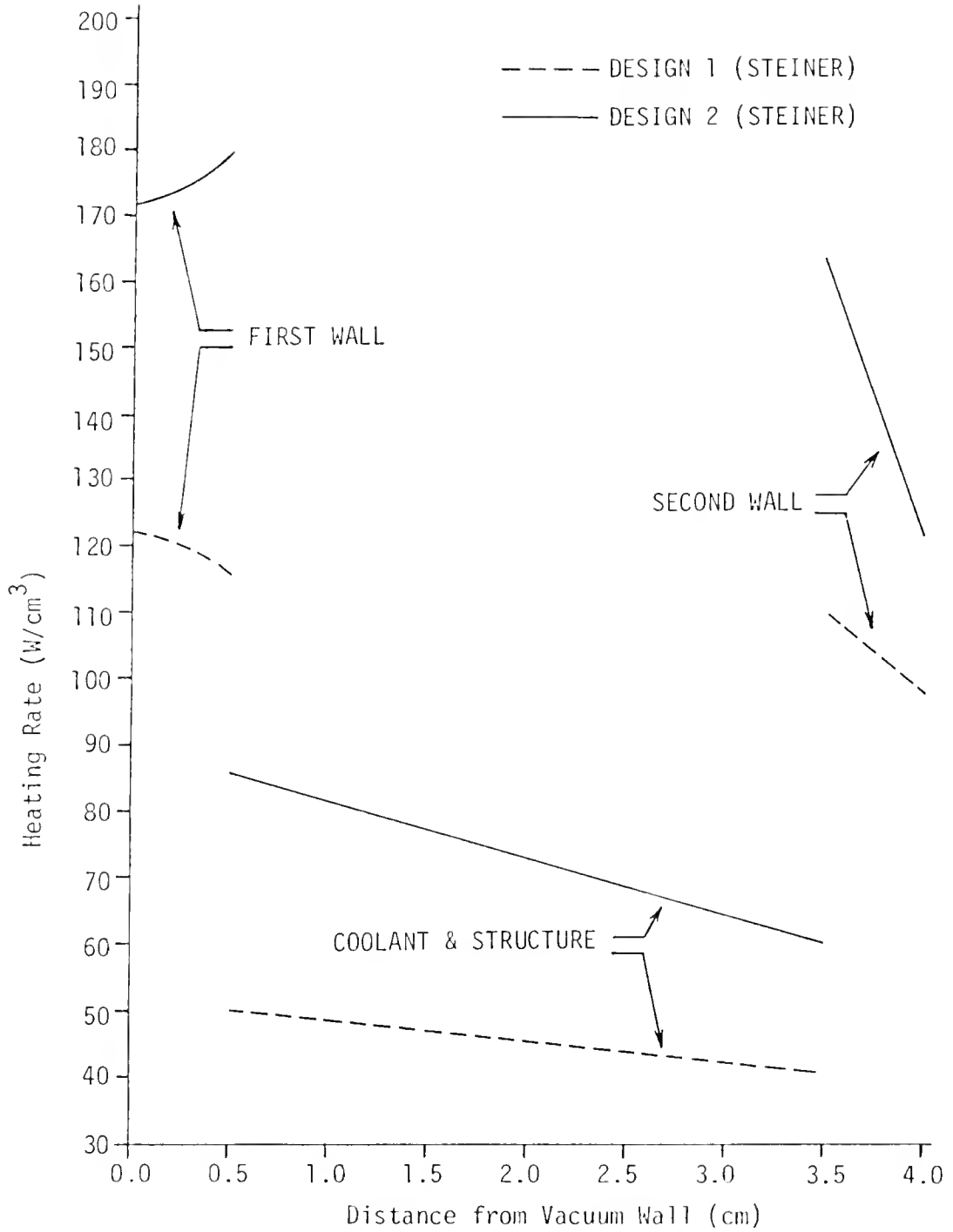
Figure 2.   Comparison of spatially-dependent heating rates for vacuum wall regions in two designs.

heating rate peak at the vacuum wall will be 5-10% more extreme than indicated. These extreme heating rates (power densities) near the first wall along with the excessive fusion neutron wall loading represent a major technological problem for all Tokamak fusion power reactors.[30,33,47]

Steiner's work supported previous work indicating that blankets employing lithium as the only coolant are superior to those employing flibe since:

1. Design 1 has a 10% higher tritium breeding ratio.

2. Design 1 has a 50% lower heat load in the niobium vacuum walls since the high gamma cross section of flibe has been removed.

3. Neutron irradiation effects within the vacuum wall are essentially the same in both designs along with excessive heating rates near the first wall.

Blow et al.[40] used Monte Carlo calculations in cylindrical geometry with first wall at 150 cm to examine Steiner's two basic 100 cm thick blanket models with varying (2-8%) niobium structural content. Good breeding ratios (1.15-1.54) were reported for all cases except the exclusive use of flibe coolant in the entire blanket where $T/n = 1.027$. Blow reported additional good breeding results ($T/n = 1.58$) for blankets of Design 1 where niobium was replaced with 2% molybdenum. Examination of molybdenum was justified because the alloy TZM (0.5% Ti, 0.1% Zr, 99.4% Mo) has the neutronic characteristics of pure molybdenum but welding characteristics similar to niobium.

A modular blanket design using heat pipes has been proposed by Werner et al.[41,42] in which neutronic behavior was examined in a 100 cm thick cylindrical annulus with 200 cm inside diameter. In relocating the "standard" vacuum wall of a thermonuclear reactor beyond the neutron-moderating, energy-converting blanket (at 320 cm), the entire moderator was placed in a cylindrical vacuum envelope in clear view of the plasma

to eliminate the neutronic losses and structural buckling problems of previous designs.

The interlocking modular blanket units incorporated heat pipes which remove radiant energy from the inner module surface and flatten the power distribution in the blanket by moving excess energy outward to power-deficient zones.[42]

Werner's blanket model contained beryllium for neutron multiplication, lithium for tritium breeding, sodium for energy generation, and niobium for structural strength. The 100 cm moderator section of the blanket was divided into two zones; Zone 1 contained 75% Li and 5% Nb while Zone 2 contained varying volume percentages of Be, Na, and Li. Both zones contained $\sim$ 20% volume for heat pipe voids. Zone 1 was used to buffer the energy density in the fluid so that all nuclear and radiant heating energy could be removed by convective heat-transfer through the heat pipes resulting in power flattening and increased average power densities.

The tradeoff between tritium breeding and energy multiplcation through use of beryllium or sodium was examined for varying volume fractions in a 90 cm thick Zone 2.[41] Increased energy generation per fusion neutron up to 23.0 MeV for beryllium and 26.05 MeV for sodium was obtained but with a reduction in the tritium breeding ratio. Unless maximum energy is very important, Werner recommended maintenance of tritium breeding-- probably because of beryllium costs and sodium activation.

Struve and Tsoulfanidis[43] used Monte Carlo methods to calculate tritium breeding ratios and heating rates for two proposed blanket designs utilizing vanadium as the structural material in lithium. Vanadium was used for its reduced activation and after-heat advantages, although it has the disadvantage of a low operating temperature.

The two blanket configurations included a basic Steiner-type[8] where the vacuum wall surrounds the plasma and a Werner-type where the vacuum wall surrounds the blanket.[42] To avoid the problem of coolant flow, Struve proposed a heat transfer fluid such as helium which would be unaffected by magnetic field lines and transparent to neutrons. It was simulated by 20% volume void in the lithium. Breeding ratios above 1.3 were obtained and agreed reasonably well with previous blanket studies using niobium structure.[8,40,42] The use of helium as a fusion blanket coolant has been investigated by Hopkins and Melese-d'Hospital[48] and by others at General Atomic Company.[31]

The spatially dependent nuclear-heating rates for the two blankets showed high vacuum wall heating and agreed with previous results. Steiner's generally higher calculated heating rates were caused by niobium blanket structure.

These detailed neutronic studies of fusion blankets indicate ample tritium breeding is possible in realistic blankets. The inability to breed tritium is not a problem in fusion designs. The real problems include providing adequate heat removal for the first wall and protecting and designing the vacuum wall to withstand the required 15 MeV neutron fluxes.[33]

These fusion reactor blanket scoping studies have formed the basis for a number of design studies for Tokamak fusion power reactors of either full commercial scale or demonstration size.[28-32] These various pure fusion Tokamak blankets use either flibe, natural lithium, or helium as coolant and flibe, natural lithium, or some lithium-bearing medium as breeding material with tritium breeding ratios from 1.15 to 1.3. Most pure fusion design studies use lithium or helium as the coolant, instead

of flibe.[33]   All blankets are on the order of 100 cm thick and some 20-25 MeV are deposited in the blanket per 14 MeV neutron entering the blanket with extreme peaking of heating rates near the first wall. The blankets are not expected then to be significantly energy multiplying.

In general the tendency is toward more compact fusioning plasmas with an associated reduction in the first wall neutron flux to well below 10 MW/m^2 of 14 MeV neutron energy transport.[28-33] The basis for such reductions is the extreme technological problems of designing a first wall which will function for at least two years or more. If such cannot be accomplished, then fusion power plants that are viable in other respects are likely to be too limited in outage maintenance time to compete economically with other electrical power sources.[33,49]

Critical Review of Hybrid Blanket Studies

Overview of Hybrid Blanket Studies

Fusion blanket designs attempt to maximize energy generation while maintaining the tritium breeding ratio. The inclusion of fissionable materials in the blanket is an obvious possibility for achieving significant power and neutron multiplication. Such a hybrid blanket must still meet the basic fusion blanket requirements of adequate tritium breeding, heat transfer, and magnet shielding as well as produce energy multiplication and/or fissile material. As with pure fusion systems, previous evaluations of hybrid concepts have been based primarily on the calculated neutronic behavior of the conceptual blanket as reflected in the following parameters:

1. Tritium breeding ratio and fissile fuel production.

2. Energy production in the blanket per fusion event.

3. Fusion plasma characteristics.

4. Neutron first wall loading.

The tritium breeding ratio must be sufficient to refuel operating hybrid systems and fuel new ones. As for pure fusion systems, adequate values are in the range $T/n = 1.15 - 1.3$ and are relatively easy to obtain.[1,3] Simultaneously, a hybrid may also be required to produce or even breed significant amounts of fissile fuel.[2,3,6]

Energy deposition in the blanket per fusion event is a very important hybrid criterion. Usually D-T fusion systems assume a blanket energy deposition, Q_B, of about 20 MeV per fusion to account for the 14.1 MeV neutron and the 4.8 MeV per $^6Li(n,\alpha)^3T$ reaction. Fusion blanket studies show this energy deposition is relatively insensitive to design or composition[33] with calculated values per fusion neutron ranging from a maximum of 26 MeV for Werner's[41] best design down to 18.3 MeV evaluated by Leonard[1] for the ORNL standard design.

Although fusion blankets are limited in their energy multiplication capabilities, this is not the case for hybrids which are evaluated for significantly increased blanket energy deposition per fusion event through fission energy multiplication. Interest in subsystem interactions and dynamics studies of such a coupled hybrid system is certainly justified when the potential for energy generation through energy multiplication in the subcritical blanket is considered.

The third area of technical assessment of hybrids involves the fusion plasma characteristics required to achieve the assumed blanket performance. This assessment is directly related to the blanket energy deposition, Q_B, per fusion neutron. The Lawson Criterion sets the plasma values of density, n, confinement time, τ, and temperature, T, required

to reach overall breakeven in energy production or scientific breakeven.[50]
The breakeven $n\tau$-value varies inversely with the total energy generated
per fusion event. Therefore, the potential value of a hybrid system is
characterized by its ability to relax the Lawson condition through effec-
tive fission increase of energy released per fusion event.

Finally, the required transport of neutron energy through the first
vacuum wall is an important figure of merit. Previous projections of 10
MW/m^2 impose stringent material problems so more recent designs attempt
to achieve wall loadings in the range 0.25 to 3.5 MW/m^2.[1,3,13] Any
hybrid relaxation of first wall loadings is a technical advantage over
pure fusion systems.

Such potential for breeding fissile fuel with fission energy multi-
plication of the fusion neutron source strength to sustain and drive the
coupled system has been examined by many researchers. Early concepts
were summarized adequately by Leonard and have little more than historical
significance.[1]

Lontai Attenuator Model

The first detailed calculations on the neutron economy of hybrid
blankets were performed by Lontai in 1965.[10] He assumed a steady-state,
D-T clyindrical plasma with a 5.0 MW/m^2 energy transport of 14 MeV
neutrons but performed the neutron balance calculations for an infinite
slab source geometry. Lontai's results were based on blanket configura-
tions using flibe coolant channelled in a graphite matrix. Neutron
balance ranges were reported for various molybdenum wall thicknesses,
UF_4 concentrations and ^6Li enrichments to increase poor tritium breeding

ratios. Such a scope of study and results reported set the stage for most of the hybrid studies which followed.

Lontai's best results were reported for a blanket concept consisting of a 1 cm molybdenum vacuum wall, 1.5 cm coolant (flibe) region, and 49 cm attenuator region containing 21% graphite by volume with 70% salt bearing uranium (LiF - BeF_2 - UF_4). The natural lithium case had insufficient tritium breeding. Adequate tritium breeding was calculated only by using lithium salt enriched to 50% ^{6}Li and varying composition. The fission energy multiplication increased by nearly a factor of two over non-fissile blankets with better heat transfer characteristics. Similar calculations for 90% enriched ^{6}Li resulted in much lower fissile fuel production with no increase in energy multiplication. Plasma requirements are not relaxed much by such small amounts of fission energy deposition; however, Lontai opti-mistically labeled the 50% ^{6}Li attenuator practical because of possible reduced plant capital costs.

Lontai's hybrid feasibility study currently has little more than historical significance because of inherent deficiencies:[1]

1. Faiure to consider values of plutonium production.

2. Failure to consider cost of maintaining high ^{6}Li enrichment.

3. Failure to consider ^{235}U present in depleted uranium.

4. Use of obsolete computer codes and poor cross section data.

Lidsky's Symbiosis Concept

A novel approach to the fusion-fission hybrid concept was proposed by L.M. Lidsky,[2,6] who analyzed the characteristics of a hybrid fusion reactor which, when coupled with a Molten Salt Converter Reactor (MSCR), would constitute a viable central station power plant.[6] The essential

feature of this symbiotic scheme was a fusion system breeding sufficient tritium and fissile nuclei to fuel itself and a power-producing fission device such as an MSCR.

A cylindrical, 1.25 m radius torus of D-T plasma was used in the symbiosis. The basic duplex blanket configuration contained a thorium-bearing blanket flibe salt composed of $LiF:BeF_2:ThF_4$ in the ratio 71:02:27 and lithium depleted in ^6Li. The neutronic properties of pure molybdenum with its large $Mo(n,2n)$ cross section, were utilized in the TZM structural alloy. Since Lidsky's fusion reactor was designed for fuel, not power production, a graphite moderating region was used to prevent thorium fission products from poisoning the blanket during operation. This is only possible at initial operation until fissile ^{233}U is produced which implies frequent refueling and possible cost penalties which Lidsky ignored. Lidsky used S_N transport theory to evaluate the neutron economy of the hybrid blanket configuration. The results for this as well as variations in the base design are shown in Table 1-V. Since simultaneous production of fissile nuclei and tritium was found to be attainable over a range of production ratios, each component of the system can be optimized for power or fuel production to utilize the strong points of both fusion reactors (neutron rich) and fission reactors (power rich).

The reactors in the symbiosis were coupled by the production of fuel for the fission reactor by the fusion reactors. Lidsky[6] also analyzed equations for the time dependence of the fuel inventories of the two reactors in the fusion-fission symbiosis combination.

Table 1-V

Neutron Economy of Lidsky's Hybrid Blanket

	Events per 14-MeV Source Neutron	
	Calculated	Range
Tritium production	1.126	
Thorium captures	0.325	0.05-0.50
Total conversion	1.451	$\geq$ 1.40

Lidsky's results demonstrated that the fuel doubling time of such a balanced hybrid system is determined entirely by the neutron-rich fusion reactor component. Lidsky's power production analysis indicated further that the net power production in such a dual system is determined primarily by the fission reactor component since the fusion power reactor is only a small perturbation on the net power of real systems. Thus each subsystem in the symbiosis can theoretically be optimized for its respective primary purpose of fuel or power production. This is an important point to remember with respect to hybrid reactor system design.

Lidsky selected a CTR-MSCR power plant with 1500 MWe output and a 10 year doubling time for symbiosis study. The MSCR was rated at 4450 MWth with a fuel conversion ratio of 0.96 operating on the ^{233}U-^{232}Th cycle. Lidsky calculated a 10 year fissile doubling time with a tritium linear fuel doubling time of 0.113 years. For a 40% thermodynamic efficiency the fusion reactor would be a net consumer of 89 MWe while the overall system was calculated to be able to provide 1690 MWe net power with 35.6% plant efficienty. Lidsky predicted net plant efficiencies above 40% for near-classical plasma confinement times.

Required plasma characteristics were encouraging since the vacuum wall loading due to 14 MeV neutrons was only 1.00 MW/m^2--well below that necessary to assure technological feasibility in pure fusion plants.[33]

In addition, there was no energy multiplication in the fusion reactor blanket of the symbiotic scheme; this assumption was clearly not accurate as soon as some fissile fuel breeding has occurred. Plasma parameters are near Lawson conditions as indicated by the hybrid parameters summary in Table 1-VI and the fact that only 295 MWth was required to support the fuel-producing fusion system.

Table 1-VI

Lidsky's Hybrid Reactor Parameters

n	$= 10^{14}$ ions/cm^3
τ	$= 0.625$ sec
T	$= 20$ keV
Wall loading	$= 1$ MW/m^2
^{233}U production	$= 1.1$ kg/day

The symbiosis has a number of advantages. First, this scheme simplifies the construction of power plants capable of breeding and processing all requisite fuel in situ. Second, the lessening of fuel cost constraints makes the modifications of existing reactors possible to avoid thermal pollution. Finally, by developing this concept, the system under construction at any time could take full advantage of the existing state of development of both fusion and fission technology without final commitment to either.

In addition to the symbiotic hybrid concept and the usual power-producing hybrid concept, Lidsky has also formalized consideration of a third hybrid concept called the augean concept. This concept involves using the hybrid blanket to burn the actinide waste from fission reactors.[2,13] The augean concept is of little interest for dynamic consideration.

Lee's Fast Fission Hybrid Concept

Lee[45] eliminated Lidsky's separate fusion and fission reactors in favor of the so-called subcritical fast fission blanket. Monte Carlo Transport theory was used to perform neutron balance calculations in infinite media of pure thorium, pure ^{238}U, and natural uranium to verify the breeding potential of hybrid blankets. The results shown in Table 1-VII are in good agreement with experimental measurements done by Weale et al.[51]

Table 1-VII

Lee's Neutron Balance in Infinite Media

Blanket	Q_B (MeV)	Breeding Reactions per 14-MeV Neutron
Thorium	64	2.7 $[^{232}Th(n,\gamma)]$
^{238}U	233	4.4 $[^{238}U(n,\gamma)]$
Natural Uranium	309	5.0 $[^{238}U(n,\gamma)]$

Lee examined blankets containing varying concentrations of niobium, lithium, and a fertile nuclide. The blanket geometry was a two-zone,

sperhical annulus having an inner radius of 200 cm and an outer radius of 300 cm with composition as listed in Table 1-VIII. For constant blanket geometry and material volume fractions, the following optimum results were obtained for depleted lithium (4% ^{6}Li) and depleted uranium (0.04% ^{235}U) per 14 MeV neutron: Q_B = 103 MeV; T/n = 0.986; ^{238}U(n,γ) reactions = 1.68. Because of the 1.68 ^{239}Pu breeding reactions per D-T fusion event, Lee chose ^{239}Pu as the fissile fuel.

Table 1-VIII

Subcritical Fast Fission Blanket Components
Studied by Lee

	Element	Volume Fraction
Zone 1 (30 cm thick)	Li	0.95
	Nb	0.05
Zone 2 (70 cm thick)	Li	0.30
	Nb	0.05
	Heavy Element	0.65

Lee also studied the neutronics effects of changes in the thickness of Zone 1 and material volume fractions in Zone 2; for the composition shown in Table 1-VIII results were reported for the following heavy element material variations:

1. Depleted uranium versus ^{235}U content.

2. Metallic and oxide mixtures of plutonium and uranium versus ^{239}Pu content.

3. Thorium versus ^{233}U content.

Best energy generation with sufficient breeding was reported for the metallic uranium blanket with 4% plutonium. This case and one poisoned with 8% fission products are summarized in Table 1-IX.

Table 1-IX

Fast Fission Hybrid Neutron Economy per 14 MeV
Neutron Calculated by Lee

Material	Tritium Production	Plutonium Conversion Ratio	Q_B (MeV)	k_{eff}
4% Pu-U	1.38	3.14	431	0.84
4% Pu-U + 8% FP	1.18	3.03	306	

The usefulness of a hybrid concept is contingent upon a short fissile fuel doubling time. Lee estimated a very high 14 MeV neutron wall loading of 12.8 MW/m^2 to obtain a 5 year plutonium doubling time for the 8% FP blanket but reports no fusion plasma characteristics. Leonard[1] later claimed that the 306 MeV blanket energy release per fusion neutron in Lee's 8% FP model would lead to a three-fourths reduction of the usual Lawson breakeven condition. However, current engineering considerations indicate that such first wall power loadings will almost certainly make fusion power unrealistic due to the need for frequent first wall replacement.[33]

Since his results indicated energy production increases of 10 to 20 times over non-fissile blankets with simultaneous adequate tritium and fissile fuel breeding, Lee concluded fast fission hybrid blankets were feasible. However, the fast fission blanket has no clear neutronic

advantage over other concepts except as a fuel producer. Considerable additional research has been reported on blankets and hybrid systems using the fast fission concept.[52-57]

All have emphasized fuel production versus power production and have worked with reduced first wall neutron loadings of 1-5 MW/m^2. The advantages of using fusion neutrons for fast fission as well as breeding fuel in situ are probably only applicable in the true symbiotic concept[6] where the hybrid is not a system energy producer but a fuel producer, since blanket multiplication is lowered for low enrichments with fast fission. Hence, the fast fission hybrid is of little interest in this current study.

Texas Fast Fission Hybrid

Parish and Draper[12] presented extensive hybrid neutronics results for their model which was also a fast fission design. They investigated the potential of 14 MeV fusion neutrons to fission fertile materials (^{232}Th and ^{238}U) while maintaining adequate fusion blanket performance. Parish and Draper based the attractiveness of this concept on the relative abundance of such fertile fuels and the elimination of dependence on breeding fissile fuel for hybrid usage. The large fission energy multiplications obtained in other studies[1,3] were not paralleled in this hybrid; however, the potential of both thorium and natural uranium-fueled fast fission blankets to produce both fission power and fissile material was demonstrated.

The use of the standard ORNL fusion blanket[44] with natural lithium coolant and niobium structure provided the model for comparison between

various calculational methods. To verify methods of analysis Parish and Draper calculated the neutronic and photonic characteristics of the standard fusion blanket model using ENDF/B-III cross section data in the ANISN[58] code for a P_3-S_4 transport approximation. The resultant standard blanket neutron economy compared well with Steiner's latest results on the same standard.[59] Good agreement was obtained for breeding (T/n = 1.445 versus T/n = 1.452) and (n,2n) reactions as well as neutron leakage despite Steiner's use of pre-ENDF/B-III cross section data. This Texas hybrid was one of the first hybrid studies to account for (n,3n) reactions which become very important in such poorly multiplying blankets.

Since high energy neutrons are needed to fission fertile fuels, the fission material regions in this concept were placed as close as possible to the vacuum walls. Low energy neutron absorption was only partially offset by (n,2n) and (n,3n) reactions.

The volume fractions of fuel, clad (niobium), and coolant (lithium) in the model were maintained constant at 0.45, 0.15, and 0.40, respectively, to approximate fuel regions in a LMFBR. The tritium breeding, fissile breeding, fission power, and spatial heat deposition by blanket region were presented in the Texas study for various blanket fuel thicknesses. The results of these calculations for two thorium-fueled blankets and four uranium-fueled blankets are presented in Tables 1-X and 1-XI.

The calculation of spatial heat deposition rates in the standard and fertile fueled blankets in this work emphasized the problems with low multiplication hybrid blankets.

Table 1-X

Neutron Economy for Thorium-Fueled Blankets

Thorium Fuel Region Thickness	Reactions/Fusion Event		
	T/n	^{232}Th(n,f)	^{232}Th(n,γ)
6 cm	1.3012	.0310	.1326
13 cm	1.0964	.0472	.3118

Table 1-XI

Neutron Economy for Uranium-Fueled Blankets

Natural Uranium Fuel Region Thickness	Reactions/Fusion Event				
	T/n	^{238}U(n,f)	^{235}U(n,f)	Total Fission	^{238}U(n,γ)
10 cm	1.3252	.133	.0133	.1463	.2487
13 cm	1.2694	.1863	.0161	.2024	.3818
20 cm	1.0865	.1837	.0259	.2096	.5320
26 cm	0.9614	.1986	.0315	.2301	.6654

For the large 10 MW/m^2 first wall neutron loading limit, the two thorium-fueled blankets showed peak power densities of 200 W/cm^3. For the 13 cm natural uranium case, the power density between the niobium walls ranged from 510 to 364 W/cm^3; the related thorium case had a range of 203 to 146 W/cm^3. Fuel was eliminated in the 3 cm region between niobium walls for all other uranium cases to prevent vacuum wall cooling problems. Since the LMFBR is designed for 500 W/cm^3 average power

density, Parish and Draper have claimed these hybrid blanket power densities are acceptable. This is doubtful because of the low power densities at blanket positions removed from the vacuum wall and the resultant unit cost of electrical and fusion power produced.

The superiority of natural uranium to thorium as a fast fission hybrid blanket fuel because of its larger fast fission cross section is illustrated in Parish's comparison of the best case for each fuel presented in Table 1-XII.

Table 1-XII

Comparison of Best Natural Uranium-Fueled and
Extrapolated Thorium-Fueled Blankets

	Uranium	Thorium
Tritium Breeding Ratio	1.09	1.15
Fusion Blanket Energy Multiplication	~ 20	0.5
Fissile Nuclei Produced per Fusion Event	0.53	0.31
Peak Power Density at Nb First Wall	409 W/cm^3	~ 200 W/cm^3

However, the low return of the fissioning blanket renders this concept uneconomical versus other concepts relying on better fissile blankets. Increasing fuel costs could make this concept more attractive at some future date but others seem more appropriate.

Light Water Hybrid Reactors

The feasibility of fusion-fission hybrid reactors based on breeding light water thermal fission systems has recently been investigated at the

Princeton Plasma Physics Laboratory.[60] Emphasis was placed on fuel-self-sufficient (FSS) hybrid power reactors fueled with natural uranium. Other Light Water Hybrid Reactors (LWHR) considered included FSS-LWHR's fueled with spent fuel from Light Water Reactors (LWR's), and LWHR's to supplement LWR's by providing a tandem LWR-LWHR power economy that would be fuel self-sufficient similar to Lidsky's symbiotic concept. Nuclear power economies based on any of these LWHRs were found to be free from the need for uranium enrichment and for the separation of plutonium. They offer a high utilization of uranium resources (including depleted uranium) and have no doubling-time limitations.

This study investigated the properties of subcritical thermal lattices for hybrid applications and concluded that light water is the best moderator for FSS hybrid reactors for power generation. Several lattice geometries and compositions of particular promise for LWHR's were identified with thicknesses up to 250 cm. The performance of several conceptual LWHR blankets was investigated and optimal blanket designs were identified for natural uranium-fueled lattices. The effect of blanket conversion efficiency and the feasibility of separating the functions of tritium breeding and of power generation to different blankets were investigated. Optimal iron-water shields for LWHR's were also determined.

The evolution of the blanket properties with burnup was evaluated along with fuel management schemes. The feasibility of using the lithium system of the blanket to control the blanket power amplitude and shape was also investigated. A parametric study of the energy balance of LWHR power plants was carried out, and performance parameters expected from LWHR's were estimated. This investigation of LWHRs also compared LWHR's

with critical systems and delineated the advantages of such hybrids in alleviating nuclear technology problems relating to resource utilization, proliferation, and safety issues. In general, this study reported the same types of information as previous studies but for a different blanket design.

PNL--Thermal Fission Hybrid

Pacific Northwest Laboratories (PNL)[1,61] initially studied a hybrid fusion reactor utilizing a subcritical thermal fission lattice around the usual cylindrical D-T plasma. The four distinct regions of the hybrid blanket configuration are illustrated in Fig. 3.

The 8 cm thick neutron convertor region was filled with niobium-clad pins of both depleted uranium carbide and natural lithium. Niobium structural walls are used along with helium coolant. The 150 cm thick thermal fission lattice, consisting of a graphite-moderated, natural uranium-fueled, helium-cooled matrix, was designed for fission power generation. The last 50 cm of blanket thickness are filled with graphite reflector and natural lithium absorber, respectively.

The ENDF/B III cross section data were used in the HRG3[62] and Battelle-Revised-Thermos (BRT-1)[63] cross section codes to obtain fast and thermal broad group data, respectively. The final neutron balance results obtained using a P_3-S_8 transport calculation in ANISN[58] are summarized in column 1 of Table 1-XIII. Neutronic effects from slight enrichment of the uranium in the fission lattice are also shown in the neutron balances of columns 2 and 3 in Table 1-XIII.
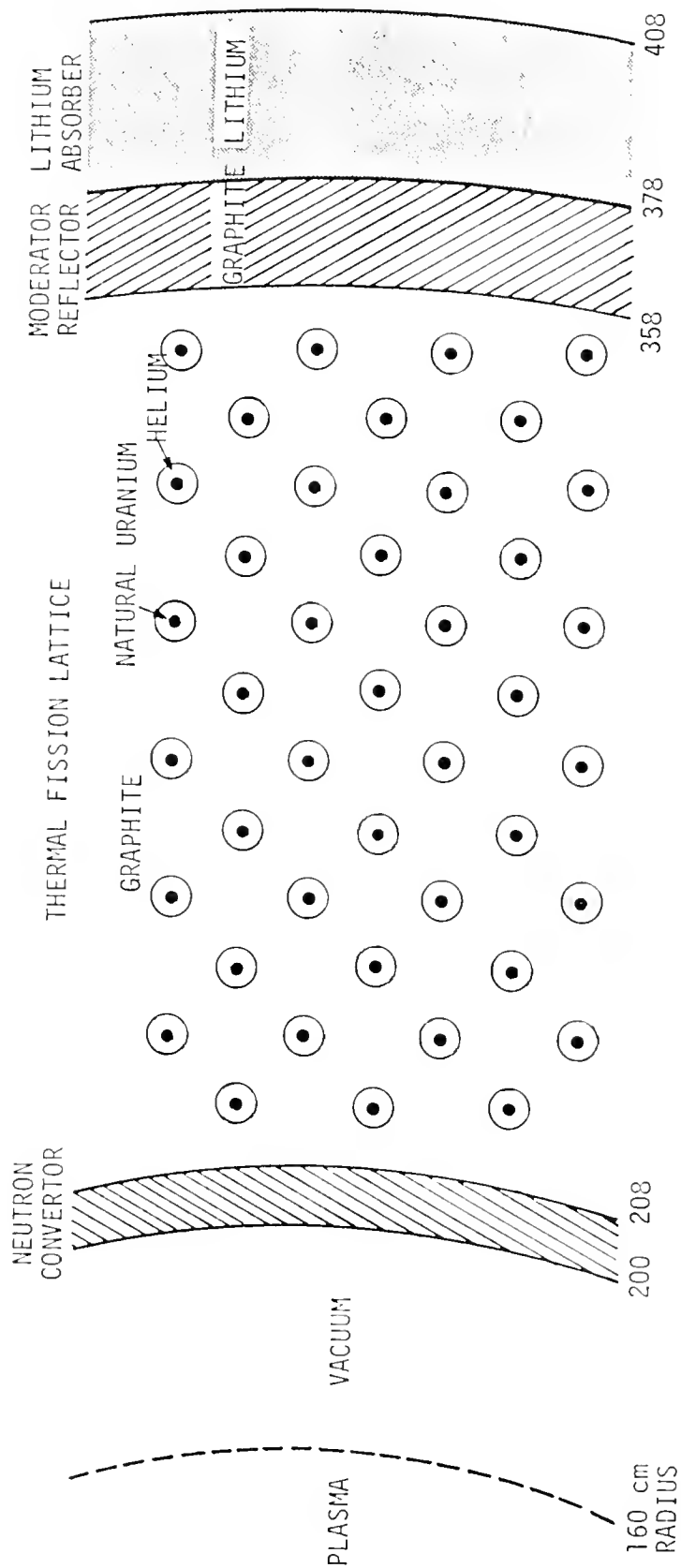
Figure 3. Early PNL fusion-fission hybrid subcritical blanket configuration.

Table 1-XIII

Early PNL Hybrid Neutron Balance

	Events per Source 14-MeV Neutron		
^{235}U Atom Percent Enrichment	0.7196	0.80	0.90
Tritium Production			
^{6}Li	0.956	1.188	1.763
^{7}Li	0.019	0.019	0.020
Total Tritium Production	0.975	1.207	1.783
Fissions			
^{238}U	0.234	0.251	0.292
^{235}U	1.936	2.776	4.863
$\dfrac{^{238}\text{U Captures}}{^{235}\text{U Absorptions}}$	1.121	0.988	0.853
Estimated k_{eff}	0.847	0.884	0.928
Q_B	455	625	1050

Based on their composite behavior with fissile enrichment, an enrichment was predicted (0.77 atom %) for which both the tritium and fissile conversion ratios could be optimized to exceed unity. The calculated energy deposition in the blanket for the best case was calculated to be about 500 MeV per source neutron corresponding to an energy multiplication of about 25. This PNL optimum hybrid is attractive since significantly 0.77% enriched uranium can be produced than the higher percentages required for fast or thermal fission breeder concepts.

This early PNL concept assumed a thermal power generation rate of 0.75 W/cm^3 corresponding to advanced, gas-cooled, uranium metal graphite

reactor capabilities which is very low. This power density was used to determine the plasma and blanket specifications shown in Table 1-XIV where the plasma requirements are substantially less than for a nonmultiplying blanket and the vacuum wall loading is very low.

Table 1-XIV

Early PNL Hybrid Specifications

Blanket	
Specific power	0.75 W/cm^3
Thermal power	20 MW/m
Vacuum wall loading	0.05 MW/m^2
Plasma	
T (keV)	nτ (steady state) (sec/cm^3)
10	3.5×10^{13}
20	1.8×10^{13}

Since a non-negligible fraction of the thermal energy produced in the blanket must be used to sustain such a plasma, the need for investigation of controls is justified, especially since the fission energy multiplication is predicted to be so high.

This preliminary PNL hybrid design was faced with drawbacks such as large size (2 m thick blanket) and low power density (0.75 W/cm^3). However, it was favored with low wall loading and plasma conditions reduced to $\sim$ 1/6 Lawson Criterion value. Since the hybrid objectives of energy multiplication with adequate breeding of tritium and fissile fuel are attainable, the PNL concept appeared to be a promising competitor for the LMFBR program. Much additional work has been performed including further scoping calculations to determine the best design of the PNL helium-cooled hybrid blanket design. These detailed parametric analytical

studies have identified and delineated the merits of the helium-cooled, thermal fission hybrid fueled with natural or slightly enriched uranium, moderated with graphite, and cooled with helium. In addition, the optimal use of lithium for breeding has been delineated.

This PNL concept of a fusion-fission system has been developed to a considerable degree as reported by many studies.[64-67] The most complete results on blanket parameters were reported by the combined efforts of Lawrence Livermore Laboratory and Pacific Northwest Laboratories.[64] Although this hybrid blanket design was intended for use in the spherical geometry of Livermore's mirror (Yin-Yang) fusion reactor concept, the basic blanket geometry is very similar to that shown in Fig. 3. Blanket modules of varying composition were analyzed using a fuel pin lattice geometry similar to that used in High-Temperature Gas-Cooled Reactors.[68] Results reported for the hybrid blanket analysis are included in Table 1-XV showing seven (7) different cases analyzed, all of approximately 200 cm thickness. The inner convertor region was closest to the plasma and contained helium coolant and stainless steel structure as well as depleted uranium to enhance neutron multiplication. The inner thin breeder contained lithium for fast neutron tritium breeder while the thicker outer lithium breeder contained lithium for thermal neutron breeding of tritium. The reflector, where used, was composed of graphite and the thermal fission lattice was composed of hexagonal unit cells of slightly enriched (as noted) fuel pins in a helium-cooled graphite matrix. The fuel pin geometry and cell pitch were optimized using S_n transport calculations.

The tritium breeding and fissile breeding ratios were very en-couraging particularly for Case 7 where both were reported to exceed

Table 1-XV

PNL Hybrid Blanket Analysis

Case	Blanket Arrangement	Tritium Breeding Ratio	Fissile Breeding Ratio	Blanket Fusion Energy Multiplication
1	8.5 cm convertor 1.5 cm breeder 150 cm lattice (1.0%)* 20 cm reflector 15 cm breeder	0.766	1.59	18.9
2	10 cm convertor-breeder mix 150 cm lattice (1.0%) 20 cm reflector 15 cm breeder	0.725	1.57	19.8
3	10 cm convertor-breeder mix 180 cm lattice (1.0 %) 10 cm breeder	0.365	1.62	25.2
4	8.5 cm convertor 1.5 cm breeder 180 cm lattice 10 cm breeder	0.737	1.55	20.0
5	8.5 cm convertor 1.5 cm breeder 180 cm lattice (1.25%) 10 cm breeder	0.893	1.22	31.8
6	8.5 cm convertor 1.5 cm breeder 180 cm lattice (1.50%) 10 cm breeder	1.26	0.984	59.6
7	8.5 cm converter 1.5 cm breeder 180 cm lattice (1.35%) 10 cm breeder	1.00	1.11	39.8

*^{235}U enrichments denoted in parentheses.

unity. In addition, the energy multiplication of the fusion power was found to be very large for this best case (M_B = 39.8).

This energy multiplication was claimed to be related to the effective neutron multiplication of the blanket and the neutrons produced per fission in the blanket by the following global parameter equation:

$$M_B = (\frac{200 \text{ MeV}}{14 \text{ MeV}})(\frac{1}{\nu})(\frac{k_{eff}}{1 - k_{eff}}) \tag{5}$$

where 200 and 14 represent the energy deposited due to fission reactions and fusion neutrons, respectively, ν is the number of neutrons released per fission and k_{eff} is the usual blanket effective neutron multiplication factor. Since this equation related global parameters and since the 14 MeV source is introduced inhomogeneously, the current work was partially directed at determining if this equation might be inadequate despite its frequent use in describing and analyzing results from calculations performed on hybrid blankets.

Review of Controlled Thermonuclear Reactor Thermal Stability Analyses

Fusioning Plasma Operational Criteria

The first determinations of operational criteria for thermonuclear reactors were performed using global or point-model reactor parameters. Rigorous descriptions of complex plasma dynamics with attendant spatial variations were usually beyond the scope of such criteria development.

The first attempt to specify fusion reactor operational criteria was undertaken by Lawson[50] and refined by Ribe et al.[69] This model assumed instantaneous heating of the plasma at an ion density, n, to a

uniform temperature, T, and confined for a time, τ, after which cooling was allowed. Conduction losses were entirely neglected. This initial work established values of temperature and the product of ion density and confinement time, $n\tau$, for a zero-power but self-sustaining thermonuclear system. A system energy balance was used in which the energy to heat the plasma, E_p, and the energy to overcome bremsstrahlung radiation losses, E_B, were supplied to produce fusion reaction energy, E_F. The energy supplied as well as the fusion reaction energy, was assumed to be recoverable and converted to useful output energy at some efficiency, n.

The minimal condition for breakeven is simply defined as follows:

$$[E_F + E_B + E_p]n \geq E_B + E_p \tag{6}$$

where n is the overall system energy conversion efficiency.

For a D-T fusion system as described above, the so-called Lawson Criterion for breakeven becomes simply:

$$n\tau = \frac{3T}{(\frac{n}{1-n})p(1-p)Q_F<\sigma v>_{DT} - bT^{1/2}} \tag{7}$$

where

$\quad$ n = fuel ion density (ions/cm^3)

$\quad$ T = plasma temperature (keV)

$\quad <\sigma v>_{DT}$ = reactivity of D-T plasma (cm^3/sec)

$\quad$ n = overall system energy conversion efficiency

$\quad$ b = proportionality constant for bremsstrahlung radiation

$\quad$ p = tritium fraction of ion density

$\quad Q_F$ = energy release per fusion reaction (keV).

The Lawson Criterion for the pure D-T fuel cycle is represented by a series of parametric curves in the efficiency as shown in the lower spectrum of curves in Fig. 4. Points on such parametric curves represent minimum n_τ and T values for breakeven fusion energy production; no net fusion energy is produced. If the energy per fusion event can be augmented by fission reactions in the hybrid blanket, then the requirements on the plasma can be significantly relaxed.

Cyclotron or impurity radiation losses are not considered in Lawson-type analyses. No stability is considered since the conditions quoted from such analyses refer to minimum requirements for overall breakeven.

Another early study of the reactor energy balance was done by Jensen et al.[70] Again the D-T reaction was of primary concern though subsidiary fusion reactions were also treated. Jensen reported on the effects of finite energy transfer rates and found self-sustaining reactors were possible over an increased parameter range, although all ion species were treated at a uniform temperature. The major shortcoming of Jensen's energy balances was its failure to consider particle confinement times of diffusion losses. Additional energy balance considerations were reported by Woods.[71]

Horton and Kammash[72] have also considered energy balances and operating conditions for the D-T fusion cycle. Since alpha particles are a significant plasma heating mechanism, energy and particle conservation equations were introduced for the alphas created in D-T fusion reactions. Both bremsstrahlung and synchrotron radiation losses were treated along with the effects of cold and energetic fuel injection. This work was distinguished by its treatment of several different models for diffusion and hence several different types of confinement time variation with

temperature and density, some of which were applied in the later stability work of Mills[15-17] and Ohta et al.[18]

A similar but more realistic condition than the Lawson Criterion for minimal operation has been developed by Mills for a system using only the D-T reaction.[15,16] This model is based upon continuous injection of cold fuel where fusion temperatures are assumed to be supported by alpha heating. Mills used particle and energy conservation equations for the ion density as follows:

$$\frac{dn}{dt} = S - n/\tau \tag{8}$$

$$n \frac{d}{dt} [\frac{3}{2} (T_i + T_e)] = p(1 - p)n^2 <\sigma v>_{DT} cQ_\alpha - \frac{3}{2} S(T_i + T_e) \tag{9}$$

where

n = fuel ion density (ions/cm^3)

S = fuel ion injection feedrate (nuclei/cm^3-sec)

p = tritium fraction of ion density

τ = confinement time against all plasma losses including fusion (sec)

Q_α = alpha particle energy from D-T fusion events (3520 keV)

c = fraction of alpha energy retained in the plasma for heating

$T_{i,e}$ = temperature for ion and electron species respectively (keV)

$<\sigma v>_{DT}$ = D-T fusion reaction reactivity or rate coefficient (cm^3/sec).

For steady-state operation with this model, Mills found that the following equilibrium condition must be maintained if operating characteristics are to remain unchanged:

$$n\tau = \frac{3(T_i + T_e)}{2p(1 - p)<\sigma v>_{DT} c Q_\alpha} \quad .$$

(10)

This result is similar to the Lawson condition but more conservative since only a fraction of the alpha particle energy is retained to sustain the plasma while none of the neutron kinetic energy is retained. In addition, the Mills condition is a steady-state condition based only on the plasma while the Lawson Criterion attempts to account for all influences on system efficiency. The constant, c, accounts for energy losses due to bremsstrahlung and synchrotron radiation. An important feature of this work is the temperature difference allowed between the ion and electron species; in general, Mills found that the electron temperature is elevated due to preferential alpha heating. Figure 4 illustrates the Lawson breakeven region for 35 to 45% efficiencies compared to the Mills' equilibrium region (c = 0.8, p = 0.25 and 0.50).[16]

Since Mills' model is concerned only with alpha heating and radiation losses within the plasma, energy release to neutrons was not considered. Though actual power generation capabilities were not considered by Mills, comparison with the zero power condition developed in Lawson's model does indicate net overall power production as expected for equilibrium operation.

Fusion devices producing values above Mills' equilibrium region in Fig. 4 can be operated only in the pulsed mode. Similarly, devices providing $n\tau$-values below the Lawson region can never operate as power-producing reactors, while those falling between the two criteria will require energetic injection of fuel. Controlling a reactor to keep it exactly at the equilibrium condition is the preferable mode of operation which leads to stability considerations.
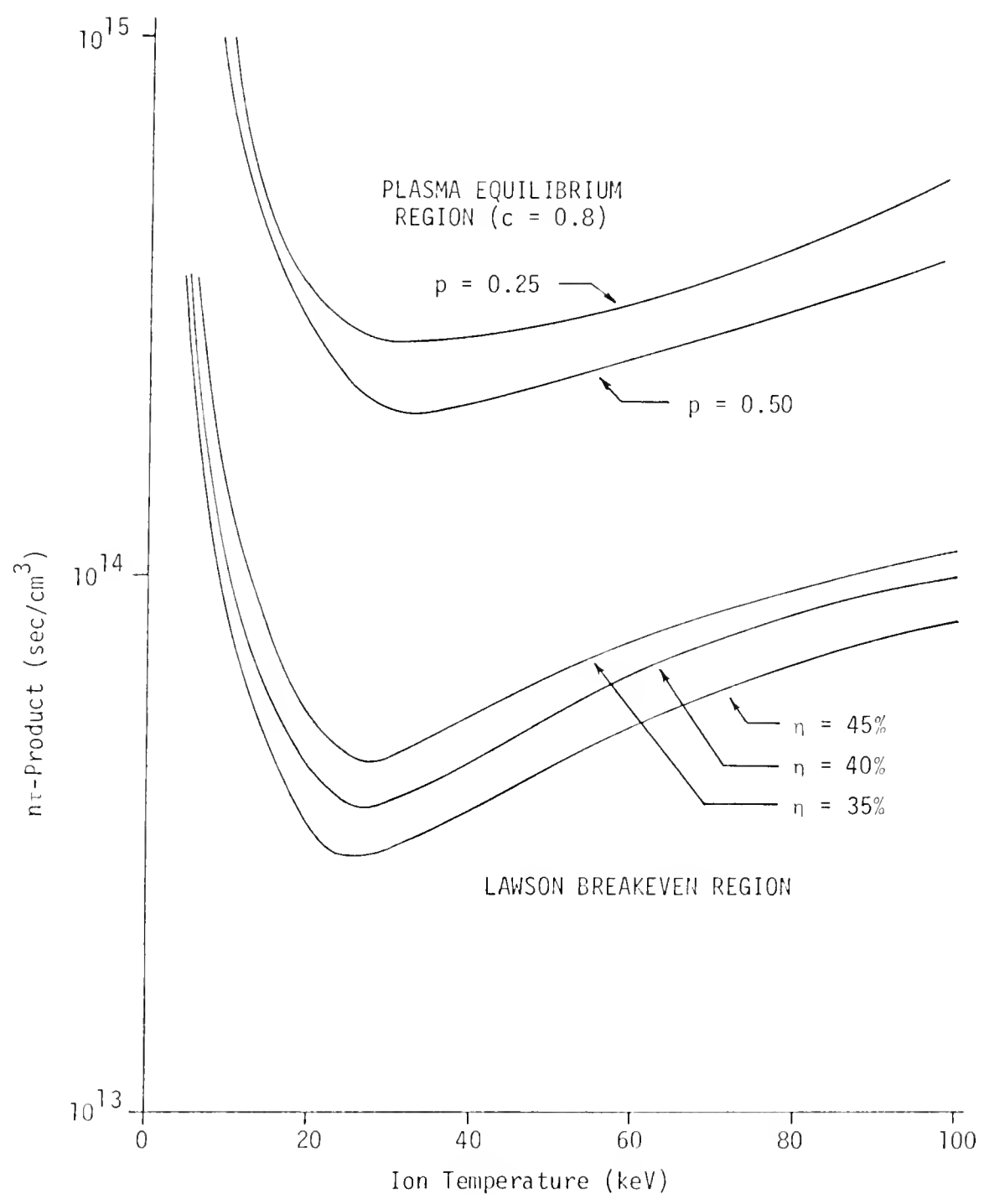
Figure 4.   Comparison of Lawson breakeven and plasma equilibrium regions.

Plasma Thermal Stability Considerations

Plasma global thermal stability studies were initiated by Mills based on the operational equilibrium studies.[15-17] Mills demonstrated that the equilibrium condition is equivalent to requiring the constancy of a function, ψ, as follows:

$$\psi = S\tau^2 p(1 - p)S \tag{11}$$

where the so-called stability function, S $(cm^2/keV-sec)$, varies with ion temperature T_i as $S \sim cT_i^a$ which exhibits a broad resonance peak around 28 keV. In the first approximation Mills treated the alpha energy retention fraction as a constant. For stable equilibrium, the logarithmic variation of $\psi(S,\tau,p,T_i)$ must vanish. Therefore, Mills found that the operational equilibrium is unstable against fluctuations in the fuel feedrate, the confinement time, the fuel mixture (unless $p = 1/2$), and the ion temperature except when the exponent in T_i^a falls to zero above 28 keV.

Although the exact behavior of the confinement time with ion temperature was not known (nor is it known today), the ψ-function formalization showed that if τ is independent of T_i, stable operation of a thermonuclear reactor below 28 keV is impossible without some form of control. Below 28 keV, departures from equilibrium are supported due to the positive slope of the stability function. It is not until the negative slope region of the stability function is reached above 28 keV that the inherent instability against fluctuations in T_i is controlled and the temperature driven back to equilibrium.

Mills[15] acknowledged a preference for operating at lower temperatures, perhaps near the 12 keV temperature for the optimal D-T reaction rate.[73]

In fact, most fusion reactor system design studies currently select operating temperatures below 20 keV.[28-32] But at temperatures below 28 keV, Mills showed that control is necessary to avoid the predicted extreme departures from equilibrium. This control can be implemented via the feedrate, the fuel mixture, the confinement time, or radiation losses dependent on injection of impurities. Initially, Mills favored control via the confinement time[15,17] but later work has emphasized feedrate control.[16] More recent studies by Ohta et al.[18] have confirmed the use of feedrate as a viable method by which to control stability.

If the confinement time is temperature-dependent, then it may be useful for inherent control by introducing temperature dependency into the ψ-function. Mills hypothesized Bohm-type diffusion ($\tau \sim T^{-1}$) as a possible inherent control to allow stable operation below the 28 keV cutoff indicated for constant confinement operating conditions.[15] For fixed feedrate and fuel mixture, Mills used the ψ-function variational method to demonstrate inherent stabilization of plasma equilibria for this Bohm-type diffusion for temperatures in the 7 to 28 keV range. By analyzing the dynamic behavior of thermonuclear plasmas, Mills established the self-stabilizing influence of Bohm diffusion below 28 keV temperatures as the perturbed plasma temperatures (ion and electron) and ion density were shown to approach equilibrium with time.[15] In this way, Mills justified operation near the 12 keV temperature to take advantage of the optimal D-T reaction rate[73] without the necessity of introducing artificial control.

Mills[17] also presented detals on calculations to evaluate the time evolution of the parameters in a fusioning plasma. The calculations accounted for bremsstrahlung and synchrotron radiation by treating energy

exchange between ion species as an instantaneous process. Results were reported only for plasma time behavior for attempted initial equilibrium operation about a temperature of 11 keV with 50% deuterium and 50% tritium fuel injection leading to ion densities of $\sim 5 \times 10^{14}$ ions/cm^3. The instability of plasma operating conditions in this region was verified for constant confinement and shown to result in rapid plasma runaway in less than three seconds. The plasma temperatures (T_i and T_e) were shown to runaway above or below ignition depending to extreme accuracy on whether or not the constant plasma confinement time was too long or too short so artificial control was found to be essential below 28 keV.

Mills[17] also investigated feedback control via the fuel mixture using the monitored plasma electron temperature. When the electron temperature was set below a preselected control temperature, the injected fuel mixture was maintained at the original 50% D, 50% T; when the temperature exceeded the control temperature, tritium injection was replaced with pure deuterium. The effect of stopping tritium injection was to reduce fusion events and lower temperature; the stabilizing effect of this mixture control feedback was achieved by making the time average of $p(1-p)$ low enough to compensate for excessive confinement time. Control to a temperature that was too low to provide the $n\tau$-equilibrium condition was found to result in the reacting plasma extinguishing itself. Mills also noted that excessive confinement time will result in severe initial temperature overshoot.

These investigations by Mills constituted the first efforts to study the dynamics and control of thermonuclear reactor plasmas. The omission of other than D-T fusion reactions and the incomplete treatment of the synchrotron radiation represent deficiencies in Mills' work. The

incomplete stability criteria development in Mills' work is its most significant deficiency.

The same stability problems of point model D-T plasmas have been investigated in more detail by Ohta et al.[18] but using the following global nonlinear balance equations for plasma density and temperature (energy):

$$\frac{dn}{dt} = S - n/\tau_n \tag{12}$$

$$\frac{d(nT)}{dt} = n^2 f(T) - \frac{nT}{\tau_E} + ST_s \tag{13}$$

where

$$f(T) = \frac{Q_\alpha <\sigma v>_{DT}}{12} - 1.12 \times 10^{-15} T^{1/2}$$

and

n = plasma ion density (ions/cm^3)

T = uniform plasma temperature (keV)

$\tau_{n,E}$ = particle and energy confinement times (1/sec)

S = fuel injection feedrate (ions/cm^3-sec)

$3T_s$ = fuel ion inject energy (keV)

Q_α = alpha particle energy from D-T fusion events (3520 keV)

$<\sigma v>_{DT}$ = D-T fusion reaction rate coefficient (cm^3/sec).

Ohta addressed only the D-T reaction; the fusion reaction was not considered an important loss mechanism in the particle conservation equation in essential agreement with Mills. Both the fusion energy source and the bremsstrahlung energy loss terms were included in f(T) but synchrotron radiation losses were neglected. Injection energy was specifically included in the energy equations as $3T_s$ for convenience of notation.

No temperature difference was allowed between the electron and ion species which is a limitation in contrast to Mills' attempt to treat differing temperatures. The advantages of Ohta's model include accounting for energy diffusion with particles and energetic ion injection as well as including an explicit expression for bremsstrahlung radiation. Ohta obtained the following form of the Mills equilibrium condition for steady-state (subscript o) evaluation of the balance equations:

$$n_0 \tau_{E_0} = \frac{\left(1 - \frac{\tau_{E_0}}{\tau_{n_0}} \frac{T_s}{T_0} \, T_0\right)}{f(T_0)} \qquad (14)$$

which indicates the reduction in required $n\tau$-values by the inclusion of Ohta's injection heating option.

Efforts by Ohta to examine steady-state plasma stability can be categorized into two areas:

1. Linear analysis establishing temperature-dependent stability criteria in possible operating regions for future fusion plasmas, and

2. Nonlinear dynamic simulation of the plasma balance equations subject to small perturbations with and without feedback effects to verify agreement with linear stability analysis and control possibilities in unstable operating regimes.

Linearized analysis will usually predict stability regimes. If a system is not stable, linearized analysis will not predict true consequences of the unstable situation--hence the need for dynamic simulations. Stability criteria to predict whether small plasma perturbations will grow or diminish with time were developed by Ohta from linearized forms of the density and temperature balance equations. The elimination of nonlinear terms is valid only for small density perturbations, $\delta n(t)$,

and small temperature perturbations, $\delta T(t)$, which Ohta assumed to vary exponentially with time.

Stability is assured provided the real part of the growth rate is negative. Ohta obtained general stability criteria by solving for the growth rate after substituting the density and temperature variations into the linearized density and temperature equations.

To proceed beyond such general stability criteria, the functional dependences of both the particle and energy confinement times were required. Because the exact density and temperature dependence of confinement time was uncertain, Ohta based the analysis upon the following functional dependence of confinement time on density and temperature: $\tau \sim n^{\ell} T^m$. It is the derivation of stability criteria on the basis of this general diffusion model that represents the major contribution of Ohta's stability analysis. To obtain useful stability criteria, Ohta used three diffusion models to get specific values for ℓ and m:

1. Constant confinement: $\tau \sim$ constant ($\ell = 0$, $m = 0$).
2. Bohm confinement: $\tau \sim T^{-1}$ ($\ell = 0$, $m = -1$).
3. Classical confinement: $\tau \sim n^{-1} T^{1/2}$ ($\ell = -1$, $m = 1/2$).

The minimum temperature satisfying the stability criteria for each confinement model is known as the critical temperature, T_c; that is, the temperature above which operating conditions are predicted to be stable as described by Mills' work. Representative temperature results predicted by these stability criteria are listed in Table 1-XVI for both charged particle and injection heating for all three diffusion models.

Ohta also dynamically simulated the balance equations to check the stability predictions of the linear analysis. For these numerical simulations, initial equilibrium temperatures were assumed; the initial

densities, however, were perturbed a small amount above and below equilibrium and the effect on the temporal behavior of the plasma density and temperature calculated as presented in Fig. 5.

Table 1-XVI

Critical Temperatures for D-T Fusion Reactors

Confinement Model	T_c (keV)	
	Charged particle Heating $(\tau_n/\tau_E = 10)$	Injection Heating* $(\tau_n/\tau_E = 1)$
τ = constant	28	21
$\tau \sim T^{-1}$	14	5
$\tau \sim n^{-1}T^{1/2}$	42	33

*Ion Injection Energy: $3T_s$ = 150 keV.

For the case of constant confinement and charged particle heating for which the critical temperature T_c is 28 keV was found also by Mills. Ohta's results are depicted in Fig. 5 for three initial equilibrium temperatures of 10 keV, 30 keV, and 50 keV. For equal magnitude density perturbations, equilibrium density is always approached with time which indicates plasma stability under isolated density perturbations. Similarly, temperature transients resulting from the density perturbations die out for cases (30 keV to 50 keV) where $T > T_c$. However, for the subcritical 10 keV initial temperature, the time evolution of temperature is unstable as shown in Fig. 5 and predicted in Table 1-XVI. Ohta's dynamic simulations supported the linear analysis stability criteria for both methods of heating and all three diffusion models. In
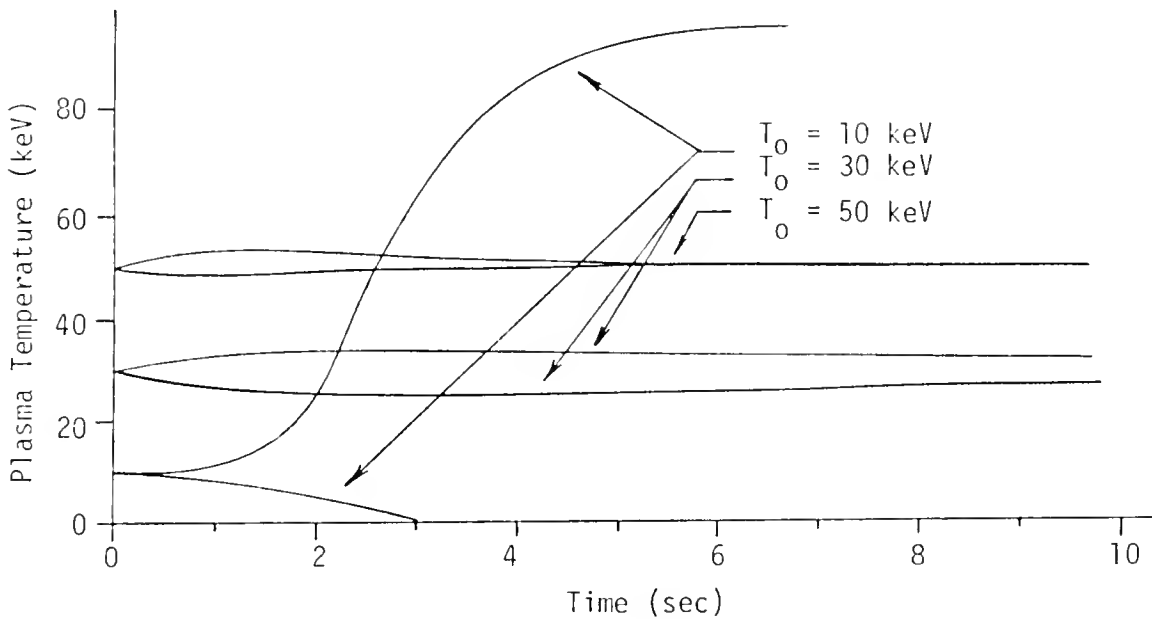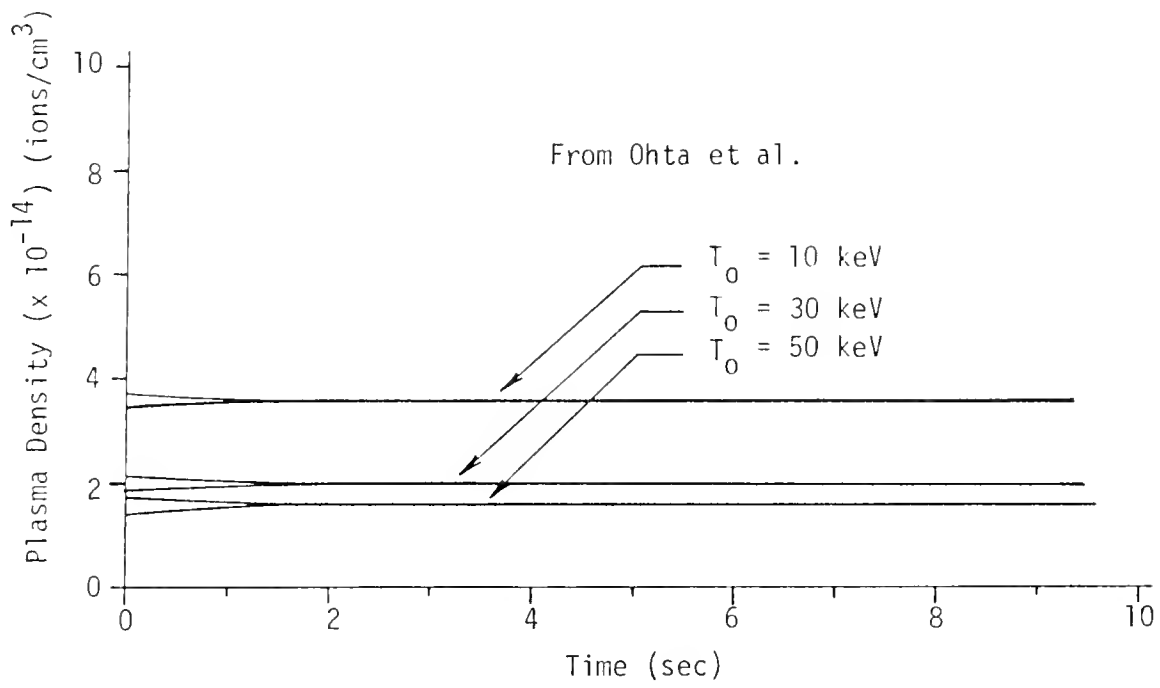
Figure 5. Time variation of point-model plasma temperature and density for constant confinement and charged particle heating.

general, the quick plasma response on the order of a few seconds was found for all these analyses of unstable plasma variations in pure fusion plasmas. This behavior agreed with previous fusion plasma analyses.

Ohta's results demonstrate the need for stabilizing control to allow fusion reactors to operate below the critical temperatures as planned by current fusion reactor design studies.[28-32] The case of feedback stabilization for the constant confinement model was also examined by Ohta et al.[18] Stability criteria were again derived from linearized balance equations. Density feedback control was introduced by adding the term, $\alpha \frac{\delta n(t)}{n_0}$, but was not able to stabilize the system because the balance equations are stable for isolated density perturbations. Since temperature instabilities can grow independently, various types of temperature feedback were introduced by adding the stabilizing feedback term, $\alpha \frac{\delta T(t)}{T_0}$, to either one or both of the perturbed linearized balance equations. New stability criteria were derived dependent on the value of the feedback coefficient, α. Although many parameters are possible for use in implementing control, feedback via the injection feedrate was preferred by Ohta et al. in agreement with Mills.[16]

Ohta demonstrated control of the temperature instability through dual temperature and density feedback which was introduced through the injection rate and its "small" variation about equilibrium as follows:

$$S(t) = S_0 + \delta S(t) = S_0 + \frac{\alpha n_0}{T_0} \delta T(t - \Delta t) \tag{15}$$

where α is the feedback coefficient and Δt is the delay time between a temperature variation, $\delta T(t)$, and the corresponding feedback effect on the injection rate. Inclusion of feedback delay time makes Ohta's results

applicable to realistic control situations. The effectiveness of feedback stabilization was found to be dependent on both feedback parameters: α and Δt. For the applicable plasma model Ohta found a stabilized region in the $\alpha \Delta t$-plane from the linear stability analysis of this feedback effect. In general larger negative feedbacks and shorter delay times were found to yield more effective stabilization. For sufficiently large Δt or small α, feedback stabilization was found to be ineffective in all subcritical ($T < T_c$) cases.

As expected, Ohta found the unrealistic case of zero delay time to be the most effective feedback. However, when the delay time and feedback coefficient were within the stability region predicted by linear analysis, an equilibrium temperature was always approached; however, the amplitude of oscillations was found to increase with delay time as the limits of the stability regime were neared. Since delay times of 2 to 3 seconds are outside the linear stability regime predicted for this case, extreme amplitude of oscillation for these delays was found as expected.

Usher and Campbell[23,24] extended point-model thermal stability analyses to other fuel cycles and other plasma diffusion models with similar results and speeds of response. In addition burnup was treated in this extension of Ohta's analysis with essentially similar results for the D-T fuel cycle.

Stacey's point model plasma stability analysis of the D-T fuel cycle extended point model plasma stability analysis of the D-T fuel cycle to include more detailed plasma behavior including four balance equations to represent the following plasma parameters:[22]

1. Ion particle density.

2. Ion energy density.

3. Alpha particle density.

4. Electron energy density.

Again the temperature instability was found in certain regimes. Effective stabilization to control operation about an unstable equilibrium point through use of controlled ion injection rate as well as controlled D-T fuel mixture was demonstrated.

The temperature instability has also been examined for radially in-homogeneous D-T fusion plasmas by Yamato, Ohta, and Mori, using particle and energy balance equations.[19-21] The results of this inhomogeneous analysis support the validity of decoupling excursions in the overall particle densities and temperatures from excursions in the spatial density and temperature distributions. When the injection of fuel is uniform, the temperature instability can develop only in the zero order mode. Stability criteria were developed similar to those for the uniform plasma with similar results, including feedback stabilization through temperature to allow operation below the critical temperature.

There have been no investigations of hybrid plasmas to examine the temperature instability discussed in this review. This is an area that requires study because large hybrid blanket energy multiplication values coupled with large plasma transients and neutron release could have con-trol as well as safety significance.

Motivation for the Research

As is evident from the preceding critical review of hybrid studies, there are many different versions of hybrids. New studies on hybrids can either design new blanket models or make use of existing designs with appropriate changes. The primary objective of this work was to analyze

the dynamic interaction of the two components of the hybrid system. Such investigations have not been reported in the literature to date. Thus, the objective was not to devise a new system but to take the somewhat arbitrary approach of selecting a previously established hybrid concept with necessary adjustments.

Many different types of hybrid machines have been proposed with many different methods of application. Power-producing Tokamak hybrids are of most interest for control and dynamics considerations and so such a model was selected for this work. Essentially this hybrid design is compatible with various hybrid advantages delineated in the recent Princeton Plasma Physics Laboratory systems study of Tokamak fusion-fission hybrid reactors which concluded that the most economical mix of power- and fuel-producing hybrids should emphasize power production.[3] An optimized hybrid machine should be a substantial power producer with a by-product of fissionable fuel, the optimum ratio of fuel production to power production being determined by economics.

An early demonstration of hybrids could allow a very reassuring program for future development of the utility industry. A guarantee of future reasonable fuel costs could promote the accelerated installation of current LWR plants to fill near-term power needs while loosening constraints on all sectors of the United States energy economy. Subsequent commercial development of hybrids could supplement LWR's, provide them with fuel, and take up the load of retired power stations followed by eventual introduction of the pure fusion reactor sometime in the coming century.

The hybrid could also prove to be inherently superior to the fast breeder reactor[3] for using the depleted uranium reserves built up from

enrichment operations run for nuclear power plants and defense purposes. The hybrid may be a better way to burn ^{238}U reserves with possible elimination of some enrichment requirements and perhaps elimination of plutonium separation if bred plutonium is burned in situ. This scenario is especially important in light of the continuing breeder controversy[5] and the recent Three Mile Island accident[11,74] which will undoubtedly delay introduction of the breeder still longer due to safety considerations.

Since the hybrid represents an alternate concept for power production and orderly progression to long-range utility application of pure fusion, its characteristics require analysis prior to its being approved for central station power production. One parameter frequently used to describe hybrid characteristics is the global relationship for the blanket neutron energy deposition per fusion neutron, Q_B, derived in Appendix A:

$$Q_B = \frac{G_f}{\bar{\nu}} \left[\frac{k_{eff}}{1 - k_{eff}} \right] + E_n + \delta_E \qquad (16)$$

where

Q_B = blanket energy deposition per entering fusion neutron

G_f = fission energy deposited in the blanket per fission event (192.9 MeV)[75]

$\bar{\nu}$ = average number of fission neutrons produced per fission event

k_{eff} = effective blanket neutron multiplication factor

E_n = energy of the fusion neutron (14.06 MeV)

δ_E = additional energy generated and deposited in the blanket due, for example, to exothermic neutron absorption reactions.

The associated blanket fusion neutron energy multiplication, M_B, is then:

$$M_B = \frac{Q_B}{E_n} \quad . \qquad (17)$$

Several forms of the global relationship of Eq. (16) have been used extensively to describe hybrid blankets.[1,64,76,77] However, no results have been reported on its validity. If the parameter is to be used as a figure of merit characterizing the multiplicative capabilities of hybrid blankets, then its applicability must be verified and its limitations established.

Hybrid blankets are expected to have substantial energy deposition per fusion event so it becomes imperative that safety studies be undertaken to examine the implications of this characteristic. For non-multiplying pure fusion blankets, the energy deposition per fusion event is expected to be about 20 MeV. For hybrid blankets, even extremely modest ones with k_{eff} = 0.8 are predicted by Eq. (16) to have 316 MeV deposited per fusion event. The energy deposition and fusion energy multiplication predicted by Eq. (16) for possible blanket k_{eff} values are listed in Table 1-XVII.

Table 1-XVII

Predicted Blanket Global Response per 14 MeV Neutron

Effective Blanket Neutron Multiplication k_{eff}	Blanket Energy Deposition* Q_B (MeV)	Blanket Fusion Neutron Energy Multiplication M_B
0.80	316	22.5
0.85	439	31.2
0.90	687	48.8
0.92	872	62.0
0.94	1181	84.0
0.95	1429	102
0.98	3654	260
0.99	7364	524

*Based on G_f = 192.9 MeV, $\bar{\nu}$ = 2.6 nts/fission, E_n = 14.06 MeV, and δ_E = 4.84 MeV

The accepted variation of blanket fusion neutron energy multiplication with blanket values of k_{eff} is depicted graphically in Fig. 6 to demonstrate the hybrid capability for high energy multiplication with increasing but still far subcritical blanket systems. Despite the impossibility of reaching a critical fission reactor state in such systems, variations in the plasma operating conditions could cause blanket energy production rates beyond the technical limitations or the technical specifications of the design. Even with no danger of supercritical behavior, large uncontrolled thermal instabilities in the plasma could lead to excessive energy deposition in the power-producing hybrid blanket. In addition, there is the possibility of criticality at low temperatures prior to power startup. If plasma startup is very quick, then the plasma neutron production may drive the blanket to large overpower ratings before the temperature defect can reduce the effective blanket neutron multiplication factor, k_{eff}.

Although relatively small quantities of thermal energy are contained in the plasma a full-scale hybrid system generating 6500 MWth of steady-state thermal power will require large numbers of 14 MeV neutrons. Even a far-subcritical blanket ($k_{eff} \simeq 0.9$) can cause considerable multiplication of the fusion neutrons available as an external source for providing fission neutrons in the blanket. The component interactions as well as the control and stability of such power-producing hybrid systems must be well-understood.

The Lawson Criterion for hybrid reactors is modified as follows to account for fusion and fission sources of thermal power with zero energy fuel injection into the plasma:
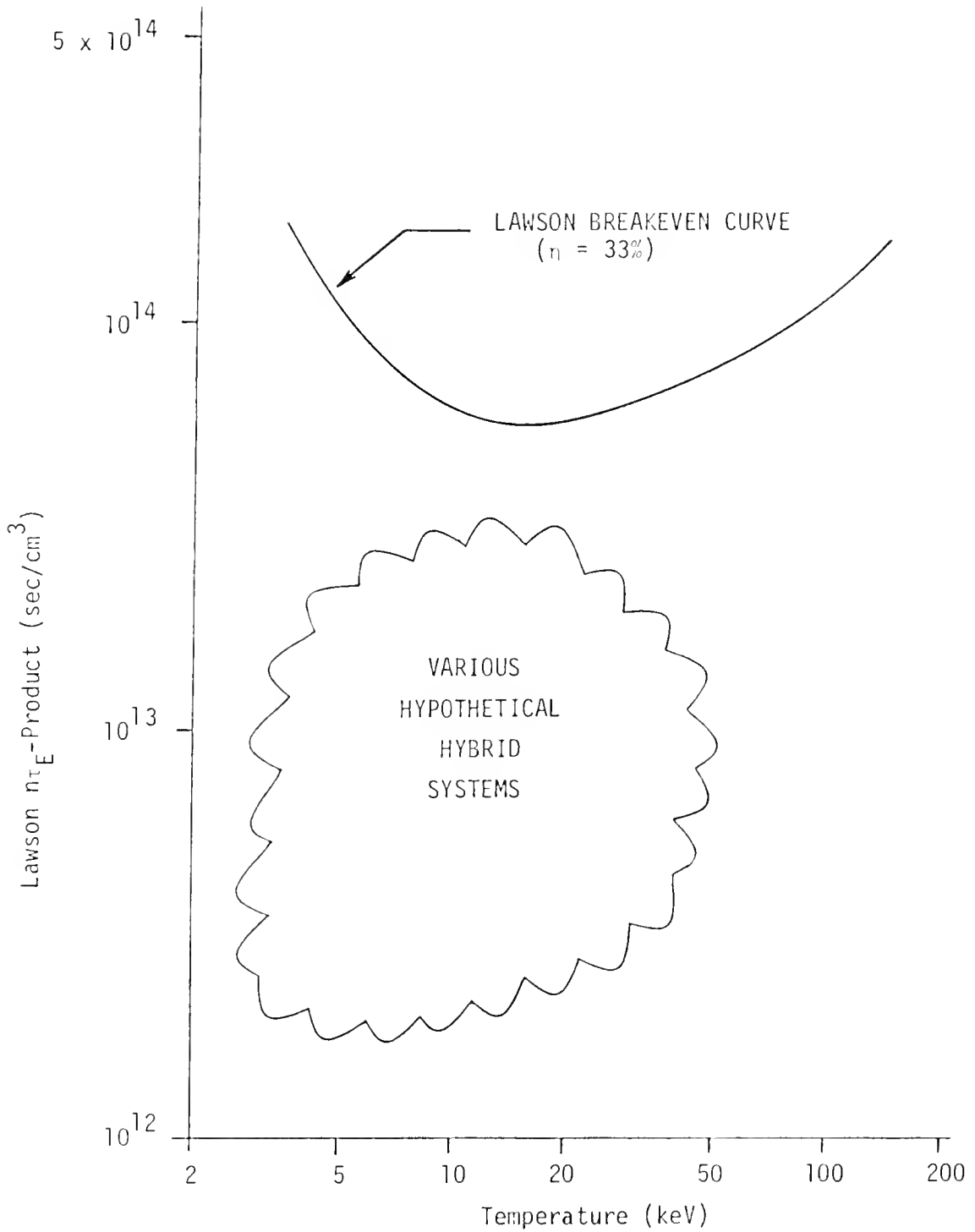
Figure 6. Typical Lawson breakeven curve for a 50-50 D-T plasma and 33% overall efficiency showing relative position of hybrid systems.

$$n\tau \geq \cfrac{12\ T}{\cfrac{\eta}{1-\eta} <\sigma v>_{DT}(Q_\alpha + Q_B) - 4bT^{1/2}} \qquad (18)$$

where Q_B is the blanket energy deposition per fusion neutron and η is the usual overall system efficiency defined for the Lawson Criterion.[50,69] Obviously, if significant energy is produced in the fissile blanket, the requisite hybrid plasma parameters can be relaxed to allow earlier utilization of fusion power in combination with a subcritical fission reactor to take full advantage of inherent hybrid safety features.

The typical effect of hybrid operation with blanket energy multiplication is a reduction in the required $n\tau$-product is depicted in Fig. 7. The production of fission energy effectively reduces the need for fusion-produced energy. The hybrid-revised Lawson Criterion of Eq. (18) is greatly relaxed because Q_B is on the order of hundreds of MeV versus the usual Q_B used for pure fusion systems which is limited to about 20 MeV including exothermic blanket reactions. As noted, this interactive multiplication demonstrates the need to examine the dynamics and controllability of hybrid systems.

Previous studies have been restricted to steady-state neutron balance calculations and associated technological limitations. There has been no analysis of the time-dependent behavior associated with hybrids, when subjected to reasonable perturbations in the characterizing parameters. In addition, there have been no reports of analysis of hybrid plasmas in the reduced reactivity regions where plasmas are not self-sustaining. The development of a model to describe the dynamics of fusion-fission coupled systems was one of the primary objectives of this research. The basis for operation, stability, and control of a coupled
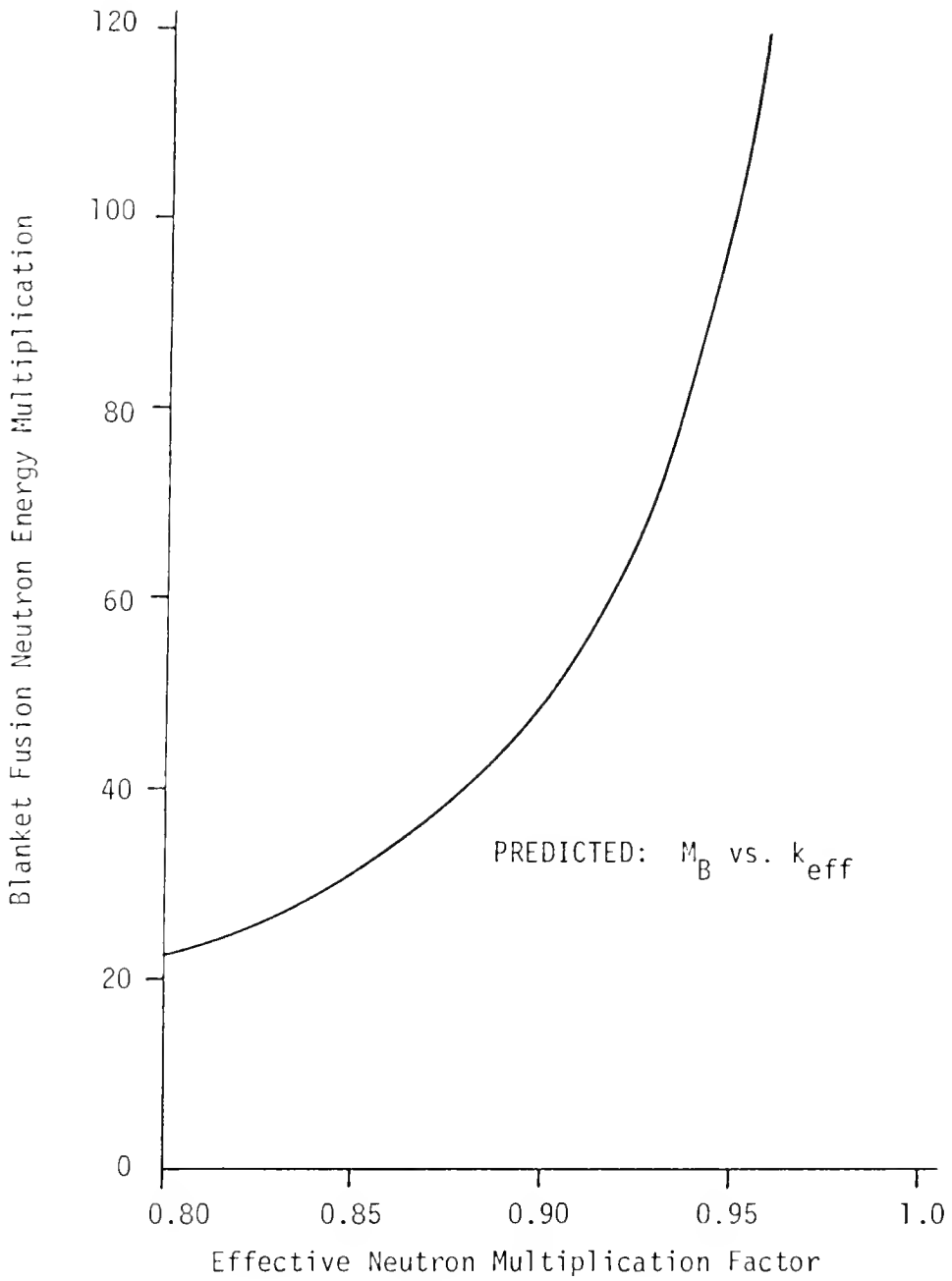
Figure 7. Predicted variation of blanket fusion neutron energy
multiplication with blanket effective neutron multiplication
factor.

hybrid system must be established when subjected to effects such as those due to the thermal instability analyzed by Mills[15-17] and by Ohta et al.[18] for pure fusion plasmas.

The desired result was a hybrid system model whose analysis would yield useful operational characteristics of hybrid machines which could then enable the hybrid to make a contribution to power production before the turn of the century. These various investigations will only be possible if both the plasma and blanket components are modeled and coupled to allow dynamics and stability analysis to be performed.

Summary of the Research

The research reported here began with the Ohta plasma model[18] with burnup effects included after Campbell and Usher[23,24] and developed plasma stability criteria based upon source feedrate perturbations and other engineering considerations for plasma changes affecting the output neutron production rate. Essentially, an effort was made to develop an analytical model for pure fusion plasma stability and control based on a global parameter treatment of a linearized fusioning plasma model using concepts of classical control theory and transfer functions. Feedback effects were also incorporated into the model which was kept independent of specific design concepts. The analytical model and its stability predictions were compared with Ohta's results to develop an engineering-oriented model which could have broad application to more sophisticated plasma models in the future. Perturbations causing plasma transients were specifically related to engineering expectations instead of theoretical hypotheses.

With the completion of this plasma stability and transfer function analysis, the effort was extended to develop a simplified hybrid model from which general stability criteria were developed for the interacting components of a hybrid system. Again, the model was kept independent of specific hybrid concepts except that the plasma confinement time was assumed to be a constant, independent of plasma temperature and density. The model was specifically developed and related to engineering considerations of hybrid system perturbations as well as dynamic simulation and control. Inherent as well as artificial feedback effects were incorporated where appropriate. The entire effort was directed to development of a simple, linearized, closed-loop model in transfer function format which could be used for future extensions of this work on dynamic and stability characteristics of hybrids. Of course the nonlinear form was retained for dynamic simulations.

The hybrid analytical model was then used to examine the properties of a particular hybrid system. The various augean and symbiotic concepts and variations proposed by Lidsky[2] and analyzed parametrically in the Princeton Study[3] were rejected for this research since they are not primarily intended for power production. This left essentially two choices: a fast fission blanket or a thermal fission blanket. To avoid the possible need for significant enrichments and to take advantage of expected higher multiplication factors, a thermal fission concept was selected. The most advanced and promising design was reported by PNL and Livermore workers under Wolkenhauer.[64]

This PNL blanket design was based primarily on existing technology and intended for use in spherical geometry with a Yin-Yang spherical mirror device[78] for a plasma core. Since this spherical concept is

severely power-limited, the only substantive change for this research was the conversion to a Tokamak-driven hybrid versus the mirror-device hybrid to promote larger power output and allow consideration of thermal instability effects.

Since the physical arrangement of the hybrid blanket selected corresponded to the reported PNL concept as nearly as possible, the results of previously performed parametric analyses of optimized region widths, ordering of zones, and region material constituents were used as the basis for extending steady-state neutronic analysis of the blanket. The Tokamak-driven blanket design used is described in Appendix B.

Detailed neutronic claculations were performed on the blanket for the selected design whose thermal lattice unit cell enrichment and global temperature were the only varied parameters. The cell enrichment was varied from natural uranium up to 1.50% enriched while the temperature was varied from 290°K up to 970°K. This work was performed using the BRT-1[63] (one thermal group) and PHROG[79] (three fast groups) codes to get 4-group constants. The 4-group CORA diffusion theory code[80] was then used for criticality calculations and acquisition of fundamental flux shapes. The doppler defect was also calculated as a function of the blanket operating temperature. Only the more promising blankets with $k_{eff} \gtrsim 0.90$ at elevated temperatures were considered in detail. This limitation minimized blanket dependence on the fusion component of the hybrid system.

Adjoint and perturbation calculations were performed on the system to provide parameters to characterize the kinetic properties of the system. Specifically, the average global delayed neutron fraction, $\overline{\beta}_{eff}$, the average prompt neutron lifetime, ℓ_p, and the so-called neutron

source weighting factors, ζ_s, of the hybrid blanket were calculated using diffusion theory.

Additional inhomogeneous calculations for blankets driven by planar sources of group 1 fast neutrons (10 MeV - 0.821 MeV) were used to approximate the fission energy source size required to produce a nominal design power of 6500 MWth. Volume source calculations were also run to investigate the difference in the worth of the diffusion theory group 1 source neutron power production depending on the point of introduction into the blanket. This investigation was accomplished to analyze the validity of the global parameter relationship for the blanket energy deposition per fusion neutron presented in Eq. (16). This relationship was expected to yield reasonable agreement with diffusion theory simulations since the source neutrons were introduced at nearly fission spectrum energies.

The series of diffusion theory results were used essentially as scoping calculations to select the best enrichment for further, more detailed and exact S_n transport theory analysis using the AMPX code package[81] available from ORNL. The blanket neutronic analysis performed with the XSDRNPM code[82] from AMPX was the first reported application of the ORNL-developed AMPX package to such hybrid studies. In P_2-S_4 analysis using the AMPX package, the fusion neutron source energy was treated more nearly as a true 14 MeV source. The required source strength for producing the 650 MW design power was determined for the toroidal system to establish finally the applicable degree of validity expected in calculating or predicting the blanket energy deposition per entering fusion neutron using Eq. (16). The flux shapes were also investigated again but for a six energy group structure to more exactly model blanket effects caused by energetic fusion neutrons.

On the basis of the XSDRNPM-predicted fusion neutron source strength required for a 6500 MWth hybrid plant, the required plasma conditions were estimated. The corresponding plasma temperature, density, constant confinement time, source feedrate, and injection energy characteristics were then parametrically varied to establish reasonable hybrid plasma operating conditions. Perturbations in various parameters with emphasis on plasma feedrate and temperature were then simulated to investigate the thermal instability of the hybrid plasma and the results compared with stability predictions and expected dynamic behavior under transient conditions. In this way the plasma component of the hybrid plant was examined with respect to the thermal instability to establish operational characteristics necessary for planning proper deployment of hybrid power plants.

Finally, since hybrid plasmas are expected to be subjected to various transient phenomena, especially thermal instability-driven transients, time variations in the design magnitude of the 14 MeV neutron source driving the blanket were considered on the basis of those transients resulting from the perturbed behavior of the hybrid plasma examined previously. Kinetics calculations representing the effects of plasma-caused perturbations on the fusion neutron source driving the blanket were run and changes in power level were examined for one spatial dimension and six delayed neutron groups. These kinetics calculations were performed using the space-time kinetics code GAKIN II[83] with six neutron groups whose group constants were obtained from the previous XSDRNPM, P_2-S_4 calculations. Although no time-dependent feedback effects were examined, the speed of response of the system was determined for typical transients and some characteristics for hybrid operational controllability were established.

CHAPTER 2

THE PLASMA MODEL

Introduction to the Plasma Model

First generation fusion power plants are expected to utilize the basic deuterium-tritium (D-T) fuel cycle

$$
{}^{2}_{1}D + {}^{3}_{1}T \longrightarrow {}^{4}_{2}He\ (3.52\ MeV) + {}^{1}_{0}n\ (14.06\ MeV)\ . \tag{19}
$$
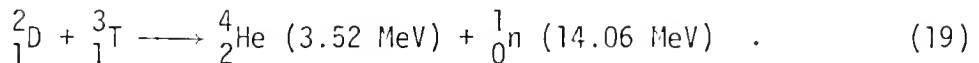
Because of its large cross section and reactivity, its minimized plasma temperature requirements and its relatively large energy release per reaction, no other fuel cycle is given serious consideration for use in early pure fusion power reactors. Certainly the near term experimental and demonstration fusion power systems are expected to use D-T fuel.[29,32,84] The United States Department of Energy effort toward implementation of central station fusion power plants has clearly recognized the superiority of this fuel cycle in the overall development programs.[85-87]

Even the utility industry has recognized the need for future choices in types of power generating systems and is supporting the effort to develop fusion reactors using the D-T fuel cycle.[88] The major magnetic confinement efforts to produce fusion power in other countries have also been directed toward the D-T fuel cycle.[89,90] Even so, D-T fueled fusion power plants are not expected to have significant impact on the utility industry until well into the next century.[91]

The complexity and difficulty involved in achieving fusion power is amply demonstrated in full scale commercial fusion power plant design studies.[28-30, 92,93] Because economic fusion power is such a large technological challenge, no factor can be dismissed which will made the development proceed more easily. The one common factor in different designs for fusion power plants in a closed, steady-state mode of operation (Tokamak) has been the universal selection of the D-T fuel cycle. Hence, although the D-T fuel cycle has the drawback of producing high energy, penetrating neutrons, its other advantages make it the only serious choice for fusion fuel for many years.

Mills[15] demonstrated that the fusion reaction rate and fusion power production are maximized for thermonuclear plasmas which have a 50% deuterium-50% tritium fuel ion composition. This 50-50 D-T mixing ratio is the most favorable fuel cycle for the production of fusion energy. With this cycle, not only is the demonstration of scientific breakeven in a self-sustaining fusioning plasma more easily accomplished but the steady-state production of net energy in a fusion power plant can be accomplished at minimized levels of plasma particle density, temperature, and confinement time.

These inherent advantages of the D-T fuel cycle in reducing plasma requirements have been illustrated in various analyses of equilibrium requirements and conditions including those of Lawson in which the n_T-criterion for energy breakeven was first presented.[50] The superiority of the 50-50 D-T fuel cycle for reaching and maintaining thermonuclear power-producing conditions has been uniformly demonstrated in extensive analyses of thermonuclear, steady-state, net energy-producing systems as reported by Mills,[94] Woods,[71] Ohta et al.,[18] as well as Usher and Campbell.[23,24]

Because fusion-fission hybrids are expected to serve as an intermediate energy-producing stepping block between current LWR plants and the eventual development of pure fusion power, the usual 50-50 D-T fuel cycle was logically selected for this hybrid analysis. This choice was aimed at optimizing the time scale for the implementation of the hybrid power-producing concept.

The Point Model Plasma

In this work, time-dependent point model balance equations were first established for the plasma ion density, $n(t)$, the plasma energy density, $3n(t)T(t)$, and the volumetric plasma neutron production rate, $q_p(t)$; these three balance equations for the plasma ion (particle) density, temperature, and neutron production rate state variables are presented as follows:

Plasma Ion (Particle) Density:

$$\frac{dn(t)}{dt} = S(t) - \frac{n(t)}{\tau_n} - \frac{n^2(t)<\sigma v>_{DT}}{2} \tag{20}$$

Plasma Energy Density:

$$\frac{d[3n(t)T(t)]}{dt} = \frac{n^2(t)<\sigma v>_{DT}Q_\alpha}{4} + T_s(t)S(t) - \frac{3n(t)T(t)}{\tau_E} - bn(t)T^{1/2}(t) \tag{21}$$

Plasma Volumetric Neutron Production Rate:

$$q_p(t) = \frac{n^2(t)<\sigma v>_{DT}}{4} \tag{22}$$

Conventional definitions for symbols used in these nonlinear point model
equations are listed below:

$n(t)$ = plasma ion density for 50-50 D-T plasma (ions/cm^3)

$T(t)$ = plasma temperature (keV)

$S(t)$ = external fuel volumetric injection rate (ions/cm^3 sec)

$q_p(t)$ = volumetric fusion neutron production rate (#/cm^3 sec)

$T_s(t)$ = external particle (ion) injection energy (keV)

τ_n = particle confinement time (sec)

τ_E = energy confinement time (sec)

Q_α = completely plasma confined fusion-produced alpha particle
energy (3520 keV)

$<\sigma v>_{DT}$ = D-T fusion reaction rate coefficient (cm^3/sec)

b = proportionality coefficient for plasma energy loss rate via
Bremsstrahlung radiation (3.36 x 10^{-15} cm^3 keV$^{1/2}$/sec).[18]

Since the plasma in this analysis was treated as a global system,
only a single average plasma temperature was considered; that is, no
distinction was made between ionic species or between ion and electron
temperatures. The inclusion of the burnup term in the plasma ion density
equation is an improvement to the model used by Ohta[18] that has been in-
corporated by others.[23,24,95] In stability studies on pure fusion devices
this burnup term and its effects have frequently been neglected because
burnup causes small changes in the stable temperature operating regimes of
D-T fusion systems. This analysis was intended for application to a
hybrid system where most of the energy would be produced in the blanket
so burnup predictions were even lower than in pure fusion devices; that
is, plasma temperature and plasma density are both expected to be lower
for hybrid plasmas than for pure fusion plasmas. However, large tempera-
ture variations in perturbed nonlinear systems can occur at which point

burnup increases due to temperature increases will be directly respon-
sible for lowering neutron yields which are proportional to the square
of the ion density. All of the alpha particle energy produced in fusion
was assumed to be deposited within the plasma to help heat the system.
Others have assumed fractional deposition,[15] but there is no loss of
applicability in assuming full alpha energy deposition.

For this initial analysis of point model kinetics, the plasma volume,
V_p, was treated as a constant; for linearized stability analysis, this is
adequate because only small plasma system perturbations were considered.
For time-dependent, nonlinear analysis energy and neutron production are
overpredicted by the assumption of constant volume since both are pro-
portional to the square of the ion density. More detailed analyses in
the future will incorporate temperature-dependent as well as magnetic
and other dynamic conditions that can affect the volume occupied by the
plasma independent of whether the plasma density has changed. Some pre-
liminary global analyses of such plasma volume variations have been
reported for pure fusion models[19-21,96] and additional work is under-
way.[27,97,98] The analysis was directed ultimately to the kinetic behavior
of the hybrid so the inclusion of the added complication of a variable
plasma volume in this initial treatment of the plasma neutron source
driving a power-producing blanket was not justified.

The inherent behavior and characteristics of the point model fusion-
ing plasma used for analysis in this study is completely described by
Eq. (20), Eq. (21), and Eq. (22). In fact, the plasma response to any
input perturbation, as well as its equilibrium characteristics are
determined by only the first two equations relating ion and energy
density. However, since this analysis of hybrid reactors was concerned

with the driven nature of the hybrid subcritical blanket, the third
equation for the specific neutron production rate was also necessary;
without neutrons produced in and hence output from the plasma, no inter-
action is possible between the two component halves of the hybrid system.
Note that these neutrons are produced in the plasma and inherently drive
the blanket; however, there is no inherent reverse effect whereby the
plasma is affected by the neutrons themselves or by the blanket itself.
The neutrons and their effects are strictly feedforward in nature.

The volumetric neutron production rate, $q_p(t)$, is an intrinsic
variable--characteristic of the condition of the plasma represented by
the state variables of ion density and temperature only. The volumetric
neutron production rate was multiplied by the effective plasma volume,
V_p, to obtain the total plasma neutron production rate, $Q_p(t)$, as
follows:

$$Q_p(t) = q_p(t) \cdot V_p \tag{23}$$

where the total neutron production rate is an extrinsic variable charac-
teristic of a specific plasma with constant effective volume, V_p. In
other words, $Q_p(t)$ is characteristic not of all plasmas in a state de-
scribed by an ion density and a temperature, but only of those specific
plasmas whose volumes satisfy Eq. (23). This extrinsic variable could
be useful for relating specific size plasmas to the corresponding hybrid
blanket; however, for this general development, the volumetric neutron
production rate was more useful since it is the intrinsic variable from
which any specific pure fusion or hybrid plasma can be analyzed. Indeed,
if pure global analysis is used throughout a fusion plasma study or even
a hybrid study, then any effect on total power production of such a

constant volume will be simply multiplicative--the larger the plasma, the greater the system power production.

The density equation was rewritten in the following simplified form:

$$\frac{dn(t)}{dt} = S(t) - \frac{n(t)}{\tau_n} - f_1(T)n^2(t) \tag{24}$$

where the temperature-dependent coefficient, $f_1(T)$, was defined as follows to simplify the burnup loss term:

$$f_1(T) = \frac{<\sigma v>_{DT}}{2} . \tag{25}$$

Similarly, Eq. (21) for the plasma energy density was also simplified preparatory to linearization by rewriting it in the following form after Ohta:[18]

$$\frac{d[n(t)T(t)]}{dt} = f_2(T)n^2(t) - \frac{n(t)T(t)}{\tau_E} + \frac{T_s S(t)}{3} \tag{26}$$

where the temperature-dependent coefficient, $f_2(T)$, was used to account for charged alpha particle heating and bremmstrahlung radiation, respectively:

$$f_2(T) = \frac{<\sigma v>_{DT} Q_\alpha}{12} - \frac{bT^{1/2}}{3} . \tag{27}$$

Although it was not so complicated, the equation for the volumetric neutron production rate was also redefined as follows:

$$q_p(t) = g(T)n^2(t) \tag{28}$$

where the temperature-dependent coefficient, $g(T)$, was defined as follows:

$$g(T) = \frac{<\sigma v>_{DT}}{4} . \tag{29}$$

It is noteworthy that $g(T)$ in the neutron production equation and $f_1(T)$ in the burnup term of the particle density equation differ only by a factor of two (2) as follows:

$$g(T) = 2f_1(T) \tag{30}$$

which simply means that two (2) ions must undergo fusion burnup for each neutron produced.

The Linearized Plasma Model

The global plasma equations were linearlized in order to facilitate analysis of stability regimes in the frequency domain. At this point, contrary to previous work,[18,23,24,95] specific perturbations were introduced into the point model plasma equations. Since the feedrate, $S(t)$, is the only external influence appearing in both the density and temperature point model equations, the feedrate was chosen as the typical source perturbation for the examination of global plasma stability. The choice was logical since the driving force for the entire fusioning energy producer is ultimately supplied by the plasma feedrate. The same dependence on feedrate is applicable for the hybrid system, since the hybrid will be entirely dependent for energy production on the plasma-produced neutrons because of the blanket subcriticality. But the production of neutrons is ultimately governed by the state of the plasma (ion density and temperature) which itself is driven and sustained by the feedrate of energetic fuel ions. Therefore, examination of the hybrid system response to perturbations in the plasma feedrate is logical for such a global plasma model.

For inherent stability and control analyses, the system response to small external or internal perturbations was a primary concern. Dependent variable perturbations about steady-state values were used to generate a dynamic variation in the point model equations. For linear analysis the following necessarily small variable perturbations were used:

$$n(t) = n_0 + \delta n(t) \quad , \tag{31a}$$

$$T(t) = T_0 + \delta T(t) \quad , \tag{31b}$$

$$S(t) = S_0 + \delta S(t) \quad , \tag{31c}$$

and

$$q_p(t) = q_{p_0} + \delta q_p(t) \tag{31d}$$

where the subscript "o" was used to designate a system variable at an initial steady-state equilibrium value about which a small perturbation in the variable, represented by δ-terms was introduced so the system could be subsequently examined for stability in linearized form. In other words, the time-dependent arbitrary perturbations in ion density, $\delta n(t)$, plasma temperature, $\delta T(t)$, source feedrate, $\delta S(t)$, and volumetric neutron production rate, $\delta q_p(t)$, were required to be small to validate the linearization of the point model equations. These perturbed variables were substituted into the point model dynamics equations along with first order linear expansions for all the density- and temperature-dependent coefficients in these equations. The objective was to obtain linearized perturbed equations from the three original nonlinear plasma dynamics equations for the plasma ion density, temperature, and volumetric neutron production rate.

The inverse confinement time coefficients were examined using procedures from previous analyses of global plasma behavior.[15,16,23,24] Both the particle and energy confinement times were assumed to depend exclusively on the plasma ion density and temperature state variables:

$$\tau_{n,E} = F(n,T) \ . \tag{32}$$

Therefore, following the example of Ohta,[18] both inverse confinement times were expanded about an initial steady-state in first order Taylor series in the dependent density and temperature variables as follows:

$$\frac{1}{\tau_n} = \frac{1}{\tau_{n_0}} + \frac{\partial(\frac{1}{\tau_n})}{\partial n}\bigg|_0 \delta n(t) + \frac{\partial(\frac{1}{\tau_n})}{\partial T}\bigg|_0 \delta T(t)$$

$$\frac{1}{\tau_n} = \frac{1}{\tau_{n_0}} + \frac{1}{\tau_{n1}}\frac{\delta n(t)}{n_0} + \frac{1}{\tau_{T1}}\frac{\delta T(t)}{T_0} \tag{33a}$$

and

$$\frac{1}{\tau_E} = \frac{1}{\tau_{E_0}} + \frac{\partial(\frac{1}{\tau_E})}{\partial n}\bigg|_0 \delta n(t) + \frac{\partial(\frac{1}{\tau_E})}{\partial T}\bigg|_0 \delta T(t)$$

$$\frac{1}{\tau_E} = \frac{1}{\tau_{E_0}} + \frac{1}{\varepsilon_{n1}}\frac{\delta n(t)}{n_0} + \frac{1}{\varepsilon_{T1}}\frac{\delta T(t)}{T_0} \ . \tag{33b}$$

The constants $1/\tau_{n1}$, $1/\tau_{T1}$, $1/\varepsilon_{n1}$, and $1/\varepsilon_{T1}$ were used to reduce the complexity of analytical manipulations. The subscript "o" was used again to denote quantities in an initial steady-state condition about which the system was somehow to be perturbed and subsequently examined for stability in linearized form.

Each of the other three temperature-dependent coefficients (no density dependence) was also expanded in a simple linear Taylor series. From the particle equation the temperature-dependent coefficient was expanded as follows:

$$f_1(T) = f_1(T_0) + \frac{\partial f_1(T)}{\partial T}\bigg|_0 \delta T(t) \quad . \tag{34}$$

The temperature-dependent bremsstrahlung and alpha heating coefficient in the energy density equation was expanded similarly:

$$f_2(T) = f_2(T_0) + \frac{\partial f_2(T)}{\partial T}\bigg|_0 \delta T(t) \quad . \tag{35}$$

Finally, the temperature-dependent coefficient in the equation for the volumetric neutron production rate becomes:

$$g(T) = g(T_0) + \frac{\partial g(T)}{\partial T}\bigg|_0 \delta T(t) \quad . \tag{36}$$

A linearized system of plasma equations can now be produced by substitution of the perturbed variables from Eq. (33) and the various coefficient expansions into the plasma model equations.

Substitution of the first order variable and coefficient expansions into the plasma particle equation yields the following equation:

$$\frac{d\delta n(T)}{dt} = S_0 + \delta S(t) - [\frac{1}{\tau_{n_0}} + \frac{1}{\tau_{n1}} \frac{\delta n(t)}{n_0} + \frac{1}{\tau_{T1}} \frac{\delta T(t)}{T_0}][n_0 + \delta n(t)]$$

$$- [f_1(T_0) + \frac{\partial f_1(T)}{\partial T}\bigg|_0 \delta T(t)][n_0 + \delta n(t)]^2 \quad . \tag{37}$$

The steady-state condition in the expanded particle equation was eliminated using the steady-state equilibrium condition.

Two additional coefficients were defined from the effect of including burnup via $f_1(T)$ in this model; specifically, the effective confinement time for particles due to any loss mechanisms is reduced by including burnup effects. Certainly, fusion of particles is a loss mechanism. The subscript "b" was used in defining inverse confinement time terms to account for the increased loss of plasma ions by fusion as follows:

$$\frac{1}{\tau_{b_1}} = 2n_o f_1(T_o) \tag{38}$$

and

$$\frac{1}{\tau_{b_2}} = n_o T_o \left. \frac{\partial f_1(T)}{\partial T} \right|_0 . \tag{39}$$

By eliminating the steady-state solution and neglecting all terms above the first order in the perturbed variables and coefficients, the following linearized equation for the perturbed plasma ion density was obtained:

$$\frac{1}{n_o} \frac{d\delta n(t)}{dt} = \frac{\delta S(t)}{n_o} - \left[\frac{1}{\tau_{n_o}} + \frac{1}{\tau_{n1}} + \frac{1}{\tau_{b_1}} \right] \frac{\delta n(t)}{n_o} - \left[\frac{1}{\tau_{T1}} + \frac{1}{\tau_{b_2}} \right] \frac{\delta T(t)}{T_o} . \tag{40}$$

The inclusion of burnup results in an additional burnup-dependent inverse confinement time term as well as the usual density- and temperature-perturbed terms. This dual effect follows directly from the dependence of burnup on both state variables. Note that the addition of inverse confinement time terms results in lowered overall particle confinement time as expected.

Next the variable and coefficient expansions were substituted into the energy density equation to obtain:

$$\frac{d}{dt}\{[n_0 + \delta n(t)][T_0 + \delta T(t)]\} = [n_0 + \delta n(t)]^2[f_2(T) + \left.\frac{\partial f_2(T)}{\partial T}\right|_0 \delta T(t)]$$

$$- [n_0 + \delta n(t)][T_0 + \delta T(t)][\frac{1}{\tau_{\epsilon_0}} + \epsilon_{n1}\delta n(t) + \epsilon_{T1}\delta T(t)] + \frac{T_s S(t)}{3}$$

(41)

where the injection energy, T_s, is constant; allowance for variation in this injection energy term is another possibility for future analysis of fusioning plasma stability and dynamic response.

The steady-state solution was eliminated from Eq. (41) as usual. All terms above first order in perturbations were also eliminated since products of perturbations are negligible with respect to first order terms. In parallel with Ohta's work, the following two coefficients $1/\tau_1$ and $1/\tau_2$ were defined to simplify the analysis:

$$\frac{1}{\tau_0} \equiv \frac{1}{T_0} [2n_0 f_2(T_0) - \frac{T_0}{\epsilon_{n1}}]$$

(42a)

and

$$\frac{1}{\tau_2} \equiv \frac{1}{n_0} [n_0^2 \left.\frac{\partial f_2(T)}{\partial T}\right|_0 - \frac{n_0}{\epsilon_{T1}}] \quad .$$

(42b)

After rearrangement of terms, the following linearized equation was obtained for the perturbed plasma energy density equation:

$$\frac{1}{n_0}\frac{d\delta n(t)}{dt} + \frac{1}{T_0}\frac{d\delta T(t)}{dt} = (\frac{1}{\tau_1} - \frac{1}{\tau_{E_0}})\frac{\delta n(t)}{n_0} + (\frac{1}{\tau_2} - \frac{1}{\tau_{E_0}})\frac{\delta T(t)}{T_0} + \frac{T_s}{3T_0}\frac{\delta S(t)}{n_1} \quad .$$

(43)

The equation for the volumetric neutron production rate was also linearized; substitution of the first order variable and coefficient expansions yielded:

$$q_{p_0} + \delta q_p(t) = [g(T_0) + \frac{\partial g(T)}{\partial T}\Big|_0 \delta T(t)][n_0 + \delta n(t)]^2 \ . \qquad (44)$$

Since all terms above first order in the perturbed variations are negligible with respect to first order perturbation terms, these higher order terms were neglected. The usual steady-state condition was also eliminated to obtain the linearized perturbed fusion neutron source equation:

$$\delta q_p(t) = 2n_0 g(T_0)\delta n(t) + n_0^2 \frac{\partial g(T)}{\partial T}\Big|_0 \delta T(t) \ . \qquad (45)$$

The three linearized point model plasma equations which account for plasma input as well as output are summarized below:

Plasma Ion Density:

$$\frac{1}{n_0} \frac{d\delta n(t)}{dt} + (\frac{1}{\tau_{n_0}} + \frac{1}{\tau_{n1}} + \frac{1}{\tau_{b_1}}) \frac{\delta n(t)}{n_0} + (\frac{1}{\tau_{T1}} + \frac{1}{\tau_{b_2}}) \frac{\delta T(t)}{T_0} = \frac{\delta S(t)}{n_0}$$
$$\qquad (46)$$

Plasma Energy Density:

$$\frac{1}{n_0} \frac{d\delta n(t)}{dt} + \frac{1}{T_0} \frac{d\delta T(t)}{dt} = (\frac{1}{\tau_1} - \frac{1}{\tau_{E_0}}) \frac{\delta n(t)}{n_0} + (\frac{1}{\tau_2} - \frac{1}{\tau_{E_0}}) \frac{\delta T(t)}{T_0} + \frac{T_s}{3T_0} \frac{\delta S(t)}{n_0} \quad (47)$$

Plasma Volumetric Neutron Production Rate:

$$\delta q_p(t) = 2n_0 g(T_0)\delta n(t) + n_0^2 \frac{\partial g(t)}{\partial T}\Big|_0 \delta T(t) \ . \qquad (48)$$

The stability of these equations was examined in the Laplace or frequency domain using the standard applicable methods of classical control theory.[99] By Laplace transforming these three linearized differential equations and rearranging terms, the following set of three linear algebraic equations was obtained in the frequency domain:

$$\frac{\Delta n(s)}{n_0} \left[s + \frac{1}{\tau_{n_0}} + \frac{1}{\tau_{n1}} + \frac{1}{\tau_{b_1}}\right] + \frac{\Delta T(s)}{T_0} \left[\frac{1}{\tau_{T1}} + \frac{1}{\tau_{b_2}}\right] = \frac{\Delta S(s)}{n_0} \quad , \tag{49}$$

$$\frac{\Delta n(s)}{n_0} \left[s + \frac{1}{\tau_{E_0}} - \frac{1}{\tau_1}\right] + \frac{\Delta T(s)}{T_0} \left[s + \frac{1}{\tau_{E_0}} - \frac{1}{\tau_2}\right] = \frac{T_s}{3T_0} \frac{\Delta S(s)}{n_0} \quad , \tag{50}$$

$$\Delta q_p(s) = 2n_0 g(T_0)\Delta n(s) + n_0^2 \left.\frac{\partial g(T)}{\partial T}\right|_0 \Delta T(s) \quad . \tag{51}$$

This set of three algebraic equations can now be analyzed to determine stability information about the plasma which is modeled by these equations. This stability analysis was performed in the frequency domain not only because algebraic equations are now involved instead of differential equations, but also because the methods of stability analysis of linearized systems of equations are easily applied in the Laplace, s, domain. Since this simplified system of three algebraic equations contains four (4) unknown transformed variables in the frequency domain, the ratio of any pair of dependent perturbations is easily determined. All other parameters were assumed to remain constant, although future analyses may allow the injection energy as well as the plasma volume to be time-dependent variables.

As noted previously, the driving input perturbation to this plasma system was represented as a variation, $\delta S(t)$, in the feedrate. The corresponding output response is a perturbation or variation, $\delta q_p(t)$, in the volumetric neutron production rate. There are other internal system changes in response to changes in feedrate such as variations in density or temperature, but the final plasma output response to a change in feedrate is a change in the neutron production rate. The changed neutron production rate is then effective in altering parameters such as energy production and temperature in the subcritical blanket surrounding the plasma in the basic hybrid design. Previous anslysis by Ohta has effectively considered the temperature change as the output; however, for hybrid analysis, the neutron production rate change is a more important engineering system output, for which the temperature is only a partial system indicator. Of course, for the hybrid power producing blanket, the plasma neutron production rate is the important system parameter ultimately.

Transfer Function Representation of Plasma Characteristics

The linearized system stability characteristics, which govern the output response of the system to an arbitrary input perturbation, are contained in the transfer function, $T(s)$, for the system. This transfer function, with its characteristic system stability information, is defined as the ratio of the output to the input variable perturbations in the s-domain for this plasma system:

$$T(s) = \frac{\Delta q_p(s)}{\Delta S(s)} \quad . \tag{52}$$

So, the transfer function for any system or element within the system is defined as the transformed output of that system or element divided by the corresponding input in the frequency domain; that is, ignoring all initial conditions, the transfer function, $T(s)$, of the plasma system is defined as that factor which when multiplied with the Laplace-transformed input, $\Delta S(s)$, yields the Laplace-transformed output, $\Delta q_p(s)$. This linearized plasma model is represented by the open-loop block diagram in Fig. 8 for which the output, $\Delta q_p(s)$ is obtained by the simple algebraic multiplication of the system transfer function and the input perturbation, $\Delta S(s)$.

The stability of a time-invariant linear system is determined from the characteristic equation. The denominator of the system transfer function set equal to zero is the characteristic equation. Consequently, if all the roots of the denominator have negative real parts, the system is demonstrated, within the constraints of the linearization, to be stable. Therefore, the system or element within an overall system characteristic information concerning stability is contained in the transfer function, $T(s)$, for the overall system or an elemental part of the system.

Basic block diagram and transfer function methodology in the frequency domain were used to show how the input perturbation, $\delta S(t)$, in the plasma feedrate can cause a corresponding output perturbation, $q_p(t)$, in the volumetric neutron production rate. This effect is shown in Fig. 9. The block flow diagram in Fig. 9 is based upon the re-arrangement of the relation for the linearized volumetric neutron production rate of Eq. (51) into the following form:
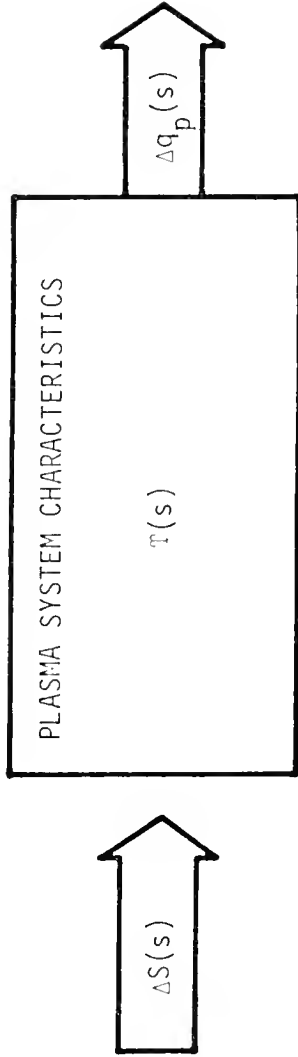
Figure 8. Transfer function formulation for a point-model fusioning plasma.
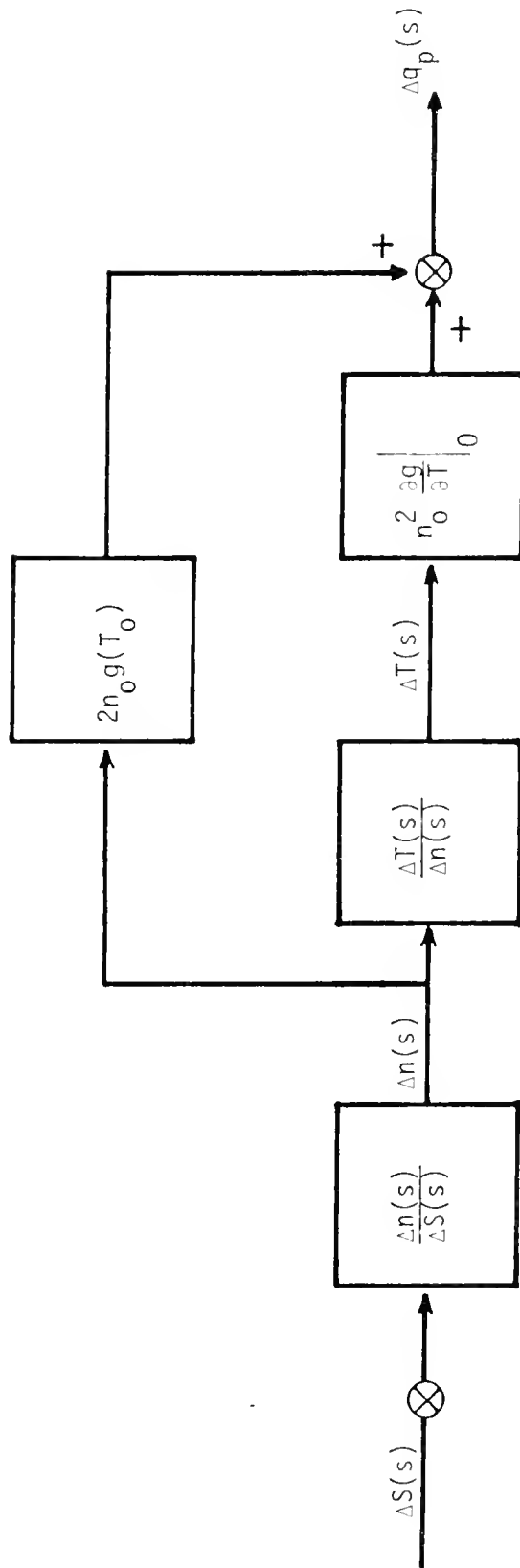
Figure 9. Block diagram for the point-model plasma system.

$$\Delta q_p(s) = 2n_0 f(T_0) \cdot \frac{\Delta n(s)}{\Delta T(s)} \cdot \Delta T(s) + n_0^2 \left. \frac{\partial g(T)}{\partial T} \right|_0 T(s) \; . \tag{53}$$

The representation of transformed equations such as Eq. (53) in block diagrams such as shown in Fig. 9 is straightforward because of the algebraic method of operation of transfer functions in the Laplace domain.

A more easily analyzed equivalent block diagram of Fig. 9 is shown in Fig. 10 after application of the appropriate block diagram transformation. The transfer function for pairs of dependent variables denoted as ratios in the block diagram were determined from the system of algebraic equation. The transfer functions for the plasma system with no feedback as they are presented here are all ratios of polynomials. The following two polynomial ratios required to analyze the frequency response of the system in the block diagrams of Fig. 9 and Fig. 10 were obtained:

$$\frac{n(s)}{S(s)} = \frac{s + a_1}{s^2 + a_2 s + a_3} \; , \tag{54}$$

$$\frac{T(s)}{n(s)} = \frac{a_4 s + a_5}{-\frac{n_0}{T_0}(s + a_1)} \; , \tag{55}$$

where the coefficients a_1, a_2, a_3, and a_4 are given by

$$a_1 = \frac{1}{\tau_{E_o}} - \frac{1}{\tau_2} - \frac{T_s}{3T_o} \left(\frac{1}{\tau_{T1}} + \frac{1}{\tau_{b_2}}\right) \quad , \tag{56a}$$

$$a_2 = \frac{1}{\tau_{E_o}} - \frac{1}{\tau_2} + \frac{1}{\tau_{n_o}} + \frac{1}{\tau_{n1}} + \frac{1}{\tau_{b_1}} - \frac{1}{\tau_{T1}} - \frac{1}{\tau_{b_2}} \quad , \tag{56b}$$

$$a_3 = \left(\frac{1}{\tau_{n_o}} + \frac{1}{\tau_{n1}} + \frac{1}{\tau_{b_1}}\right)\left(\frac{1}{\tau_{E_o}} - \frac{1}{\tau_2}\right) + \left(\frac{1}{\tau_{T1}} + \frac{1}{\tau_{b_2}}\right)\left(\frac{1}{\tau_1} - \frac{1}{\tau_{E_o}}\right) \quad , \tag{56c}$$

$$a_4 = 1 - \frac{T_s}{3T_o} \quad , \tag{56d}$$

$$a_5 = \frac{1}{\tau_{E_o}} - \frac{1}{\tau_1} - \frac{T_s}{3T_o} \left(\frac{1}{\tau_{n_o}} + \frac{1}{\tau_{n1}} + \frac{1}{\tau_{b_1}}\right) \quad . \tag{56e}$$

The elemental transfer functions $\Delta n(s)/\Delta S(s)$ and $\Delta T(s)/\Delta n(s)$ given in Eqs. (54) and (55) as well as the simpler factors, $2n_o g(T_o)$ and $n_o^2 \left.\frac{\partial g}{\partial T}\right|_o$, operate in the transfer function methodology via algebraic multiplication of transform inputs to produce the various transform outputs shown in the block diagram in Fig. 9. A third elemental transfer function is required to complete the block diagram representation of the linearized set of three trnasformed equations applicable for this plasma model; this transfer function is presented as the only remaining ratio of perturbed, frequency-dependent variables as shown in Eq. (57):

$$\frac{\Delta T(s)}{\Delta S(s)} = \frac{-\frac{T_o}{n_o} \left[(1 - \frac{T_s}{3T_o})s + a_4\right]}{s^2 + a_2 s + a_3} \quad . \tag{57}$$

The verification of the identity presented in Eq. (57) was used to check not only the algebraic multiplication of these elemental transfer functions but also the correctness of the transfer function relations in Eqs. (54), (55), and (57):

$$\frac{\Delta n(s)}{\Delta S(s)} = \frac{\Delta T(s)}{\Delta S(s)} \cdot \frac{\Delta n(s)}{\Delta T(s)} \tag{58}$$

where $\frac{\Delta n(s)}{\Delta T(s)}$ is simply the inverse of $\frac{\Delta T(s)}{\Delta n(s)}$ from Eq. (55).

The transfer function, $\frac{\Delta T(s)}{\Delta n(s)}$, is presented for completeness because the linearized neutron source Eq. (51) can be rearranged as follows in contrast to the form in Eq. (53):

$$q_p(s) = 2n_o g(T_o)\Delta n(s) + n_o^2 \left.\frac{\partial g}{\partial T}\right|_0 \frac{\Delta T(s)}{\Delta n(s)} \cdot \Delta n(s) . \tag{59}$$

The point model plasma system using this form of the linearized volumetric neutron production rate is represented by the somewhat different block diagram shown in Fig. 11. The requirement for the transfer function element, $\frac{\Delta T(s)}{\Delta S(s)}$, is explicitly indicated. The block diagram of Fig. 11 is reduceable to the simplified form shown in Fig. 12 which again is different from its equivalent counterpart in Fig. 10. The algebraic nature of the equations allows formulation for optimum system coordination.

The two reduced block diagram representations of Fig. 10 and Fig. 12 are completely equivalent since each reduces to the overall plasma model shown in Fig. 13 where the input is a transform perturbation in the feedrate and the output is a corresponding transform perturbation in the volumetric neutron production rate in the plasma.
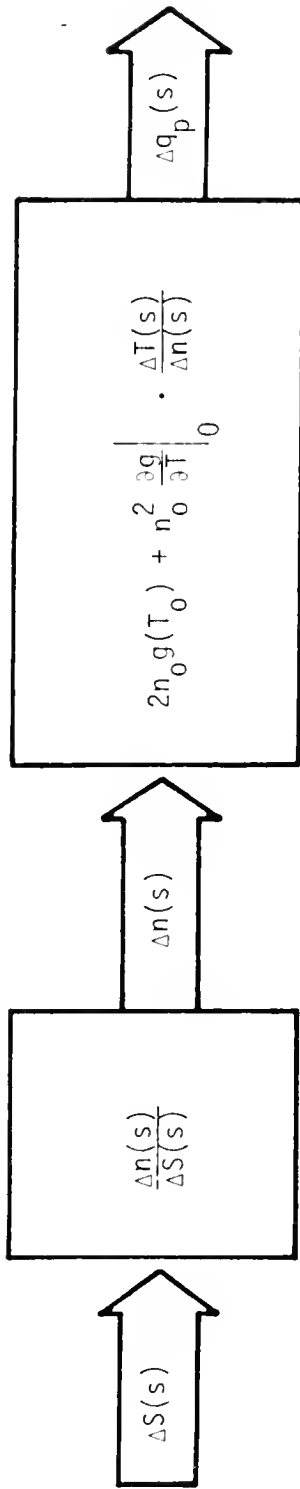
Figure 10. Partially-reduced block diagram for the point-model plasma system.
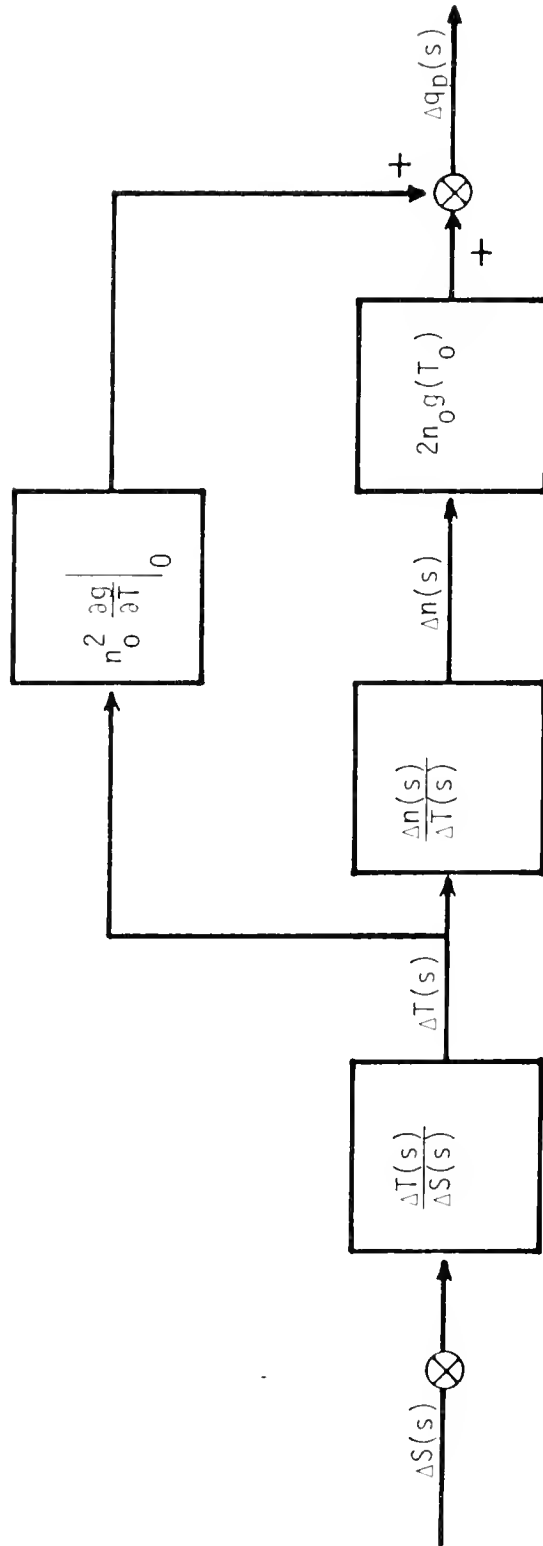
Figure 11. Alternate block diagram for the point-model plasma system.
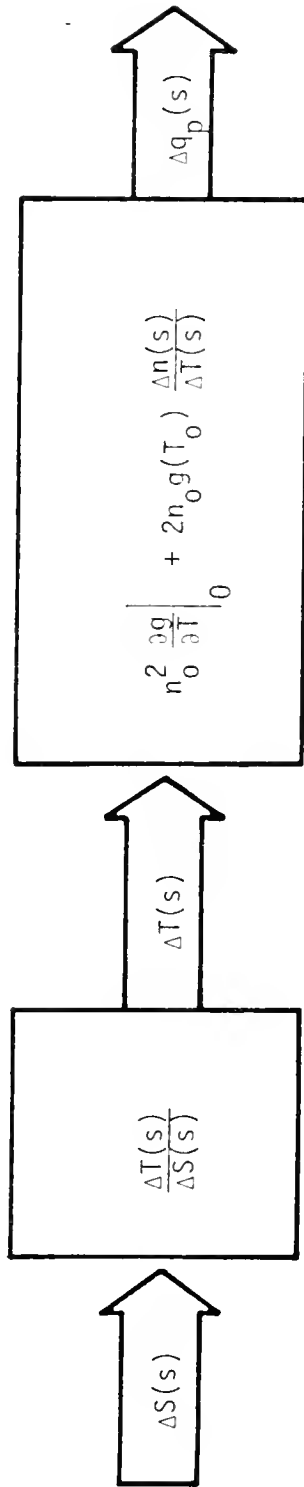
Figure 12. Partially-reduced block diagram for the alternate point-model plasma system formulation.

$$n_o^2 \left.\frac{\partial g}{\partial T}\right|_0 \cdot \frac{\Delta T(s)}{\Delta S(s)} + 2n_o g(T_o) \frac{\Delta n(s)}{\Delta S(s)}$$

$\Delta q_p(s)$

$\Delta S(s)$
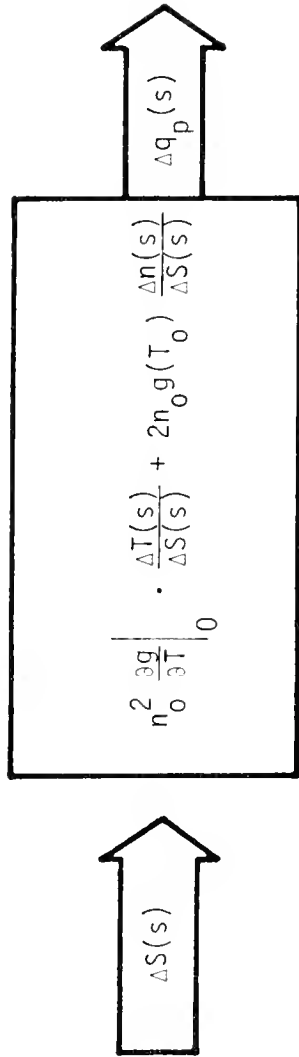
Figure 13. Reduced open-loop block diagram for the point-model plasma.

The overall open loop transfer function for the point-model plasma system is presented in Eq. (60) as the perturbed neutron source output divided by the initiating perturbation in the plasma feedrate as follows:

$$\frac{\Delta q_p(s)}{\Delta S(s)} = n_o^2 \left. \frac{\partial g(T)}{\partial T}\right|_0 \cdot \frac{\Delta T(s)}{\Delta S(s)} + 2n_o g(T_o) \cdot \frac{\Delta n(s)}{\Delta S(s)} \quad . \tag{60}$$

The elemental transfer functions, $\Delta n(s)/\Delta S(s)$ and $\Delta T(s)/\Delta S(s)$, and Eqs. (54) and (57) were used to evaluate the overall open-loop plasma transfer function. After substitution and simplifying rearrangement of terms, the overall transfer function for the point model plasma without feedback becomes

$$\frac{\Delta q_p(s)}{\Delta S(s)} = \frac{s\left[2n_o g(T_o) - n_o T_o \left.\frac{\partial g}{\partial T}\right|_0 a_4\right] + 2n_o g(T_o)a_1 - n_o T_o \left.\frac{\partial q}{\partial T}\right|_0 a_5}{s^2 + a_2 s + a_3} \quad . \tag{61}$$

Equation (61) is the overall open-loop plasma source feedrate transfer function; this result is similar in application and meaning to the source transfer function derived for fissile subcritical assemblies where a neutron source perturbation causes a changed flux or neutron level in the system.[99]

Stability Analysis of the Linearized Plasma Model

Individual elements in block diagrams used to model mechanical, electrical, or other physical systems are usually required to be stable—that is, to have stable impulse responses. In contrast, the individual elements in the open-loop plasma block diagrams in Fig. 9 and Fig. 11 do not necessarily have stable impulse responses. For example, the elemental

transfer function, $\Delta n(s)/\Delta T(s)$, may well be unstable when considered independently since it has the same number of zeroes and poles. This situation occurs because of the effort to compartmentalize the plasmas system and its describing linearized equations in the Laplace domain in order to analyze the overall system. No such independent element exists in the plasma; both the density and the temperature state variables are interdependent and this separation has no clear physical meaning. However, this overall transfer function was still analyzed to determine the conditions for system stability which are contained in the characteristic equation of the overall system transfer function.

The system characteristic equation was obtained from the system transfer function by setting the polynomial in its denominator equal to zero as follows:

$$
0 = s^2 + a_2 s + a_3 = s^2 + s \left(\frac{1}{\tau_{E_0}} - \frac{1}{\tau_2} + \frac{1}{\tau_{n_0}} + \frac{1}{\tau_{n1}} + \frac{1}{\tau_{b_1}} - \frac{1}{\tau_{T1}} - \frac{1}{\tau_{b_2}} \right)
$$

$$
+ \left(\frac{1}{\tau_{n_0}} + \frac{1}{\tau_{n1}} + \frac{1}{\tau_{b_1}} \right) \left(\frac{1}{\tau_{E_0}} - \frac{1}{\tau_2} \right) + \left(\frac{1}{\tau_{T1}} + \frac{1}{\tau_{b_2}} \right) \left(\frac{1}{\tau_1} - \frac{1}{\tau_{E_0}} \right) \quad . \quad (62)
$$

This characteristic equation was used to determine the open-loop stability of the modeled plasma; that is, if all the roots of the denominator have negative real parts, the system is inherently stable to small disturbances in the feedrate. The Routh Stability Criterion was selected from the several methods of stability analysis available from classical control theory. The Routh array in Fig. 14 was constructed from the coefficients of the characteristic equation.

$$\begin{array}{cc} 1 & a_3 \\ a_2 & 0 \\ a_3 & 0 \\ 0 & \end{array}$$

Figure 14. Routh array for open-loop point model fusioning plasma with burnup.

Within the limits of the assumptions of small perturbations to obtain linearized equations, the requirements of the Routh criterion for absolute stability are that there be no sign changes in column 1 of the array. Therefore, for the plasma system model represented by the open-loop black diagram of Fig. 9, the inequality requirements for absolute stability are twofold:

$$a_2 = \frac{1}{\tau_{E_0}} - \frac{1}{\tau_2} + \frac{1}{\tau_{n_0}} + \frac{1}{\tau_{n1}} + \frac{1}{\tau_{b_1}} - \frac{1}{\tau_{T1}} - \frac{1}{\tau_{b_2}} > 0 \qquad (63a)$$

and

$$a_3 = \left(\frac{1}{\tau_{n_0}} + \frac{1}{\tau_{n1}} + \frac{1}{\tau_{b_1}}\right)\left(\frac{1}{\tau_{E_0}} - \frac{1}{\tau_2}\right) + \left(\frac{1}{\tau_{T1}} - \frac{1}{\tau_{b_2}}\right)\left(\frac{1}{\tau_1} - \frac{1}{\tau_{E_0}}\right) > 0 . \qquad (63b)$$

These stability criteria are identical to those of Ohta[18] but were obtained differently using a system-related phys8cal model of the plasma behavior and its sources of perturbations via the feedrate. The two conditions of Eqs. (63a) and (63b) represent general stability criteria

for the modeled plasma. Unless some assumptions are made concerning diffusion properties in the plasma, this type of analysis cannot proceed any further.

Because understanding and treatment of diffusion in fusioning plasmas are clouded by anomalous behavior and the lack of data on diffusion in full scale thermonuclear plasmas, plasma diffusion behavior has been represented by a wide range of different analytical models. The three most frequently used analytical diffusion models[100] are

1. Constant confinement where $\tau_{n,E}$ = constant.
2. Classical confinement where $\tau_{n,E} \propto n^{-1}T^{1/2}$.
3. Bohm confinement where $\tau_{n,E} \propto T^{-1}$.

These three postulated types of diffusion can be used to model a wide range of expected possibilities for diffusion in future fusioning plasmas when they are produced for steady-state operation. The constant confinement case has frequently been chosen not only for simplicity but also because its predictions of diffusion losses fall between the most encouraging model (classical) and the least advantageous model (Bohm) for attaining fusion reactor conditions.

Following Ohta et al.[18] the confinement time was conveniently represented in all these diffusion models by a general dependence on density and temperature:

$$\tau \sim n^{\ell}T^m \tag{64}$$

where (a) $\ell = m = 0$ for constant confinement, (b) $\ell = -1$, $m = 1/2$ for classical confinement, and (c) $\ell = 0$, $m = -1$ for Bohm confinement.

The assumption of constant confinement time was made to simplify the open-loop transfer function of Eq. (61) by the elimination of all

terms containing the inverse confinement time expansion terms $1/\tau_{n1}$ and $1/\tau_{T1}$. The following resultant open-loop transfer function was obtained:

$$\frac{\Delta q_p(s)}{\Delta S(s)} = \frac{s[2n_0 g(T_0) - n_0 T_0 \left.\frac{\partial g}{\partial T}\right|_0 a_4] + 2n_0 g(T_0)a_b - n_0 T_0 \left.\frac{\partial g}{\partial T}\right|_0 a_7}{s^2 + a_8 s + a_9} \tag{65}$$

where the reduced coefficients are given by

$$a_6 = \frac{1}{\tau_{E_0}} - \frac{1}{\tau_2} - \frac{T_s}{3T_0}\frac{1}{\tau_{b_2}} \quad, \tag{66a}$$

$$a_7 = \frac{1}{\tau_{E_0}} - \frac{1}{\tau_1} - \frac{T_s}{3T_0}\left(\frac{1}{\tau_{n_0}} + \frac{1}{\tau_{b_1}}\right) \quad, \tag{66b}$$

$$a_8 = \frac{1}{\tau_{E_0}} - \frac{1}{\tau_2} + \frac{1}{\tau_{n_0}} + \frac{1}{\tau_{b_1}} - \frac{1}{\tau_{b_2}} \quad, \tag{66c}$$

$$a_9 = \left(\frac{1}{\tau_{n_0}} + \frac{1}{\tau_{b_1}}\right)\left(\frac{1}{\tau_{E_0}} - \frac{1}{\tau_2}\right) + \frac{1}{\tau_{b_2}}\left(\frac{1}{\tau_1} - \frac{1}{\tau_{E_0}}\right) \quad. \tag{66d}$$

The linearized response of the open-loop plasma volumetric neutron pro-
duction rate to a small perturbation in the plasma feedrate is contained
in this transfer function. The characteristic equation to be examined
for stability was reduced to the simplified expression in Eq. (67) which
was obtained by setting the denominator of the transfer function of
Eq. (65) equal to zero:

$$0 = s^2 + a_8 s + a_9 =$$

$$s^2 + s\left(\frac{1}{\tau_{E_0}} - \frac{1}{\tau_2} + \frac{1}{\tau_{n_0}} + \frac{1}{\tau_{b_1}} - \frac{1}{\tau_{b_2}}\right) + \left(\frac{1}{\tau_{n_0}} + \frac{1}{\tau_{b_1}}\right)\left(\frac{1}{\tau_{E_0}} - \frac{1}{\tau_2}\right) + \frac{1}{\tau_{b_2}}\left(\frac{1}{\tau_1} - \frac{1}{\tau_{E_0}}\right) \quad. \tag{67}$$

The further simplified Routh array for Eq. (67) is presented in Fig. 15.

$$1 \qquad\qquad a_9$$

$$a_8 \qquad\qquad 0$$

$$a_9 \qquad\qquad 0$$

$$0$$

Figure 15.   Routh array: Open-loop plasma model with constant confinement.

The dual stability requirements become simply:

$$a_8 = \frac{1}{\tau_{E_o}} - \frac{1}{\tau_2} + \frac{1}{\tau_{n_o}} + \frac{1}{\tau_{b_1}} - \frac{1}{\tau_{b_2}} > 0 \qquad (68a)$$

and

$$a_9 = \left(\frac{1}{\tau_{n_o}} + \frac{1}{\tau_{b_1}}\right)\left(\frac{1}{\tau_{E_o}} - \frac{1}{\tau_2}\right) + \frac{1}{\tau_{b_2}}\left(\frac{1}{\tau_1} - \frac{1}{\tau_{E_o}}\right) > 0 \; . \qquad (68b)$$

When the effects of burnup were also neglected, then the two inverse confinement times accounting for burnup disappeared so that the stability requirements become simply:

$$\frac{1}{\tau_{E_o}} - \frac{1}{\tau_2} + \frac{1}{\tau_{n_o}} > 0 \qquad (69a)$$

and

$$\frac{1}{\tau_{n_o}} \left(\frac{1}{\tau_{E_o}} - \frac{1}{\tau_2} \right) > 0 \qquad \qquad (69b)$$

which are the same stability results as those obtained by Ohta.[18] Here, however, the results were obtained in a manner related directly to reasonably expected perturbations of the plasma feedrate from the engineering viewpoint of affecting the resultant volumetric neutron production rate emitted from the plasma to drive the blanket for energy production. Further, this is a completely general approach which can be applied whenever such plasma systems are analyzed.

Typical steady-state fusioning plasma equilibrium conditions were used to demonstrate that the burnup-related terms, $1/\tau_{b_1}$ and $1/\tau_{b_2}$, are negligible with respect to the equilibrium inverse particle confinement time, $1/\tau_{n_o}$, as well as the equilibrium inverse energy confinement time, $1/\tau_{E_o}$. The negligible effect of burnup for both pure fusion designs such as UWMAK-III[30] and hybrid designs such as that developed in this study was easily demonstrated using equilibrium operating conditions for the two types of systems: pure fusion and hybrid fusion-fission. This comparison was simply based on comparing particle confinement times excluding burnup effects to particle confinement times including burnup effects. In other words, the characteristic fusion time, τ_F, is defined as follows:

$$\tau_F = \frac{2}{n(t) \langle \sigma v \rangle_{DT}} \qquad . \qquad \qquad (70)$$

The effect of this confinement time on the temperature and density of the plasma is shown to be negligible in Appendix C, in comparison to similar effects of the ordinary particle confinement time.

Although the comparisons of Appendix C are presented between equilibrium parameters for the two systems, the small perturbations applicable in the linearized analysis maintain the validity of the comparison. In addition, the types of nonlinear transients of most interest in this analysis involve relatively small, $\pm$ 5% perturbations in some operating conditions. This study of hybrid reactors was concerned with the transient behavior over time intervals on the order of a few seconds. The total resultant nonlinear temperature transients were not expected to be large within the five to fifteen seconds of interest for such operational perturbations. As noted in Appendix C, if very large nonlinear, short time transients are considered or even if slowly changing transients are allowed to grow for long periods of time, then assumptions in the plasma model used here will be invalid. For example, if large temperature variations are obtained by nonlinear time variations in the parameters of the plasma model, then the results will be invalid because they violate the basic assumption of constant plasma volume.

As expected, stability analysis of such full scale point model D-T fusioning plasmas has demonstrated that the stability criteria as well as time-dependent transient development due to departures of plasma temperature from equilibrium are nearly identical for the two pure fusion cases.[23,24,95] In other words, whether burnup is included or removed from consideration makes little difference in stability criteria and transient plasma development for which the current plasma model is applicable. The calculations of Appendix C support such results.

When the general confinement model of Eq. (64) was used to obtain expressions for $1/\tau_{nl}$, $1/\tau_{Tl}$, $1/\tau_1$, and $1/\tau_2$ from their original definitions in Eqs. (33a), (33b), (42a), and (42b), respectively, the two

general stability requirements in Eqs. (69a) and (69b) were expanded
to yield:

Stability Condition I:

$$\frac{1}{\tau_{E_0}} - [n_0 \left.\frac{\partial f_2(T)}{\partial T}\right|_0 - T_0 \left.\frac{\partial(\frac{1}{\tau_E})}{\partial T}\right|_0] + \frac{1}{\tau_{n_0}} + n_0 \left.\frac{\partial(\frac{1}{\tau_n})}{\partial n}\right|_0 - T_0 \left.\frac{\partial(\frac{1}{\tau_n})}{\partial T}\right|_0 > 0 \tag{71}$$

Stability Condition II:

$$[\frac{1}{\tau_{n_0}} + n_0 \left.\frac{\partial(\frac{1}{\tau_n})}{\partial n}\right|_0][\frac{1}{\tau_{E_0}} - n_0 \left.\frac{\partial f_2(T)}{\partial T}\right|_0 + T_0 \left.\frac{\partial(\frac{1}{\tau_E})}{\partial T}\right|_0]$$

$$+ T_0 \left.\frac{\partial(\frac{1}{\tau_n})}{\partial T}\right|_0 \cdot [\frac{2n_0 f_2(T)}{T_0} - n_0 \left.\frac{\partial(\frac{1}{\tau_E})}{\partial n}\right|_0 - \frac{1}{\tau_{E_0}}] > 0 \ . \tag{72}$$

Several definitions were then introduced in parallel with Ohta's
treatment to simplify the application of these stability criteria. First,
the ratio of particle to energy confinement time in the steady-state was
designated by the constant, R:

$$R = \frac{\tau_{n_0}}{\tau_{E_0}} \tag{73}$$

which is predicted to exceed unity for the full-scale, power-producing
fusioning plasmas considered in large conceptual design studies.[30,32,101,102]
This predicted behavior of the R-ratio is consistent with theoretical
results indicating that particles of higher energy diffuse out of plasma
devices more quickly than lower energy particles do. In addition, R-values
above unity account for other anomalous energy losses.[100]

The second identity is related to Lawson's $n\tau_E$-criterion; that is, at steady-state, the Lawson relation using the more meaningful energy confinement time is defined by

$$F(T_o) \equiv n_o \tau_{E_o} \tag{74}$$

which is a more restrictive condition used by Ohta in contrast to Lawson's original criterion using the particle confinement time, τ_n. The variation of this relation with temperature is presented in Fig. 16 for both charged particle heating and injection heating cases in general agreement with results presented in Ohta's paper. The derived stability criteria are dependent on the behavior of the $F(T)$ function.

Finally, to simplify notation, a combination of recurring parameters was defined by the following constant:

$$\xi_2 \equiv 1 - \frac{1}{R} \frac{T_s}{3T_o} \quad . \tag{75}$$

The three parameters defined in Eqs. (73), (74), and (75) together with Eq. (64) for the general confinement model were used to simplify the two expanded versions of the stability conditions given in Eqs. (71) and (72).

After appropriate substitution as well as combination and rearrangement of terms, the two stability criteria originally determined by Ohta[18] were obtained as follows:

Criterion I:

$$\left. \frac{\partial F}{\partial T} \right|_o > \left[m - \frac{(1 - \ell + m)}{R} \right] \frac{F_o}{\xi_2 T_o} \tag{76}$$
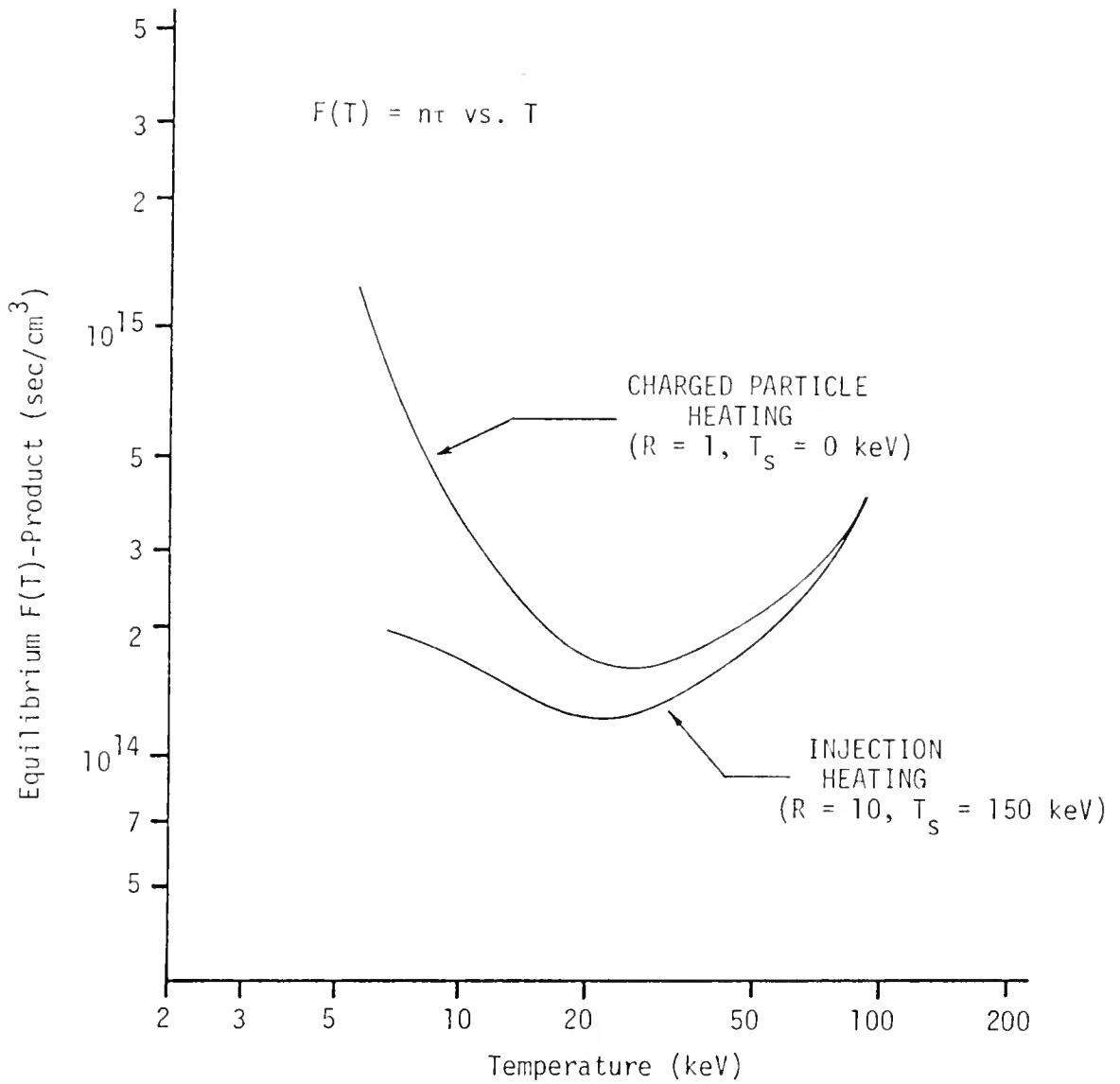
Figure 16. Variation of $F(T) = n_i$ with temperature.

Criterion II:

$$\frac{\partial F}{\partial T}\bigg|_0 > \frac{2mF_0}{T_0} \tag{77}$$

where stability is shown to be strongly dependent on the Lawson $n_0 \tau_{E_0}$ - product and its derivative at the existing equilibrium plasma condition.

For the three previously defined diffusion models, these two stability criteria are summarized in Table 2-I. The confinement time effects are contained only in the F_0-term via τ_{E_0} and to a less effective degree, in the ξ_2-term via the R-ratio.

Table 2-I

Stability Criteria for a D-T Fusion Reactor

Confinement Model	Stability Criteria	Critical Temperature (T_c) (keV)	
		CPH*	IH**
τ_E = constant	$\frac{T_0}{F_0} \frac{\partial F}{\partial T}\bigg|_0 > 0$	28	21
$\tau_E \sim T^{-1}$ (Bohm)	$\frac{T_0}{F_0} \frac{\partial F}{\partial T}\bigg|_0 > -2$ $\frac{T_0}{F_0} \frac{\partial F}{\partial T}\bigg|_0 > -1/\xi_2$	14	5
$\tau_E \sim T^{1/2} n^{-1}$ (Classical)	$\frac{T_0}{F_0} \frac{\partial F}{\partial T}\bigg|_0 > 1/2$ $\frac{T_0}{F_0} \frac{\partial F}{\partial T}\bigg|_0 > \frac{1}{2\xi_2} (1 - 5/R)$	42	33

*Charged particle heating ($T_s = 0$) R = 1, $\xi_2 = 1$.
**Injection heating ($T_s \neq 0$) T_s = 150 keV, R = 10.

These results are identical to those presented by Ohta; the fusioning plasma is stable and self-controlling only if its operating steady-state temperature exceeds the critical temperature limits defined by the two stability criteria for each model.

Since most full scale fusion power plant designs are predicted to utilize plasmas at steady-state temperatures in the range of 15-20 keV, these plasmas are expected to require feedback control due to the thermal instability problem.[30,92,93,102] A similar but significantly lower range of plasma operating temperatures is anticipated for the core of hybrid reactors. The hybrid plasma discussed in Chapter 4 will operate in the steady-state equilibrium condition at a temperature of only 8.0 keV. Therefore, feedback control was selected to ensure plasma stability for closed loop pure fusion plasma operation at low temperatures.

In accordance with Ohta's efforts to demonstrate global plasma stability, an artificial feedback mechanism was incorporated to effect changes in the plasma sustaining feedrate via corresponding changes in the plasma temperature as follows:

$$\delta S(t) = \alpha_1 \frac{n_0}{T_0} \delta T(t - t_{d_1}) \quad . \tag{78}$$

The delay time, t_{d_1}, was incorporated to account for the possible lag time between the occurrence of a change in the steady-state plasma temperature, $\delta T(t)$, and the corresponding application of a change in the feedrate, $\delta S(t)$. The inclusion of this delay time, at least in the hypothetical model, is necessitated by the limitations on engineering speed of response. The factor, n_0/T_0, was used to normalize the feedback relationship from

energy to particle density while the factor, α_1, was designated as the temperature (plasma) feedback coefficient with units of inverse seconds.

To examine stability for this feedback case, this plasma source feedrate perturbation was transformed to the Laplace domain to obtain the following exponential equation:

$$\Delta S(s) = \alpha_1 \frac{n_0}{T_0} e^{-t_{d_1} s} \Delta T(s) \quad . \tag{79}$$

Due to the exponential delay term, this feedback equation is not purely algebraic and linear in the transform domain. Since the delay time was assumed small, the equation was linearized by expanding the exponential term in a first order Taylor series to obtain the desired algebraic form for the transformed feedback equation:

$$\Delta S(s) = \alpha_1 \frac{n_0}{T_0} (1 - t_{d_1} s) \Delta T(s) \quad . \tag{80}$$

The transform feedback relation of Eq. (80) is in the polynomial form suited to the Laplace domain stability analysis methods which were applied to the open-loop system. Note that, if delay time is neglected in the application of feedback, then this equation can be simplified to the following form:

$$\Delta S(s) = \alpha_1 \frac{n_0}{T_0} \Delta T(s) \quad . \tag{81}$$

This form was actually applied to the hybrid plasma model developed in Chapter 3.

The four linearized equations which were developed in the Laplace domain--one each for plasma ion density, plasma energy density or

temperature, and plasma volumetric neutron production rate plus a fourth linearized equation for plasma feedrate dependent on plasma temperature-- were rewritten for ease of handling as follows:

Plasma Ion (Particle) Density:

$$(s + \frac{1}{\tau_{n_0}} + \frac{1}{\tau_{n1}}) \frac{\Delta n(s)}{n_0} = \frac{\Delta S(s)}{n_0} - \frac{1}{\tau_{T1}} \frac{\Delta T(s)}{T_0} \tag{82}$$

Plasma Energy Density:

$$(s + \frac{1}{\tau_{E_0}} - \frac{1}{\tau_1}) \frac{\Delta n(s)}{n_0} + (s + \frac{1}{\tau_{E_0}} - \frac{1}{\tau_2}) \frac{\Delta T(s)}{T} = \frac{T_s}{n_0 T_0} \Delta S(s) \tag{83}$$

Plasma Volumetric Neutron Production Rate:

$$\Delta q_p(s) = g(T_0) \Delta n(s) + n_0 \left. \frac{\partial g(T)}{\partial T} \right|_0 \Delta T(s) \tag{84}$$

Plasma Temperature Feedback:

$$\Delta S(s) = \alpha_1 \frac{n_0}{T_0} (1 - t_{d_1} s) \Delta T(s) \quad . \tag{85}$$

The block diagram applicable to this neutron-producing plasma system with feedback is presented in Fig. 17 where the only change from the reduced schematic in Fig. 12 is the stabilizing feedback loop. The open-loop elemental transfer function, $\Delta T(s)/\Delta S(s)$, was presented in Eq. (57). By applying block diagram reduction methods, the transfer function for this closed loop system was determined from Fig. 17 to be as shown in Eq. (84).
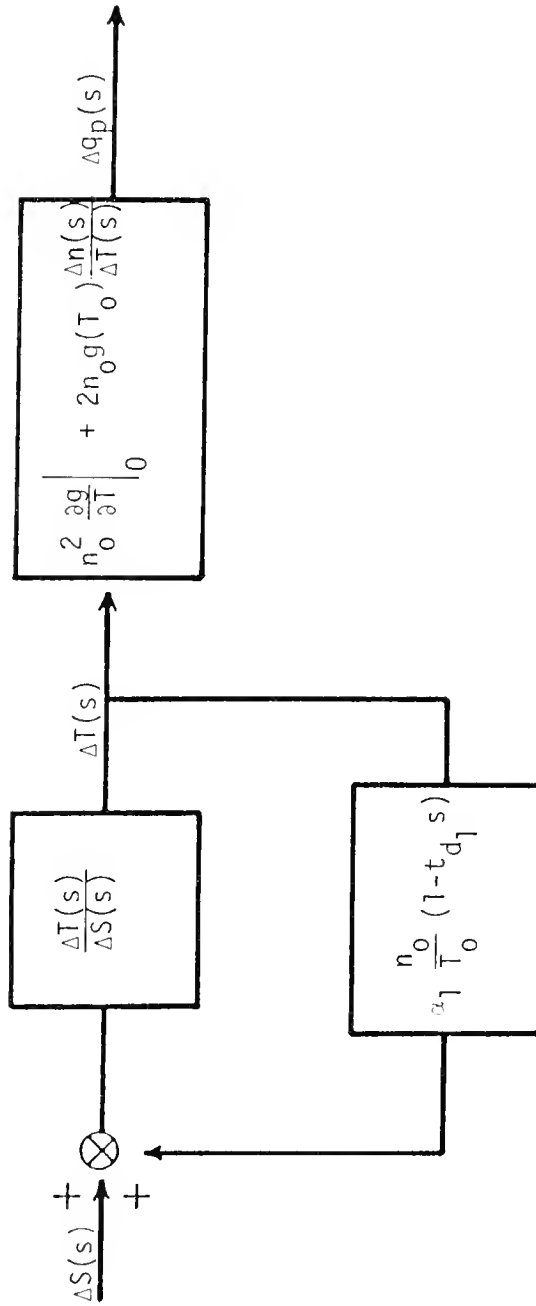
Figure 17. Block diagram for the point-model plasma with temperature feedback to the feedrate.

$$\frac{\Delta q_p(s)}{\Delta S(s)} = \frac{-\dfrac{T_0}{n_0}\left[n_0^2\left.\dfrac{\partial g}{\partial T}\right|_0(a_4 s + a_7) - \dfrac{2n_0^2 g(T_0)a_6}{T_0}\right]}{s^2 + a_{10}s + a_{11} - \alpha_1(1 - t_{d_1}s)(a_4 s + a_7)} \quad , \tag{86}$$

where the reduced coefficients, a_{10} and a_{11}, apply for negligible burnup and are given by

$$a_{10} = \frac{1}{\tau_{E_0}} - \frac{1}{\tau_2} + \frac{1}{\tau_{n_0}} + \frac{1}{\tau_{n1}} - \frac{1}{\tau_{T1}} \tag{87a}$$

$$a_{11} = \left(\frac{1}{\tau_{n_0}} + \frac{1}{\tau_{n1}}\right)\left(\frac{1}{\tau_{E_0}} - \frac{1}{\tau_2}\right) + \frac{1}{\tau_{T1}}\left(\frac{1}{\tau_1} - \frac{1}{\tau_{E_0}}\right) \quad . \tag{87b}$$

The assumption of constant confinement time was employed not only to simplify analysis of this transfer function but also because the constant confinement model is an effective average for the spectrum of possible diffusion behavior in fusion systems. Diffusion losses are probably overpredicted by the unrealistic Bohm diffusion model ($\tau \sim T^{-1}$) because of the so-called collisionless regime at relatively high plasma temperatures and possibly underpredicted by the classical diffusion model ($\tau \sim n^{-1}T^{1/2}$).[100] For this hybrid analysis the constant confinement model was used exclusively as an effective average diffusion behavior because this study was concerned primarily with typical parameters and behavior rather than actual design base calculations.

By combining terms into polynomials in the s-domain, the overall closed-loop plasma transfer function was reduced to

$$\frac{\Delta q_p(s)}{\Delta S(s)} = \frac{\left[g(T_0) - T_0\left.\dfrac{\partial g}{\partial T}\right|_0 a_4\right]s + g(T_0)\left(\dfrac{1}{\tau_{E_0}} - \dfrac{1}{\tau_2}\right) - T_0\left.\dfrac{\partial g}{\partial T}\right|_0 a_{12}}{a_{13}s^2 + a_{14}s + a_{15}} \quad , \tag{88}$$

where the reduced coefficients, a_{12}-a_{15}, apply for negligible burnup with constant confinement and are given by

$$a_{12} = \frac{1}{\tau_{E_0}} - \frac{1}{\tau_1} - \frac{T_s}{3T_0} \frac{1}{\tau_{n_0}} \quad , \tag{89a}$$

$$a_{13} = 1 + \alpha_1 t_{d_1} a_4 \quad , \tag{89b}$$

$$a_{14} = \frac{1}{\tau_{E_0}} - \frac{1}{\tau_2} + \frac{1}{\tau_{n_0}} - \alpha_1 a_4 + \alpha_1 t_{d_1} a_{12} \quad , \tag{89c}$$

$$a_{15} = \frac{1}{\tau_{n_0}} (\frac{1}{\tau_{E_0}} - \frac{1}{\tau_2}) - \alpha_1 a_{12} \quad . \tag{89d}$$

Application of the Routh criterion to the characteristic equation for this transfer function yielded the following three stability conditions (criteria).

Stability Criterion I:

$$a_{13} = 1 + \alpha_1 t_{d_1} (1 - \frac{T_s}{3T_0}) > 0 \tag{90a}$$

Stability Criterion II:

$$a_{14} = \frac{1}{\tau_{E_0}} - \frac{1}{\tau_2} + \frac{1}{\tau_{n_0}} - \alpha_1 (1 - \frac{T_s}{3T_0}) - \frac{\alpha_1 \xi_2 t_{d_1}}{\tau_{E_0}} > 0 \tag{90b}$$

Stability Criterion III:

$$a_{15} = \frac{1}{\tau_{n_0}} (\frac{1}{\tau_{E_0}} - \frac{1}{\tau_2}) + \frac{\alpha_1 \xi_2}{\tau_{E_0}} > 0 \quad . \tag{90c}$$

These criteria are presented dependent on Criterion I being positive which is the case only when the injection energy, T_{s_0}, exceeds the thermal temperature, T_0, by a factor of three or more since Criterion I implies $\alpha_1 > [t_{d_1}(\frac{T_s}{3T_0} - 1)]^{-1}$. Should the reverse be true for Criterion I, then the direction of the inequalities in Eqs. (90b) and (90c) must be reversed; that is, all three coefficients of the characteristic polynomial are required to be the same sign, regardless of whether it is positive or negative. Of course, from an engineering point of view, the injection energy makes no sense unless it is much larger than the equilibrium plasma temperature, T_0; otherwise, the capital investment used to inject energetic particles would be wasted. In fact, pure fusion machines are expected to operate with injection energies of hundreds of keV versus plasma temperatures of tens of keV.[29,30,92] The recent successful injection heating experiments on the Princeton Large Torus (PLT) Tokamak system support this heating method. Temperatures above 5 keV and possibly as high as 7 keV were reached for the first time in a large Tokamak device.[9,103]

For the case when feedback is applied, Criteria II and III remain very similar to those which were developed without feedback. Criterion I is completely new since it is introduced essentially because of the feedback. No confinement times are involved in Criterion I which depends only on the feedback coefficient and its delay time in addition to the ratio of injected energy to plasma temperature. Although the open loop (no feedback) plasma model is found to be unstable with respect to feedrate perturbations for certain temperature ranges, the closed loop system can be made stable to small perturbations over much of the previously unstable temperature range.

Again, these results for plasma stability agree with those of Ohta; but in this development, the system concept of transfer functions is used with more reliance on the physics of the plasma system to justify examining perturbations in feedrate as the governing plasma parameter. The present analysis has much broader application to more sophisticated systems as needed. Note that it is the feedrate alone--assuming as is usually done,[15,18,19,21-24] that the injection energy is constant--that affects the plasma content and behavior, as an external influence in these global models. All other influences on the plasma depend on the model used and parameters within the system itself. Only the feedrate, $S(t)$, or the feed energy, $T_S(t)$, affects the plasma from an external source.

Some studies have attempted to look at other external influences on the plasma. Specifically, the primary effect considered by these other studies has been the effect of a changing magnetic field and concurrently (causally) a changing plasma volume.[96,97] To include such effects in this model would have needlessly increased the complexity and number of equations needed to represent the fusioning plasma and its dynamic behavior. Such increased complexity was not justified because the fusioning plasma is only the driver of the hybrid, dual fusion-fission system which is the primary subject of this analysis. Therefore, the basic plasma model as utilized here to drive a hybrid blanket is complete.

The very important result was noted that these three stability criteria are the same as those obtained by Ohta et al.[18] Although the plasma neutron production rate is now included, this additional complication of the overall model does not affect stability requirements which was expected. Essentially, the previously applied point-model plasma and

its related stability were given more general applicability by the development of the transfer function basis in this work. This approach also allows more general model development. It is also important to realize that linearized analysis usually predicts correctly whether or not a system or a model is stable. However, if the system is unstable, linearized analysis is not capable of predicting the true consequences resulting from input perturbations.

CHAPTER 3

A HYBRID REACTOR ANALYTICAL MODEL

Development of the Hybrid Model

Consideration was next given to an analytical model which could be used to describe the dynamic behavior of the fusion-fission hybrid system. This same model, in linearized form, was used to establish stability criteria for the hybrid system. The plasma model for a power-producing fusion reactor has already been presented in Chapter 2 and was assumed to apply directly to the hybrid reactor plasma core. Although the plasma will not be self-sustaining for the hybrid case, the plasma core must still be in steady-state equilibrium for the neutron production rate required to meet the power rating of the hybrid system. Since the hybrid plasma is not expected to be self-sustaining, more energy will be required to confine and maintain it than is produced by fusion reactions.

The same three equations for plasma particle density, $n(t)$, plasma energy density, $3n(t)T(t)$, and plasma volumetric neutron production rate, $q_p(t)$, were used to describe the global dynamic behavior of the hybrid reactor plasma core as follows:

Plasma Ion Density:

$$\frac{dn(t)}{dt} = S(t) - \frac{n(t)}{\tau_n} - f_1(T)n^2(t) \qquad (91)$$

Plasma Energy Density:

$$\frac{d[n(t)T(t)]}{dt} = f_2(T)n^2(t) - \frac{n(t)T(t)}{\tau_E} + \frac{T_s S(t)}{3} \tag{92}$$

Plasma Volumetric Neutron Production Rate:

$$q_p(t) = g(T)n^2(t) \quad . \tag{93}$$

In the absence of any feedback effects, the global dynamic behavior of the plasma core of the hybrid is completely determined by these three equations where temperature-dependent coefficients are defined as before:

$$f_1(T) = \frac{<\sigma v>_{DT}}{2} \quad , \tag{94a}$$

$$f_2(T) = \frac{<\sigma v>_{DT} Q_\alpha}{12} - bT^{1/2}(t) \quad , \tag{94b}$$

and

$$g(T) = \frac{<\sigma v>_{DT}}{4} \quad . \tag{94c}$$

Only ion density and plasma temperature are needed to describe completely the state of the plasma in this model; that is, only the density and energy equations are actually needed for stability analysis of the plasma in isolation. However, to analyze the hybrid system, the specific neutron production rate was explicitly included in the model as noted in Chapter 2. In addition, since the neutrons produced by the plasma are its only means of effecting changes in the hybrid blanket flux distributions and power production in this model, the plasma volumetric neutron source equation was required for physical interpretation and

modeling of the functioning hybrid. These three equations completely
determine the nonlinear dynamic behavior of the hybrid plasma under the
assumption that no feedback is applied.

To determine the global stability criteria for the hybrid system,
the same procedure was applied as for the pure fusion system. The plasma
model consists of essentially the same equations although the plasma
itself is considerably less reactive as shown in Table C-I of Appendix C.
The linearized perturbed form of the plasma equations was obtained and
linear stability of the hybrid was determined for small perturbations in
the steady-state equilibrium operation of the hybrid plasma core which
is not self-sustaining. Burnup in the fusioning plasma was neglected
from the beginning in the formulation of the hybrid linearized model
because the inclusion of burnup effects was demonstrated in Appendix C
as well as in comparison with previous analyses of pure fusion
plasmas[23,24,95] to be nearly negligible in its effect on the less
reactive hybrid plasmas of interest in this analysis. Therefore, such
small burnup-induced effects on total particle confinement time were
completely eliminated in the simplified linearized plasma model equa-
tions. The linearized plasma equations in the perturbed variables are
repeated without burnup from Eqs. (46), (47), and (48) in Chapter 2 as
follows:

Plasma Ion Density:

$$\frac{1}{n_0} \frac{d\delta n(t)}{dt} = -\left(\frac{1}{\tau_{n_0}} + \frac{1}{\tau_{n1}}\right) \frac{\delta n(t)}{n_0} - \frac{1}{\tau_{T1}} \frac{\delta T(t)}{T_0} + \frac{\delta S(t)}{n_0} \tag{95}$$

Plasma Energy Density:

$$\frac{1}{n_0} \frac{d\delta n(t)}{dt} + \frac{1}{T_0} \frac{d\delta T(t)}{dt} = (\frac{1}{\tau_1} - \frac{1}{\tau_{E_0}}) \frac{\delta n(t)}{n_0} + (\frac{1}{\tau_2} - \frac{1}{\tau_{E_0}}) \frac{\delta T(t)}{T_0} + \frac{T_s}{3T_0} \frac{\delta S(t)}{n_0}$$

(96)

Plasma Volumetric Neutron Production Rate:

$$\delta q_p(t) = 2n_0 g(T_0) \, \delta n(t) + n_0^2 \left. \frac{\partial g(T)}{\partial T} \right|_0 \delta T(t) \ .$$

(97)

Except for feedback effects, the linearized stability analysis of the hybrid plasma core was completely determined by these three linearized plasma equations just as for the pure fusion system.

The fissile hybrid blanket model was developed using the point reactor kinetics equations which were used to describe the kinetic behavior of the neutron population in the blanket. Typically, seven point reactor kinetics equations are applicable. One equation gives the neutron density, $N(t)$, which can be related to neutron flux or power by a multiplicative factor; one additional equation applies each precursor concentration, $C_i(t)$, corresponding to one of six possible delayed neutron groups. This model is summarized in the following well-known fission reactor formulation of global reactor kinetics:[104]

$$\frac{dN(t)}{dt} = [\frac{\rho(t) - \bar{\beta}}{\Lambda}] N(t) + \sum_{i=1}^{6} \lambda_i C_i(t) + q_{B_{eff}}(t)$$

(98)

and

$$\frac{dC_i(t)}{dt} = \frac{\beta_i}{\Lambda} N(t) - \lambda_i C_i(t) \qquad i = 1,2,\ldots 6$$

(99)

where the symbols used in these equations were defined as follows:

$N(t)$ = neutron density in the blanket $(\#/cm^3)$

$C_i(t)$ = effective delayed neutron precursor concentration for ith delayed neutron group in the blanket $(\#/cm^3)$

$\rho(t)$ = blanket reactivity

$q_{B_{eff}}(t)$ = effective neutron source strength in the blanket $(\#/cm^3\text{-sec})$

$\overline{\beta}$ = total effective delayed neutron fraction in the fissile blanket

β_i = effective delayed neutron fraction of the ith group of precursors in the blanket

Λ = neutron generation time in the blanket (sec)

λ_i = decay constant for the ith group of precursors (1/sec).

The effective delayed neutron fractions and the neutron generation time in the fissile blanket were assumed time-independent for the hybrid model.

The effective neutron source strength was defined by the following equation:

$$q_{B_{eff}}(t) = \frac{1}{\Lambda f} \int_{\vec{r}} \int_{E} q_{B_{ACT}}(\vec{r},E,t)\phi_0^+(\vec{r},E)d\vec{r}dE \qquad (100)$$

where angular dependence has been neglected and,

$\phi_0^+(\vec{r},E)$ = the adjoint flux for the critical reference system as a function of position, r, and energy, E

$q_{B_{ACT}}(\vec{r},E,t)$ = the true or actual source strength as a function of position, energy, and time

f = the production operator.

Standard definitions for the production operator, f, as well as $C_i(t)$, $\bar{\beta}$, β_i, $\rho(t)$, and Λ, can be found in the usual references on reactor kinetics.[105,106]

The effective neutron source strength, $q_{B_{eff}}(t)$, is a weighted quantity which was used to account, in lumped parameter fashion, for the neutron source in the fissile hybrid blanket due to the fusion neutrons produced in the plasma. This fusion neutron source represents a unique characteristic of fissile hybrid blankets versus the usual fission reactor kinetic analysis on subcritical fissile systems; for example, neutron sources are used to produce an easily monitored neutron flux level in a subcritical fuel assembly prior to startup in a power reactor.[107,108]

The blanket neutron energy deposition per fusion event, Q_B, is a global parameter which consists of three terms derived in Appendix A due to fission energy deposition, fusion neutron energy deposition, and exothermic reaction energy deposition as follows:

$$Q_B = \frac{G_f}{\bar{\nu}} \left[\frac{k_{eff}}{1 - k_{eff}}\right] + E_n + \delta_E \tag{101}$$

where

> G_f = fission energy deposited in the blanket per fission event
>
> $\bar{\nu}$ = average number of fission neutrons produced per fission event
>
> k_{eff} = effective blanket neutron multiplication factor
>
> E_n = energy associated with a source neutron entering the blanket
>
> δ_E = any additional energy deposited in the blanket due to exothermic neutron absorption reactions for example.

The resultant blanket neutron energy multiplication factor, M_B, is simply the ratio of energy deposited in the blanket (Q_B) to energy input to the

blanket as follows:

$$M_B = Q_B/E_n \tag{102}$$

which is also strictly global; despite its extensive use in previous analyses of hybrid blankets and their neutronics,[1,64,76,77] results obtained in this work and reported in Chapter 5 indicate that Eq. (101) is inadequate for a spatially-dependent analysis of multiplying hybrid blanket properties. Estimation of the theoretical global power involves only the use of a relationship such as

$$P_{B_{EST}} = Q_p(t) \cdot Q_B = Q_p(t) \, M_B E_n \tag{103}$$

where $Q_p(t)$ is the total fusion neutron production rate. This estimated blanket power production, $P_{B_{EST}}$, incorporates the shortcomings associated with the blanket neutron energy deposition factor so it is of no use for scaling as shown in Appendix A.

The hybrid blanket is driven to power production by a surface inhomogeneous source leaving the plasma. For the hybrid model the surface source strength, $q_s(t)$, from the plasma was expressed as follows:

$$q_s(t) = \frac{Q_p(t)}{A_s} \tag{104}$$

where A_s is the inner blanket surface area facing the plasma and $Q_p(t)$ is the total plasma neutron production rate. The total plasma neutron production rate was derived as follows:

$$Q_p(t) = q_p(t) \cdot V_p \tag{105}$$

where V_p is the constant plasma volume and $q_p(t)$ is the lumped plasma volumetric neutron production rate.

For use in a point kinetics calculation, this actual surface source was converted to an effective surface source using Eq. (100). This is the usual adjoint-weighted source term used in the point kinetics equations. Note that the integration involved in this definition would have to be transformed from a volume to a surface integral in this case.

Alternatively, a surface conversion coefficient, ζ_1, can be determined by comparing the results of lumped parameter or point-model blanket power (neutron density) calculations using the blanket neutron energy multiplication in Eq. (103) with the results of space- and energy-dependent power (neutron density or flux) calculations performed using diffusion theory, transport theory, or some other space-dependent neutronic model for determining actual neutron density distributions and power levels in a fissile medium. So the surface conversion coefficient for use in the hybrid model was defined as follows:

$$\zeta_1 = \frac{P_{B_{ACT}}}{P_{B_{EST}}} \tag{106}$$

where $P_{B_{ACT}}$ is the actual or true system power calculated from the surface source in a space- and energy-dependent calculation, and $P_{B_{EST}}$ is the estimated power generation. Calculations described in Chapter 5 found the actual power was less than the estimated power so that the conversion coefficient, ζ_1, is less than unity--at least for the thermal fission hybrid system considered in Chapter 5. Since the neutron source enters the blanket at a surface and not within the main blanket volume, the

surface conversion coefficient was expected to be less than one although
the increased energy of fusion neutrons over fission spectrum neutrons
was expected to compensate for most, if not all, of the decreased neutron
worth. The surface source conversion coefficient was used to relate the
geometrically "equivalent" surface source, $q_s(t)$, to the effective sur-
face source for inclusion in the point kinetics equations as follows:

$$q_{B_{eff}} = \zeta_1 q_s(t) \tag{107}$$

and

$$q_{B_{eff}} = \zeta_1 \frac{V_p}{A_s} q_p(t) \tag{108}$$

where the effective surface source is related directly to the plasma
neutron volumetric production rate. Note that such an effective area
source requires the point kinetics equations to be modified to get a
dimensionally consistent set.

Each of the calculations performed to obtain the actual blanket
power generation involved an inhomogeneous, multigroup, spatially-
dependent, steady-state calculation over the blanket while the corres-
ponding theoretical global power calculation involved only the use of a
relationship such as Eq. (103). For a given total neutron source pro-
duction rate or source strength in the plasma, $Q_p(t)$, the estimation of
blanket power generation, $P_{B_{EST}}$, was performed using global blanket cal-
culations based on the blanket energy deposition factor, Q_B. Some energy
dependence was included by basing the average neutrons per fission on
the neutron spectrum involved in the inhomogeneous calculation. Implicit
in such global calculations is the assumption that the planar source

of neutrons can be treated in a manner that is not spatial vary-
ing.

Depending on the available computational tools, it may be desirable
or necessary to work with an "equivalent" volumetric source rather than
a surface source. In fact, this is usually the case so that there is
no need to correct dimensions in the point kinetics equations. It is
more convenient to work with volume sources in the kinetic equations
because the other terms are related to volumes. The corresponding volu-
metric neutron source strength in the hybrid blanket can be written as
follows:

$$q_B(t) = \frac{A_s}{V_B} q_s(t) \tag{109}$$

where V_B is the effective hybrid fissile blanket volume. This equation is
again based on purely geometric equivalence or conservation of neutrons
and is also written as follows:

$$q_B(t) = \frac{Q_p(t)}{V_B} \quad . \tag{110}$$

Note that this volumetric source, $q_B(t)$, conserves neutrons but not their
effectiveness. It is simply an "equivalent" volumetric source obtained
from geometrical consideration of the actual surface source just as
$q_s(t)$ was for the surface case. When this neutron source strength,
$q_B(t)$, is properly weighted, it provides a simple conceptual input for
the source term which is used to drive the subcritical fissile blanket.
This weighted or effective inhomogeneous source term, along with the
other kinetic parameters, was used in the point model fission kinetic
equations to obtain the variation of neutron density (or power or flux)

with time following source insertion or alteration as well as any other type of neutronic perturbation in the blanket system. However, the underlying assumption for use of the kinetics equations in general, and the source definition in Eq. (109) in particular, is that a global or point model treatment of the blanket is valid. This "equivalent" volumetric source, $q_B(t)$, is not sufficient for use in the point-model equations but must first be converted to an effective source in the same way that the surface source was converted, except the actual calculation involves a distributed volume source, $q_B(t)$, instead of a surface source, $q_s(t)$. The source term, $q_B(t)$, is presented only as a volume-normalized source in Eq. (110); however, the fusion neutron source driving the blanket is actually a nearly planar (large radius toroidal surface for the actual blanket model presented in Appendix B) source of 14.06 MeV neutrons entering the hybrid blanket through the inner surface containing the plasma. Such a geometry is not conducive inherently to a global treatment--at least, not without some further assumptions. Of course, the neutrons are also not introduced with a fission spectrum which is another reason why they are not amenable to a simple global treatment.

Equation (100) can be directly used to perform this conversion of the "equivalent" volume source to an effective volume source in order to obtain the adjoint-weighted volumetric neutron source for inclusion in the point kinetics equations. Alternatively, a second conversion coefficient, ς_2, can be defined. This volume conversion coefficient was obtained from the same equation as the surface conversion coefficient:

$$\varsigma_2 = \frac{P_{B_{ACT}}}{P_{B_{EST}}} \, , \tag{111}$$

except that the actual power, $P_{B_{ACT}}$, was obtained from a space-dependent and energy-dependent neutronics calculation using a distributed volume source instead of a surface source. The estimated power was obtained from the same global energy multiplication/deposition relation in Eq. (103). So the volume conversion coefficient relates the geometrically "equivalent" volume source to the effective volume source for inclusion in the point kinetics equations as follows:

$$q_{B_{eff}}(t) = \zeta_2 \, q_B(t) \qquad (112)$$

or

$$q_{B_{eff}}(t) = \zeta_2 \, \frac{A_s}{V_B} \, q_s(t) \qquad (113)$$

and

$$q_{B_{eff}}(t) = \zeta_2 \, \frac{V_p}{V_B} \, q_p(t) \qquad (114)$$

where the conversion coefficient, ζ_2, relates the effective neutron source, $q_{B_{eff}}$, required (as by flux distribution calculations using an actual surface driving source) to the calculated source strength, q_B, obtained by simple global analysis using only geometric effects as in Eqs. (109) and (110). Essentially, the inclusion of either conversion coefficient, ζ_1 or ζ_2, in this model recognizes the inhomogeneous nature of surface fusion neutron sources and the resultant inadequacy of a simple global representation of the source itself.

Analysis of neutron density (or power) transients using the point-model kinetics equations is limited to amplitude changes; the point-model formulation cannot account for changes in the neutron flux shape during

a transient. As the name indicates, the point model is applicable to a global reactor or blanket treatment (a zero-dimensional system) during a transient. Of course, the plasma model is also zero-dimensional since Eqs. (91-93) cannot account for spatial variations in any of the plasma parameters such as ion density, temperature, or volumetric neutron production rate.

In more sophisticated transient analyses using the adiabatic or quasistatic methods, the slow variation or the shape function is used to justify point-model calculations of transient neutron density changes over relatively long intervals with companion recalculations of the applicable changed shape function at widely spaced intervals. In this way relatively long transients or transients involving significant spatial changes in the neutron population can be analyzed.[105,106] Such is <u>not</u> the case for pure point-model analysis.

A generalized neutron density variable, $N(\vec{r}, E, \vec{\Omega}, t)$, can be written as a function of position, energy, direction of neutron movement, and time, respectively. Since the neutron energy, E, and direction of motion, $\vec{\Omega}$, variables are of secondary concern in this dynamic analysis, the neutron density can be reduced to a dependence on only position and time as $N(\vec{r}, t)$.

The point reactor concept is based on a reassignment of the spatial and temporal dependence of the neutron density as the product of an amplitude function, $N(t)$, and a shape function, $\psi(\vec{r}, t)$, as follows:

$$N(\vec{r}, t) = N(t) \cdot \psi(\vec{r}, t) \ . \tag{115}$$

All spatial variations in the neutron density are contained in the normalized shape function, $\psi(\vec{r}, t)$, which is assumed in this global model to

be slowly varying in time. Such a global reduction to consideration of only temporal variations is a common method of analysis if transient shapes are not expected to vary appreciably from steady-state equilibrium distributions.[105]

When the point reactor kinetics equations are applied to a reactor such as the hybrid blanket, only the magnitude of the neutron density (or equivalently the power or flux) is taken into account during any hypothetical transient. Temporal changes in the neutron density shape function cannot be analyzed with these equations; only temporal changes in the magnitude of the neutron density are contained in the amplitude function, $N(t)$. Therefore, the application of the point model equations yields the magnitude of the neutron density during a transient assuming the final shape, $\psi(\vec{r},t)$, at time, t, is unchanged from the initial shape, $\psi(\vec{r},t_0)$, at time, t_0. If the transient under consideration is sufficiently large, asymmetrically introduced, or allowed to run long enough so the flux shape changes significantly then results based on the point model will be inadequate to describe the exact dynamic behavior of the neutron population. Although inaccurate, such results can still be used to indicate trends and, for small transients, yield approximate values of maximum power densities and possible destruction or excessive power density zones. Such point-model results cannot be used for final design analysis for which the full space-time analysis of transients is required. Nevertheless, the point-model dynamics results can be used for studying stability and transients in reactor systems. Therefore, the basic assumption implied in using these point-model equations to model the kinetic behavior of a subcritical hybrid blanket is that the shape function for the spatial dependence of the neutron density does not change

significantly over the time scale during which these equations are used to describe transient behavior.

This assumption is very adequate when the sizes of typical "realistic" hybrid plasma transients are considered. Calculations for typical hybrid plasma perturbations in Chapter 4 demonstrate that relatively small transients in plasma neutron production result from typical ($\pm$ 5%) perturbations in different hybrid plasma equilibrium conditions such as plasma temperature, plasma ion density, source feedrate, and injection energy.

Because the hybrid blanket will be subcritical, the effects of delayed neutrons are expected to be less important in the subcritical blanket of the hybrid system than in a critical power-producing reactor. The delayed neutrons will not be needed to maintain power-producing capability. In fact, since proposed operating parameters for the hybrid blanket indicate subcriticality at room temperature, the typical temperature defect in core reactivity due to heat up and ultimate buildup of blanket poisons indicates that the blanket will be far subcritical during actual hybrid power operation. This large negative reactivity will make delayed neutrons even less important.[109] Therefore, the six delayed neutron groups were combined into one effective group with no loss in applicability of the model to typical hybrid systems. The seven point reactor kinetics equations were reduced to the usual pair of equations for the neutron density, $N(t)$, and the total precursor concentration, $C(t)$:

$$\frac{dN(t)}{dt} = [\frac{\rho(t) - \bar{\beta}}{\Lambda}] N(t) + \bar{\lambda} C(t) + q_{B_{eff}}(t) \tag{116}$$

and

$$\frac{dC(t)}{dt} = \frac{\overline{\beta}}{\Lambda} N(t) - \overline{\lambda}C(t) \tag{117}$$

where $C(t)$ is the effective precursor concentration for all six delayed groups; $q_{B_{eff}}(t)$ is the effective blanket neutron source whether an effective surface source or an effective volume source; and $\overline{\lambda}$ is the average decay constant for six groups of delayed neutron precursors:

$$\overline{\lambda} = \frac{\overline{\beta}}{\displaystyle\sum_{i=1}^{6} \frac{\beta_i}{\lambda_i}} \quad . \tag{118}$$

The Linearized Hybrid Model

Equation (112) for the neutron density is nonlinear due to the reactivity-density product term, $\rho(t)N(t)/\Lambda$; therefore, these equations were linearized prior to stability analysis. These equations are, however, far less nonlinear than the plasma model equations developed in Chapter 2. The following usual small perturbation expansions of the dependent variables about an initial equilibrium were used:

$$N(t) = N_0 + \delta N(t) \; , \tag{119a}$$

$$C(t) = C_0 + \delta C(t) \; , \tag{119b}$$

$$\rho(t) = \rho_0 + \delta\rho(t) \; , \tag{119c}$$

$$q_{B_{eff}}(t) = q_{B_{eff_0}} + \delta q_{B_{eff}}(t) \quad , \tag{119d}$$

where the variations in the reactivity and the inhomogeneous volume source in the blanket were both retained. This simultaneous retention of the

reactivity as well as the blanket source perturbation is unique to hybrid blanket system analysis where both perturbations are required in determining how the neutron density and power changes in the symbiotic blanket system are dependent on the plasma feedrate. No other work has considered or even commented upon this set of unique conditions in a hybrid model.

After substitution of the perturbed variables of Eqs. (119a)-(119d) into the point-model reactor kinetics equations, the following pair of expanded kinetics formulations were obtained:

$$\frac{d\delta N(t)}{dt} = (\frac{\rho_o - \overline{\beta}}{\Lambda})N_o + (\frac{\rho_o - \overline{\beta}}{\Lambda})\delta N(t) + \frac{N_o \delta\rho(t)}{\Lambda} + \frac{\delta\rho(t)\delta N(t)}{\Lambda} + \overline{\lambda}C_o + \overline{\lambda}\delta C(t)$$

$$+ q_{B_{eff_o}} + \delta q_{B_{eff}}(t) \tag{120}$$

$$\frac{d\delta C(t)}{dt} = \frac{\overline{\beta}}{\Lambda} N_o + \frac{\overline{\beta}}{\Lambda} \delta N(t) - \overline{\lambda}C_o - \lambda\delta C(t) \quad . \tag{121}$$

Because of the assumption of small perturbations, the second order, non-linear term, $\delta\rho(t)\delta N(t)/\Lambda$, was neglected as usual. The two initial equilibrium conditions were also eliminated so that linearized perturbed point reactor kinetics equations of the following form were produced:

Perturbed Blanket Neutron Density:

$$\frac{d\delta N(t)}{dt} = (\frac{\rho_o - \overline{\beta}}{\Lambda}) \delta N(t) + \frac{N_o}{\Lambda} \delta\rho(t) + \overline{\lambda}\delta C(t) + \delta q_{B_{eff}}(t) \tag{122}$$

Perturbed Precursor Concentration:

$$\frac{d\delta C(t)}{dt} = \frac{\overline{\beta}}{\Lambda} \delta N(t) - \overline{\lambda}\delta C(t) \quad . \tag{123}$$

These linearized perturbed point kinetics equations are in the same form encountered in fission reactor kinetics with one exception--both the inhomogeneous effective volumetric neutron source strength perturbation, $\delta q_{B_{eff}}(t)$, and the reactivity perturbation, $\delta \rho(t)$, of the blanket are incorporated in this model simultaneously. This unique feature of hybrid reactor kinetics analysis introduces considerable interplay of variable dependences in the hybrid model.

In the linearized kinetics analysis of ordinary fission reactors, one or the other of these two variations of transient-producing terms is completely negligible. In the usual analysis of subcritical systems, the reactivity perturbation due to a source variation for a zero-power system is expected to be zero while the source variation is itself retained; similarly, in the kinetic analysis of critical or supercritical power-producing reactors, the source perturbation in the presence of a reactivity variation is assumed to be zero since inhomogeneous source variations have a negligible effect on a critical power-producing system.[110]

For example, in a subcritical assembly--perhaps a research system or a LWR during fuel loading--interest is directed toward the so-called source perturbation and the associated-source transfer function, $\Delta N(s)/\Delta q_{B_{eff}}(s)$, for stability analysis. It is this quantity in ordinary subcritical reactor kinetics which is likened to the volumetric source feedrate transfer function, $\Delta q_p(s)/\Delta S(s)$, derived in Chapter 2 for characterization of plasma stability. Both transfer functions represent output neutron densities (or power) due to input source perturbations in either the ion feedrate for the plasma or the neutron source for the subcritical assembly. On the other hand, in a critical power-producing

system such as a large PWR or even a research reactor at power, the changes in reactivity, $\delta\rho(t)$, and the corresponding reactivity transfer function, $\Delta N(s)/\Delta\rho(s)$, are the quantities of interest. Any perturbations due to an inhomogeneous source are negligible in a transient analysis.

In the hybrid blanket, the effective volumetric neutron source, $q_{B_{eff}}(t)$, will be so large that its perturbations were included along with perturbations in the reactivity because both the fusioning plasma with its volumetric driving source of neutrons, $q_p(t)$, and the fissioning blanket with its driven reactivity, $\rho(t)$, are required to sustain the overall system in a power-producing mode. Since both the effective neutron source and the reactivity are needed, perturbations in both variables were included in the linearized hybrid kinetics equations. Only for the hybrid case, where the inhomogeneous source is so large and the blanket is subcritical, is there a need to account for the effects of both perturbed variables simultaneously in determining system stability and dynamic behavior.

In addition, Eq. (114) for the volumetric neutron source conversion coefficient was used to relate the effective volumetric neutron source in the blanket to the volumetric neutron production rate in the fusioning plasma as follows:

$$q_{B_{eff}}(t) = \frac{\varsigma_2 \, V_p \, q_p(t)}{V_B} \quad . \tag{124}$$

The surface neutron conversion coefficient could have been used but volumes are more applicable. As usual perturbations in both volumetric sources about the steady-state $[q_{B_{eff}}(t) = q_{Beff_0} + \delta q_{B_{eff}}(t)$ and $q_p(t) = q_{p_0} + \delta q_p(t)]$ were used to obtain the following perturbed and linearized

volumetric neutron conversion coefficient equation:

$$\delta q_{B_{eff}}(t) = \frac{\zeta_2 \ V_p \ \delta q_p(t)}{V_B}$$

(125)

where the steady-state condition has been eliminated.

Because the hybrid is a power-producing system, a power scaling equation was required to relate neutron density to power density as follows:

$$p(t) = G_f \ \overline{\Sigma}_f \ \overline{v} \ N(t)$$

(126)

where

$p(t)$ = power density in the fissile hybrid blanket (W/cm^3)

G_f = average energy per fission (ergs/fission)

$\overline{v}$ = average neutron velocity in the fissile blanket (cm/sec)

$\overline{\Sigma}_f$ = average macroscopic fission cross section of the fissile blanket (1/cm).

The three multiplicative coefficients ($G_f, \overline{v}, \overline{\Sigma}_f$) were assumed constant as in typical transient analyses. Certainly for the short-term blanket transients caused by plasma perturbations considered here, these coefficients will not change significantly. Although already in linear form, this scaling equation was converted into perturbed form to be compatible with the global plasma and blanket kinetics equations which were perturbed for linear stability analysis. The blanket power density was represented as the sum of a steady-state, equilibrium power level plus the usual small perturbation, $p(t) = p_0 + \delta p(t)$. The resultant perturbed form of the linear power density scaling equation was obtained as follows:

$$\delta p(t) = G_f \, \overline{\Sigma}_f \, \overline{v} \, \delta N(t) \, , \tag{127}$$

since only the neutron density was allowed to vary with time.

At this point some form of heat transfer relationship was needed to provide the overall hybrid model with a means of removing energy from the system. Based on the typical heterogeneous unit cell arrangement consisting of helium coolant, graphite moderator, and fuel material, a lumped parameter model using three temperature nodes could have been used to represent the heat transfer processes in the blanket. No generality would be lost by such an assignment of constituents and nodes in the unit cell since other fuels, other moderators, and other coolants could be treated in the same way. They were not included here to prevent un-necessary complication in the basic hybrid model.

For this initial linearized analysis of system stability and kinetic behavior, a single temperature node was selected for the fissile blanket. The blanket temperature was treated as a global parameter just as the neutron density was treated in the neutron dynamics model of Eqs. (98) and (99). By utilizing a single average blanket temperature, T_B, the simplicity of the model was retained along with the interaction of plasma and blanket effects.

This global blanket temperature model can be employed for linear stability studies as well as for the dynamics analysis of the hybrid system. Although informative dynamics results can be obtained, more detailed multinodal temperature analysis of the blanket will be required prior to selection of a hybrid design for final analysis and installation. The present study was not so concerned with the temperature-dependence in the blanket but only its general behavior through development of the overall hybrid model.

To proceed with development of the hybrid analytical model, the global blanket temperature was related to power. A single, effective helium coolant temperature, $\overline{T}_C$, was assumed along with Newton's law of cooling to obtain an overall fissile blanket energy balance as follows:

$$c_{p_B} m_B \frac{dT_B(t)}{dt} = p(t)V_B - hA_C[T_B(t) - \overline{T}_C] \qquad (128)$$

where

c_{p_B} = fissile blanket average specific heat (ergs/gm°K)

m_B = fissile blanket mass (gm)

$T_B(t)$ = average fissile blanket temperature (°K)

$p(t)$ = average fissile blanket power density W/cm^3)

h = effective average blanket conductance between graphite modulator and helium coolant (W/cm^2-°K)

A_C = total effective coolant channel area across which heat flows from the graphite moderator to the helium coolant (cm^2)

$\overline{T}_C$ = average bulk helium coolant temperature (°K)

V_B = effective fissile blanket volume (cm^3).

The steady-state condition was represented by

$$0 = p_o V_B - hA_C(T_{B_o} - \overline{T}_C) \qquad (129)$$

where the coolant temperature was essentially assumed constant and T_{B_o} was used to represent the average blanket temperature for the initial equilibrium state. Certainly, variations in the fuel and moderator temperatures would be expected to be much larger than variation in the temperature of the coolant which can have more or less heat removed in a heat exchanger to keep it constant. Since coolant temperatures do not vary as much as

fuel temperatures anyway, the helium coolant temperature was eliminated from Eqs. (128) and (129) to obtain the following result:

$$c_{p_B} m_B \frac{dT_B(t)}{dt} = V_B p(t) - p_0 V_B - hA_C [T_B(t) - T_{B_0}] \quad . \tag{130}$$

This equation has frequently been employed in linear stability studies.[111] To make this equation compatible with the previously linearized hybrid equations, small variations about the equilibrium state were again utilized:

$$T_B(t) = T_{B_0} + \delta T_B(t) \tag{131a}$$

$$p(t) = p_0 + \delta p(t) \quad . \tag{131b}$$

These perturbed variables of Eqs. (131a) and (131b) were substituted into Eq. (130) to obtain the following linearized equation in the perturbations:

$$c_{p_B} m_B \frac{d\delta T_B(t)}{dt} = V_B \delta p(t) - hA_C \delta T_B(t) \quad . \tag{132}$$

With the development of this blanket temperature equation, the feedforward part of the linearized hybrid system model is complete; however, feedback effects are also necessary to complete a general hybrid analytical model.

Incorporation of Feedback Effects into the Hybrid Model

At this point the analytical hybrid model was sufficiently developed to trace the dynamic effects due to an initial perturbation in the plasma feedrate from effects on the plasma density and temperature through

effects on the blanket neutron density and power production and finally to changes in the global blanket temperature. The global equations presented can be used to analyze the dynamic behavior and, in linearized form, to predict the stability limits of the point-model system in the absence of controlling feedback effects. However, several feedback terms were required to complete the overall analytical model of global fusion-fission reactor dynamics. Although the linearized hybrid dynamics model is valid only for small perturbations, the influence of feedback effects on stability criteria cannot be ignored. This is especially true since uncontrolled pure fusion plasmas are predicted unstable to temperature perturbations for proposed operating temperatures and expected confinement characteristics.[18,23,24] Indeed, much the same condition was found to hold for hybrid plasmas in Chapter 4 depending on the equilibrium operating conditions selected.

First, the neutron-producing plasma subsystem may be unstable to temperature and other perturbations at expected thermonuclear operating temperatures in the hybrid core below 28 keV for the constant confinement model ($\tau \sim$ constant). Therefore, the artificial temperature feedback previously applied for pure fusion systems was incorporated into the hybrid model as follows:

$$S(t) = S_0 + \alpha_1 \frac{n_0}{T_0} [T(t) - T_0]u(t - t_{d_1}) \qquad (133)$$

which was used to show that the feedback due to a plasma temperature variation from a steady-state temperature, T_0, is applied to the feed-rate after a delay time, t_{d_1}, via the delayed unit step function,

$u(t - t_{d_1})$. The factor, n_0/T_0, was used to normalize the temperature variation to the feedrate so that the feedback coefficient, α_1, has units of inverse seconds. The usual perturbed formulation, $\delta S(t)$, about equilibrium was introduced to obtain the following feedback equation:

$$\delta S(t) = \alpha_1 \frac{n_0}{T_0} \delta T(t - t_{d_1}) \quad . \tag{134}$$

A second, less effective source of artificial feedrate feedback was incorporated through variations in the global blanket temperature. In this model blanket power fluctuations can cause changes in the effective blanket temperature. This feedback was applied to the plasma feedrate in the following form similar to that for the plasma temperature feedback:

$$S(t) = S_0 + \alpha_2 \frac{n_0}{T} [T_B(t) - T]u(t - t_{d_2}) \tag{135}$$

where the normalization factor, n_0/T_{B_0}, was used so this externally controlled or artificial power feedback coefficient, α_2, would have the same units of inverse seconds as the artificial plasma temperature feedback coefficient. The usual perturbed formulation of this feedback equation was obtained:

$$\delta S(t) = \alpha_2 \frac{n_0}{T_{B_0}} \delta T_B(t - t_{d_2}) \quad . \tag{136}$$

These two delayed, artificial feedback effects in Eqs. (132) and (134) were combined into a single analytical expression relating perturbations in plasma temperature and blanket temperature to the driving plasma

feedrate via delayed artificial feedback effects:

$$\delta S(t) = \alpha_1 \frac{n_o}{T_o} \delta T(t - t_{d_1}) + \alpha_2 \frac{n_o}{T_{B_o}} \delta T_B(t - t_{d_2}) \ . \tag{137}$$

The remaining feedback effect is a natural result of temperature changes within the blanket. The reactivity of the hybrid blanket was treated as a sum

$$\rho(t) = \rho_o + \rho_F(t) \tag{138}$$

where ρ_o is the reactivity (negative by design) of the subcritical blanket in the initial, steady-state, equilibrium condition and $\rho_F(t)$ is the additional reactivity of either sign added due to feedback effects resulting from departures from the initial equilibrium.

The blanket temperature was assumed to be the only parameter whose change would inherently affect the fissile blanket reactivity. The usual linear truncation of the Taylor series expansion representing the general nonlinear relation between reactivity and blanket temperature was included as follows:

$$\rho(t) = \rho_o + \alpha_T[T_B(t) - T_{B_o}] \tag{139}$$

where

α_T = the overall effective prompt temperature coefficient of reactivity

$T_B(t)$ = the average blanket temperature

T_{B_o} = the reference initial steady-state temperature for the equilibrium operation of the blanket system.

This natural temperature feedback was primarily based upon the doppler effect within the fuel for which there is little delay. Therefore, the assumption of instantaneous feedback on the blanket reactivity is reasonable. The model is simplistic, however, since the feedback effects are based on criticality evaluations of the fissile blanket for different equilibrium operating temperatures. Therefore, the net reactivity feedback effect was applied with no delay in this model in Eq. (139) as if the blanket temperature feedback were due exclusively to effects within the fuel such as doppler broadening.

Since primary interest is in the stability of the linearized hybrid model as well as short-term response to small perturbations in the plasma feedrate, only prompt reactivity feedback effects were included to maintain a simplified model upon which later analyses can expand to include the many delayed effects which must be considered prior to final design of the hybrid blanket.

Feedback directly to the reactivity, $\rho(t)$, via control rod assemblies may also be present but would be relatively long-acting. Such control rods would allow end-of-life operation in the event that optimum plasma operation were to be reached with no reserve capability remaining to increase the fusion source sufficiently to overcome reduced blanket multiplication. Hence, to maintain blanket power level given by

$$P_{B_{ACT}}(t) \propto Q_p(t) \cdot Q_B \tag{140}$$

in the presence of a decreasing reactivity, the energy production per fusion neutron must be increased by removing control rods and increasing the effective neutron multiplication factor of the blanket.

The entire question of control rod feedback was ignored in developing this linearized model. Only short-term feedback effects were considered to ensure stability for small perturbations where flux shapes in the fission blanket remain nearly constant.

Nonlinear and Linearized Hybrid Model Summary

The basic set of nonlinear global model equations derived to describe the dynamic behavior of a point-model, fusion-fission hybrid system is summarized in the following set of ten (10) equations:

Plasma Ion Density:

$$\frac{dn(t)}{dt} = S(t) - \frac{n(t)}{\tau_n} - \frac{<\sigma v>_{DT} n^2(t)}{2} \tag{141a}$$

Plasma Energy Density:

$$\frac{d[n(t)T(t)]}{dt} = \frac{<\sigma v>_{DT} Q_\alpha n^2(t)}{12} - bT^{1/2}(t)n^2(t) - \frac{n(t)T(t)}{\tau_E} + \frac{T_s S(t)}{3} \tag{141b}$$

Plasma Volumetric Neutron Production Rate:

$$q_p(t) = \frac{<\sigma v>_{DT} n^2(t)}{4} \tag{141c}$$

Blanket Neutron Density:

$$\frac{dN(t)}{dt} = [\frac{\rho(t) - \bar{\beta}}{\Lambda}] N(t) + \bar{\lambda}C(t) + q_{B_{eff}}(t) \tag{141d}$$

Blanket Delayed Neutron Precursor Concentration:

$$\frac{dC(t)}{dt} = \frac{\overline{\beta}}{\Lambda} N(t) - \overline{\lambda} C(t) \tag{141e}$$

Plasma to Blanket Neutron Conversion Coefficient:

$$q_{B_{eff}}(t) = \zeta_2 \frac{V_p}{V_B} q_p(t) \tag{141f}$$

Blanket Power Density:

$$p(t) = G_f \overline{\Sigma}_f \overline{v} N(t) \tag{141g}$$

Blanket Temperature and Heat Removal:

$$c_{p_B} m_B \frac{dT_B(t)}{dt} = p(t) V_B - h A_C [T_B(t) - \overline{T}_C] \tag{141h}$$

Blanket Temperature (Doppler) Feedback:

$$\rho(t) = \rho_0 + \alpha_T [T_B(t) - T_{B_0}] \tag{141i}$$

Plasma Feedrate Feedback (Blanket and Plasma Temperature):

$$S(t) = S_0 + \frac{\alpha_1 n_0}{T_0} [T(t) - T_0] u(t - t_{d_1}) + \frac{\alpha_2 n_0}{T_{B_0}} [T_B(t) - T_{B_0}] u(t - t_{d_2}) . \tag{141j}$$

At this point the entire perturbed and linearized set of coupled dynamics equations for the hybrid system is also summarized. First, two

global equations for plasma particle and energy density were applied in the plasma:

$$\frac{1}{n_0} \frac{d\delta n(t)}{dt} = -\left(\frac{1}{\tau_{n_0}} + \frac{1}{\tau_{n1}}\right) \frac{\delta n(t)}{n_0} - \frac{1}{\tau_{T1}} \frac{\delta T(t)}{T_0} + \frac{\delta S(t)}{n_0} \quad (142)$$

$$\frac{1}{n_0} \frac{d\delta n(t)}{dt} + \frac{1}{T_0} \frac{d\delta T(t)}{dt} = \left(\frac{1}{\tau_1} - \frac{1}{\tau_{E_0}}\right) \frac{\delta n(t)}{n_0} + \left(\frac{1}{\tau_2} - \frac{1}{\tau_{E_0}}\right) \frac{\delta T(t)}{T_0} + \frac{T_s}{3T_0} \frac{\delta S(t)}{n_0} \; .$$

$$(143)$$

In addition, two point-model reactor kinetics equations for neutron density and precursor concentration were applied in the blanket with one effective group of delayed neutrons:

$$\frac{d\delta N(t)}{dt} = \left(\frac{\rho_0 - \overline{\beta}}{\Lambda}\right) \delta N(t) + \frac{N_0}{\Lambda} \delta\rho(t) + \overline{\lambda}\delta C(t) \quad (144)$$

$$\frac{d\delta C(t)}{dt} = \frac{\overline{\beta}}{\Lambda} \delta N(t) - \overline{\lambda}\delta C(t) \; . \quad (145)$$

These two sets of basic describing equations for plasma and blanket dynamics were coupled in the feedforward direction by the linearized fusion neutron source equation for the perturbed plasma output:

$$\delta q_p(t) = 2n_0 g(T_0)\delta n(t) + n_0^2 \left.\frac{\partial t}{\partial T}\right|_0 \delta T(t) \quad (146)$$

and by the relationship for the surface conversion coefficient, ζ_1, or the volume conversion coefficient, ζ_2, giving the neutron worth for the perturbed blanket input as follows:

$$\delta q_{B_{eff}}(t) = \zeta_1 \frac{V_p}{A_S} \cdot \delta q_p(t) \qquad (147a)$$

$$\delta q_{B_{eff}}(t) = \zeta_2 \frac{V_p}{V_B} \cdot \delta q_p(t) \quad . \qquad (147b)$$

For the effective volumetric source applied in this work, Eq. (147b) was used. Since this analysis was concerned with the stability of the system for producing power and keeping within design limitations, two other linearized, perturbed equations were required--the scaling equation relating blanket power to neutron density and the blanket heat removal equation relating the average blanket temperature to the blanket power level:

$$\delta p(t) = G_f \overline{\Sigma}_f \overline{v} \, \delta N(t) \qquad (148)$$

and

$$c_{p_B} m_B \frac{d \delta T_B(t)}{dt} = \delta p(t) - h A_c \delta T_B(t) \quad . \qquad (149)$$

The feedback equations were also included to complete a closed-loop model for this hybrid system. First, the blanket temperature feecback affecting the reactivity was included as follows:

$$\delta \rho(t) = \alpha_T \delta T_B(t) \qquad (150)$$

where only prompt temperature effects such as those associated with doppler feedback were considered.

Two additional artificial feedback effects were incorporated into a single equation to affect the plasma feedrate via plasma temperature

variations with delay, t_{d_1}, and via blanket temperature variations with delay, t_{d_2}:

$$\delta S(t) = \alpha_1 \frac{n_0}{T_0} \delta T(t - t_{d_1}) + \alpha_2 \frac{n_0}{T_{B_0}} \delta T_B(t - t_{d_2}) \quad . \tag{151}$$

Each of these feedback effects, natural as well as artificial, is activated only when there is departure from the initial equilibrium state of the power-producing hybrid system. Because the blanket temperature feedback effect on the plasma feedrate is a duplicate of the plasma temperature feedback on the feedrate, this effect is included in a dotted box as unnecessary for basic stability analysis. It was included in this hybrid model to close the overall loop but it would be included in a realistic model only as a backup for the feedback based on the plasma temperature variation unless allowance were made for some mechanism by which the coolant channels could be blocked or the coolant lost so that the blanket temperature increased independent of the driving fusion source. This addition, however, would no longer satisfy the hybrid model established here.

Transfer Function Representation of the Hybrid

The entire set of ten (10) linearized perturbed hybrid model equations was transformed to the Laplace domain to simplify the linearized stability analysis of the hybrid model; the transformed equations were rearranged into the following formulation:

$$\frac{\Delta n(s)}{n_0} \left[s + \frac{1}{\tau_{n_0}} + \frac{1}{\tau_{n1}} \right] + \frac{\Delta T(s)}{T_0} \frac{1}{\tau_{T1}} = \frac{\Delta S(s)}{n_0} \tag{152}$$

$$\frac{\Delta n(s)}{n_o} \left[s + \frac{1}{\tau_{E_o}} - \frac{1}{\tau_1} \right] + \frac{\Delta T(s)}{T_o} \left[s + \frac{1}{\tau_{E_o}} - \frac{1}{\tau_2} \right] = \frac{T_s}{3T_o} \frac{\Delta S(s)}{n_o} \tag{153}$$

$$\frac{\Delta N(s)}{n_o} \left[s + \frac{\overline{\beta} - \rho_o}{\Lambda} \right] = \frac{N_o}{\Lambda} \Delta\rho(s) + \overline{\lambda}\Delta C(s) + \Delta q_{B_{eff}}(s) \tag{154}$$

$$\Delta C(s)[s + \overline{\lambda}] = \frac{\overline{\beta}}{\Lambda} \Delta N(s) \tag{155}$$

$$\Delta q_{B_{eff}}(s) = \zeta_2 \cdot \frac{V_p}{V_B} \cdot \Delta q_p(s) \tag{156}$$

$$\Delta q_p(s) = n_o^2 \left. \frac{\partial g}{\partial T} \right|_0 \Delta T(s) + 2n_o g(T_o)\Delta n(s) \tag{157}$$

$$\Delta p(s) = G_f \overline{\Sigma}_f \overline{v} \Delta N(s) \tag{158}$$

$$\Delta T_B(s) \left[s + \frac{hA_C}{c_{p_B} m_B} \right] = \frac{V_B}{c_{p_B} m_B} \Delta p(s) \tag{159}$$

$$\Delta\rho(s) = \alpha_T \Delta T_B(s) \tag{160}$$

$$\Delta S(s) = \alpha_1 \frac{n_o}{T_o} e^{-st_{d_1}} \Delta T(s) + \alpha_2 \frac{n_o}{T_o} e^{-st_{d_2}} \Delta T_B(s) \quad . \tag{161}$$

This system of equations is completely linearized in the Laplace domain except for Eq. (161) where the delayed feedback effects on the plasma feedrate in the time domain result in exponential terms in the frequency domain. The previous assumption of short delay times was used to justify expanding the exponential terms in Eq. (161) in first order Taylor series

to yield truncated first order polynomials as follows:

$$e^{-t_{d_1} s} \simeq 1 - t_{d_1} s \tag{162a}$$

$$e^{-t_{d_2} s} \simeq 1 - t_{d_2} s \quad . \tag{162b}$$

These expansions allow valid small-transient predictions of stability while maintaining the ease of treatment associated with transfer functions whose numerators and denominators are polynomials in the frequency variable, s.

Dynamic analysis of large transients is not possible with this model and was not the concern of this stability analysis. Of course, the basic assumption of negligible burnup would also no longer be valid for very large transients. The following linearized approximation for Eq. (161) was obtained:

$$\Delta S(t) = \alpha_1 \frac{n_o}{T_o} (1 - t_{d_1} s) \Delta T(s) + \alpha_2 \frac{n_o}{T_B} (1 - t_{d_2} s) \Delta T_B(s) \quad . \tag{163}$$

At this point the procedure followed for the point-model plasma equations in Chapter 2 was repeated to produce a block diagram for the overall fusion-fission hybrid system. Some simplification of this system of algebraic equations was needed. First, since it effectively spans the predictions of several theories on diffusion in fusioning plasmas and also greatly simplified the stability analysis, the constant confinement model was utilized for plasma diffusion. As a result, both

expansion terms, $1/\tau_{n1}$ and $1/\tau_{T1}$, were set to zero in Eq. (152). This assumption is consistent with the feedback controlled plasma system described in Chapter 2.

Second, the two blanket reactor kinetics equations were combined as usual to eliminate the precursor concentration variation as follows:

$$\Delta N(s)\left[s + \frac{\overline{\beta} - \rho_0}{\Lambda} - \frac{\overline{\lambda}\,\overline{\beta}}{\Lambda(s + \overline{\lambda})}\right] = \frac{N_0}{\Lambda}\,\Delta\rho(s) + \Delta q_{B_{eff}}(s) \quad . \tag{164}$$

Note that neither the blanket source transfer function, $\Delta N(s)/\Delta q_{B_{eff}}(s)$, nor the blanket reactivity transfer function, $\Delta N(s)/\Delta\rho(s)$, can be isolated in this hybrid model; the symbiotic relationship is absolute--both the blanket source perturbation, $\Delta q_{B_{eff}}(s)$, and the blanket reactivity perturbation, $\Delta\rho(s)$, were retained for this analytical model as explained following Eq. (123). This is a significant difference in comparison with traditional fission reactor kinetics studies. One or the other of the two perturbations is always neglected for ordinary stability analysis of fissile systems.[99]

The transfer function formulation in Eq. (165) was obtained upon rearrangement of Eq. (164):

$$\Delta N(s) = \left[\frac{s + \overline{\lambda}}{s^2 + \left(\frac{\overline{\beta} - \rho_0}{\Lambda} + \overline{\lambda}\right)s - \frac{\overline{\lambda}\rho_0}{\Lambda}}\right]\left[\frac{N_0}{\Lambda}\,\Delta\rho(s) + \Delta q_{B_{eff}}(s)\right] \tag{165}$$

where the first factor, involving a first order polynomial in s divided by a quadratic in s, is the usual factor derived for the source or reactivity transfer function of fission reactors. This factor was identified as the blanket reactor transfer function, $B(s)$, after the similar form used in ordinary fission reactor kinetics:

$$B(s) \equiv \frac{s + \bar{\lambda}}{s^2 + (\frac{\bar{\beta} - \rho_0}{\Lambda} + \bar{\lambda})s - \frac{\lambda\rho_0}{\Lambda}} \quad .$$ (166)

The plasma block diagram presented in Fig. 9 of Chapter 2 is com-
pletely applicable for the plasma subsystem of the hybrid. The only
difference in the hybrid plasma case is the less reactive nature of the
plasma which is no longer self-sustaining. To account for the presence
of both source and reactivity perturbations in the blanket kinetics
equation, the summation method presented in Fig. 18 was utilized in the
overall hybrid system diagram for the linearized, perturbed hybrid model
and its associated overall transfer function.

In addition, the power scaling factor relating neutron density to
power density in Eq. (158) was used in the form of a transfer function
as follows:

$$\frac{\Delta p(s)}{\Delta N(s)} = G_f \; \bar{v} \; \bar{\Sigma}_f \quad .$$ (167)

Finally, the transfer function relating blanket temperature changes to
blanket power density changes was obtained from the perturbed blanket
heat transfer relation in Eq. (159) as follows:

$$\frac{T_B(s)}{p(s)} = \frac{V_B / c_{p_B} m_B}{s + \frac{hA_C}{c_{p_B} m_B}} \quad .$$ (168)

These various subsystems including the plasma diagram of Fig. 9 in
Chapter 2, and the blanket kinetics diagram of Fig. 18, together with the
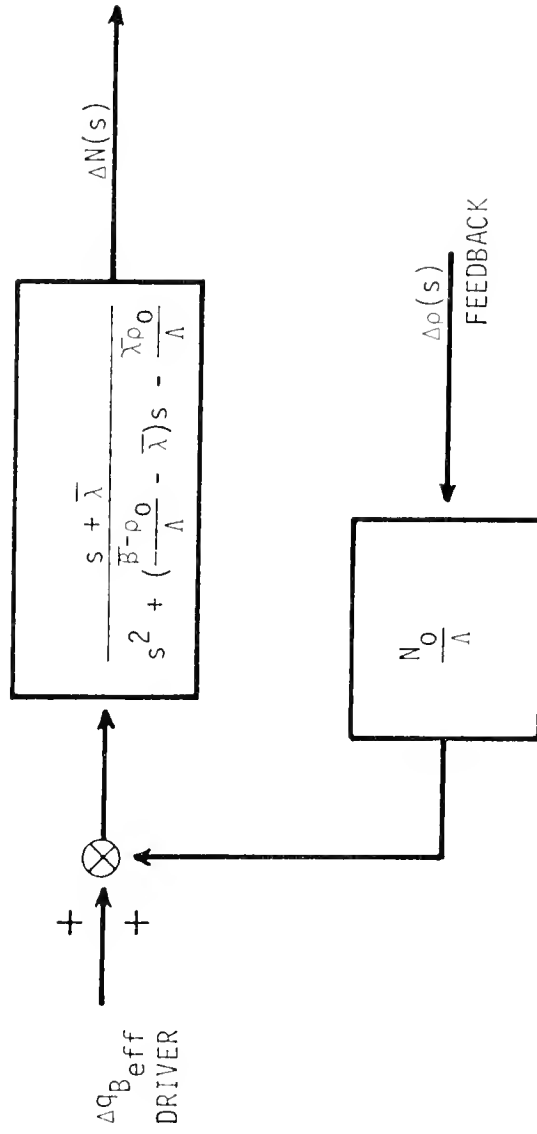
Figure 18. Block diagram schematic for point-model blanket kinetics retaining both source and reactivity perturbations.

connecting relations and feedback components were combined to yield the overall fusion-fission hybrid block diagram presented schematically in Fig. 19. This overall block diagram relating transfer functions for the various components of the linearized hybrid model was entirely derived from the linearized, Laplace-domain model presented in Eqs. (152)-(160) plus Eq. (163). Figure 19 graphically illustrates the linear dependence of the perturbed hybrid system with the various interactions of blanket and plasma effects.

The linearlized and perturbed equations of the model are based on the entire set of ten original model Eqs. (141a)-(141j) of which five are nonlinear. Therefore, although the block diagram in Fig. 19 is informative and useful for stability analysis, it is not applicable in transient analysis involving the temporal evolution of perturbed systems unless the perturbations are small and the time interval to be examined is short.

The usual rules of block diagram control systems were applied to obtain the overall transfer function for the hybrid system, $\Delta T_B(s)/\Delta S(s)$. This ratio is a natural result; however, the ratio of blanket power to plasma feedrate might be more directly useful for this model because of the basic simplicity of the blanket temperature description given in Eq. (130).

First, the overall hybrid transfer function, $\Delta T_B(s)/\Delta S(s)$, was obtained without any artificial feedback. The artificial feedback coefficients (α_1 and α_2) were set to zero to simplify the open-loop, plasma-related portion of the hybrid system so that the open-loop plasma source transfer function of Eq. (169) was obtained in agreement with Eq. (61) of Chapter 2:

THE BASIC HYBRID MODEL*
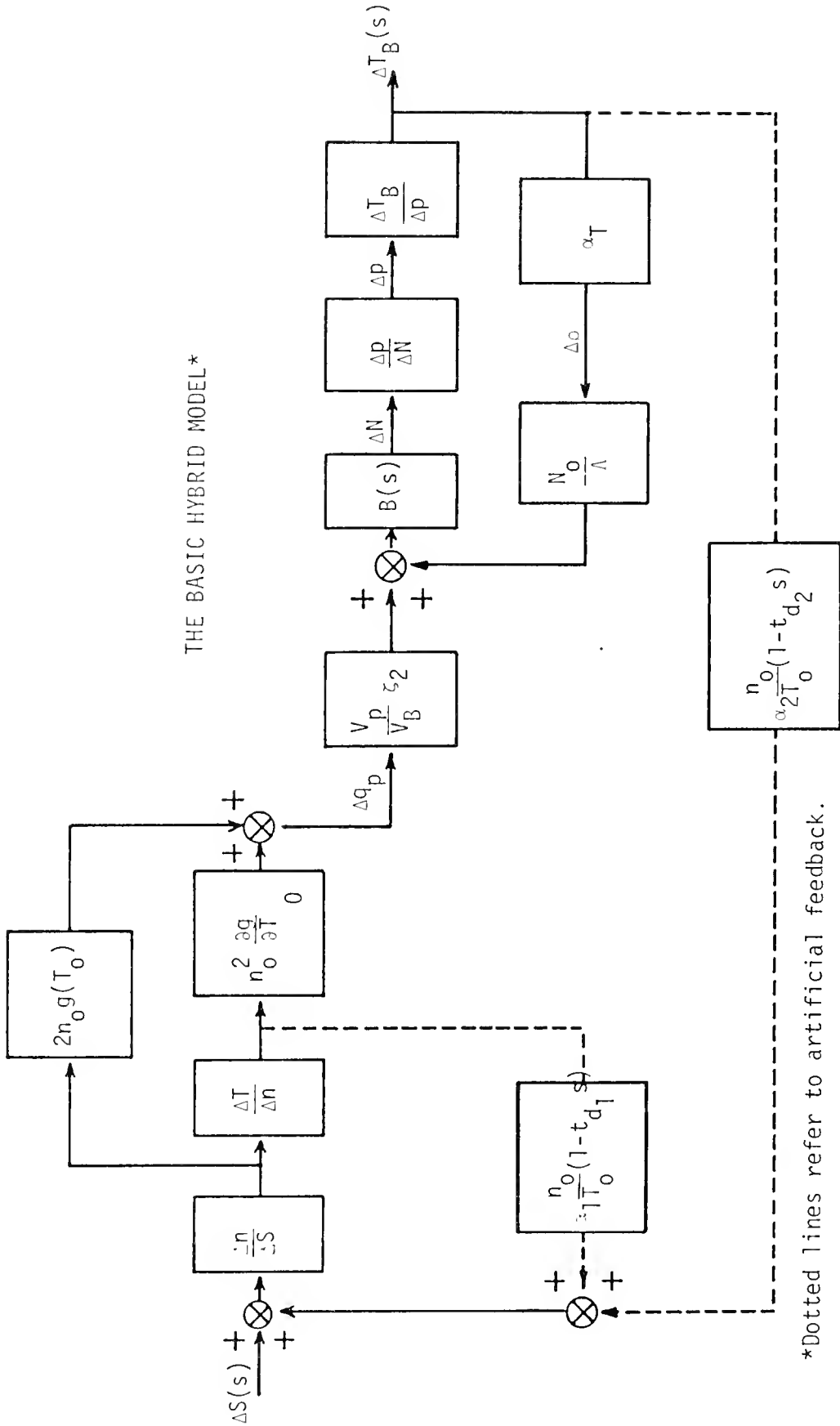
Figure 19. Block diagram of the linearized global fusion-fission hybrid reactor model.

*Dotted lines refer to artificial feedback.

$$\frac{\Delta q_p(s)}{\Delta S(s)}\bigg|_{\substack{\text{open}\\\text{loop}}} = \frac{s[2n_o g(T_o) - n_o T_o \frac{\partial g}{\partial T}\big|_0 a_4] + 2n_o g(T_o)(\frac{1}{\tau_{E_o}} - \frac{1}{\tau_2}) - n_o T_o \frac{\partial g}{\partial T}\big|_0 a_{12}}{s^2 + s(\frac{1}{\tau_{E_o}} - \frac{1}{\tau_2} + \frac{1}{\tau_{n_o}}) + \frac{1}{\tau_{n_o}}(\frac{1}{\tau_{E_o}} - \frac{1}{\tau_2})}$$

(169)

where the terms, $1/\tau_{T1}$ and $1/\tau_{n1}$, were set to zero for constant confine-
ment and the terms, $1/\tau_{b_1}$ and $1/\tau_{b_2}$, were assumed negligible for the
low-burnup hybrid plasma. The coefficient, a_4, is defined in Eq. (56d)
and the coefficient, a_{12}, is defined in Eq. (89a).

Therefore, the open-loop plasma source transfer function,
$\Delta q_p(s)/\Delta S(s)$, can be incorporated as shown in Fig. 13 of Chapter 2 to
simplify the plasma subsystem. Alternatively, this same result for
$\Delta q_p(s)/\Delta S(s)$ could be obtained directly using the linearized hybrid
model by substituting Eqs. (152) and (153) into Eq. (157) and solving
for the open-loop plasma source transfer function presented in Eq. (169).
The other feedforward elements of the blanket system including the
blanket reactor transfer function, the power scaling factor, and the
transfer function relating blanket temperature changes to blanket power
changes were combined to produce the reduced hybrid block diagram
depicted in Fig. 20. After reduction of the blanket reactivity feed-
back loop, the simplified hybrid system block diagram of Fig. 21 was
obtained where the blanket temperature feedback effect has been combined
into the overall forward loop using a single blanket transfer function,
$T_B(s)$, given by:

$$T_B(s) = \frac{G_f \bar{v} \bar{\Sigma}_f V_B(s + \bar{\lambda})/c_{p_B}}{[s + \frac{hA_c}{c_{p_B} m_B}][s^2 + (\frac{\bar{\beta} - \rho_o}{\Lambda} + \bar{\lambda})s - \frac{\bar{\lambda}\rho_o}{\Lambda}] + a_{16}(s + \bar{\lambda})}$$

(170)
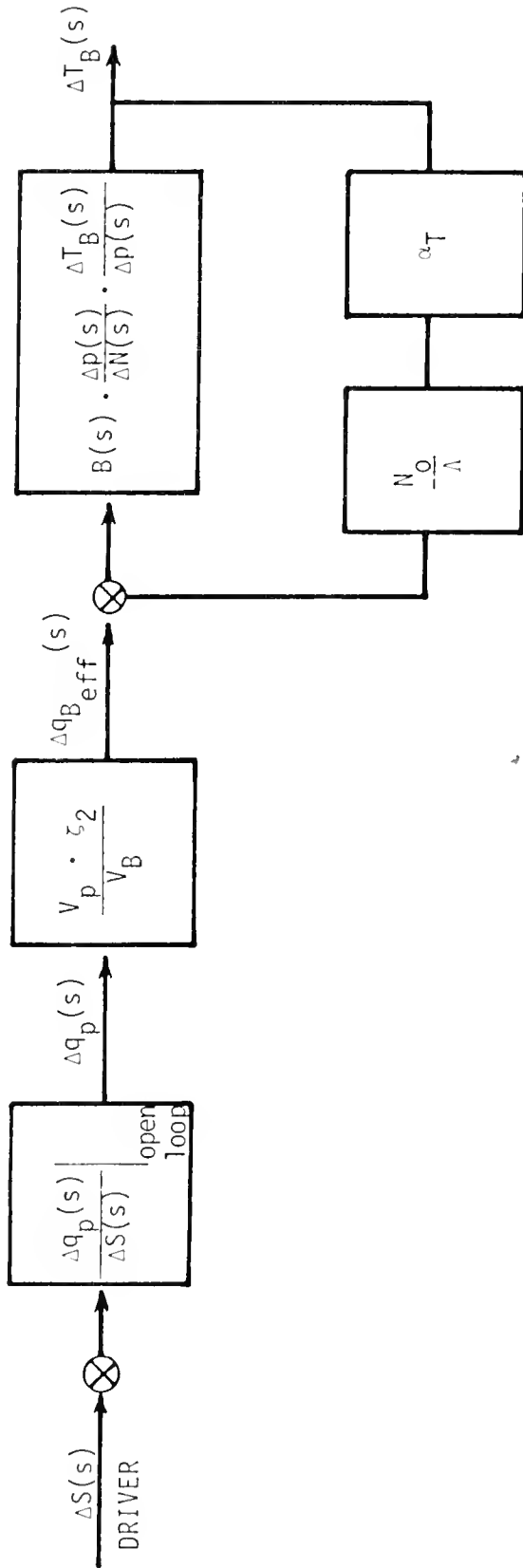
Figure 20. Partially-reduced hybrid block diagram with no artificial feedback.

$\Delta S(s)$ DRIVER PERTURBATION

$\Delta q_p(s)$

$\Delta q_{B_{eff}}$

$\Delta T_B(s)$ BLANKET TEMPERATURE PERTURBATION DUE TO DRIVER

$\left. \dfrac{\Delta q_p(s)}{\Delta S(s)} \right|_{open\ loop}^{*}$

$\dfrac{V_p \cdot \zeta_2}{V_B}$

$\tau_B(s)$
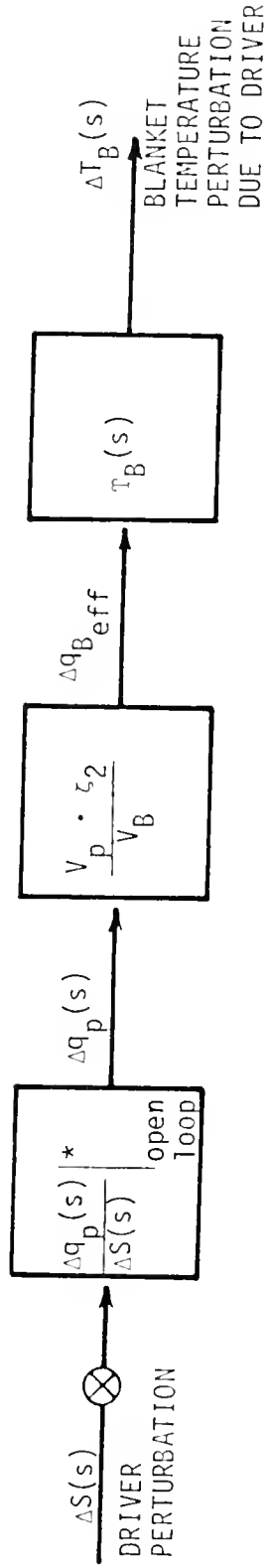
*Open-loop plasma has no feedback.

Figure 21. Simplified reduced hybrid system block diagram with no artificial feedback.

where the reducing coefficient, a_{16}, is given by

$$a_{16} = \frac{N_o \ \alpha_T \ G_f \ \overline{v} \ \overline{\Sigma}_f \ V_B}{\Lambda} \quad . \tag{171}$$

From Fig. 21 which is representative of the modeled hybrid system with inherent blanket temperature feedback but without artificial feedback, the overall, open-loop transfer function was obtained as follows:

$$\frac{\Delta T_B(s)}{\Delta S(s)}\bigg|_{\substack{\text{open} \\ \text{loop}}} = \frac{\Delta q_p(s)}{\Delta S(s)}\bigg|_{\substack{\text{open} \\ \text{loop}}} \cdot \frac{V_p \zeta_2}{V_B} \cdot \frac{G_f \ \overline{v} \ \overline{\Sigma}_f \ V_B/c_{p_B} m_B}{[s + \frac{hA_c}{c_{p_B} m_B}][s^2 + (\frac{\overline{\beta} - \rho_o}{\Lambda} + \overline{\lambda})s - \frac{\overline{\lambda}\rho_o}{\Lambda}] + a_{16}}$$

$$\tag{172}$$

where the plasma elemental source transfer function, $\Delta q_p(s)/\Delta S(s)$, is given in Eq. (169) and does not include the effect of artificial temperature feedback on the feedrate.

When the artificial plasma temperature feedback on the feedrate was included, the closed-loop transfer function for the plasma resembled that of Eq. (86) in Chapter 2 without $1/\tau_{n1}$ and $1/\tau_{T1}$ due to using the constant confinement model and without $1/\tau_{b_1}$ and $1/\tau_{b_2}$ which are negligible for the less reactive hybrid plasmas. The pertinent plasma portion of the overall hybrid diagram of Fig. 19 is repeated in Fig. 22 for which the closed-loop (now including artificial feedback) source transfer function is given in Eq. (173):

$$\frac{\Delta q_p(s)}{\Delta S(s)}\bigg|_{\substack{\text{closed} \\ \text{loop}}} = \frac{-\frac{T_o}{n_o} [n_o \frac{\partial g}{\partial T}\bigg|_0 (a_4 s + a_{12}) - \frac{n_o}{T_o} g(T_o)(s + \frac{1}{\tau_{E_o}} - \frac{1}{\tau_2})]}{s^2 + s(\frac{1}{\tau_{E_o}} - \frac{1}{\tau_2} + \frac{1}{\tau_{n_o}}) + \frac{1}{\tau_{n_o}} (\frac{1}{\tau_{E_o}} - \frac{1}{\tau_2}) - \alpha_1(1 - t_{d_1} s)(a_4 + a_{12})} \quad .$$

$$\tag{173}$$
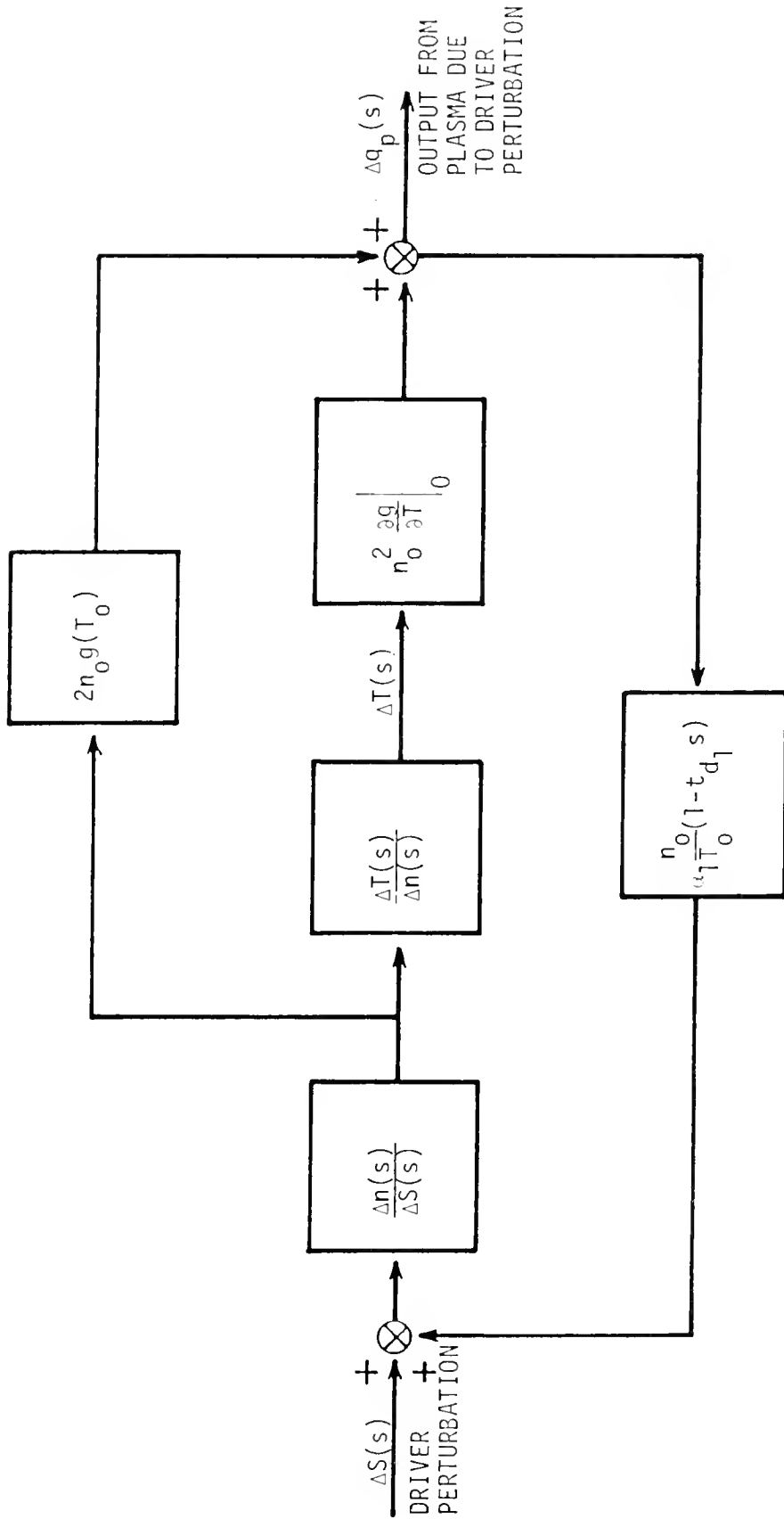
Figure 22. Closed-loop block diagram for the linearized point-model plasma with temperature feedback to the feedrate.

The overall, closed-loop, hybrid system transfer function, $\Delta T_B(s)/\Delta S(s)$, presented in Eq. (174) remains in the same form as Eq. (172) except that the closed-loop plasma source transfer function given in Eq. (173) replaces the open-loop one used in Eq. (172).

$$\left.\frac{\Delta T_B(s)}{\Delta S(s)}\right|_{\substack{\text{closed}\\\text{loop}}} = \left.\frac{\Delta q_p(s)}{\Delta S(s)}\right|_{\substack{\text{closed}\\\text{loop}}} \cdot \frac{V_p \zeta_2}{V_B} \cdot \frac{G_f \overline{v}\,\overline{\Sigma}_f V_B/c_{p_B} m_B}{s^3 + a_{17}s^2 + a_{18}s + a_{19}} \tag{174}$$

where the polynomial coefficients, a_{17}, a_{18}, and a_{19} are given by

$$a_{17} = \frac{hA_C}{c_{p_B} m_B} + \frac{\overline{\beta} - \rho_0}{\Lambda} + \overline{\lambda} \quad, \tag{175a}$$

$$a_{18} = (\frac{hA_C}{c_{p_B} m_B})(-\frac{\overline{\beta} - \rho_0}{\Lambda} + \overline{\lambda}) - \frac{\overline{\lambda}\rho_0}{\Lambda} - \frac{N_0 \alpha_T G_f \overline{v}\,\overline{\Sigma}_f V_B}{\Lambda} \quad, \tag{175b}$$

$$a_{19} = \frac{-N_0 \alpha_T G_f \overline{v}\,\overline{\Sigma}_f V_B \overline{\lambda}}{\Lambda} - \frac{\overline{\lambda}\rho_0}{\Lambda}(\frac{hA_C}{c_{p_B} m_B}) \quad. \tag{175c}$$

Stability Criteria for the Hybrid System

The Routh Criterion was applied to this overall transfer function which includes both inherent (doppler) feedback and artificial plasma temperature feedback. Since the poles of the denominator in Eq. (174) decide the stability of the system and since the plasma and the blanket are only interacting in the feedforward mode via the source conversion coefficient, ζ_2, the Routh Criterion was applied individually to each multiplicative segment of the overall hybrid transfer function. Stability

criteria for the closed-loop plasma source transfer function, $\Delta q_p(s)/\Delta S(s)$, were obtained using the Routh Criterion which supplied the three stability criteria of Eqs. (90a)-(90c) in Chapter 2. Similarly the Routh array of Fig. 23 for the second polynomial in the denominator of Eq. (174) was used to obtain three stability criteria based on blanket parameters.

1	a_{18}	0
a_{17}	a_{19}	0
$a_{18} - \dfrac{a_{19}}{a_{17}}$	0	0
a_{19}	0	0
0		

Figure 23. Routh array for the cubic denominator for blanket effects in the overall hybrid transfer function.

The results obtained by applying the Routh Stability Criterion consist of six stability criteria in all which are presented in Eqs. (176a)-(176f).

Stability Criterion I:

$$1 + \alpha_1 t_{d_1} \left(1 - \frac{T_s}{3T_0}\right) > 0 \qquad (176a)$$

Stability Criterion II:

$$\frac{1}{\tau_{E_0}} - \frac{1}{\tau_2} + \frac{1}{\tau_{n_0}} - \alpha_1 (1 - \frac{T_s}{3T_0}) - \frac{\alpha_1 \xi_2 t_{d_1}}{\tau_{E_0}} > 0 \qquad (176b)$$

Stability Criterion III:

$$\frac{1}{\tau_{n_0}} (\frac{1}{\tau_{E_0}} - \frac{1}{\tau_2}) + \frac{\alpha_1 \xi_2}{\tau_{E_0}} > 0 \qquad (176c)$$

Stability Criterion IV:

$$\frac{\bar{\beta} - \rho_0}{\Lambda} + \bar{\lambda} + \frac{hA_C}{c_{p_B} m_B} > 0 \qquad (176d)$$

Stability Criterion V:

$$[\frac{-\lambda \rho_0}{\Lambda} + \frac{hA_C}{c_{p_B} m_B} (\frac{\bar{\beta} - \rho_0}{\Lambda} + \bar{\lambda}) - G_f \bar{v} \bar{\Sigma}_f V_B \alpha_T \frac{N_0}{\Lambda}]$$

$$+ \frac{[\frac{\lambda \rho_0}{\Lambda} (\frac{hA_C}{c_{p_B} m_B}) + G_f \bar{v} \bar{\Sigma}_f V_B \alpha_T \frac{N_0}{\Lambda}]}{[\frac{\bar{\beta} - \rho_0}{\Lambda} + \bar{\lambda} + \frac{hA_C}{c_{p_B} m_B}]} > 0 \qquad (176e)$$

Stability Criterion VI:

$$[\frac{-\lambda \rho_0}{\Lambda} (\frac{hA_C}{c_{p_B} m_B}) - G_f \bar{v} \bar{\Sigma}_f V_B \bar{\lambda} \alpha_T \frac{N_0}{\Lambda}] > 0 \quad . \qquad (176f)$$

The first three stability criteria were obtained from the closed-loop plasma source transfer function and are repeated from Eqs. (90a)-(90c) in Chapter 2; the second three criteria were obtained from the closed-loop blanket transfer function using the Routh array of Fig. 23 where all first column coefficients were required to be positive for a stable hybrid system. All six of these criteria must be satisfied simultaneously; when appropriate hybrid system values are included, all six conditions can be met provided feedback is included. Indeed, the three blanket conditions are met automatically for realistic systems, regardless of the specific system because of blanket subcriticality $(\rho_0 < 0)$.

The secondary artificial feedback on the plasma feedrate (with delay time, t_{d_2}) is important only for backup control or for treating blocked coolant channels or failure to remove sufficient blanket heat while in a steady-state condition. This artificial feedback is not intended for primary plasma transient control. The plasma source feedback based on plasma temperature variations is more reliable and faster acting to control plasma perturbations directly. In addition, this work was not really concerned with blanket heat transfer considerations except as needed to complete the simplified hybrid model developed in this analysis. Therefore, aside from including the second artificial feedback term in the overall hybrid nonlinear model as well as in the linearized block diagram, it was given no further consideration. Such an artificial feedback term from the overall transformed response, $\Delta T_B(s)$, back to the original transformed perturbation, $\Delta S(s)$, does show the possibility of a completely closed loop model. Therefore, the completed hybrid model for this study is complete although somewhat restrictive. The model does allow consideration of many types of perturbations and resulting transients.

CHAPTER 4

HYBRID PLASMA OPERATIONAL CONSIDERATIONS

Introduction to Hybrid Plasma Time-Dependent Behavior

The blanket neutronic analysis described in Chapter 5 was used to determine the required volumetric neutron generation rate in the plasma to produce 6500 MWth in the hybrid system. Calculations were performed to determine the specific hybrid plasma core conditions required to drive the hybrid blanket described in Appendix B. Additional calculations were also performed to establish the stability and the transient behavior of the hybrid plasma when subjected to small perturbations. Before specific transient hybrid plasma phenomena were examined, scoping studies were performed to investigate and characterize various hybrid plasma equilibrium states and establish ranges of the plasma equilibrium temperature, T_o, and ion density, n_o, required to produce the proper neutron source to drive the power-producing system.

The CLASSIC2 Code[112] was used for this hybrid plasma analysis since it employs a point-model system of equations similar to those presented in Chapter 2. The CLASSIC2 Code was used to describe both equilibrium and time-dependent plasma conditions which could affect the surrounding fissile hybrid blanket. The point-model CLASSIC2 Code is described in Appendix D along with input requirements for using the code to examine specific equilibrium and time-dependent plasma conditions.

The basic point-model plasma equations applied in CLASSIC2 are repeated here:

$$\frac{dn(t)}{dt} = S(t) - \frac{n(t)}{\tau_n} - \frac{<\sigma v>_{DT} n^2(t)}{2} \tag{177}$$

$$\frac{d[n(t)T(t)]}{dt} = \frac{<\sigma v>_{DT} Q_\alpha n^2(t)}{12} + \frac{S(t)T_s(t)}{3} - \frac{n(t)T(t)}{\tau_E} - \frac{bT^{1/2}(t)n^2(t)}{3} \tag{178}$$

where the only difference when compared with the model presented in Chapter 2 is the explicit allowance for time-dependent variations in the injection energy, $T_s(t)$. An important parameter which must also be specified in the input to the CLASSIC2 Code is the R-ratio defined as the ratio of particle and energy confinement times, τ_n/τ_E, as in Chapter 2.

In all the hybrid analyses both confinement times were assumed to vary identically with temperature and density. In agreement with the generality of this hybrid model and the uncertainty connected with any actual selection of a confinement model, the constant confinement model was chosen for use with the CLASSIC2 Code.

The volumetric fusion neutron production rate, $q_p(t)$, was computed in CLASSIC2 using Eq. (141c) repeated as follows from Chapter 3:

$$q_p(t) = \frac{<\sigma v>_{DT} n^2(t)}{4} \tag{179}$$

where the data for the fusioning plasma reactivity, $<\sigma v>_{DT}$, was obtained from the standard work by Greene.[113] For reference purposes, Greene's reactivity data obtained using a Maxwellian distribution of plasma ion

speeds to weight the cross section is presented in Fig. C1 of Appendix C. These data were used as standard input for CLASSIC2.

As suggested by Ohta et al.[18,21] as well as Mills,[15] two standard feedback options are available with CLASSIC2. One option is plasma temperature feedback on the plasma source feedrate; the other option is plasma temperature feedback on the plasma injection energy. Many other feedback choices on such parameters as confinement time variation and impurity concentration to affect bremsstrahlung have been hypothesized, but these two choices have been proposed as most easily implemented.

In agreement with the closed-loop hybrid plasma model presented in Chapter 3, the plasma temperature feedback on the source feedrate option was utilized in all the time-dependent hybrid analysis using CLASSIC2. The feedrate feedback used with CLASSIC2 is of the form given in Eq. (180) which is similar to Eq. (141j):

$$S(t) = S_0 + K_s[T_0 - T(t)] \qquad (180)$$

where the total feedback coefficient, K_s, corresponds to the following formulation in the hybrid model of Chapter 3:

$$K_s = -\alpha_1 n_0/T_0 \quad . \qquad (181)$$

The total feedback coefficient employed in the code is not normalized and has units of ions/cm^2-sec-keV compared to the normalized feedback coefficient, α_1, which has units of inverse seconds.

One other simplification is incorporated in CLASSIC2 which sets the feedback to react instantaneously to a change in plasma temperature. Very short response times have been utilized in magneto-hydrodynamic

plasma feedback studies as well as in plasma position control studies to effect control over gross plasma breakdown and escape where response times in the range of a millisecond down to hundreds of microseconds are considered possible for engineering implementation of the feed-back.[97,98,114] Based on these short times, the assumption of instantaneous feedback effectiveness is not a great restriction on the model. This was found to be particularly true in the dynamic response of the hybrid plasma following various 5% parameter perturbations. The time constants such as the energy and particle confinement times in the basic point-model plasmas examined using Eqs. (177) and (178) were on the order of seconds. The application of feedback within a few tenths of a second was not expected to be very different from instantaneous application in its effectiveness; that is, the effectiveness of any feedback on the feed-rate was not expected to depend strongly on the speed of response in the possible millisecond to tenths of seconds range.

In particular, increasing values of the total feedback coefficient can be postulated to overcome any small delays necessitated by engineer-ing problems in applying the feedback. Although full-scale fusioning plasmas are expected to be limited in the size of allowable feedback, previous work has shown and the results of this work support the fact that the magnitude of the feedback coefficient in a transient simulation can be made very large to overcome delayed implementation for low-reactivity, highly-driven plasmas of the type used in hybrids.[115,116] Hence, a large range of feedback coefficients was used to simulate or account for the possibility of a wide range of feedback effects varying from very large feedback effects applied with some delay time down to relatively small feedback effects implemented instantaneously.

Independent of feedback considerations of CLASSIC2 Code utilized six basic input parameters for the point-model plasma represented by Eqs. (177) and (178). Initially, the R-ratio was selected and then any three of the remaining five variables of ion density, n, temperature, T, evergy confinement time, τ_E, source feedrate, S, and injection energy, T_s, were specified. From this basic selection corresponding equilibrium conditions for the remaining two variables were established and, as desired, time-dependent transients were examined by perturbing any one of four equilibrium variables of ion density, temperature, feedrate, or injection energy.

The basic assumption in CLASSIC2 and the entire global plasma analysis is that the plasma occupies a constant volume. Ordinarily, an increase in volume is expected to accompany an increase in temperature since the plasma pressure is given approximately by the following equation of state:

$$P(t) = n_T(t)T(t) \tag{182}$$

where

$\quad\quad T(t)$ = plasma temperature (keV)

$\quad\quad n_T(t)$ = plasma total particle (ions and electrons) density ($\#/cm^3$)

$\quad\quad P(t)$ = plasma pressure (keV/cm^3).

Obviously, if temperature increases, then pressure is expected to respond. Nevertheless, this deficiency in failing to account for pressure and volume changes was disregarded as unimportant in this work for the relatively small transients of primary concern. So the work of establishing some base calculations for hybrid plasma transients was expected

to overestimate neutron production rates since the neutron production rate would decrease if the plasma were allowed to expand against the confining magnetic field. Therefore, the predicted neutron production rates were conservative but sufficiently accurate for reasonably small transients in operational hybrid plasmas. Accounting for this effect would represent additional complexity without supplying additional fundamental information on plasma transient behavior as it affects the overall hybrid system.

The consideration of small transients or short time intervals was most important for analysis of the linearized model on which stability predictions were based. When transients were considered for large time intervals, it was only for comparison purposes since the model is not strictly applicable for large temperature transients (either above or below the original equilibrium state).

Although relatively small temperature transients were of primary concern, the resultant volumetric fusion neutron source transients were not expected to be quite so small. For a plasma with a Maxwellian Distribution of ion energies, plasma reactivity shows extremely rapid, nonlinear variation with temperature as shown in Appendix C. A sensitivity analysis of the volumetric neutron production rate for the 8 keV temperature selected for the hybrid plasma core showed that small fractional changes in temperature can yield over three times that same fractional increase in the neutron production rate; that is, the neutron production rate is very sensitive to the plasma ion temperature. This dependence is explained in Appendix C where the following formulation is presented for the sensitivity, $S_{DT}(T)$:

$$\frac{dq_p}{q_p} = S_{DT}(T) \cdot \frac{dT}{T} \quad . \tag{183}$$

The dimensionless sensitivity factor, $S_{DT}(T)$, varies smoothly with temperature; therefore, for a temperature change, $\frac{dT}{T}$, the neutron production rate was expected to increase fractionally by a factor, $S_{DT} \cdot \frac{dT}{T}$. Variation of the sensitivity factor in the temperature range of interest for hybrid work (5-20 keV) is shown in Figure C1. The sensitivity factor is largest (~ 3.2) at low energies and decreases as temperature increases until it reaches unity at the 60 keV peak in reactivity.

Selecting a Spectrum of Hybrid Plasma Equilibrium Conditions

To begin consideration of the hybrid, the plasma particle and energy relations of Eqs. (177) and (178) were solved for a spectrum of equilibrium conditions from which reasonable selections were made for more specific operating equilibria. Further transient analysis was performed only on those cases selected as most interesting for an actual hybrid system.

Equilibrium particle densities, n_o, and temperatures, T_o, were predetermined by the neutron production rate required to drive the hybrid blanket for proper design power levels. These predetermined values of ion density ($n_o = 9.56 \times 10^{13}$ ions/cm^3) and temperature ($T_o = 8.0$ keV) were needed to guarantee proper blanket power production. The proper design value for the neutron production rate was dependent only on the density and temperature since the plasma volume was fixed. From these two preset values, an entire range of energy confinement times was selected for investigation for a possible set of operational equilibrium conditions. The range investigated included energy confinement times up

to 5 seconds in increments of 0.1 seconds for successively varied R-ratios of 1.0, 1.5, 2.0, 2.5, 3.0, and 10.0.

The confinement time cannot actually be fixed at a value but is rather characteristic of or dependent upon the plasma operating conditions which are represented by the particle density and the temperature in the plasma. The R-ratio characterizes the plasma; that is, the plasma conditions such as collision frequency, contained magnetic field as well as temperature and density determine the R-ratio from detailed plasma dynamics effects. However, the selection of such a large range of values of energy confinement time did certainly quarantee inclusion of those values which a functioning hybrid plasma could be expected to achieve operationally with some modification of constraining magnetic fields.

The feedrates and injection energies required to satisfy plasma equilibrium operation for the given ranges of the R-ratio and energy confinement time were initially examined over a wide spectrum of possible sets of plasma operational equilibrium conditions. To reduce the parameter variation and hence the number of different sets of plasma conditions to be examined, the range of confinement times was narrowed to the more interesting and tractable range of 1.5 sec $\leq \tau_E \leq$ 2.0 sec. In addition, only integer values of the R-ratio (1, 2, 3, and 10) were examined in detail since this variation still encompasses predicted plasma system R-ratios.[30,101,102] Operational values of the R-ratio are currently predicted to be much lower than the unrealistic R-ratios in the range of 10-50 for which many previous fusion control studies have been performed.[17,18]

Scoping calculations within the indicated limited variable ranges yielded the data on equilibrium operating conditions presented in

Table 4-I. After the equilibrium particle density, n_0, and the tempera-
ture, T_0, were set, for each value of energy confinement time, τ_{E_0}, a
unique corresponding set of values of the equilibrium injection energy,
T_{S_0}, and source feedrate, S_0, was determined using CLASSIC2. Therefore,
the information contained in Table 4-I consists of six unique sets of
possible equilibrium operating conditions for n_0, T_0, τ_{E_0}, S_0, and T_0
presented for each of four (4) values of the R-ratio.

The various equilibrium conditions set forth in Table 4-I were used
to determine where these plasma equilibrium conditions place the hybrid
plasma on a Mills-like equilibrium curve.[16] For a given R-ratio and
assumed density and temperature conditions (n_0 = 9.56 x 10^{13} ions/cm^3
and T_0 = 8.0 keV) to give the required volumetric neutron production
rate, the corresponding feedrate, injection energy, and energy confinement
time were determined as presented in Table 4-I or similar presentations.
Based on these three quantities (S_0, T_{S_0}, and τ_{E_0}) plus the R-ratio, the
corresponding variation of $n_0 \tau_{E_0}$ with plasma temperature was determined
by evaluating new equilibrium conditions for various temperatures; that
is, for the specified values of R and n_0 in Table 4-I, the required
corresponding values of τ_{E_0} were determined as a function of T_0. A
specific set of such curves corresponding to the equilibrium cases listed
in Table 4-II are depicted in Fig. 24. All of the curves in Fig. 24
contain the required density and temperature points for proper neutron
production for the case of τ_E = 1.7 sec.

Table 4-I

Selected Spectrum of Equilibrium Operating Conditions for the
Hybrid Plasma With Constant Confinement

$R^{\star}$	τ_{E_0} (sec)	$n_0 \tau_{E_0}$ (sec/cm^3)	S_0 (ions/cm^3-sec)	T_{s_0} (keV)
1	1.5	1.434×10^{14}	6.401×10^{13}	17.50
	1.6	1.530×10^{14}	6.003×10^{13}	17.07
	1.7	1.625×10^{14}	5.652×10^{13}	16.64
	1.8	1.721×10^{14}	5.339×10^{13}	16.21
	1.9	1.816×10^{14}	5.060×10^{13}	15.78
	2.0	1.912×10^{14}	4.808×10^{13}	15.35
2	1.5	1.434×10^{14}	3.215×10^{13}	34.85
	1.6	1.530×10^{14}	3.016×10^{13}	33.98
	1.7	1.625×10^{14}	2.840×10^{13}	33.11
	1.8	1.721×10^{14}	2.684×10^{13}	32.24
	1.9	1.816×10^{14}	2.544×10^{13}	31.38
	2.0	1.912×10^{14}	2.418×10^{13}	30.51
3	1.5	1.434×10^{14}	2.153×10^{13}	52.04
	1.6	1.530×10^{14}	2.020×10^{13}	50.73
	1.7	1.625×10^{14}	1.903×10^{13}	49.42
	1.8	1.721×10^{14}	1.799×10^{13}	48.11
	1.9	1.816×10^{14}	1.705×10^{13}	46.81
	2.0	1.912×10^{14}	1.622×10^{13}	45.50
10	1.5	1.434×10^{14}	6.655×10^{12}	168.3
	1.6	1.530×10^{14}	6.257×10^{12}	163.8
	1.7	1.625×10^{14}	5.905×10^{12}	159.2
	1.8	1.721×10^{14}	5.593×10^{12}	154.7
	1.9	1.816×10^{14}	5.313×10^{12}	150.2
	2.0	1.912×10^{14}	5.062×10^{12}	145.8

*Power production conditions were the same in all cases: $T_0 = 8.0$ keV,
$n_0 = 9.56 \times 10^{13}$ ions/cm^3, and $q_{p_0} = 1.41 \times 10^{11}$ nts/cm^3-sec.

The plot's y-axis reads "Equilibrium $n\tau_E$-Product ($\times 10^{-14}$) (sec/cm^3)" and the x-axis reads "Plasma Temperature (keV)".

These equilibrium curves apply for no injection energy ($T_S = 0$) as well as for injection energy and source feedrate corresponding to equilibrium conditions for $n_0 = 9.56 \times 10^{13}$ ions/cm^3, $T_0 = 8.0$ keV, and $\tau_E = 1.7$ sec for the R-ratios indicated.

$T_S = 0$ (all R-ratios)

$R = 1$ ($T_S \neq 0$)
$R = 2$ ($T_S \neq 0$)
$R = 10$ ($T_S \neq 0$)
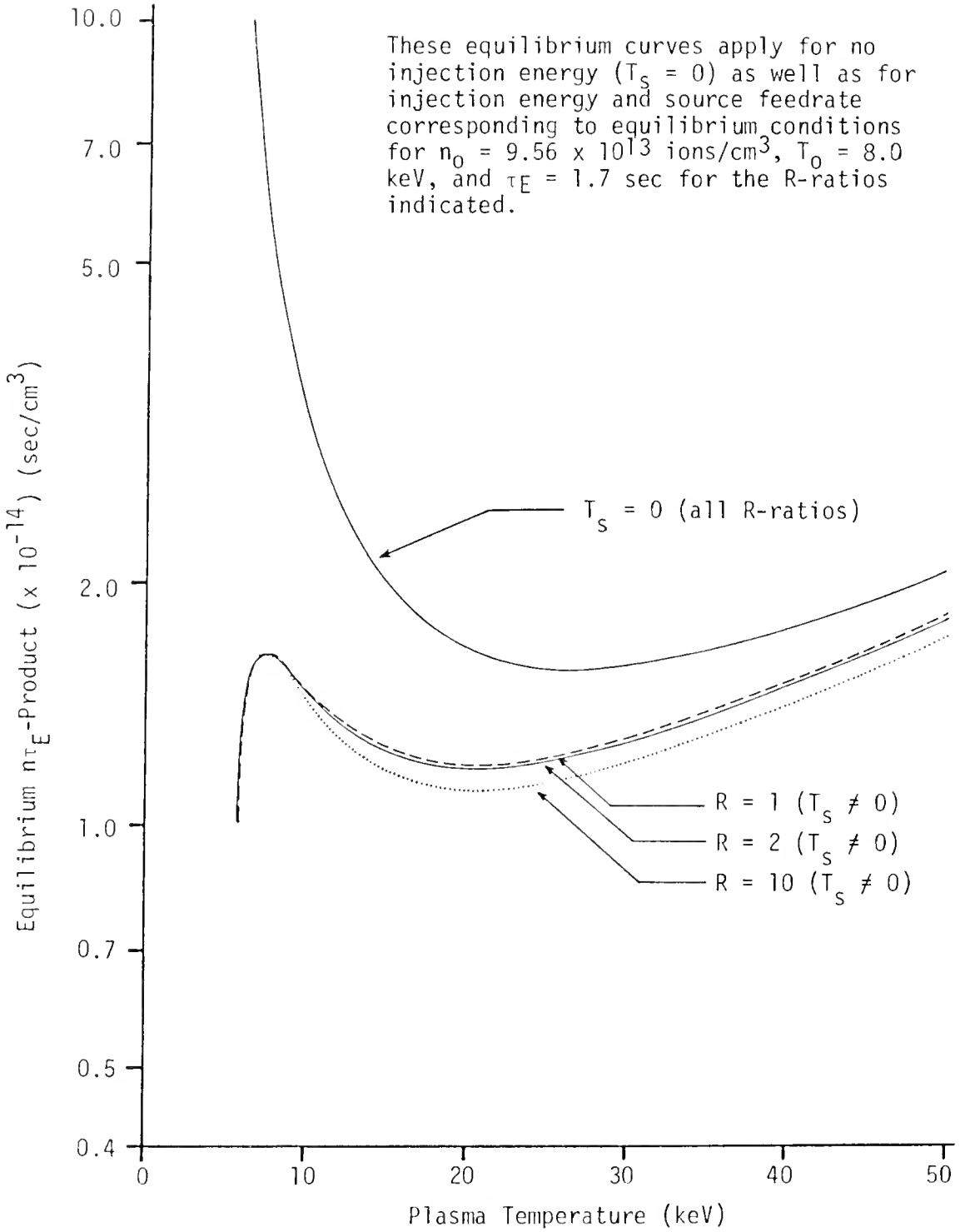
Figure 24. Equilibrium curves for various equilibrium plasma conditions.

Table 4-II

Hybrid Plasma Equilibrium Operating Conditions for τ_{E_o} = 1.7 sec
to Meet Required Power Production

R	n_o (ions/cm^3)	T_o (keV)	τ_{E_o} (sec)	S_o (ions/cm^3-sec)	T_{s_o} (keV)
1	9.56×10^{13}	8.00	1.7	5.652×10^{13}	16.64
2	9.56×10^{13}	8.00	1.7	2.840×10^{13}	33.11
3	9.56×10^{13}	8.00	1.7	1.903×10^{13}	49.42
10	9.56×10^{13}	8.00	1.7	5.905×10^{12}	159.2

After S_o and T_{s_o} were selected as equilibrium values for the hybrid steady-state, CLASSIC2 was rerun for each R-ratio with the S_o and T_{s_o} values for each equilibrium as temperature was allowed to vary from 4 to 50 keV. Equilibrium conditions were determined for each temperature yielding products of equilibrium density and energy confinement time as a function of temperature. The resultant variation of the equilibrium $n_o \tau_{E_o}$-product is shown in Fig. 24. The corresponding equation for the equilibrium $n_o \tau_{E_o}$-product at steady-state is simply:

$$n_o \tau_{E_o} = \frac{3T - \dfrac{T_s}{R}}{\dfrac{<\sigma v>_{DT} Q_\alpha}{4} + \dfrac{<\sigma v>_{DT} T_s}{2} - bT^{1/2}}$$

(184)

where burnup is included.

For comparison purposes the same plasma simulations were repeated for a hypothetical zero injection energy. The resultant equilibrium $n_o \tau_{E_o}$-curves were no longer dependent on feedrate or R-ratios since the equilibrium Mills condition, again including burnup, is given by

$$n_0 \tau E_0 = \frac{3T}{\frac{\langle \sigma v \rangle_{DT} Q_\alpha}{4} - bT^{1/2}}$$

(185)

which only varies with plasma temperature and not with burnup. The resultant equilibrium curve for the case of zero injection energy is also presented in Fig. 24 where the curve is located above the curves obtained with injection energy and exhibits the characteristic parabolic shape.

Essentially, the curves in Fig. 24 indicate that the hybrid plasma is low in reactivity and will require significant blanket conversion of energy to sustain the system. Although many more curves were generated, this Mills-like set of curves including the initial equilibrium condition of $\tau_{E_0} = 1.7$ sec and R = 2 is representative of reasonable operating conditions.

Based on the equilibrium operating data presented in Table 4-I, certain operating ranges were eliminated. For example, the case of R = 10 was eliminated from further consideration for several reasons. First, the injection energies required (140-170 keV) represent significant technological problems, especially at the injection rates required for the low temperature hybrid system. There is no need to make the hybrid more complex than necessary. If the hybrid is to be used as an inter-mediate step in the development of pure fusion, it must be based on technology available in the near term.

Second, the presence of large beam energies with associated large feedrates requires different methods of analysis to evaluate the particle and energy equations. Specifically, the beam-plasma reactivity must be accounted for in such cases as shown in recent work.[115-117] Effects of

non-Maxwellian fusion reactions of the injected beam with the thermal plasma and the resultant finite slowing down time of the injected beam particles cannot be neglected in a Two-Component Torus.

To reduce the number of sets of operating equilibrium conditions to be examined still further, the R = 1 and R = 3 cases were also removed from consideration. The R = 1 case was removed from further consideration because the required source feedrates are nearly as large as the plasma particle density. In addition, the $T_s/3T_0$ ratio is less than unity which is not a condition of interest for hybrids. Such a condition also presents unique problems in determining equilibrum conditions. If plasmas can be self-ignited and sustained, then a Tokamak fusion-fission hybrid will have no place in the power industry except as a possible breeder of fissile fuel in an Augean production system.[2] In addition, the required injection energy was found to be so low (15-17 keV) that it probably would not justify the system complication required to implement it. Such energies are simply not under consideration for presently planned pure fusion or hybrid systems. Of the remaining two cases, the R = 3 case was eliminated in favor of R = 2 simply because some very significant pure fusion design studies such as UWMAK-III[30] and others[29,101] have been based on low R-ratios in the vicinity of R = 2.

After R = 2 was selected as reasonably representative of possible fusion devices, the remaining six cases showing a range for the energy confinement time were each examined to determine operational properties for the hybrid system as well as to determine the effects that increasing confinement efficiency has on the capability of the hybrid plasma to be controlled. Since the sensitivity of the neutron production rate to temperature changes was calculated to be about 2.7 at plasma temperatures

of 8 keV, even small temperature transients were expected to result in significant increases or decreases in the size of the neutron source driving the blanket.

If hybrid blankets are to be optimized for first wall region power density as carefully as pure fusion blankets, then such surges in neutrons and power production will be very important design considerations. They may severely limit overpower ratings as well as average blanket operating power densities.

The complete equilibrium conditions selected for further analysis are presented in Table 4-III. Sample analyses of transients and equilibrium conditions at R = 1 and R = 3 indicated little difference from the R = 2 case in the plasma conditions and responses to perturbations. Essentially the speed of transient development and difficulty of control were found to increase with the R-ratio because the R-ratio is an indicator of the efficiency with which particles are confined and able to compensate the driving source to promote transient development.

Table 4-III

Equilibrium Plasma Conditions Selected for Transient Analysis
With R = 2 and q_{p_o} = 1.41 x 10^{11} nts/cm^3-sec

n_o (ions/cm^3)	T_o (keV)	τ_{E_o} (sec)	S_o (ions/cm^3 sec)	T_{s_o} (keV)
9.56 x 10^{13}	8.0	1.5	3.215 x 10^{13}	34.85
9.56 x 10^{13}	8.0	1.6	3.016 x 10^{13}	33.98
9.56 x 10^{13}	8.0	1.7	2.840 x 10^{13}	33.11
9.56 x 10^{13}	8.0	1.8	2.684 x 10^{13}	32.24
9.56 x 10^{13}	8.0	1.9	2.544 x 10^{13}	31.38
9.56 x 10^{13}	8.0	2.0	2.418 x 10^{13}	30.51

For preset density and temperature values, the equilibrium feedrate and injection energy values were determined for the preselected R = 2 value and equilibrium energy confinement times ranging from 1.5 to 2.0 sec. Then the Mills-Condition curves were generated for each confinement time value. The effects of burnup were included using CLASSIC2. The resultant values for the six equilibria summarized in Table 4-III are presented graphically in Fig. 25. The results are presented graphically in Fig. 25 to illustrate the $n_0 \tau_{E_0}$-curves on which each of the six sets of equilibrium operating hybrid plasma conditions fall. The case of generating these curves for zero injection energy is also included for comparison. Figure 25 showing the hybrid plasma position demonstrates the driven nature of hybrid plasma which means significant blanket fission energy generation will be needed to sustain the plasma and produce net energy for the utility grid.

For more efficient, larger confinement times, lower values of feedrate and injection energy are required for equilibrium as summarized in Table 4-III. Since the driving feedrate and injection energy tend to impede plasma transient development, it is not surprising that plasmas with higher confinement times were found to be less controllable when subjected to perturbations displacing the plasma from the hypothetical equilibrium states presented in Table 4-III.

Each of the six sets of equilibrium operating conditions in Table 4-III was examined for its response to a variety of different perturbations. Since the confinement time was chosen to be time-invariant, and since a spectrum of possible values was examined, there was no point in perturbing the confinement times. The perturbations examined included instantaneous positive and negative 5% step changes in each of four
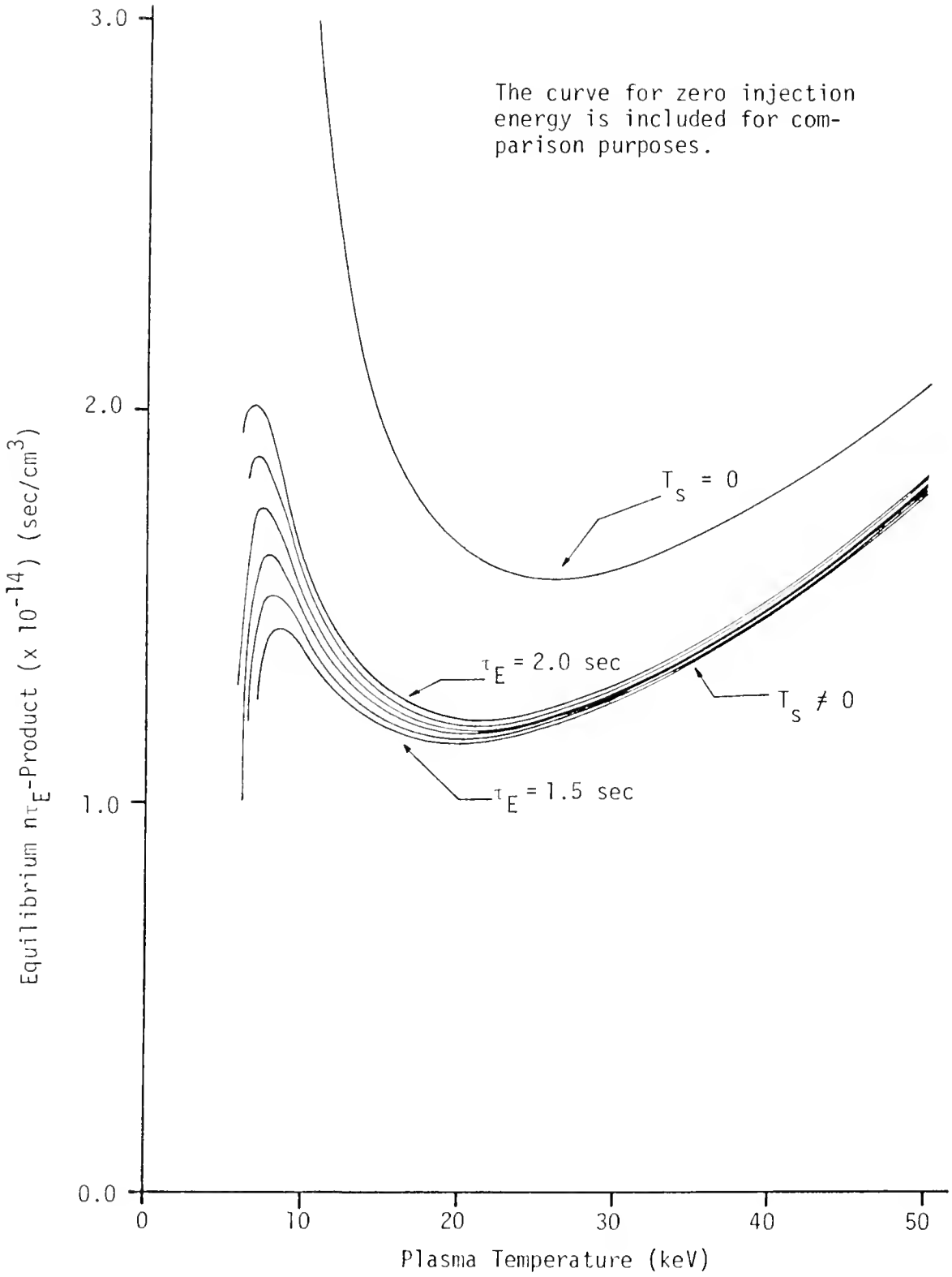
Figure 25. Mills steady-state curves including burnup for R = 2.

equilibrium variables (n, T, S, T_s). Variations in the confinement
time were not considered because it is actually dependent on the state
of the system and cannot realistically be changed independently, but only
in response to some other system parameter change such as density or
temperature.

Uncontrolled Plasma Response to Perturbations

Although a standard 5% perturbation of the equilibrium parameter was
selected for examining the time-dependent response of the hybrid plasma,
some other larger and smaller perturbations were also examined. But the
spectrum of system equilibria examined subject to 5% perturbations is
adequate since larger perturbations become increasingly non-perturbing
and more like large-scale disruptions or accident conditions. Responses
to several smaller perturbations in the range of 0.5-1.0% of an equilib-
rium parameter were examined and showed very sluggish system response
indicative of the non-interesting nature of exceedingly small perturba-
tions in the simplified hybrid plasma model. This sluggish behavior
was especially evident for lower R-ratios and low energy confinement
times because the hybrid plasma is not self-sustaining but maintained by
the feedrate. Because its state is retarded from movement by the driving
feedrate, the hybrid was found to react slowly even for 5% perturbations.

Each of the eight system perturbations ($\pm$ 5% n_o, $\pm$ 5% T_o, $\pm$ 5% S_o,
and $\pm$ 5% T_{s_o}) was introduced into the six different equilibrium hybrid
plasmas represented by the R = 2 sets of equilibrium conditions pre-
sented in Table 4-III. These sets of conditions are referred to as
hypothetical hybrid equilibrium states.

To explain the general transient results of these perturbations, the basic global plasma equations relating particle density and temperature are repeated here in slightly different form from Eqs. (177) and (178) as follows:

$$\frac{dn(t)}{dt} - \frac{n(t)}{\tau_n} - \frac{<\sigma v>_{DT} n^2(t)}{2} = S(t) \qquad (186)$$

$$\frac{d[n(t)T(t)]}{dt} - \frac{<\sigma v>_{DT} Q_\alpha n^2(t)}{12} + \frac{n(t)T(t)}{\tau_E} + \frac{bT^{1/2}(t)n^2(t)}{3} = \frac{S(t)T_s(t)}{3} . \qquad (187)$$

The source feedrate, $S(t)$, and the injection energy, $T_s(t)$, are so-called extrinsic variables; that is, $S(t)$ and $T_s(t)$ act as inhomogeneous source terms similar to inhomogeneous neutron source terms in the point-model reactor kinetics equations. For low-reactivity plasmas such as those used to drive subcritical fission lattices, the analogy is very appropriate and useful. Such extrinsic variables are characteristic only of some predetermined, externally applied conditions. Without the source feedrate to drive the fusioning plasma, the plasma subsystem cannot survive; the same is essentially true for the flux distribution in a subcritical assembly such as the hybrid blanket. Without an inhomogeneous neutron source, there can be no power-producing, neutron flux distribution in the subcritical blanket assembly despite the presence of fissionable fuel.

The extrinsic nature of the source feedrate and the injection energy variables is best illustrated by noting that they affect the global plasma behavior by an external driving force which can be removed or retained based on engineered actions taken external to the global plasma. Neither of these variables is intrinsically or inherently affected by

the transient behavior or time development of the plasma itself. No plasma conditions are inherently effecting changes in the feedrate or injection energy. This feedforward, irreversible nature of the driving variables, S and T_s, is illustrated in Fig. 26.

Perturbations in the source feedrate or in the injection energy are really step changes externally introduced into the plasma. CLASSIC2 modeled the changes in these variables as permanent until the initial alteration was removed or changed with time by some external action represented as artificial or engineered feedback. The time scale for such removal may range from instantaneous up to many seconds or even minutes depending on the physical nature of the perturbation and the corresponding feedback engineered into the system. However, there is nothing in the system response that can inherently remove or affect changes in an external driving force represented by the perturbed feedrate or the perturbed injection energy. This type of perturbation remains effective and unchangeable until removed by some external action which contrasts directly with perturbations in the temperature or the particle density which disappear with time as the plasma undergoes transient development.

Physically, these changes in S or T_s are not internal perturbations but rather correspond to external system malfunctions where either the injection rate or the injection energy might be suddenly set to a new value different from its equilibrium value. This may be a temporary or even permanent (as far as one fusioning plasma duty cycle is concerned) value different from the design conditions for these driving variables. Therefore, when step changes in the extrinsic variables were introduced into the system, the plasma simply underwent a transient response to
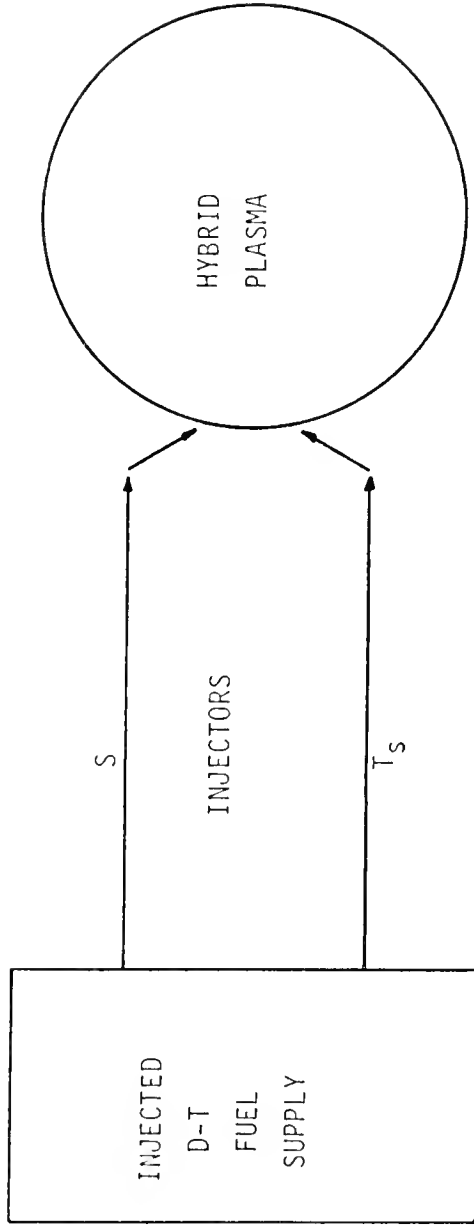
Figure 26. Illustration of the feedforward effectiveness of the source feedrate and the injection energy on plasma equilibrium conditions and transient behavior.

reach a new equilibrium where the feedrate or the injection energy assumed equilibrium values corresponding to the new value of the perturbed feedrate or injection energy.

In contrast, the plasma density and the plasma temperature are intrinsic variables, just as the neutron density and the precursor concentration are in a fissioning assembly. In contrast to the inhomogeneous source terms, changes in other plasma variables or operating conditions result in changes in such intrinsic variables: There variables are characteristic of the state of the system described. If the state is changed, then the describing variables must change. For example, if the density is changed, then the temperature is expected to change automatically depending on how the density is changed; the essential compensation of intrinsic variables is inherent to describe the evolution state of the system. However, the externally-fixed source feedrate and injection energy will not change unless some external effect is introduced.

This conceptually simple dichotomy of variables is important to the proper understanding of the dynamic response of the hybrid plasma to the different types of perturbations for which it was examined. The transient growth or decay of the plasma from an equilibrium state can be characterized according to the general category of the perturbed variable. Thus the transient development of the hybrid plasma was qualitatively categorized prior to examination of the actual perturbations because the plasma was expected to behave differently for perturbations in temperature and ion density versus perturbations in the inhomogeneous feedrate and injection energy.

Perturbations in the plasma temperature or the particle density, about an equilibrium condition were found to result in the plasma returning to the original system temperature, density, and neutron production rate or evolving to some other operating regime depending on the stability of the global plasma system at the state coordinates in effect as a result of the perturbation. Depending on the proximity to a stable operating regime, the system was found to react more or less quickly to adjust its state coordinates to the parameter perturbations; for the intrinsic variables, the perturbations were lost within the evolving system response.

The final equilibrium plasma states (density, n_F, temperature, T_F, and volumetric neutron production rate, q_{p_F}) resulting from $\pm$ 5% step changes in each of the four plasma variables are presented in Tables 4-IV through 4-XI. Each table contains entries for each of the six initial hypothetical hybrid equilibrium conditions presented in Table 4-III. These results in Tables 4-IV through 4-XI were obtained by perturbing each plasma state and following the resultant nonlinear temperature development until the plasma temperature (and density) reached steady state. The plasma conditions were found to return to the initial state involved or some other different final state characteristic of the $R = 2$, τ_{E_0}, S_0, and T_{s_0} conditions established at the outset for the particular perturbation run in question.

No further consideration was given to the density perturbations. Previous work has shown that density feedback cannot be used to control an inherently unstable plasma. Here, the insensitivity of the density to the plasma state involved was demonstrated by the relatively small fractional changes exhibited by the final densities recorded in Tables

Table 4-IV

Final Uncontrolled Hybrid Plasma Equilibrium Conditions Following
a +%5 Perturbation in the Temperature

$R*$	τ_E (sec)	$n_F\tau_E$ (sec/cm^3)	n_F (ions/cm^3)	T_F (keV)	q_{p_F} (nts/cm^3-sec)
1	1.5	1.434×10^{14}	9.560×10^{13}	8.00	1.410×10^{11}
	1.6	1.455×10^{14}	9.093×10^{13}	38.06	1.601×10^{12}
	1.7	1.539×10^{14}	9.051×10^{13}	40.90	1.629×10^{12}
	1.8	1.622×10^{14}	9.011×10^{13}	43.58	1.665×10^{12}
	1.9	1.705×10^{14}	8.974×10^{13}	46.13	1.682×10^{12}
	2.0	1.788×10^{14}	8.939×10^{13}	48.55	1.693×10^{12}
2	1.5	1.434×10^{14}	9.560×10^{13}	8.00	1.410×10^{11}
	1.6	1.397×10^{14}	8.730×10^{13}	36.24	1.438×10^{12}
	1.7	1.472×10^{14}	8.658×10^{13}	38.92	1.467×10^{12}
	1.8	1.547×10^{14}	8.592×10^{13}	41.42	1.485×10^{12}
	1.9	1.621×10^{14}	8.531×10^{13}	43.78	1.495×10^{12}
	2.0	1.695×10^{14}	8.473×10^{13}	46.03	1.499×10^{12}
3	1.5	1.434×10^{14}	9.560×10^{13}	8.00	1.410×10^{11}
	1.6	1.350×10^{14}	8.437×10^{13}	34.74	1.310×10^{12}
	1.7	1.418×10^{14}	8.343×10^{13}	38.30	1.334×10^{12}
	1.8	1.486×10^{14}	8.258×10^{13}	39.68	1.347×10^{12}
	1.9	1.554×10^{14}	8.180×10^{13}	41.90	1.352×10^{12}
	2.0	1.621×10^{14}	8.106×10^{13}	44.00	1.352×10^{12}
10	1.5	1.434×10^{13}	9.560×10^{13}	8.00	1.410×10^{11}
	1.6	1.166×10^{13}	7.286×10^{13}	28.75	8.517×10^{11}
	1.7	1.210×10^{14}	7.118×10^{13}	30.81	8.592×10^{11}
	1.8	1.255×10^{14}	6.970×10^{13}	32.71	8.603×10^{11}
	1.9	1.299×10^{14}	6.839×10^{13}	34.47	8.570×10^{11}
	2.0	1.344×10^{14}	6.721×10^{13}	36.11	8.507×10^{11}

*Power-producing initial equilibrium conditions were the same for all
cases: $T_0 = 8.0$ keV, $n_0 = 9.56 \times 10^{13}$ ions/cm^3, and $q_{p_0} = 1.41 \times 10^{11}$
nts/cm^3-sec.

Table 4-V

Final Uncontrolled Hybrid Plasma Equilibrium Conditions Following
a -5% Perturbation in the Temperature

R^*	τ_E (sec)	$n_F \tau_E$ (sec/cm^3)	n_F (ions/cm^3)	T_F (keV)	q_{p_F} (nts/cm^3-sec)
1	1.5	1.434×10^{14}	9.560×10^{13}	8.00	1.410×10^{11}
	1.6	1.530×10^{14}	9.560×10^{13}	8.00	1.410×10^{11}
	1.7	1.625×10^{14}	9.560×10^{13}	8.00	1.410×10^{11}
	1.8	1.724×10^{14}	9.576×10^{13}	7.056	9.734×10^{10}
	1.9	1.821×10^{14}	9.584×10^{13}	6.536	7.663×10^{10}
	2.0	1.918×10^{14}	9.592×10^{13}	6.100	6.141×10^{10}
2	1.5	1.434×10^{14}	9.560×10^{13}	8.00	1.410×10^{11}
	1.6	1.530×10^{14}	9.560×10^{13}	8.00	1.409×10^{11}
	1.7	1.628×10^{14}	9.574×10^{13}	7.573	1.204×10^{11}
	1.8	1.727×10^{14}	9.593×10^{13}	6.977	9.428×10^{10}
	1.9	1.826×10^{14}	9.610×10^{13}	6.477	7.487×10^{10}
	2.0	1.925×10^{14}	9.625×10^{13}	6.044	6.001×10^{10}
3	1.5	1.434×10^{14}	9.560×10^{13}	8.00	1.410×10^{11}
	1.6	1.530×10^{14}	9.560×10^{13}	8.00	1.409×10^{11}
	1.7	1.629×10^{14}	9.583×10^{13}	7.531	1.187×10^{11}
	1.8	1.730×10^{14}	9.613×10^{13}	6.914	9.207×10^{10}
	1.9	1.831×10^{14}	9.637×10^{13}	6.414	7.295×10^{10}
	2.0	1.932×10^{14}	9.659×10^{13}	5.987	5.858×10^{10}
10	1.5	1.434×10^{14}	9.560×10^{13}	8.00	1.410×10^{11}
	1.6	1.532×10^{14}	9.560×10^{13}	7.99	1.366×10^{11}
	1.7	1.648×10^{14}	9.698×10^{13}	7.066	1.007×10^{11}
	1.8	1.762×10^{14}	9.787×10^{13}	6.485	7.797×10^{10}
	1.9	1.873×10^{14}	9.860×10^{13}	6.012	6.191×10^{10}
	2.0	1.986×10^{14}	9.929×10^{13}	5.581	4.875×10^{10}

*Power-producing initial equilibrium conditions were the same for all
cases: $T_0 = 8.0$ keV, $n_0 = 9.56 \times 10^{13}$ ions/cm^3, and $q_{p_0} = 1.41 \times 10^{11}$
nts/cm^3-sec.

Table 4-VI

Final Uncontrolled Hybrid Plasma Equilibrium Conditions Following
a 5% Step Increase in the Steady-State Source Feedrate

R^*	τ_E (sec)	$n_F \tau_E$ (sec/cm^3)	n_F (ions/cm^3)	T_F (keV)	q_{p_F} (nts/cm^3-sec)
1	1.5	1.433×10^{14}	9.556×10^{13}	37.47	1.754×10^{12}
	1.6	1.521×10^{14}	9.509×10^{13}	40.53	1.802×10^{12}
	1.7	1.609×10^{14}	9.465×10^{13}	43.36	1.833×10^{12}
	1.8	1.696×10^{14}	9.424×10^{13}	46.06	1.854×10^{12}
	1.9	1.783×10^{14}	9.385×10^{13}	48.60	1.867×10^{12}
	2.0	1.870×10^{14}	9.348×10^{13}	51.07	1.874×10^{12}
2	1.5	1.377×10^{14}	9.180×10^{13}	35.72	1.577×10^{12}
	1.6	1.456×10^{14}	9.100×10^{13}	38.59	1.614×10^{12}
	1.7	1.534×10^{14}	9.026×10^{13}	41.23	1.635×10^{12}
	1.8	1.612×10^{14}	8.958×10^{13}	43.73	1.547×10^{12}
	1.9	1.690×10^{14}	8.894×10^{13}	46.10	1.652×10^{12}
	2.0	1.767×10^{14}	8.835×10^{13}	48.35	1.652×10^{12}
3	1.5	1.331×10^{14}	8.876×10^{13}	34.28	1.439×10^{12}
	1.6	1.403×10^{14}	8.771×10^{13}	36.99	1.467×10^{12}
	1.7	1.475×10^{14}	8.676×10^{13}	39.52	1.484×10^{12}
	1.8	1.546×10^{14}	8.589×10^{13}	41.86	1.490×10^{12}
	1.9	1.616×10^{14}	8.508×10^{13}	44.08	1.490×10^{12}
	2.0	1.686×10^{14}	8.432×10^{13}	46.20	1.486×10^{12}
10	1.5	1.151×10^{14}	7.672×10^{13}	28.47	9.368×10^{11}
	1.6	1.197×10^{14}	7.483×10^{13}	30.67	9.464×10^{11}
	1.7	1.244×10^{14}	7.318×10^{13}	32.68	9.478×10^{11}
	1.8	1.291×10^{14}	7.173×10^{13}	34.54	9.438×10^{11}
	1.9	1.338×10^{14}	7.043×10^{13}	36.27	9.362×10^{11}
	2.0	1.385×10^{14}	6.924×10^{13}	37.90	9.264×10^{11}

*Power-producing initial equilibrium conditions were the same for all cases: $T_0 = 8.0$ keV, $n_0 = 9.56 \times 10^{13}$ ions/cm^3, and $q_{p_0} = 1.41 \times 10^{11}$ nts/cm^3-sec.

Table 4-VII

Final Uncontrolled Hybrid Plasma Equilibrium Conditions Following a 5% Step Decrease in the Steady-State Source Feedrate

R^*	τ_E (sec)	$n_F \tau_E$ (sec/cm³)	n_F (ions/cm³)	T_F (keV)	q_{p_F} (nts/cm³-sec)
1	1.5	1.364×10^{14}	9.092×10^{13}	7.406	1.017×10^{11}
	1.6	1.455×10^{14}	9.095×10^{13}	7.201	9.349×10^{10}
	1.7	1.547×10^{14}	9.099×10^{13}	6.921	8.276×10^{10}
	1.8	1.639×10^{14}	9.104×10^{13}	6.598	7.121×10^{10}
	1.9	1.731×10^{14}	1.731×10^{13}	6.263	6.031×10^{10}
	2.0	1.823×10^{14}	9.115×10^{13}	5.935	5.074×10^{10}
2	1.5	1.365×10^{14}	9.102×10^{13}	7.386	1.011×10^{11}
	1.6	1.457×10^{14}	9.108×10^{13}	7.172	9.264×10^{10}
	1.7	1.550×10^{14}	9.117×10^{13}	6.882	8.163×10^{10}
	1.8	1.643×10^{14}	9.128×10^{13}	6.557	7.022×10^{10}
	1.9	1.736×10^{14}	9.139×10^{13}	6.208	5.894×10^{10}
	2.0	1.830×10^{14}	9.149×10^{13}	5.885	4.968×10^{10}
3	1.5	1.367×10^{14}	9.112×10^{13}	7.367	1.006×10^{11}
	1.6	1.460×10^{14}	9.122×10^{13}	7.142	9.174×10^{10}
	1.7	1.553×10^{14}	9.136×10^{13}	6.841	8.042×10^{10}
	1.8	1.647×10^{14}	9.152×10^{13}	6.514	6.916×10^{10}
	1.9	1.742×10^{14}	9.168×10^{13}	6.163	5.797×10^{10}
	2.0	1.837×10^{14}	9.184×10^{13}	5.832	4.857×10^{10}
10	1.5	1.380×10^{14}	9.197×10^{13}	7.201	9.561×10^{11}
	1.6	1.478×10^{14}	9.239×10^{13}	6.904	8.466×10^{10}
	1.7	1.579×10^{14}	9.290×10^{13}	6.559	7.280×10^{10}
	1.8	1.682×10^{14}	9.345×10^{13}	6.187	6.094×10^{10}
	1.9	1.785×10^{14}	9.397×10^{13}	5.838	5.103×10^{10}
	2.0	1.890×10^{14}	9.451×10^{13}	5.483	4.165×10^{10}

*Power-producing initial equilibirum conditions were the same for all cases: $T_0 = 8.0$ keV, $n_0 = 9.56 \times 10^{13}$ ions/cm³, and $q_{p_0} = 1.41 \times 10^{11}$ nts/cm³-sec.

Table 4-VIII

Final Uncontrolled Hybrid Plasma Equilibrium Conditions Following
a +5% Perturbation in the Ion Density

R^*	τ_E (sec)	$n_F \tau_E$ (sec/cm^3)	n_F (ions/cm^3)	T_F (keV)	q_{p_F} (nts/cm^3-sec)
1	1.5	1.434×10^{14}	9.560×10^{13}	8.00	1.410×10^{11}
	1.6	1.455×10^{14}	9.093×10^{13}	38.06	1.601×10^{12}
	1.7	1.539×10^{14}	9.051×10^{13}	40.90	1.639×10^{12}
	1.8	1.622×10^{14}	9.011×10^{13}	43.58	1.665×10^{12}
	1.9	1.705×10^{14}	8.974×10^{13}	46.13	1.682×10^{12}
	2.0	1.788×10^{14}	8.939×10^{13}	48.55	1.693×10^{12}
2	1.5	1.434×10^{14}	9.560×10^{13}	8.00	1.410×10^{11}
	1.6	1.397×10^{14}	8.730×10^{13}	36.24	1.438×10^{12}
	1.7	1.472×10^{14}	8.658×10^{13}	38.92	1.467×10^{12}
	1.8	1.547×10^{14}	8.592×10^{13}	41.42	1.485×10^{12}
	1.9	1.621×10^{14}	8.531×10^{13}	43.78	1.495×10^{12}
	2.0	1.695×10^{14}	8.473×10^{13}	46.02	1.499×10^{12}
3	1.5	1.434×10^{14}	9.560×10^{13}	8.00	1.410×10^{11}
	1.6	1.530×10^{14}	9.560×10^{13}	8.00	1.410×10^{11}
	1.7	1.629×10^{14}	9.583×10^{13}	7.531	1.187×10^{11}
	1.8	1.730×10^{14}	9.613×10^{13}	6.914	9.207×10^{10}
	1.9	1.554×10^{14}	8.180×10^{13}	41.90	1.352×10^{12}
	2.0	1.621×10^{14}	8.106×10^{13}	44.00	1.352×10^{12}
10	1.5	1.434×10^{14}	9.560×10^{13}	8.00	1.410×10^{11}
	1.6	1.530×10^{14}	9.560×10^{13}	7.99	1.409×10^{11}
	1.7	1.649×10^{14}	9.698×10^{13}	7.065	1.003×10^{10}
	1.8	1.762×10^{14}	9.787×10^{13}	6.485	7.795×10^{10}
	1.9	1.873×10^{14}	9.860×10^{13}	6.012	6.190×10^{10}
	2.0	1.986×10^{14}	9.929×10^{13}	5.581	4.875×10^{10}

*Power-producing initial equilibrium conditions were the same for all
cases: $T_0 = 8.0$ keV, $n_0 = 9.56 \times 10^{13}$ ions/cm^3, and $q_{p_0} = 1.51 \times 10^{11}$
nts/cm^3-sec.

3333

Table 4-IX

Final Uncontrolled Hybrid Plasma Equilibrium Conditions Following
a -5% Perturbation in the Ion Density

R^*	τ_E (sec)	$n_F\tau_E$ (sec/cm^3)	n_F (ions/cm^3)	T_F (keV)	q_{p_F} (nts/cm^3-sec)
1	1.5	1.434×10^{14}	9.560×10^{13}	8.00	1.410×10^{11}
	1.6	1.434×10^{14}	9.560×10^{13}	8.00	1.410×10^{11}
	1.7	1.625×10^{14}	9.560×10^{13}	7.988	1.391×10^{11}
	1.8	1.724×10^{14}	9.576×10^{13}	7.056	9.733×10^{10}
	1.9	1.821×10^{14}	9.584×10^{13}	6.536	7.663×10^{10}
	2.0	1.918×10^{14}	9.592×10^{13}	6.100	6.141×10^{10}
2	1.5	1.434×10^{14}	9.560×10^{13}	8.00	1.410×10^{11}
	1.6	1.530×10^{14}	9.560×10^{13}	8.00	1.410×10^{11}
	1.7	1.628×10^{14}	9.574×10^{13}	7.573	1.204×10^{11}
	1.8	1.727×10^{14}	9.593×10^{13}	6.976	9.428×10^{10}
	1.9	1.826×10^{14}	9.610×10^{13}	6.477	7.487×10^{10}
	2.0	1.925×10^{14}	9.625×10^{13}	6.044	6.001×10^{10}
3	1.5	1.434×10^{14}	9.560×10^{13}	8.00	1.410×10^{11}
	1.6	1.350×10^{14}	8.437×10^{13}	34.74	1.310×10^{12}
	1.7	1.418×10^{14}	8.343×10^{13}	37.30	1.334×10^{12}
	1.8	1.486×10^{14}	8.258×10^{13}	39.68	1.347×10^{12}
	1.9	1.831×10^{14}	9.637×10^{13}	6.414	7.295×10^{10}
	2.0	1.932×10^{14}	9.659×10^{13}	5.987	5.858×10^{10}
10	1.5	1.123×10^{14}	7.483×10^{13}	26.43	8.331×10^{11}
	1.6	1.166×10^{14}	7.286×10^{13}	28.75	3.517×10^{11}
	1.7	1.210×10^{14}	7.118×10^{13}	30.81	8.592×10^{11}
	1.8	1.255×10^{14}	6.970×10^{13}	32.71	8.603×10^{11}
	1.9	1.299×10^{14}	6.839×10^{13}	34.47	8.570×10^{11}
	2.0	1.344×10^{14}	6.721×10^{13}	36.11	8.507×10^{11}

*Power-producing initial equilibrium conditions were the same for all cases: $T_0 = 8.0$ keV, $n_0 = 9.56 \times 10^{13}$ ions/cm^3, and $q_{p_0} = 1.41 \times 10^{11}$ nts/cm^3-sec.

Table 4-X

Final Uncontrolled Hybrid Plasma Equilibrium Conditions Following
a 5% Step Increase in the Steady-State Injection Energy

R^*	τ_E (sec)	$n_F \tau_E$ (sec/cm^3)	n_F (ions/cm^3)	T_F (keV)	q_{p_F} (nts/cm^3-sec)
1	1.5	1.370×10^{14}	9.135×10^{13}	35.50	1.556×10^{12}
	1.6	1.454×10^{14}	9.090×10^{13}	38.54	1.609×10^{12}
	1.7	1.538×10^{14}	9.048×10^{13}	41.34	1.645×10^{12}
	1.8	1.622×10^{14}	9.009×10^{13}	43.99	1.670×10^{12}
	1.9	1.705×10^{14}	8.973×10^{13}	46.49	1.686×10^{12}
	2.0	1.788×10^{14}	8.938×10^{13}	48.90	1.696×10^{12}
2	1.5	1.320×10^{14}	8.801×10^{13}	33.94	1.406×10^{12}
	1.6	1.396×10^{14}	8.724×10^{13}	36.76	1.447×10^{12}
	1.7	1.471×10^{14}	8.653×10^{13}	39.41	1.474×10^{12}
	1.8	1.546×10^{14}	8.589×10^{13}	41.86	1.490×10^{12}
	1.9	1.620×10^{14}	8.528×10^{13}	44.19	1.498×10^{12}
	2.0	1.694×10^{14}	8.471×10^{13}	46.40	1.502×10^{12}
3	1.5	1.279×10^{14}	8.530×10^{13}	32.60	1.285×10^{12}
	1.6	1.348×10^{14}	8.428×10^{13}	35.32	1.320×10^{12}
	1.7	1.417×10^{14}	8.336×10^{13}	37.83	1.341×10^{12}
	1.8	1.485×10^{14}	8.252×10^{13}	40.16	1.352×10^{12}
	1.9	1.553×10^{14}	8.175×10^{13}	42.33	1.356×10^{12}
	2.0	1.621×10^{14}	8.103×10^{13}	44.40	1.355×10^{12}
10	1.5	1.115×10^{14}	7.435×10^{13}	27.36	8.493×10^{11}
	1.6	1.160×10^{14}	7.250×10^{13}	29.55	8.629×10^{11}
	1.7	1.205×10^{14}	7.089×10^{13}	31.54	8.676×10^{11}
	1.8	1.251×10^{14}	6.948×10^{13}	33.37	8.665×10^{11}
	1.9	1.296×10^{14}	6.822×10^{13}	35.07	8.615×10^{11}
	2.0	1.341×10^{14}	6.707×10^{13}	36.67	8.541×10^{11}

*Power-producing initial equilibrium conditions were the same for all
cases: $T_0 = 8.0$ keV, $n_0 = 9.56 \times 10^{13}$ ions/cm^3, and $q_{p_0} = 1.41 \times 10^{11}$
nts/cm^3-sec.

Table 4-XI

Final Uncontrolled Hybrid Plasma Equilibrium Conditions Following
a 5% Step Decrease in the Steady-State Injection Energy

R^*	τ_E (sec)	$n_F\tau_E$ (sec/cm^3)	n_F (ions/cm^3)	T_F (keV)	q_{p_F} (nts/cm^3-sec)
1	1.5	1.437×10^{14}	9.579×10^{13}	6.576	7.803×10^{10}
	1.6	1.533×10^{14}	9.583×10^{13}	6.359	7.018×10^{10}
	1.7	1.630×10^{14}	9.587×10^{13}	6.115	6.183×10^{10}
	1.8	1.726×10^{14}	9.591×10^{13}	5.859	5.382×10^{10}
	1.9	1.823×10^{14}	9.596×10^{13}	5.579	4.549×10^{10}
	2.0	1.920×10^{14}	9.601×10^{13}	5.317	3.867×10^{10}
2	1.5	1.440×10^{14}	9.598×10^{13}	6.550	7.740×10^{10}
	1.6	1.537×10^{14}	9.606×10^{13}	6.327	6.937×10^{10}
	1.7	1.634×10^{14}	9.614×10^{13}	6.080	6.107×10^{10}
	1.8	1.732×10^{14}	9.623×10^{13}	5.818	5.288×10^{10}
	1.9	1.830×10^{14}	9.633×10^{13}	5.539	4.478×10^{10}
	2.0	1.928×10^{14}	9.642×10^{13}	5.272	3.786×10^{10}
3	1.5	1.443×10^{14}	9.618×10^{13}	6.524	7.675×10^{10}
	1.6	1.541×10^{14}	9.629×10^{13}	6.294	6.852×10^{10}
	1.7	1.639×10^{14}	9.642×10^{13}	6.045	6.027×10^{10}
	1.8	1.738×10^{14}	9.656×10^{13}	5.777	5.198×10^{10}
	1.9	1.837×10^{14}	9.670×10^{13}	5.499	4.404×10^{10}
	2.0	1.937×10^{14}	9.685×10^{13}	5.226	3.702×10^{10}
10	1.5	1.465×10^{14}	9.768×10^{13}	6.327	7.173×10^{10}
	1.6	1.569×10^{14}	9.809×10^{13}	6.068	6.315×10^{10}
	1.7	1.675×10^{14}	9.854×10^{13}	5.789	5.450×10^{10}
	1.8	1.782×10^{14}	9.901×10^{13}	5.497	4.611×10^{10}
	1.9	1.890×10^{14}	9.949×10^{13}	5.209	3.860×10^{10}
	2.0	1.999×10^{14}	9.995×10^{13}	4.931	3.208×10^{10}

*Power-producing initial equilibrium conditions were the same for all
cases: $T_0 = 8.0$ keV, $n_0 = 9.56 \times 10^{13}$ ions/cm^3, and $q_{p_0} = 1.41 \times 10^{11}$
nts/cm^3-sec.

4-IV through 4-XI. Regardless of the perturbation involved, the density was never found to change by more than 15% and, in most cases, by less than 5% of the initial value. Since the plasma density was noted to react weakly to other variable perturbations, it was rejected as a useful controlling intrinsic variable.

In comparison, the temperature was found to change by nearly an order of magnitude for many of the +5% perturbations summarized in Tables 4-IV, 4-VI, 4-VIII, and 4-X. Similarly, the temperature was found to decrease by as much as 40% or more for -5% perturbations whose final states are summarized in Tables 4-V, 4-VII, 4-IX, and 4-XI. This behavior demonstrated the controlling capability of the temperature variable. Therefore, beyond the results in Tables 4-VIII and 4-IX, perturbations in the density were discarded from further consideration in favor of temperature perturbations.

Both feedrate and injection energy are extrinsic variables which were found to drive the plasma to new equilibrium states when perturbed unless an external influence or feedback effect was utilized to eliminate the perturbing step change with some delay time. Feedback dependent on the feedrate was selected for control of the plasma over feedback dependent on the injection energy. This choice was based on the appearance of the feedrate variable in both the temperature and energy equations of the basic plasma model versus the injection energy variable which appears only in the energy equation. Therefore, to eliminate redundancy, no further consideration was given to the injection energy perturbations beyond the results presented in Tables 4-X and 4-XI.

In addition, only the hypothetical hybrid states with R = 2 were considered for further time-dependent analysis.

Predicted Stability Versus Point-Model Response

The final states presented in Tables 4-IV through 4-XI represent only comparative information on stability since the plasma model used for these calculations is not valid for the large 30-40 keV temperature changes indicated in some of the transients. However, the results in Table 4-IV for positive perturbations do indicate that the plasma is stable for the case where τ_{E_0} = 1.5 sec and unstable for all other values of the energy confinement time. However, for negative perturbations, Table 4-V indicates that the hybrid plasma is stable for both τ_{E_0} = 1.5 sec and τ_{E_0} = 1.6 sec, and unstable for larger confinement times. For the designated R-ratio (R = 2) as well as equilibrium ion density (n_0 = 9.56 x 10^{13} ions/cm^3 sec) and temperature (T_0 = 8.0 keV) required for design blanket power production, the stability criteria based on the linear analysis of Chapter 3 predicted that these plasma systems would be stable to small temperature perturbations for all constant confinement times up to and including τ_{E_0} = 1.6 sec. Similarly, all such plasma systems were predicted to be unstable for larger confinement times. These stability predictions were based on linearized variations using arbitrarily small perturbations and are summarized in Table 4-XII where K_s is the feedback coefficient defined in Eqs. (180) and (181).

Table 4-XII

Summary of Predicted Stabilization Requirements for Instantaneous
Temperature Feedback on the Feedrate

τ_{E_0} (sec)*	S_0 (nts/cm^3-sec)	T_{S_0} (keV)	K_S (1/cm^3-sec-keV)	$\frac{K_S}{S_0}$ (1/keV)
0.5	9.588×10^{13}	43.59	0.00	0.00
1.0	4.808×10^{13}	39.20	0.00	0.00
1.5	3.215×10^{13}	34.85	0.00	0.00
1.6	3.016×10^{13}	33.98	0.00	0.00
1.7	2.840×10^{13}	33.11	5.478×10^{11}	0.0161
1.8	2.684×10^{13}	32.24	1.029×10^{12}	0.0384
1.9	2.544×10^{13}	31.38	1.482×10^{12}	0.0583
2.0	2.418×10^{13}	30.51	1.842×10^{12}	0.0762
2.5	1.940×10^{13}	26.20	2.801×10^{12}	0.1444
3.0	1.622×10^{13}	21.92	3.080×10^{12}	0.1899

*Power-producing initial equilibrium conditions were the same for all
cases: $R = 2$, $T_0 = 8.0$ keV, $n_0 = 9.56 \times 10^{13}$ ions/cm^3, and $q_{p_0} = 1.41 \times 10^{11}$ nts/cm^3-sec.

Similar stability predictions dependent on the energy confinement
times were also obtained for cases of equilibrium plasmas with different
R-ratios (1, 3, and 10). The only difference noted for changes in the
R-ratio was that the range of stable energy confinement times was reduced
as the R-ratio increased. However, the $\pm$ 5% perturbations in temperature
also did not yield the same stability limits on the confinement time for
these other values of the R-ratio. The predicted values such as those
in Table 4-XII were obtained from stability criteria presented in Eqs.

(90a)-(90c) in Chapter 2 and defined by the total feedback coefficient, K_s, in Eqs. (180) and (181). In every case summarized in Table 4-IV, the results of the positive perturbation simulations verified stable operating conditions only for τ_{E_0} = 1.5 sec. In contrast the results of the negative perturbations agreed with the linearized stability predictions such as those in Table 4-XII.

Since the results of the dynamic simulations presented in Table 4-VI do not agree with linearized predictions for positive temperature perturbations some explanation was required. Essentially, this disagreement has not appeared in other studies because such low plasma temperatures at 8.0 keV have not been seriously considered for point-model plasma conditions in pure fusion devices.

As presented in Fig. 25, the Mills Equilibrium Curves characteristically turn down at low temperature in the range of 7-9 keV for cases of interest for hybrid study. The peaking effect at low temperatures is a unique feature of highly-driven systems such as the Two-Component Torus[115] and hybrid plasmas. The characteristic shape essentially means that there are three equilibrium sets of operating conditions (n_0, T_0, τ_{E_0}, T_{s_0}, S_0) corresponding to each equilibrium $n_0 \tau_{E_0}$-value selected for hybrid operation.

Previous analysis[18] and the presentation in Chapter 2 has shown that a positive slope region on the $n_0 \tau_{E_0}$-curve implies stability for constant confinement. Therefore, if the equilibrium 8-keV hybrid conditions are located to the left of the peak, linear analysis predicts stability. However, if perturbations are inserted to study transient behavior and establish stability based on the actual nonlinear plasma equations, even relatively small positive perturbations may move the system to a new set

of nonequilibrium conditions with the same $n_0 \tau_{E_0}$-value but on a different equilibrium curve where the slope may be negative. If this situation occurs, the system will appear to be unstable for perturbations in temperature and the system will not return ultimately to the original equilibrium state from which it was perturbed.

This behavior is exactly the situation which was found for the +5% temperature perturbation for the $\tau_{E_0} = 1.6$ sec hypothetical hybrid equilibrium condition. When the state was perturbed using a very small, +0.5% temperature perturbations, then the system did return to a temperature of 8.0 keV to verify inherent stability for the $\tau_{E_0} = 1.5$ sec and $\tau_{E_0} = 1.6$ sec hypothetical hybrid plasma states as predicted. This situation was found to prevail for all the positive perturbations whose nonlinear transient simulation showing instability did not agree with the linearized model predictions of stability.

As a specific example, the initial R = 2, $\tau_{E_0} = 1.6$ state was predicted to be stable from linearized analysis which implied arbitrarily small perturbations in temperature about the initial equilibrium state represented by n_0, T_0, τ_{E_0}, S_0, and T_{s_0}. This initial equilibrium state (labeled A) was situated on a Mills curve as simulated in Fig. 27. When n_0 and τ_{E_0} were specified and a +5% perturbation introduced for temperature, then Mills' equilibrium $n_0 \tau_{E_0}$-condition in Eq. (184) implied the need for a new injection energy, T_{s_0}', and feedrate, S_0', because $n_0 \tau_{E_0}$ was constrained to remain unchanged. However, with the new parameters, the state was at position B in Fig. 27 which was on a new Mills curve corresponding to the perturbed temperature. When small enough perturbations were used to initiate the nonlinear simulation, the linearized predictions of stability were found in all cases to agree with the nonlinear results.
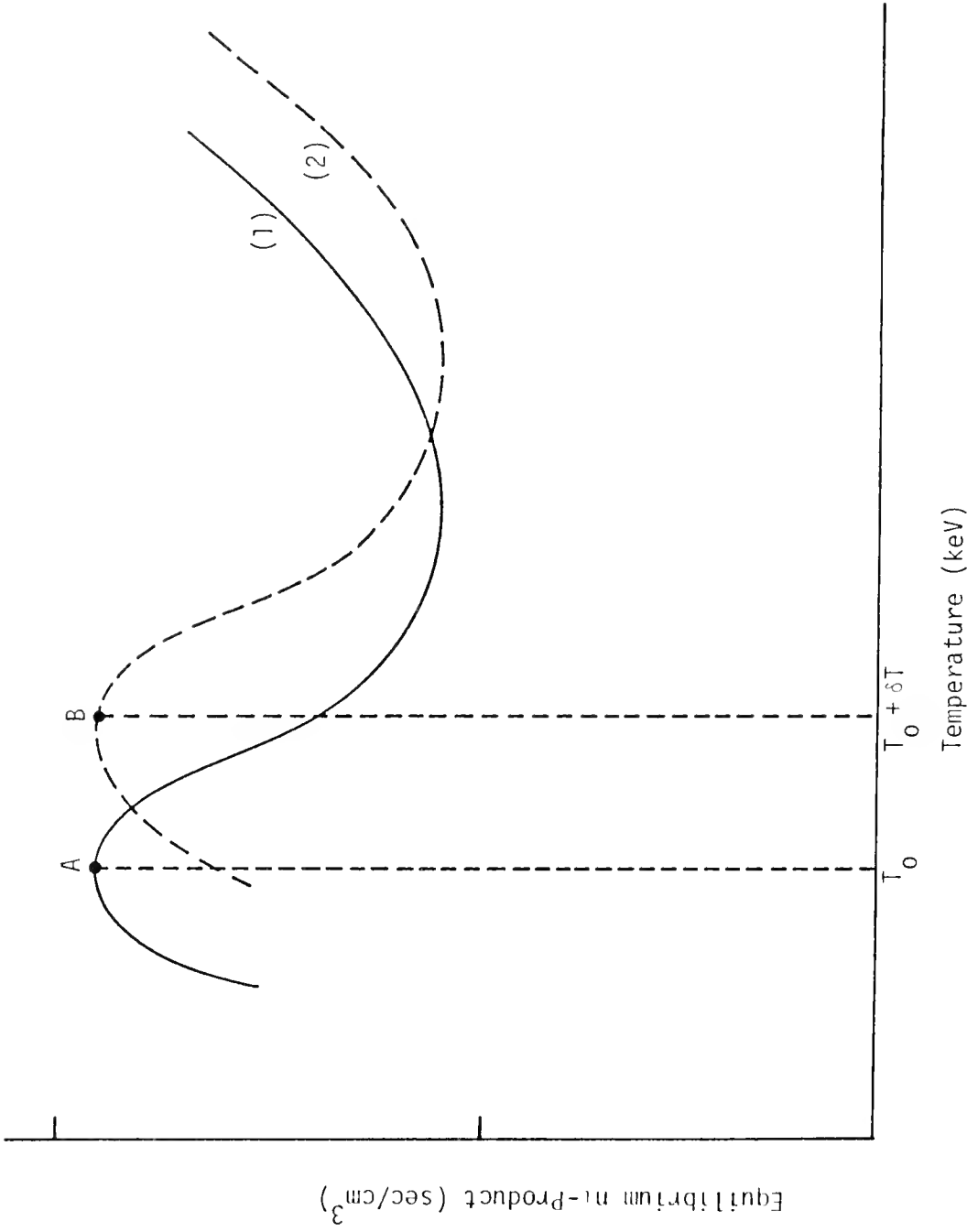
Figure 27. Arbitrary equilibrium curve (1) with a hypothetical stable hybrid state at point A plus a possible equilibrium curve (2) containing a perturbed unstable state at point B.

The stability predictions were verified by perturbing the equilibrium hypothetical hybrid states with even smaller perturbations, and the transients were allowed to continue to steady state for all cases. In every case, the predictions of instability were supported by the transient evolution of the plasma to a new equilibrium temperature above (for +5% δT) or below (for -5% δT) the original temperature. Therefore, the stability predictions based on linear analysis were found to agree with the nonlinear response of the plasma to model perturbations in the temperature provided the perturbations were small enough. The linearized predictions were more reliable in predicting stability for infinitesimal perturbations in the plasma temperature. This presentation explains the discrepancies and shows that the linear and nonlinear stability predictions are in agreement. The apparent disagreement was caused by the selection of significant 5% perturbations near a maximum in the $n_0 \tau_{E_0}$-curves illustrated in Fig. 27. The usefulness and general applicability of linear analysis to predict plasma stability for global plasma behavior was verified for the extremely poor quality plasma proposed for hybrids. There is essentially no limit to the plasma model complexity which can be treated with such analysis.

The prediction that changes in the extrinsic driving feedrate will always lead to new, different equilibrium states was also tested. Positive and negative 5% perturbations in the feedrate of the equilibrium were simulated by linear transient development. Subsequent transient behavior of the plasma was recorded for sufficient time to allow all

systems examined to reach steady-state conditions. In all cases the results in Tables 4-VI and 4-VII demonstrate that feedrate perturbations in the form of permanent external changes in feedrate always drive the plasma to a new state at a higher final temperature when a positive perturbation is introduced and at a lower temperature when a negative perturbation is introduced. It was also found, as noted in Tables 4-VI and 4-VII, that the larger R is and the larger τ_{E_0} is, the further from the initial equilibrium temperature the system goes when perturbed and unstable; this agrees with the concept of better confinement allowing more plasma fusion reactions versus source fusion reactions.

The end-of-transient results in Tables 4-IV through 4-XI are comparative only. Since such large temperature changes are represented in some cases, the plasma model assumption of constant volume becomes invalid. However, for stability verification of the point-model systems, the results are completely reliable as presented.

Short-Term Plasma Transient Response

Short term plasma temperature and neutron production rate variations are of interest for their effect on the blanket in the first seconds immediately following the variations from steady-state conditions. Since the volumetric neutron production rate was found to depend primarily on temperature, the volumetric neutron source rate and the temperature were examined in detail for their time-dependent variations in response to perturbations in the temperature and source feedrate for the six hypothetical hybrid plasma equilibrium states listed in Table 4-III.

Because the neutron production rate is very sensitive to temperature, the initial prompt change in neutron level following ± 5% temperature

perturbations can cause a significant change in blanket power level. Because the sensitivity, S_{DT}, is nearly 3 to 1 as shown in Appendix C, the prompt fractional increase in neutron production levels was shown to begin 15% above equilibrium. However, following the positive and negative 5% temperature perturbations and the associated prompt changes, the time-dependent response of temperature and volumetric neutron production rate showed two surprising characteristics. First, the time-dependent response was found to develop slowly; second, the variation was found to be nearly linear for the first few seconds.

The time-dependent variations of temperature and neutron production rate were examined for all six equilibrium hypothetical hybrid plasma states. The short-term variations are presented in Fig. 28 and Fig. 30 for the temperature responses to $\pm$ 5% perturbations and in Fig. 29 and Fig. 31 for the corresponding variation of the volumetric neutron production rate. The time-dependent responses to perturbations and all later responses are presented for a uniform 15 second interval. Beyond 15 seconds, significant increases of plasma neutrons would be compensated by multiply-redundant safety systems or other control systems engineered to prevent blanket power levels from exceeding design overpower levels.

Similarly, significant decreases of power beyond a reasonable recovery point would also be prevented by proper controls. If the plasma were to be subjected to such temperature transients over 15 second intervals and had not been corrected somehow, then the ordinary magneto-hydrodynamic and positioning instabilities which act in much less than a second were assumed to have already quenched or dissipated the hybrid plasma. In some cases, such as for the +5% perturbation for τ_{E_0} = 2.0 sec, the plasma temperature depicted in Fig. 28 changed sufficiently in
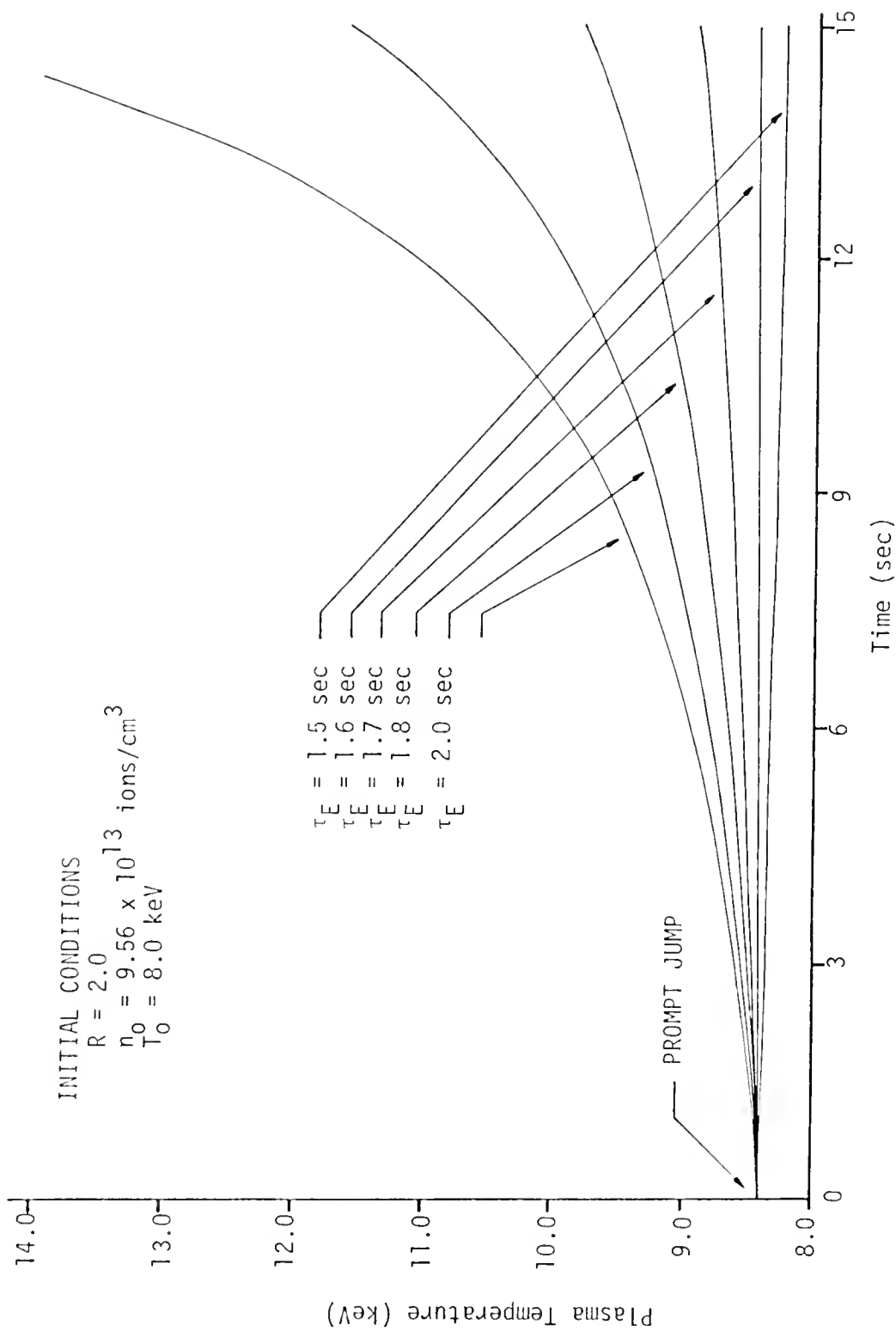
Figure 28. Variation of plasma temperature following a 5% step increase in the temperature of the six hypothetical hybrid equilibrium states.
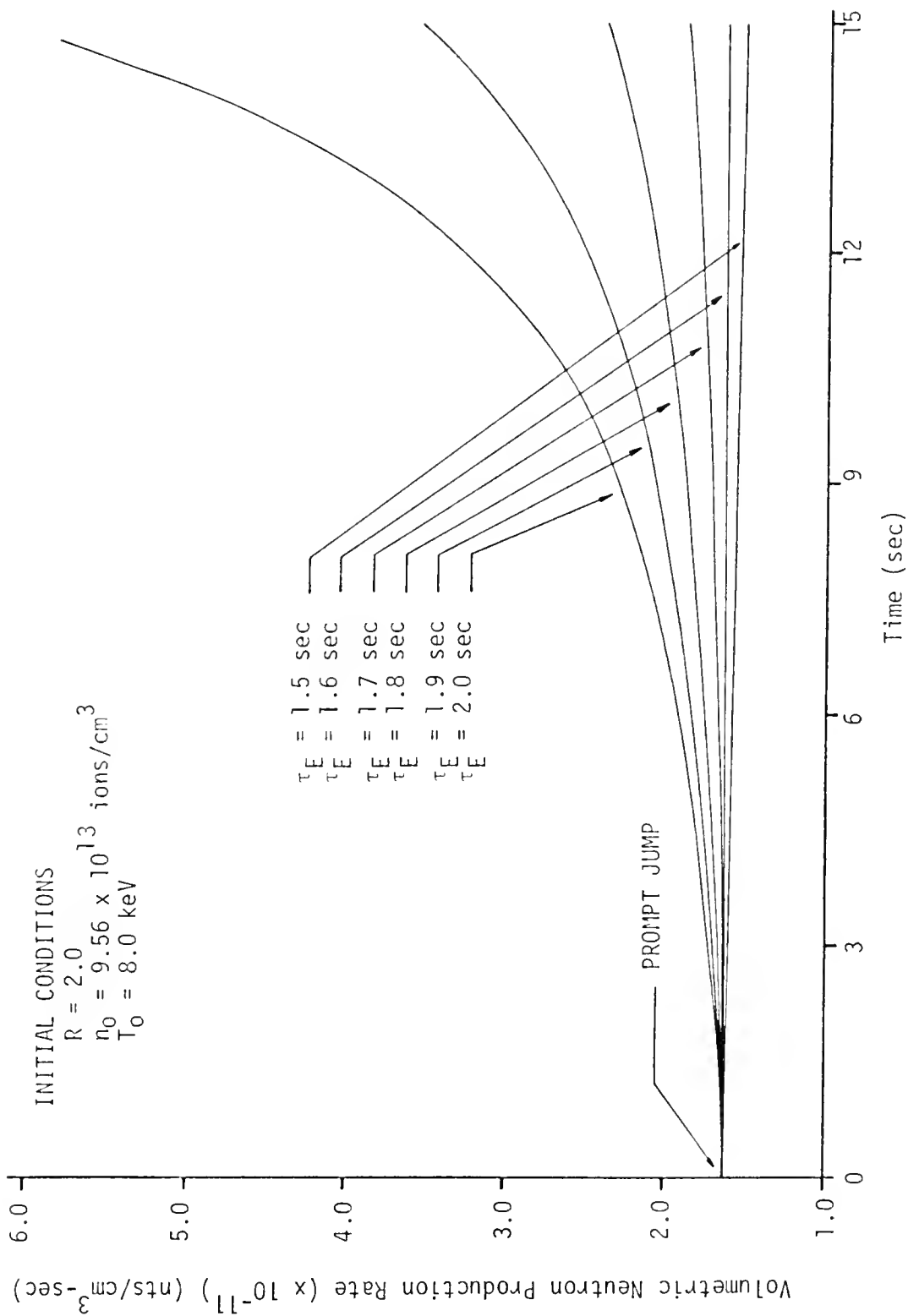
Figure 29. Variation of plasma volumetric neutron production rate following a 5% step increase in the temperature of the six hypothetical hybrid equilibrium states.
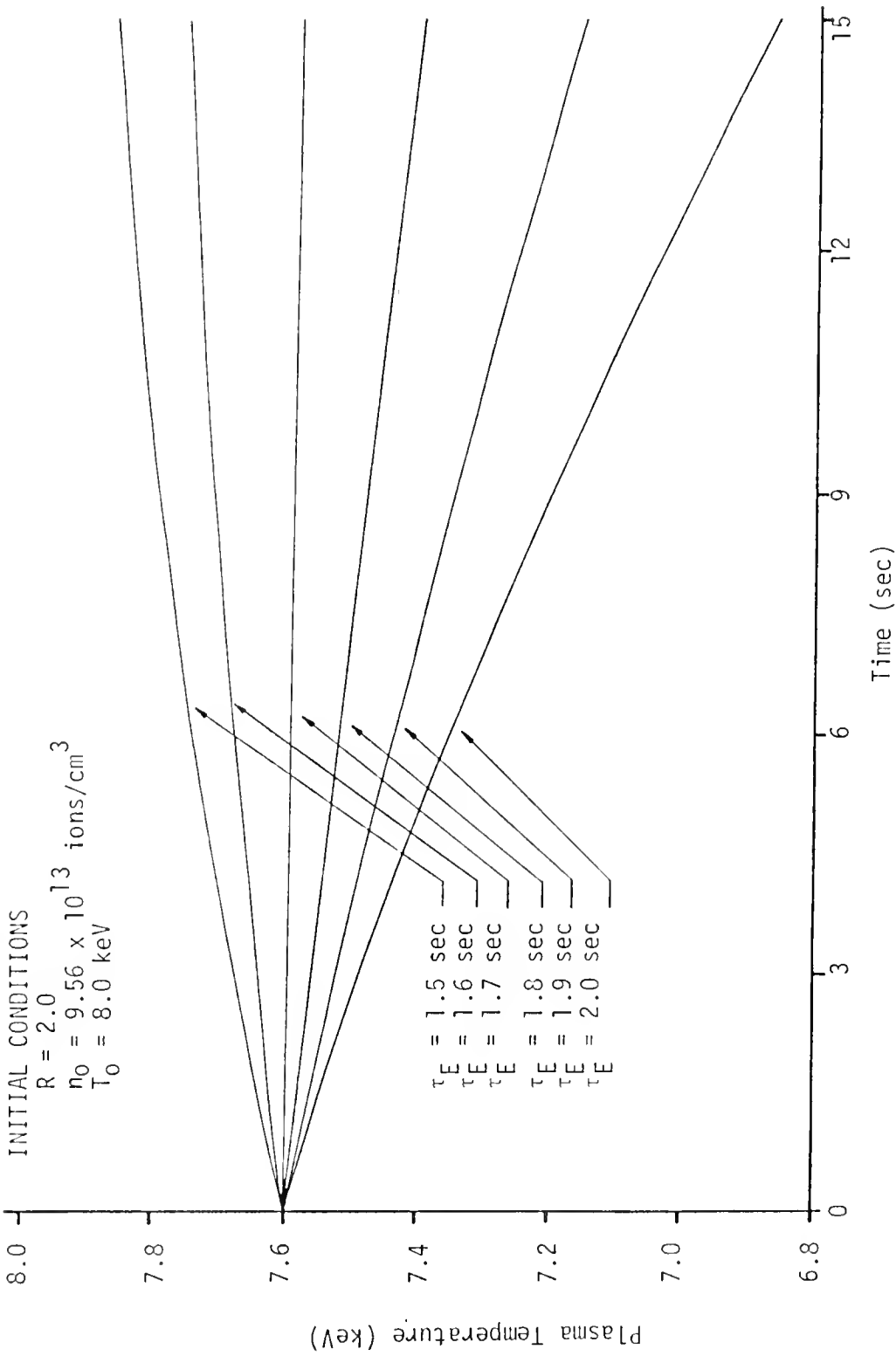
Figure 30. Variation of plasma temperature following a 5% step decrease in the temperature of the six hypothetical hybrid equilibrium states.
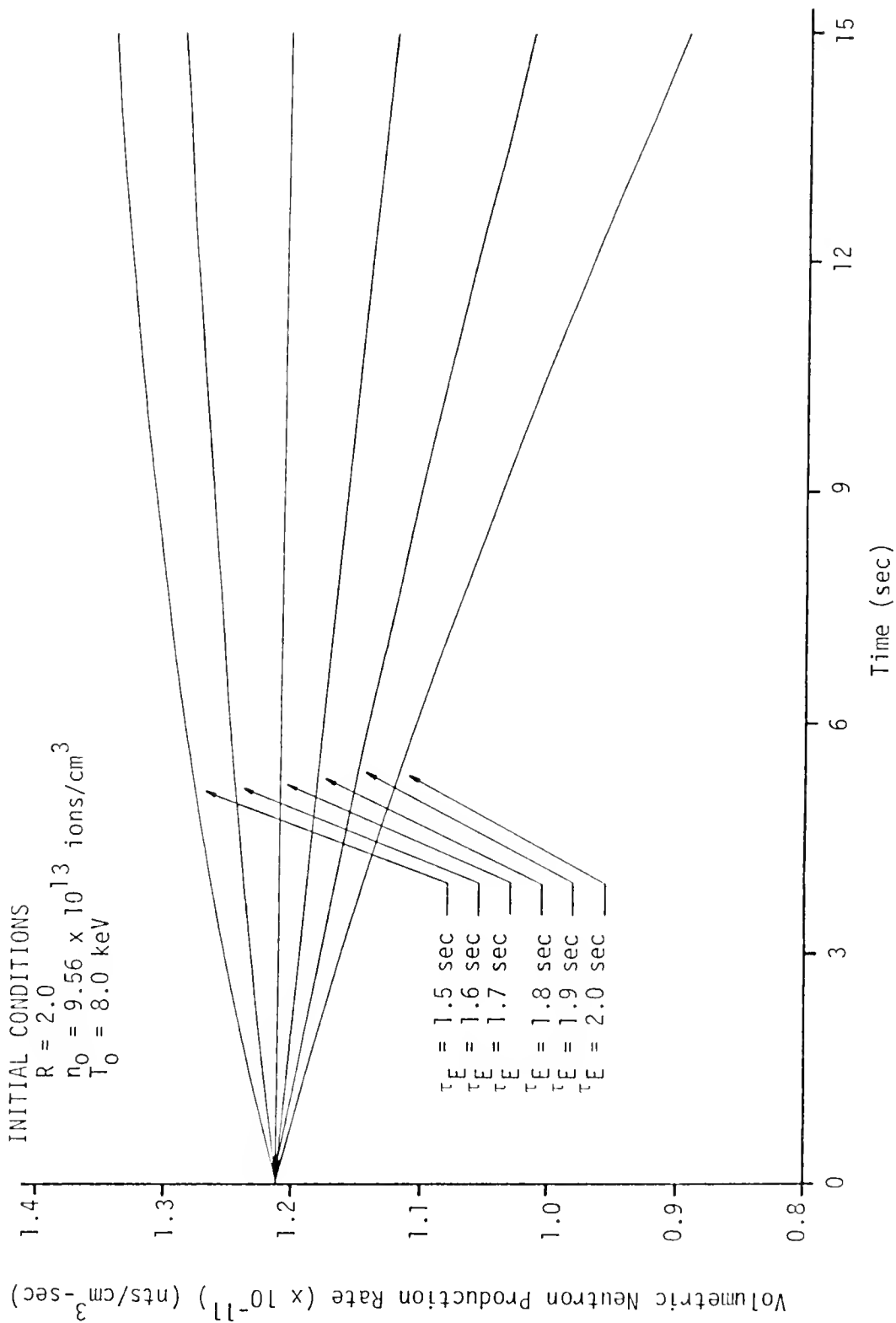
Figure 31. Variation of plasma volumetric neutron production rate following a 5% step decrease in the temperature of the six hypothetical hybrid equilibrium states.

the 15 second interval that the constant volume, point-model result was no longer valid. In fact, all of the temperature and neutron levels were found to grow more quickly and nonlinearly after about 10 seconds for the larger confinement times (τ_{E_0} = 1.8-2.0 sec). When the system was well-damped and stable as for the lower confinement times, then the temperature exhibited slow changes and less need to act to control the transients. Therefore, although the 15 second limit for observing transient nonlinear behavior was somewhat arbitrary, there are also valid reasons for not having observed results beyond this time limit.

The relatively linear response of the plasma temperature is shown in the time development of these quantities in Figs. 28-31. Although the linearity of response was demonstrated for $\pm$ 5% perturbations, the responses to the +5% perturbations became very nonlinear beyond 8-9 seconds for the larger (τ_{E_0} > 1.8 sec) confinement times as shown in Figs. 28 and 29. However, following the -5% temperature perturbations, the time-dependent increase for stable states and the decrease for unstable equilibirum states were found to be very linear over the entire 15 second interval depicted in Figs. 30 and 31.

In addition to the unexpected linearity of the time-dependent un-controlled responses of neutron production and temperature, another unexpected result was represented by the slow response of the hybrid plasma states to these 5% perturbations. This slow response following the initial 15% jump in neutron production rate implies that the blanket power will increase very quickly to a level that corresponds to the initially increased neutron production rate. The time involved will be on the order of a fraction of a second depending on the time taken for the increased source of 14 MeV neutrons to reach an equilibrium level in

the thermal hybrid blanket described in Appendix B. Since the neutron lifetime was found to be less than a millisecond for the subcritical blanket, this means that the power rise in the blanket will be practically instantaneous when compared to the 5 or 10 seconds needed for significant further increases in the plasma neutron production rate.

The relatively prompt rise in blanket power will be followed by a new steady state that then changes slowly driven by the additional slow variation in the plasma neutron production level. This behavior is especially supported because the hybrid blanket has such a low effective neutron multiplication factor ($k_{eff} \approx 0.92$). The spatial harmonics will die out quickly and the new steady-state flux shapes will build in quickly although a negative blanket power coefficient will limit the fractional increase in steady-state power to something less than the associated fractional increase in the plasma volumetric neutron production level.

The sluggish plasma response following the initial instantaneous temperature variation was particularly evident for the two least con- fined (τ_{E_o} = 1.5 sec and τ_{E_o} = 1.6 sec) equilibrium states under positive perturbations. The plasma never showed more than 1% variation in either temperature or neutron production rate following the initial instan- taneous increases from T = 8.0 keV to T = 8.4 keV and q_p = 1.41 x 10^{11} nts/cm^3-sec to q_p = 1.62 x 10^{11} nts/cm^3-sec. Even the fastest growing temperature transient in response to a positive perturbation for τ_{E_o} = 2.0 sec did not reach 9 keV from the perturbed 8.4 keV state for over 6 seconds, at which time the neutron source had increased from its equilibrium value by somewhat less than 40%. Times on the order of seconds are extremely long for plasma-related development. The cor- responding blanket power increase of nearly 40% would be excessive in

fission reactors and pure fusion blankets but perhaps not so in hybrids, where the design limitations on average blanket power densities will be much reduced compared to pure fusion machines. For pure fusion reactor blankets, the power density has been predicted to be very peaked at the first wall which will be limiting. This extreme power peaking near the first wall for pure fusion devices is illustrated for the UWMAK-III[30] design in Fig. 32. However, for hybrids, the neutron flux and hence the power production, as presented in Chapter 5, were found to be spread more evenly throughout the blanket since the main source of power in the graphite-moderated, thermal hybrid blanket is the diffuse central fissile region which is relatively uncoupled from the 14 MeV neutron source entering the blanket especially in a graphite-moderated thermal hybrid blanket.

As noted the perturbations in plasma temperature also resulted in relatively slow transients for the plasma neutron production rates as shown in Fig. 29 for +5% perturbations, and Fig. 31 for -5% perturbations. This response was expected because the neutron production rate depends on temperature through the reactivity; it also depends on the square of the density, but density is not a responsive variable as noted previously.

The resultant decrease in neutron level shown in Fig. 31 and the corresponding decreased blanket power generation would not represent a direct safety problem but rather a problem in power supply. Even the unstable case of τ_{E_0} = 1.7 sec did not exhibit a measurable decrease below the initial perturbed temperature of 7.6 keV during the 15 second interval of interest. The most unstable and fastest transient occurred
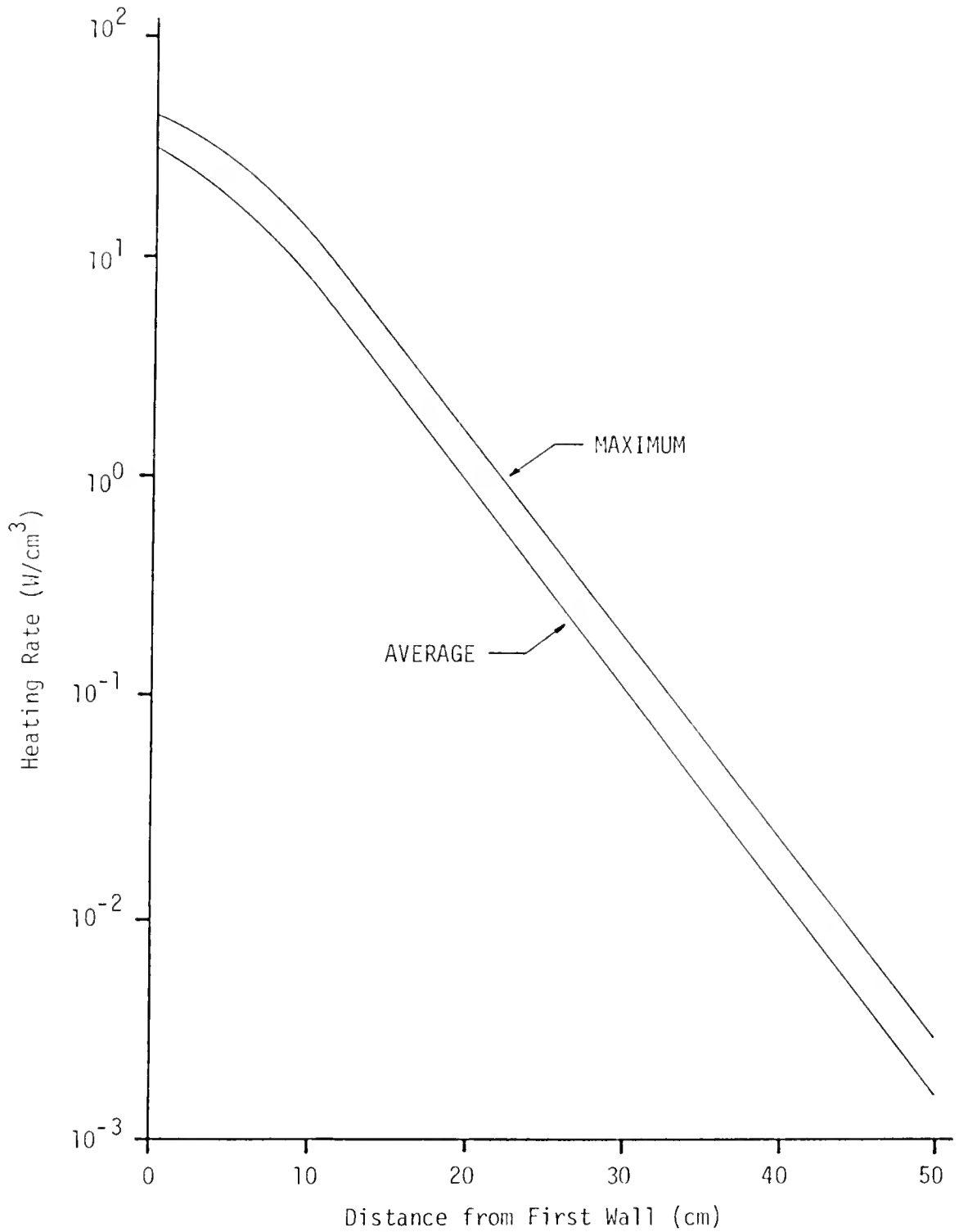
Figure 32.   Variation of the heating rate in the first wall region of
             the UWMAK-III design.

for the hybrid equilibrium state at τ_{E_0} = 2.0 sec which required over 6 seconds to decrease 30% from its unperturbed level.

Ordinary Tokamak designs plan plasma shutdown intervals for ash removal and cleanup. The UWMAK-III and other proposed Tokamak fusion reactors have been designed with unique operating cycles in which the "burning" of the fusion plasma has to be shut down periodically; however, long duty cycles with 30 to 100 minutes burntime and 1 to 6 minutes downtime have been reported.[30,92] Since the power conversion system cannot tolerate even momentary cutoff from the heat source, some means to store thermal energy for use during every reactor downtime will be required. The large thermal capacity of the thermal fission, graphite-moderated hybrid blanket plus the slow decrease of the neutron production rate following the initial -5% perturbation can be used to prevent the power conversion system from detecting the reactor downtime before remedial action can be taken.

Much the same situation was found to apply for transient development following perturbations in the feedrate. However, there was no prompt effect on the plasma neutron production rate or on the blanket power generation. Since the effect on temperatures and hence neutron production rates is indirect for the extrinsic feedrate parameter, the plasma required some time to respond with a temperature or neutron production level variation following a step change in the feedrate. Unlike the temperature perturbation case, the perturbation itself does not represent a direct and immediate change in the plasma temperature or the neutron production rate driving the fissile blanket.

The indirect perturbation of the temperature and neutron production rate is more interesting because the case can be applied more directly

to a physically realizable and expected continuous perturbation in the plasma. The continuous variation of the temperature and neutron production rates determined for $\pm$ 5% step changes in feedrate are presented in Figs. 33-36. The continuous development shown from the initial feedrate perturbation contrasts with the prompt effect involved in the temperature and neutron production levels following the temperature perturbations. The same linearity was noted for the first 6 seconds follwoing positive perturbations in the feedrate; however, for negative perturbations of the six equilibrium states, the resultant variation of temperature and neutron level was found again to be nearly linear over the entire 15 second interval as shown in Fig. 33 for the temperature variation and to a lesser extent in Fig. 34 for the variation of neutron production rate with time. This behavior agrees with the corresponding temporal response to negative temperature perturbations presented previously in Fig. 30 and Fig. 31.

When the plasma system was assumed to be more efficient at energy confinement for larger energy confinement times, the general transient effects of positive perturbations in the feedrate and the temperature were found to be more pronounced for the uncontrolled cases. The increasing confinement time of the equilibrium state increased the tendency to "run away" thermally. For example, after 10 seconds, the time-dependent nonlinear simulation of temperature for both temperature and positive feedrate perturbations yielded the values presented in Table 4-XIII. The dramatic effect of confinement efficiency on speed of response to perturbations was found regardless of the stability of the equilibrium state. The temperature values listed in the second column of Table 4-XIII show that the same +5% feedrate perturbation drives the
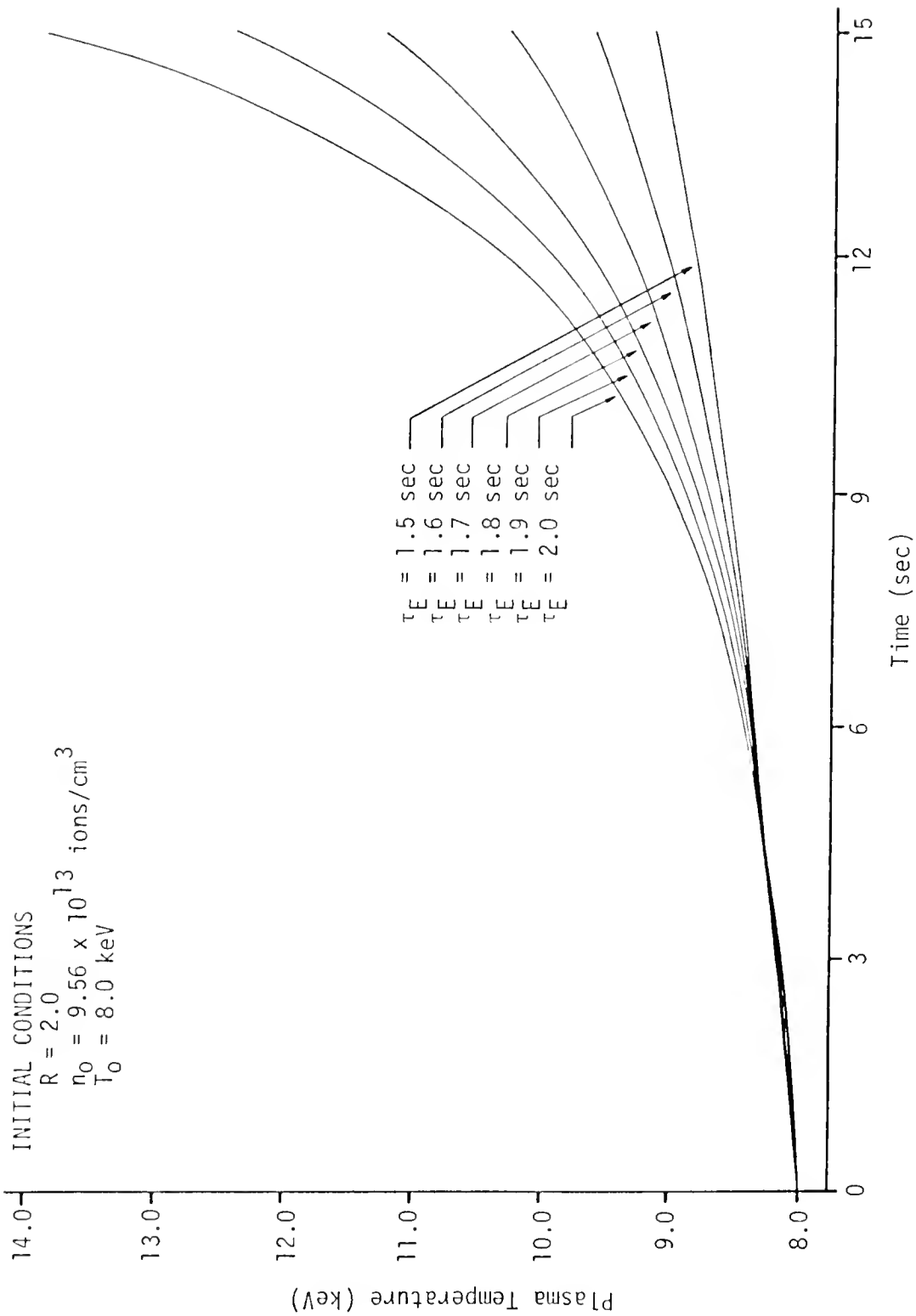
Figure 33. Variation of plasma temperature following a 5% step increase in the feedrates for the six hypothetical hybrid equilibrium states.
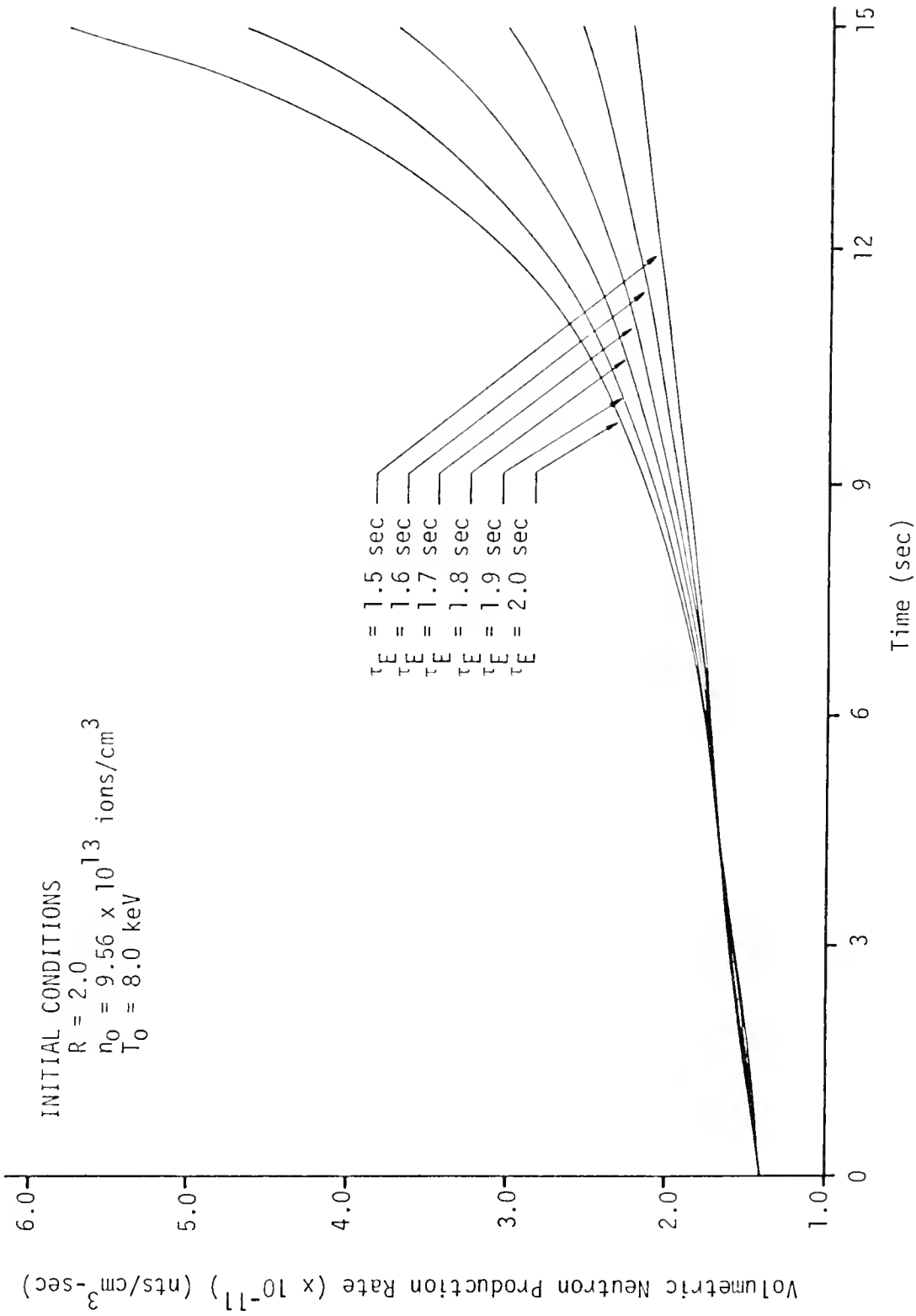
Figure 34. Variation of plasma volumetric neutron production rate following a 5% step increase in the feedrates of the six hypothetical hybrid equilibrium states.
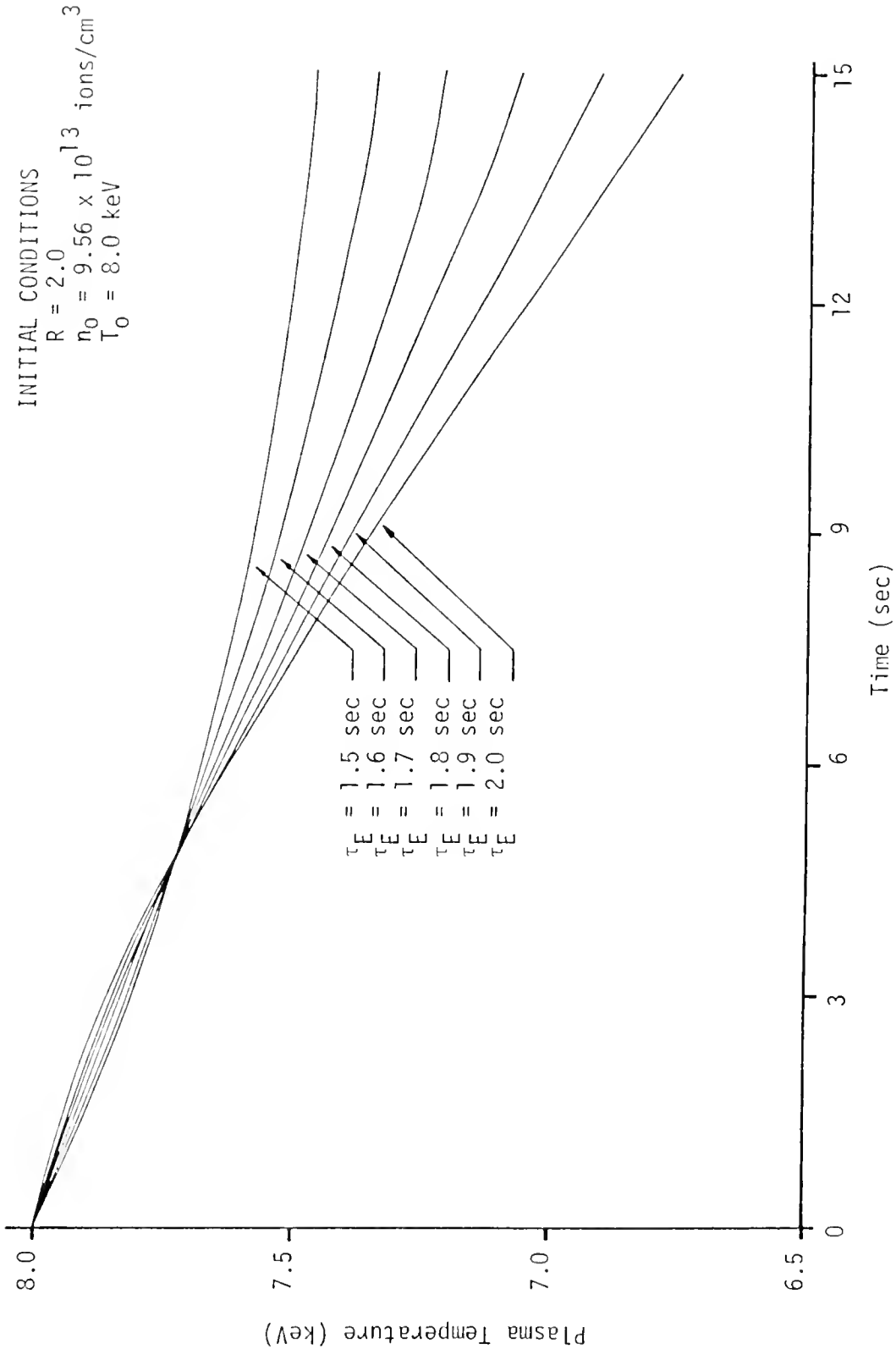
Figure 35. Variation of plasma temperature following a 5% step decrease in the feedrates for the six hypothetical hybrid equilibrium states.
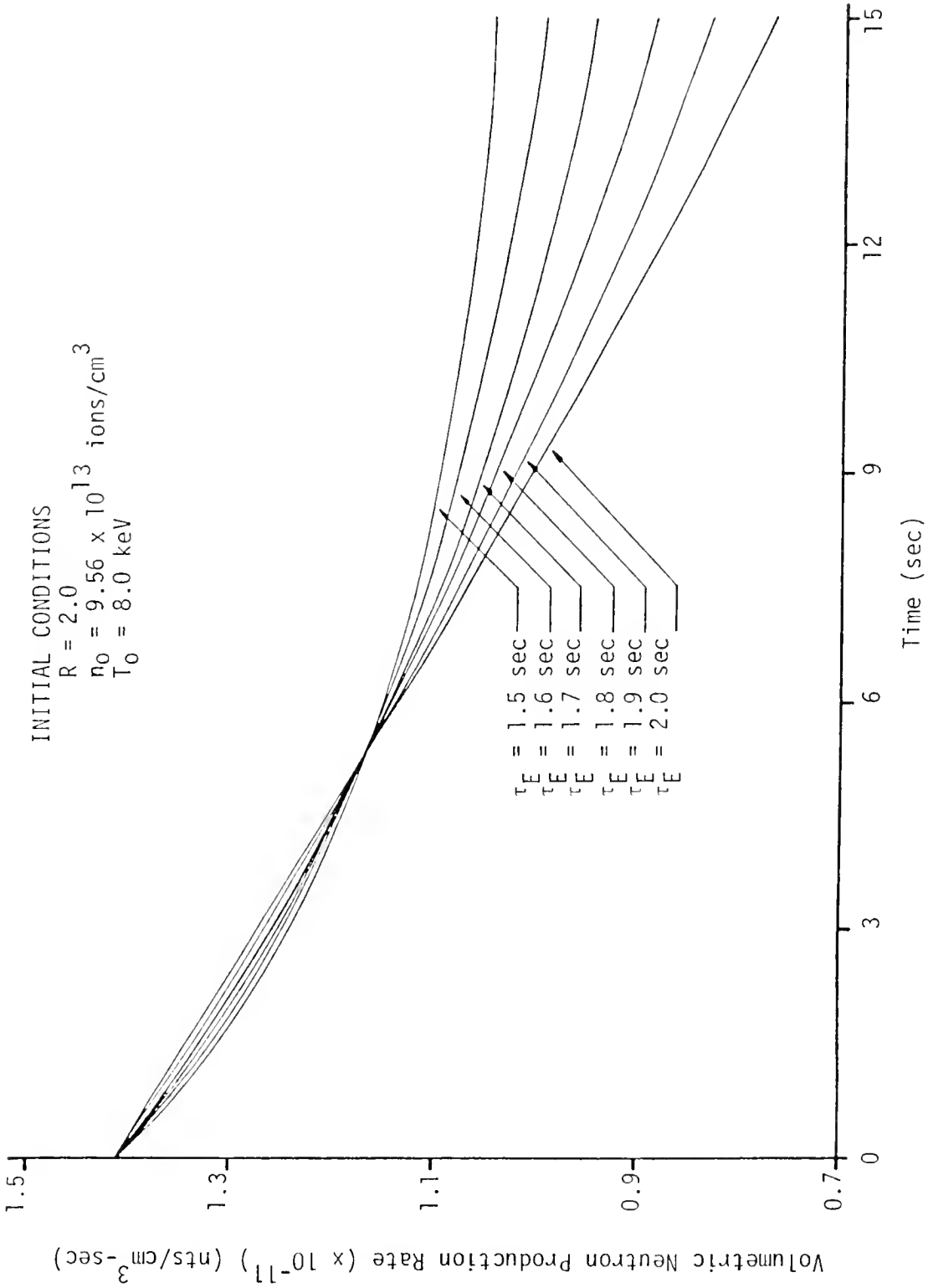
Figure 36. Variation of plasma volumetric neutron production rate following a 5% step decrease in the feedrates for the six hypothetical hybrid equilibrium states.

equilibrium plasma temperature to a new, larger value much more quickly for larger energy confinement times. Similarly, the values tabulated in the third column of Table 4-XIII show that temperature runs away more easily for larger energy confinement times when unstable ($\tau_E \geq 1.7$ sec) and the temperature returns to equilibrium less quickly for larger energy confinement times when stable ($\tau_E \leq 1.6$ sec). Although this dependence of speed of response on the energy confinement time was not unexpected, it is fortunate that the plasma behaves in this manner since it will allow selection of less effective confinement by more easily engineered Tokamak designs which can then be much more easily controlled. This is a point to remember in selecting a controllable hybrid reactor plasma operating regime if a choice is possible.

Table 4-XIII

Comparison of Confinement Time Effects on Plasma Temperature at 10 sec Following +5% Perturbation in Feedrate versus +5% Perturbation in Temperature for Six Hypothetical Hybrid Equilibrium States

Energy Confinement Time τ_{E_0} (sec)	Temperature at 10 sec After +5% δS T (keV)	Temperature at 10 sec After +5% δT T (keV)
1.5	8.678	8.289
1.6	8.805	8.442
1.7	8.937	8.668
1.8	9.067	8.931
1.9	9.194	9.394
2.0	9.313	9.944

Plasma Response With Feedback

Since there are no known inherent plasma controlling feedback mechanisms, different types of externally applied feedback have been proposed to control the temperature and hence the neutron production rate in fusioning plasmas.[15,18] Control of the thermal instability through temperature feedback on the feedrate has been most often proposed. Since the hybrid plasma temperature was found to undergo relatively slow transients, externally applied feedback in the form of delayed compensation of the feedrate perturbing step change was investigated; the following form of feedback was used for positive or negative perturbations:

$$S(t) = S_0 \pm \delta S(t)[u(t) - u(t - t_D)] \tag{188}$$

where $u(t)$ is the unit step function at initiation of the step perturbation and $u(t - t_D)$ is the compensating unit step function acting with delay time, t_D.

The application of this feedrate feedback was used to shut off the perturbation at time, t_D, after initiation; such action corresponds to a controller detecting changes in the feedrate from equilibrium requirements and then acting to restore the equilibrium feedrate. All six hypothetical hybrid equilibrium states were examined for response to such effects.

Typical results of different delay times for the shutoff of the feedrate perturbation are presented in Figs. 37-42 for positive initial feedrate step changes and in Figs. 43-48 for negative initial feedrate step changes. Only three of the six hypothetical hybrid equilibrium states are presented; however, the three cases selected represent a
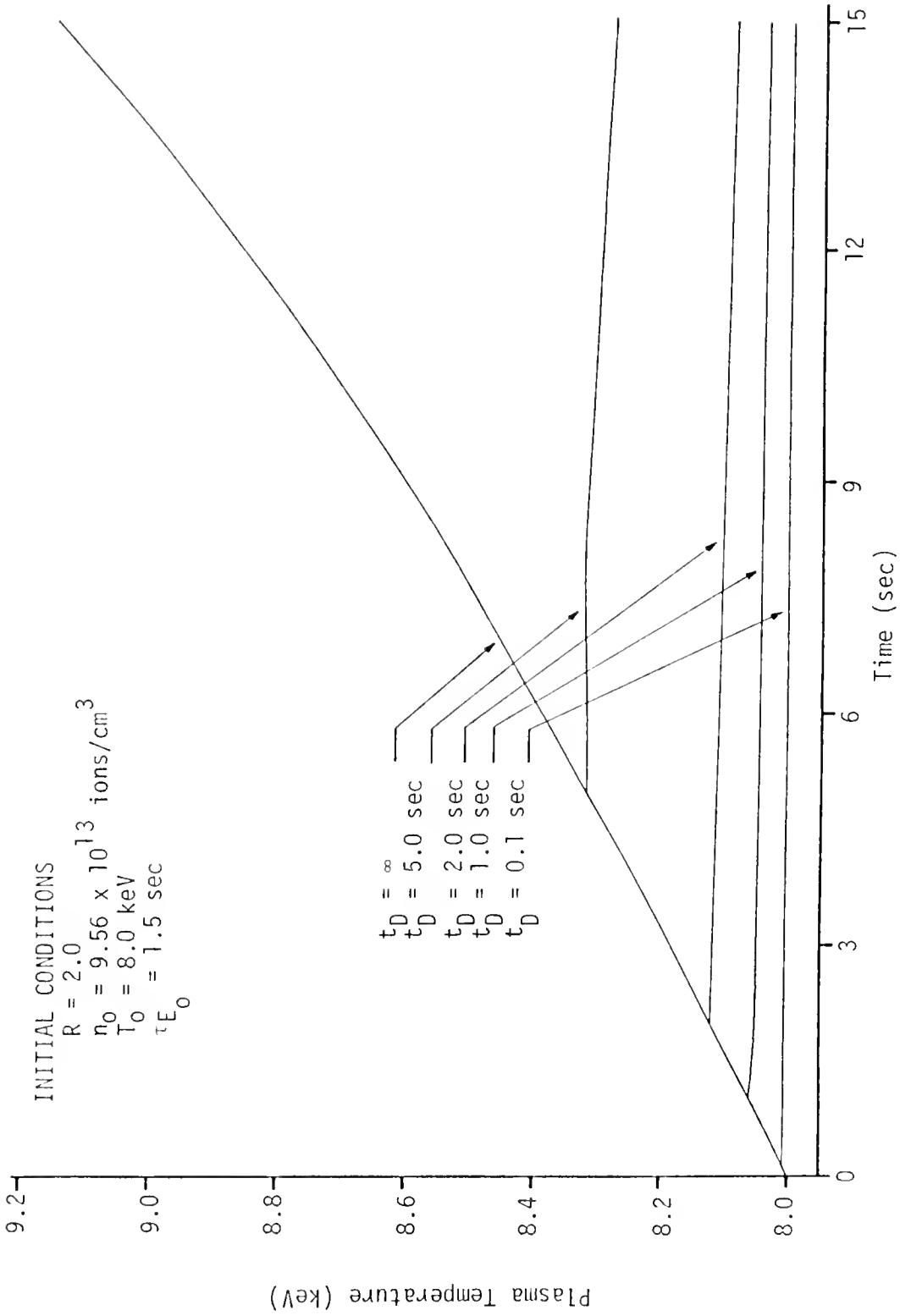
Figure 37. Variation of plasma temperature following a 5% step increase in the feedrate of an equilibrium state at τ_{E_O} = 1.5 sec with delayed shutoff times.
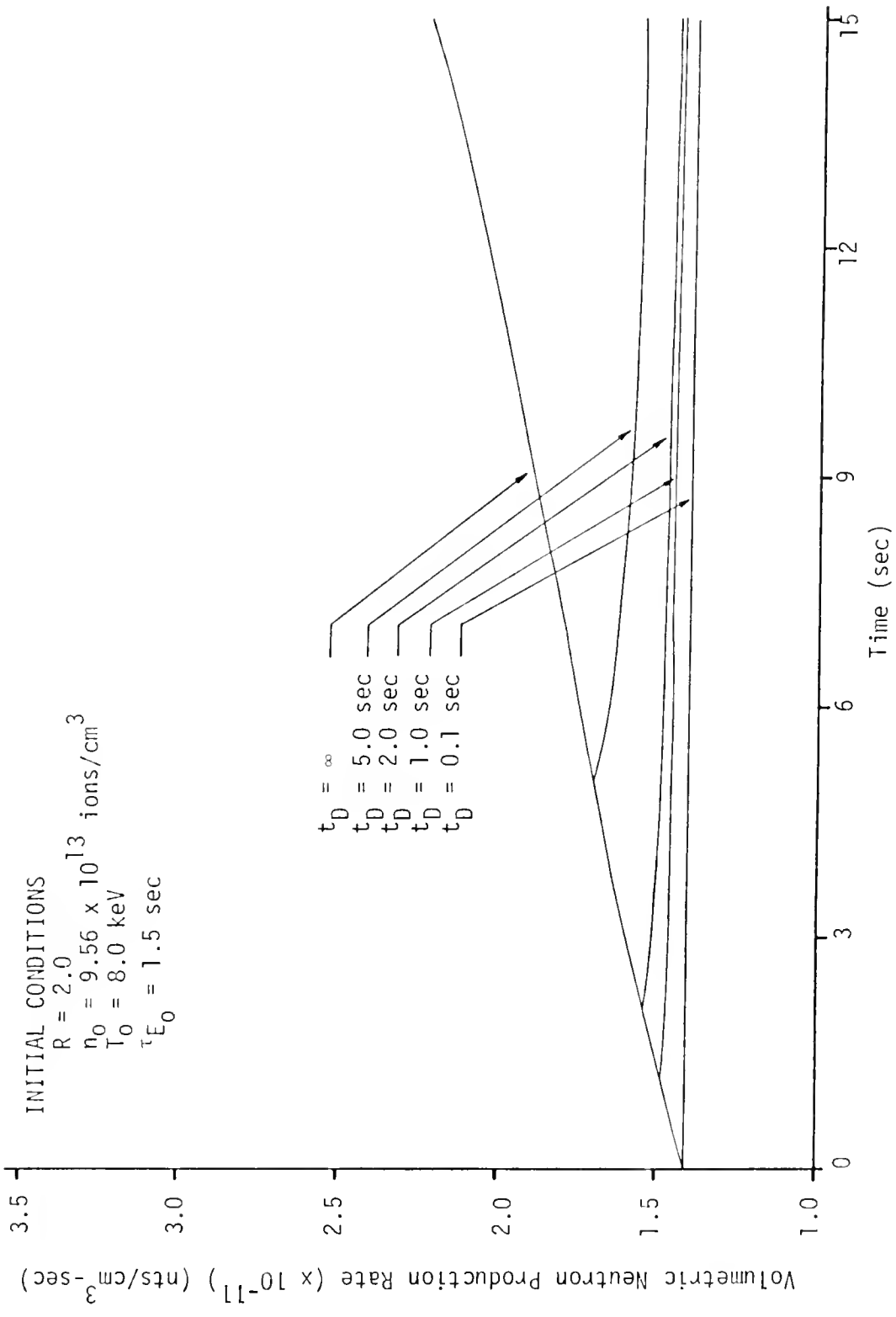
Figure 38. Variation of plasma volumetric neutron production rate following a 5% step increase in the feedrate of an equilibrium state at $\tau_{E_0} = 1.5$ sec with delayed shutoff times.
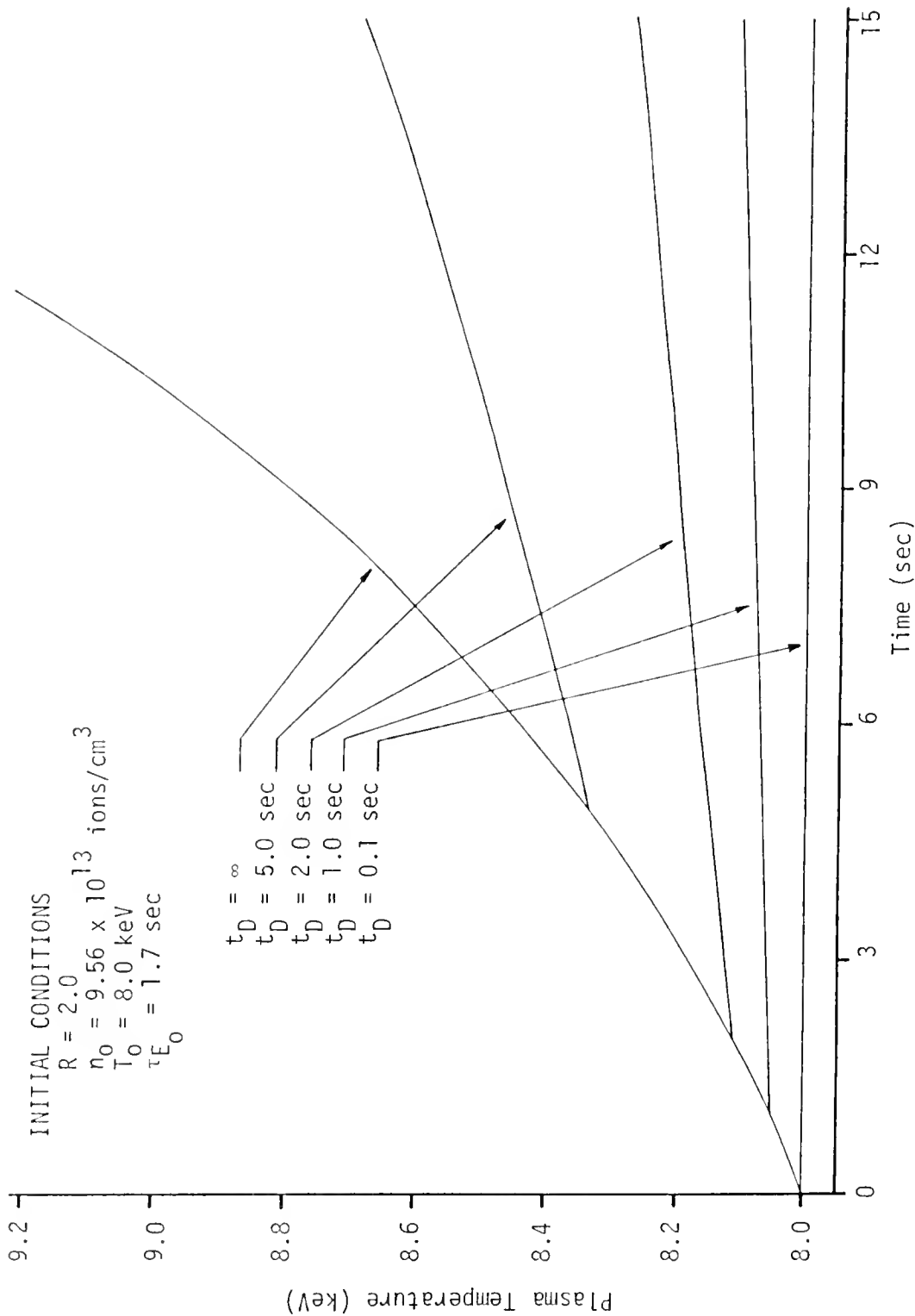
Figure 39. Variation of plasma temperature following a 5% step increase in the feedrate of an equilibrium state at $\tau_{E_O} = 1.7$ sec with delayed shutoff times.
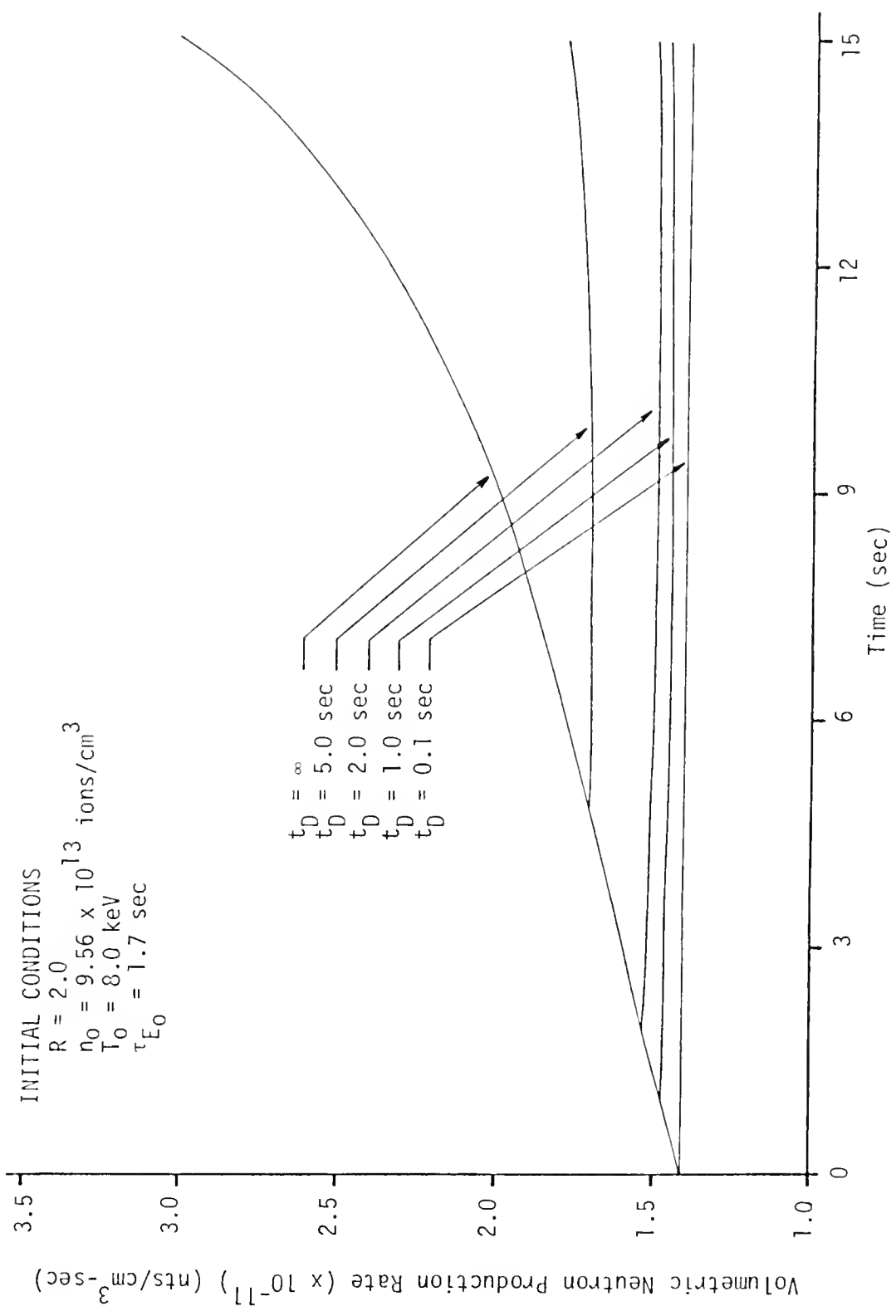
Figure 40. Variation of plasma volumetric neutron production rate following a 5% step increase in the feedrate of an equilibrium state at τ_{E_0} = 1.7 sec with delayed shutoff times.
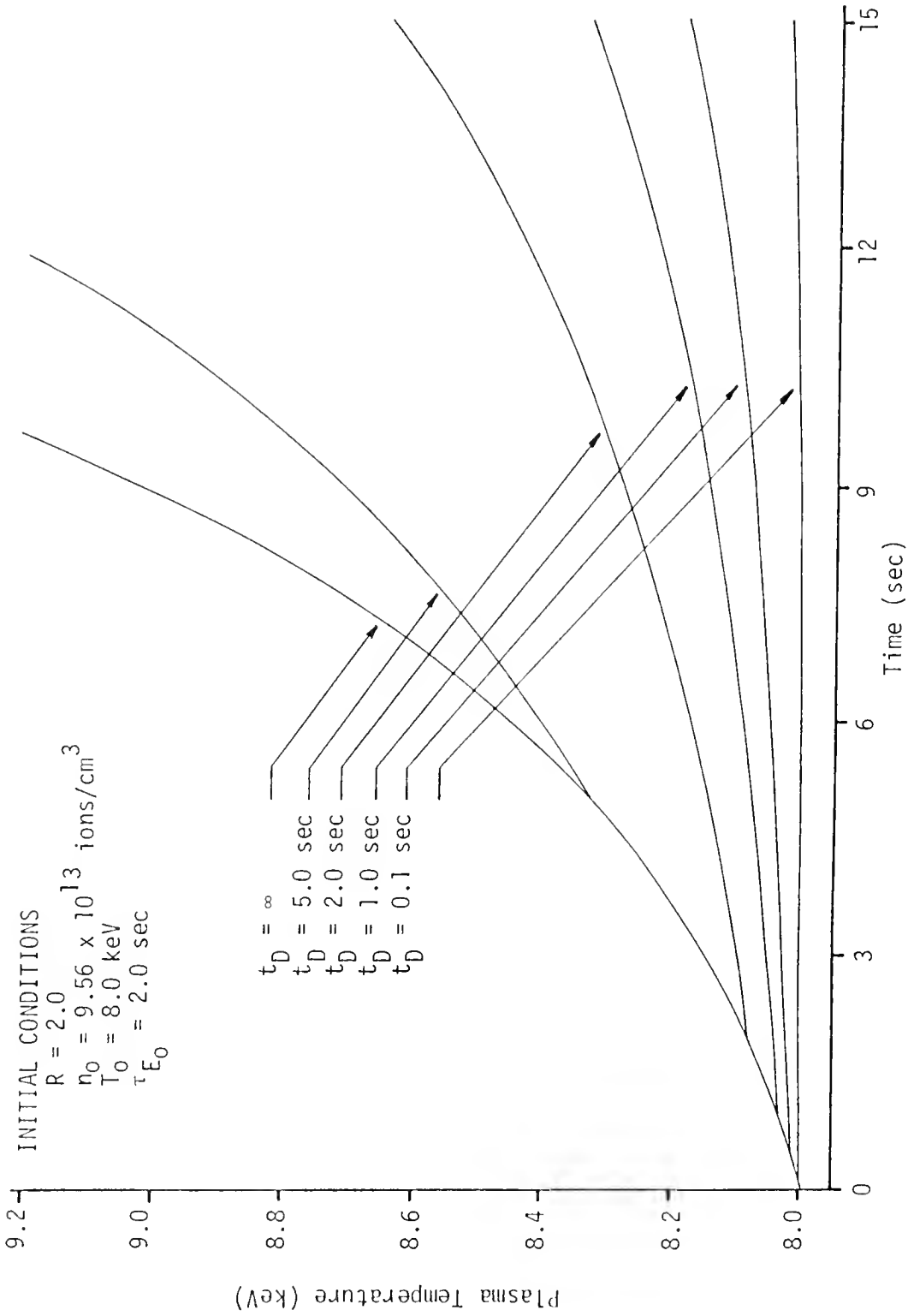
Figure 41. Variation of plasma temperature following a 5% step increase in the feedrate of an equilibrium state at τ_{E_O} = 2.0 sec with delayed shutoff times.
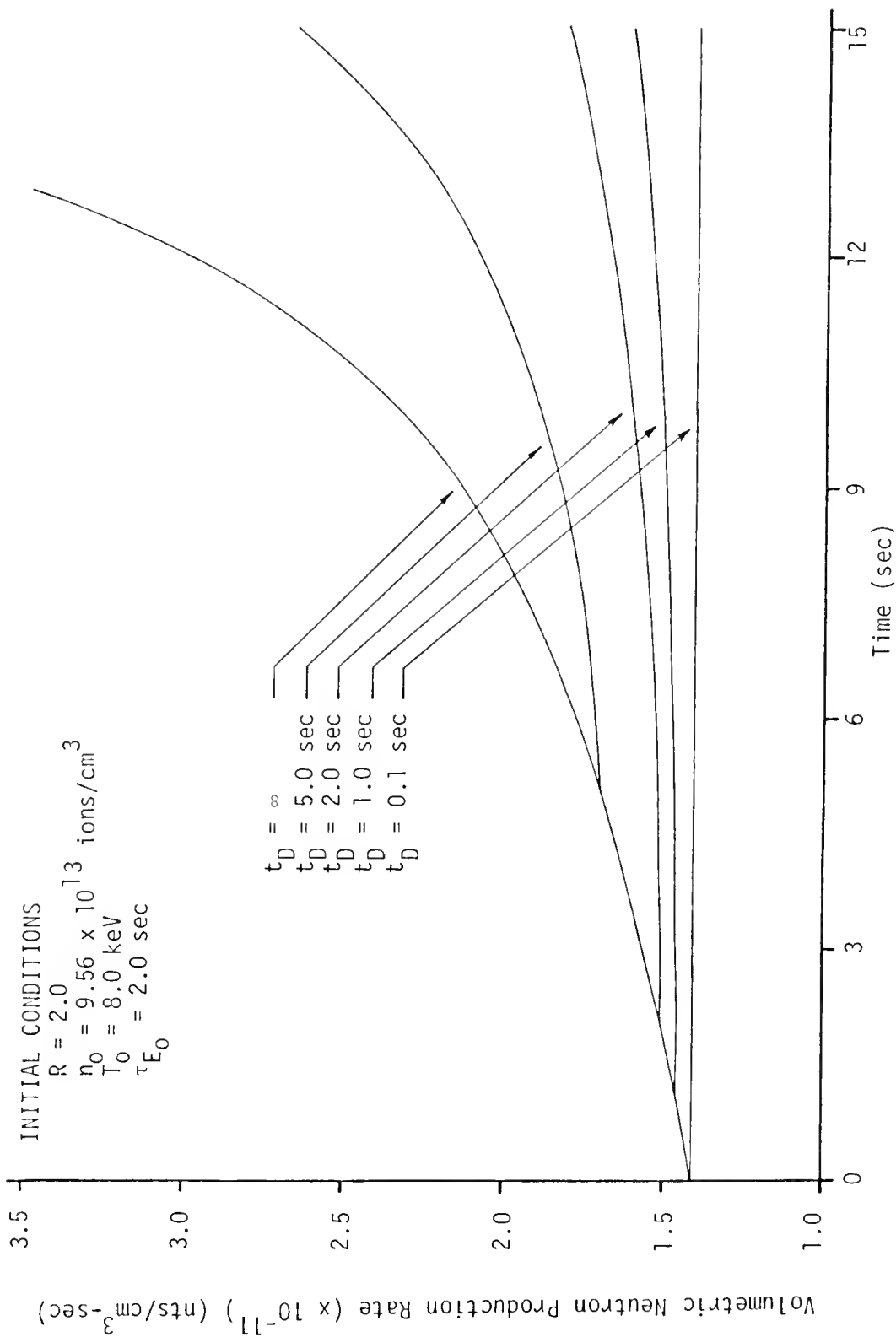
Figure 42. Variation of plasma volumetric neutron production rate following a 5% step increase in the feedrate of an equilibrium state at τ_{E_O} = 2.0 sec with delayed shutoff times.
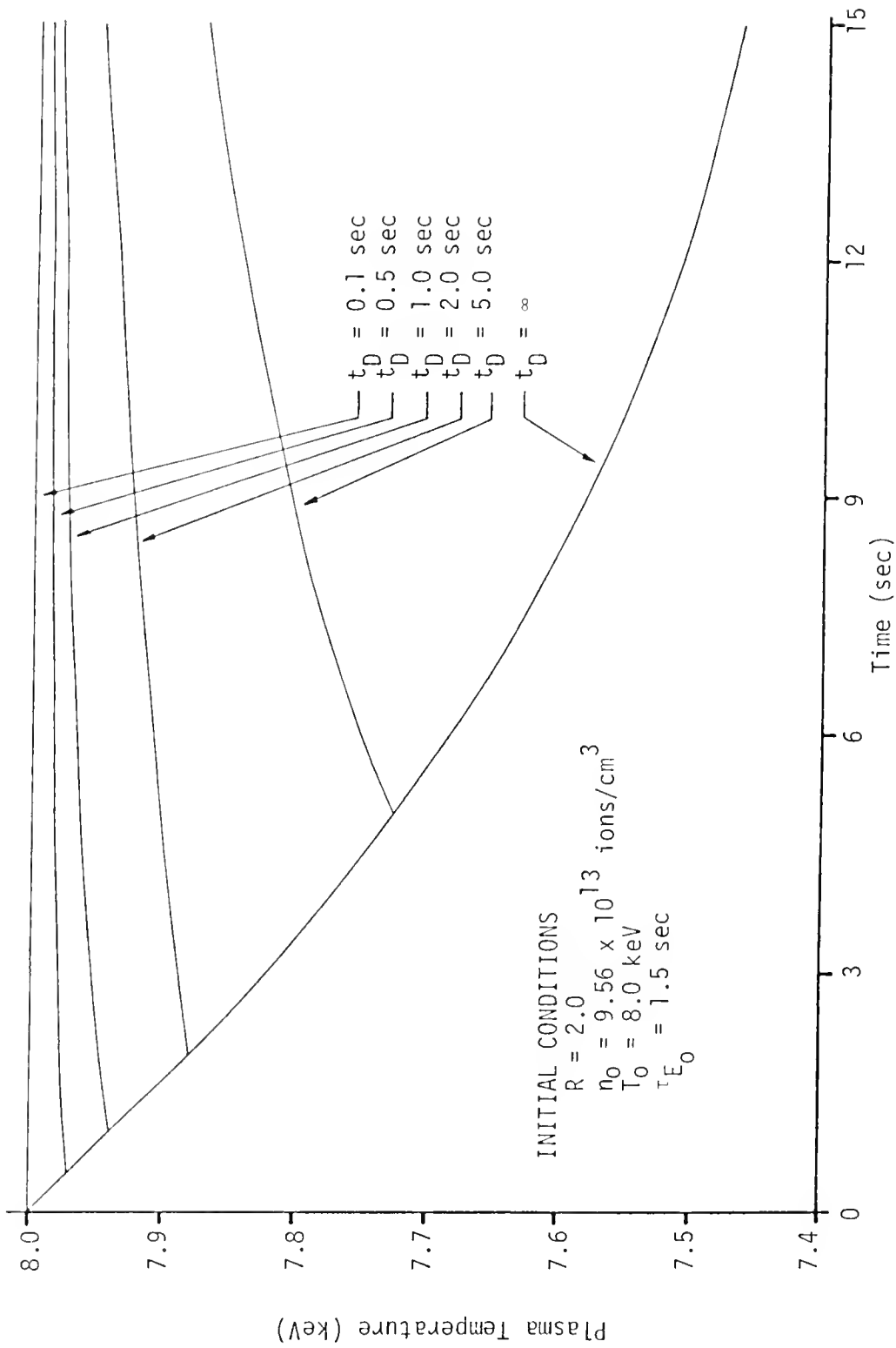
Figure 43. Variation of plasma temperature following a 5% step decrease in the feedrate of an equilibrium state at $\tau_{E_0} = 1.5$ sec with delayed shutoff times.
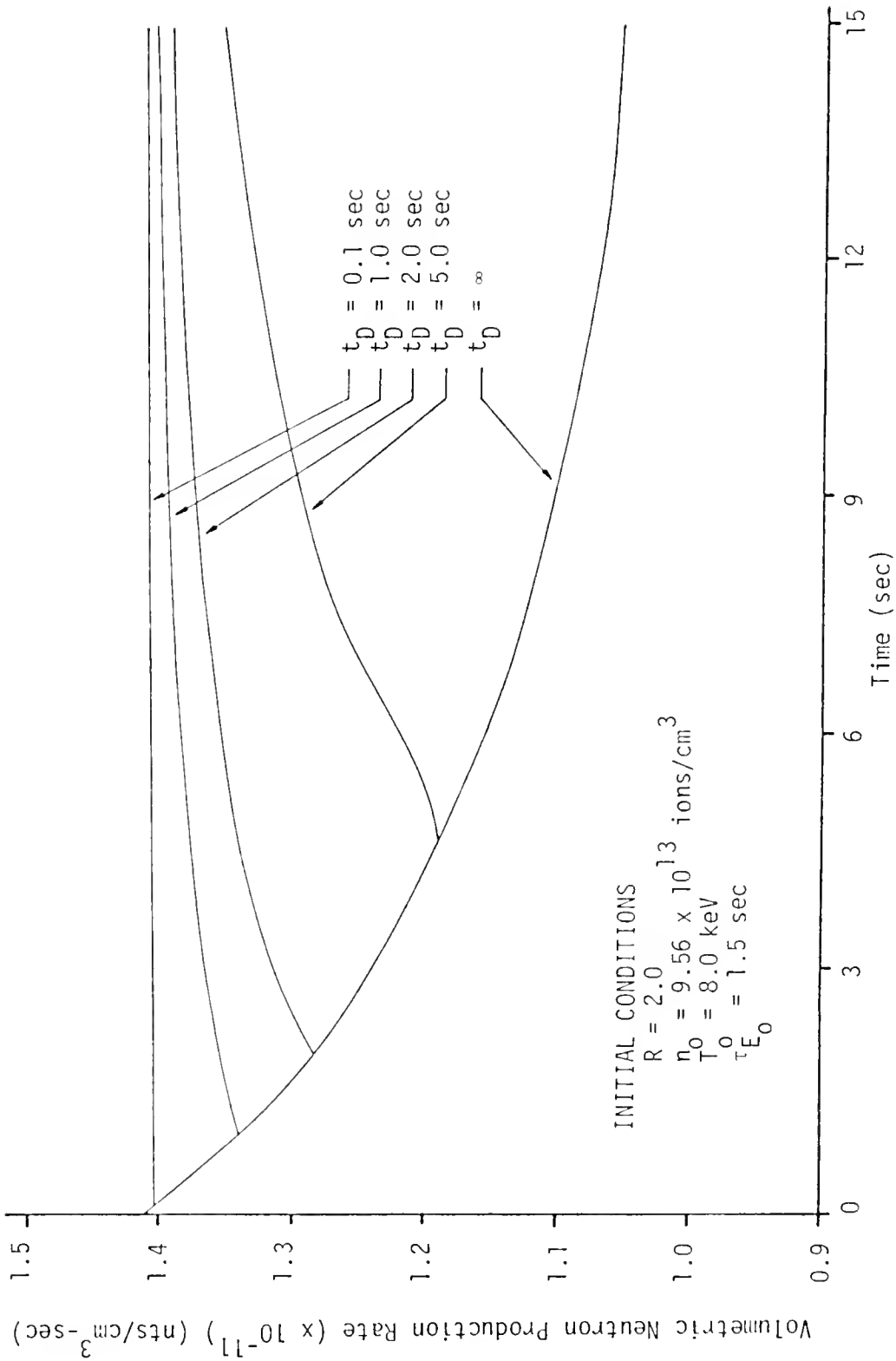
Figure 44. Variation of plasma volumetric neutron production rate following a 5% step decrease in the feedrate of an equilibrium state at $\tau_{E_O} = 1.5$ sec with delayed shutoff times.
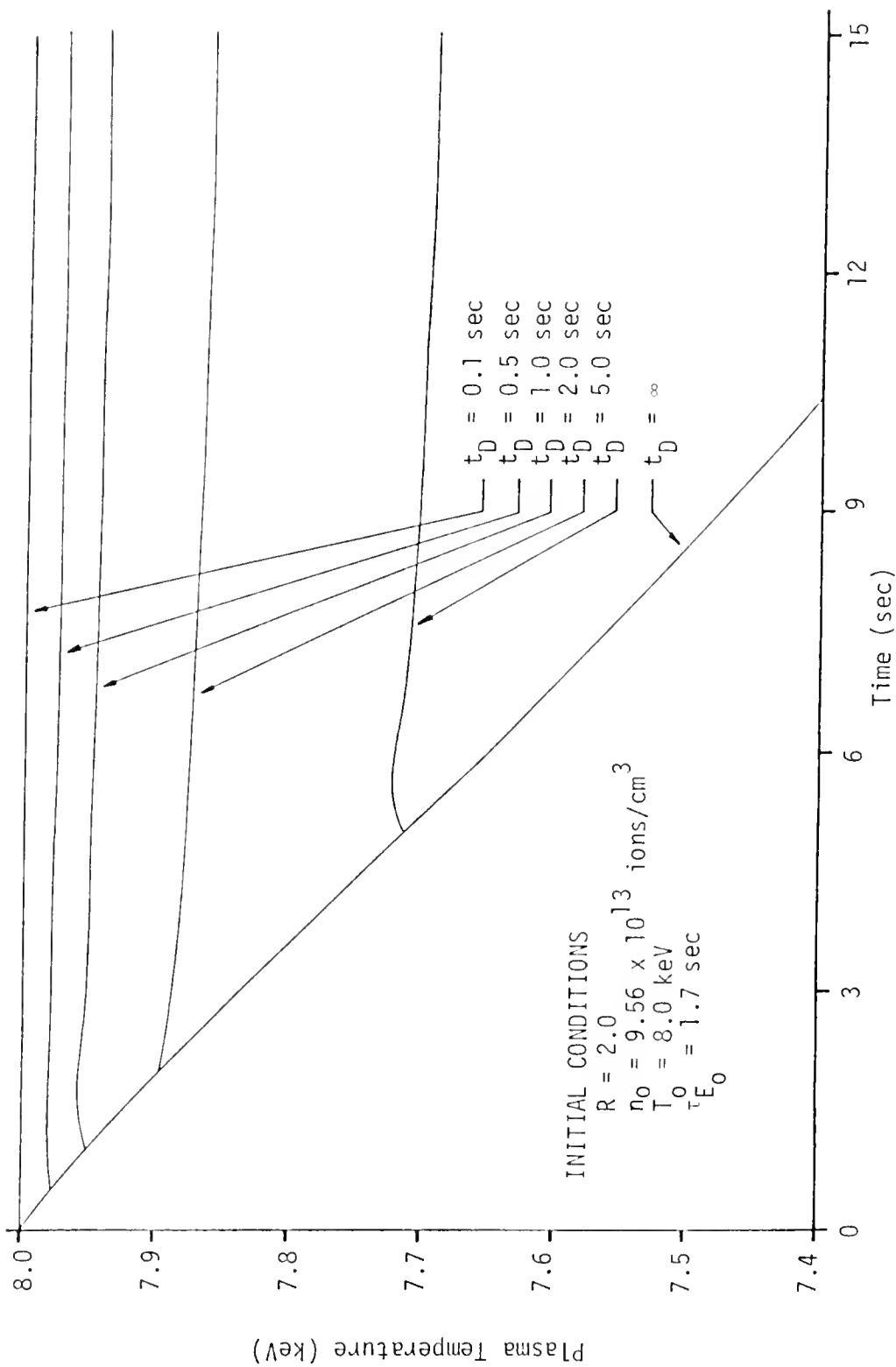
Figure 45. Variation of plasma temperature following a 5% step decrease in the feedrate of an equilibrium state at $\tau_{E_o} = 1.7$ sec with delayed shutoff times.
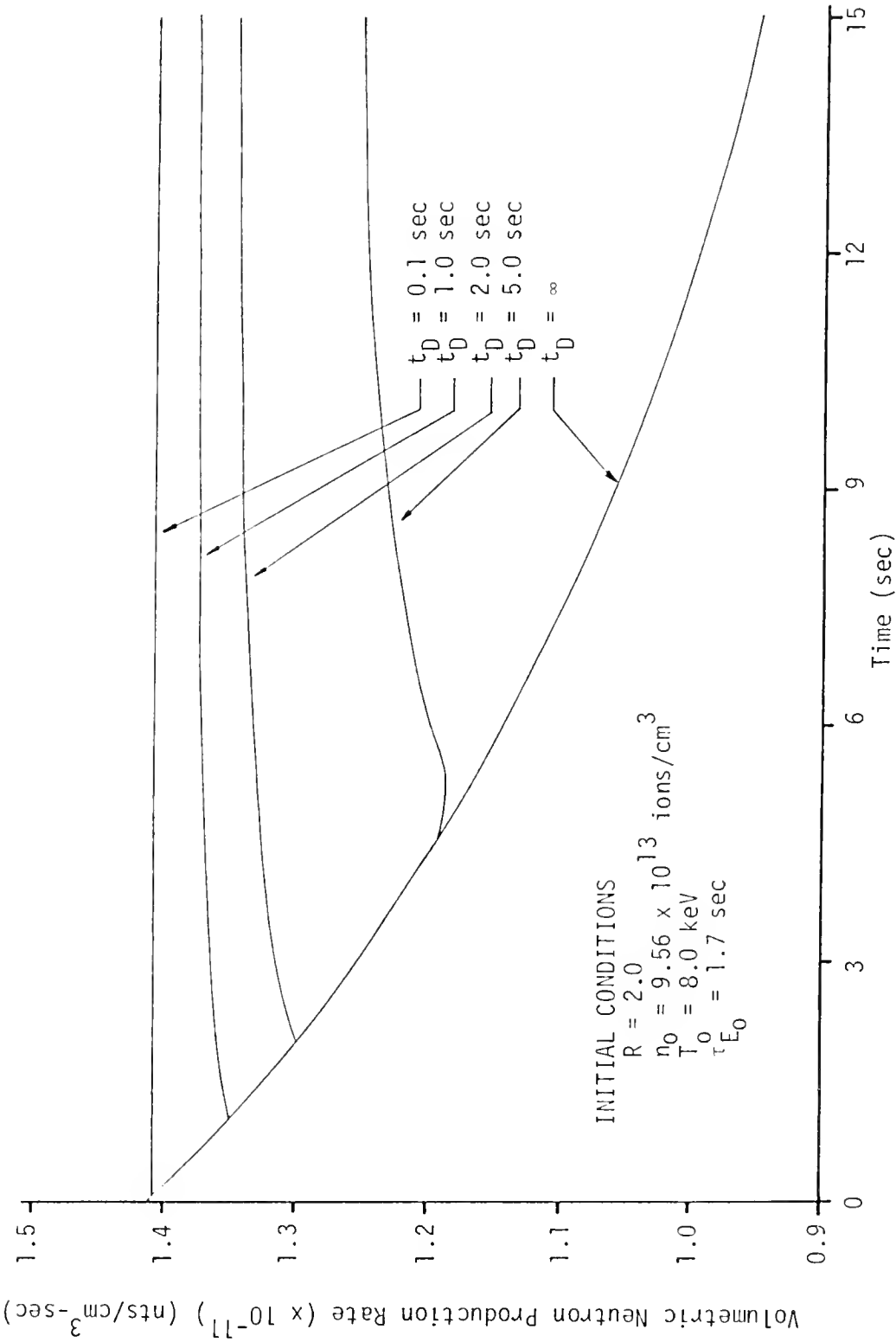
Figure 46. Variation of plasma volumetric neutron production rate following a 5% step decrease in the feedrate of an equilibrium state at τ_{E_O} = 1.7 sec with delayed shutoff times.
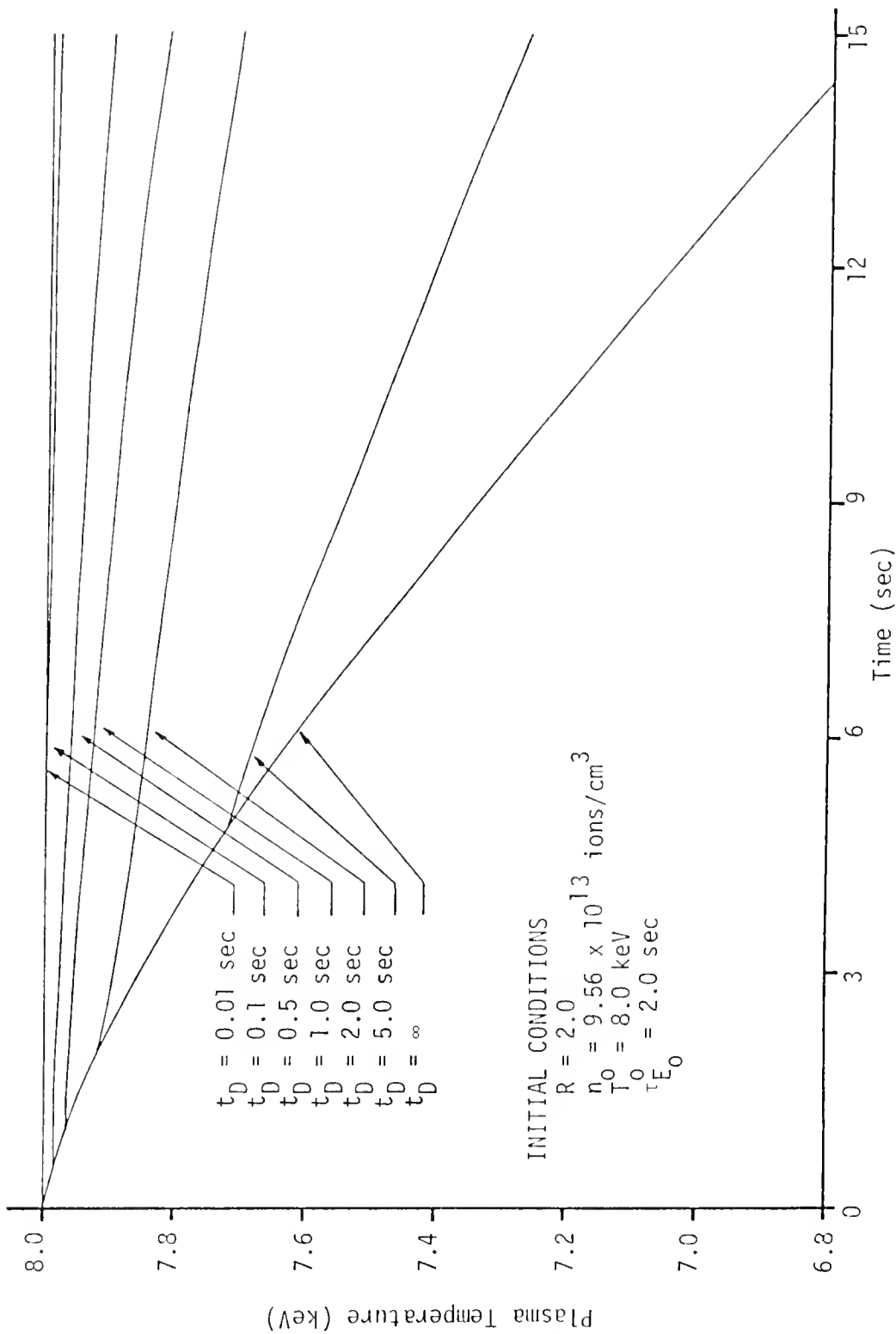
Figure 47. Variation of plasma temperature following a 5% step decrease in the feedrate of an equilibrium state at τ_{E_O} = 2.0 sec with delayed shutoff times.
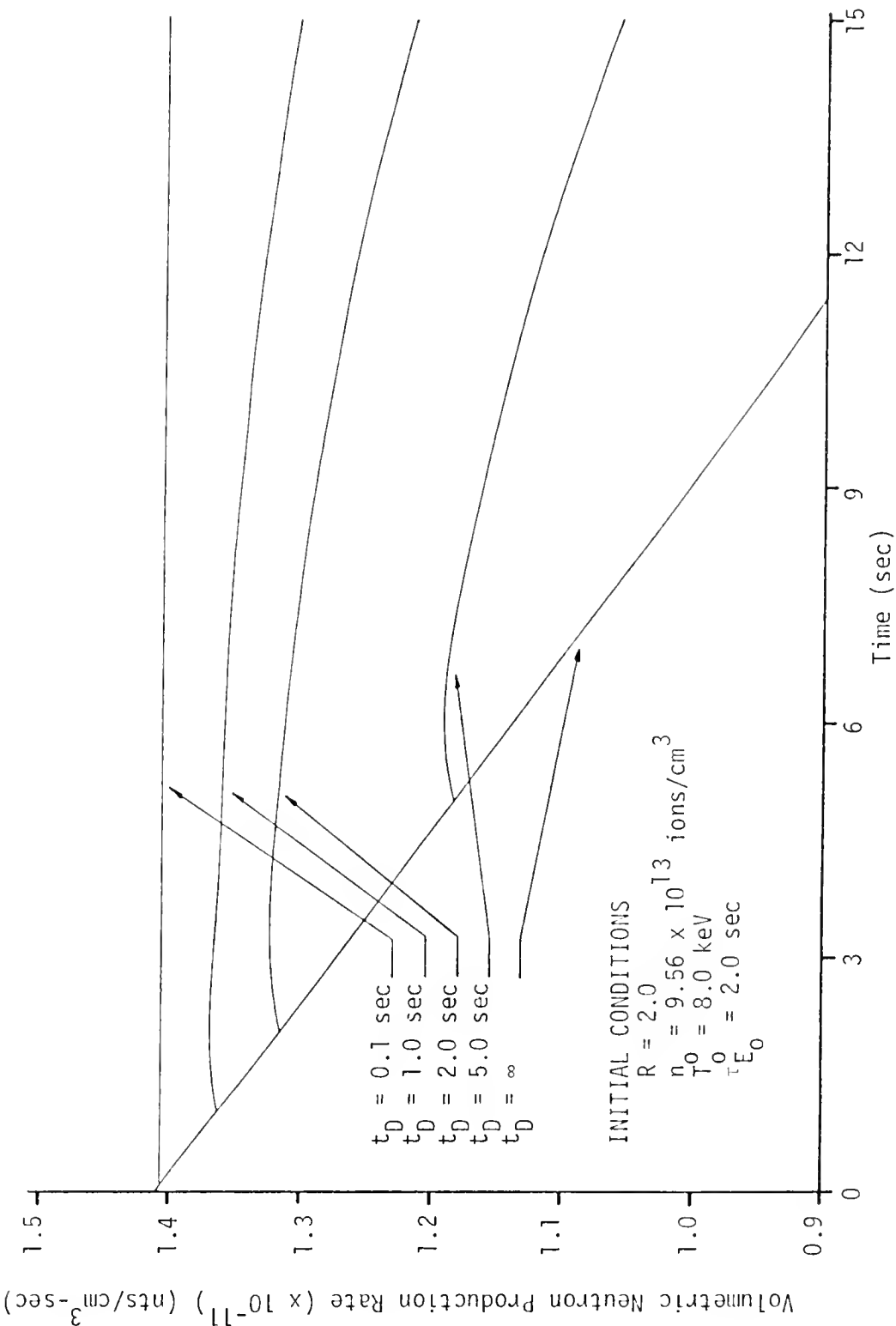
Figure 48. Variation of plasma volumetric neutron production rate following a 5% step decrease in the feedrate of an equilibrium state at τ_{E_O} = 2.0 sec with delayed shutoff times.

stable initial plasma state (τ_{E_0} = 1.5 sec), a slowly developing slightly unstable state (τ_{E_0} = 1.7 sec), and the fastest responding unstable state (τ_{E_0} = 2.0 sec).

The stability and ultimate return to the initial equilibrium states is not demonstrated definitively in the standard 15 second response intervals depicted in Figs. 37-48. Actually, whether the state is stable or not when the source perturbation is turned off is immaterial. The important point is the determination that the temperature and the neutron production rate are limited to small increases and decreases by the simple feedback mechanism of turning off the feedrate perturbations as shown in Figs. 37-48.

All of the cases for delayed shutoff of the externally induced feedrate perturbation were run for delayed shutoff times, t_D, ranging from 0.01 seconds up to 5 seconds after the initial step feedrate perturbation. Regardless of the delay time, all transients were found to be limited to some degree. However, only the τ_{E_0} = 1.5 sec stable initial state eventually returned to its original equilibrium state. The unstable perturbed states for confinement times of 1.7 sec and 2.0 sec eventually underwent transients to new equilibrium states which left them on the original Mills curve but at higher or lower equilibrium temperatures than the original 8.0 keV state. As indicated above, this eventual growth or decay to new equilibrium states was not of much concern in this study since the important consideration was the short-term response. For this reason shutting off of the source perturbation is a very effective feedback mechanism because of the reduced transient response in the 15 second interval shown in Figs. 37-48. Although the 0.1 second delay time may be somewhat optimistic for feedback application,

the feedback for larger delay times was also found to be effective.
Therefore, this simple feedback mechanism is certainly a control possi-
bility. Except for this work, no studies have examined such a simple
mechanism of feedback to control and eventually overcome feedrate per-
turbations.

Although step change perturbations in the feedrate eventually drove
the plasma to new equilibrium states if left in effect, another control
possibility, other than simple shutoff of the perturbation, was investi-
gated. This alternative made use of temperature sensing feedback as
follows:

$$\delta S(t) = K_s[T_0 - T(t)] \tag{189}$$

where K_s is the usual feedrate feedback coefficient used to apply tem-
perature-dependent feedback while the original feedrate perturbation was
still in effect. For these cases the control effectiveness was varied
by increasing the magnitude of the feedrate feedback coefficient to com-
pensate for the feedrate perturbation being left on. Although the more
unstable states required larger feedback coefficients for effective
compensation, even the hybrid equilibrium state with $\tau_E = 2.0$ sec was
hard to be controlled back to the original 8.0 keV temperature and cor-
responding neutron production rate.

Sample cases of feedrate feedback effectiveness for controlling
plasma temperature for +5% feedrate perturbations are presented in
Figs. 49-51 for three energy confinement times of 1.5 seconds, 1.7
seconds, and 2.0 seconds. Figures 52-54 represent the results of the
corresponding -5% feedrate perturbations. Only temperature variations
are depicted in Figs. 59-54 since the neutron production rate variations
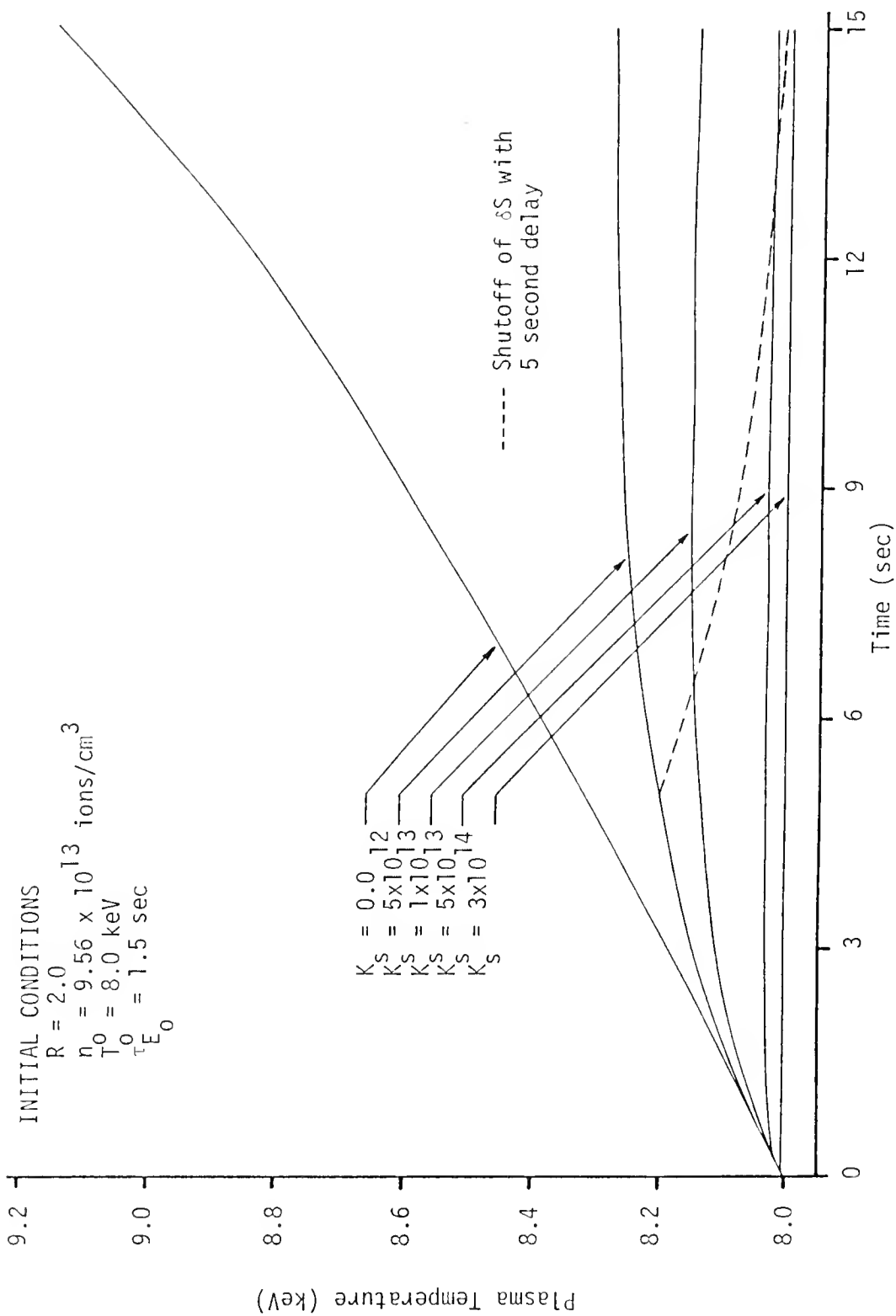
Figure 49. Variation of plasma temperature with temperature feedback following a 5% step increase in the feedrate of the τ_{E_0} = 1.5 sec equilibrium state plus delayed shutoff of δS.

–235–
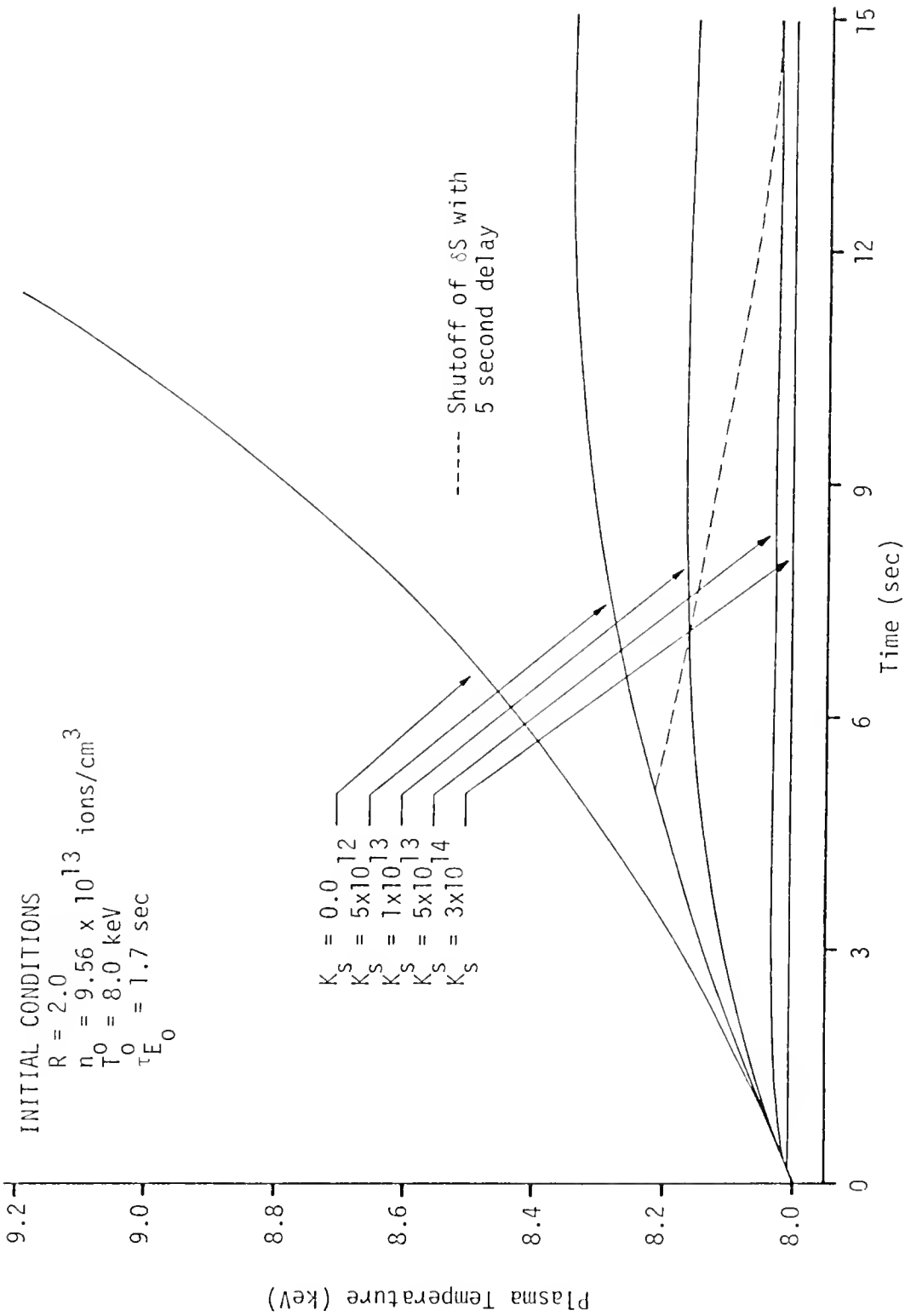
Figure 50. Variation of plasma temperature with temperature feedback following a 5% step increase in the feedrate of the $\tau_{E_o} = 1.7$ sec equilibrium state plus delayed shutoff of δS.
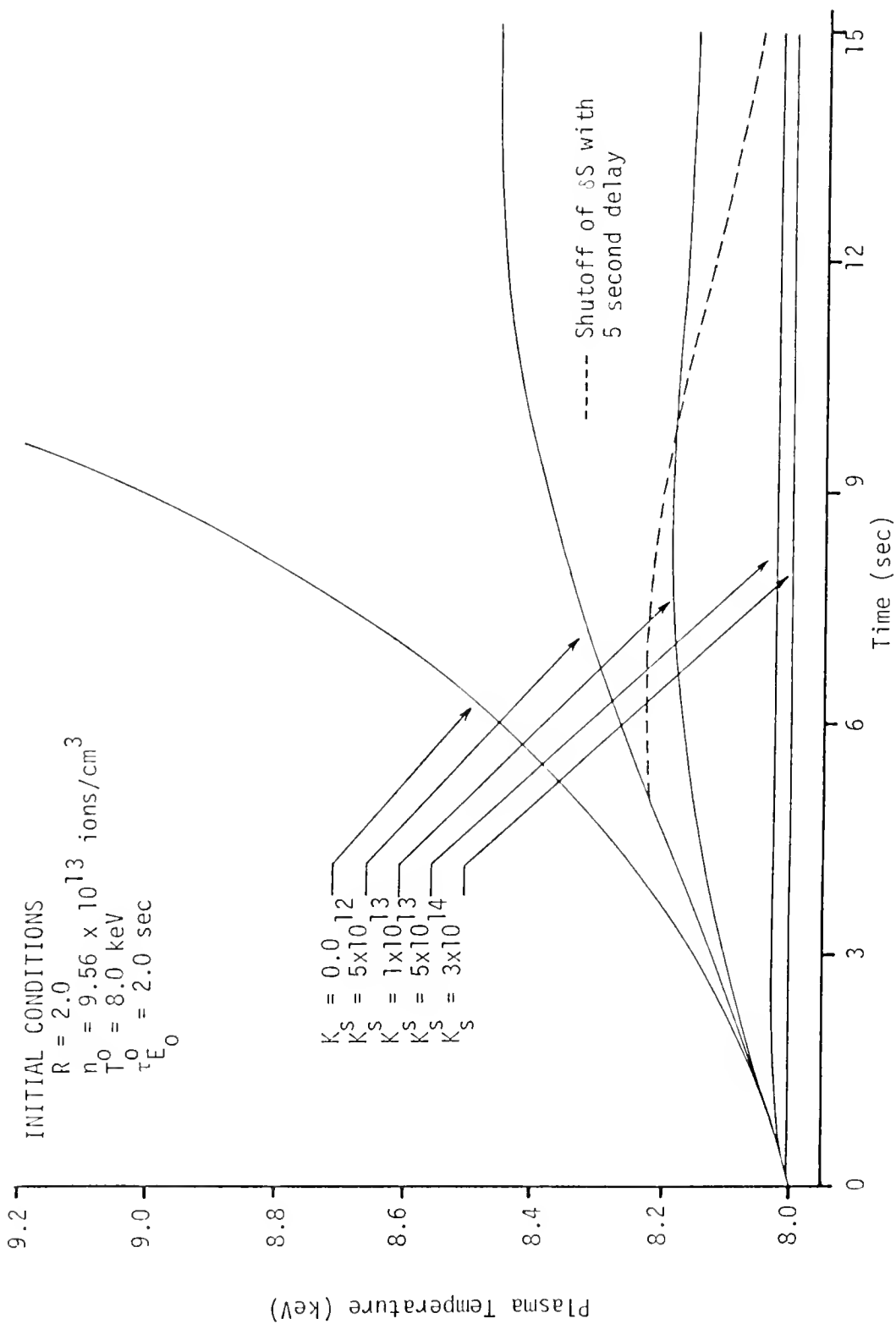
Figure 51. Variation of plasma temperature with temperature feedback following a 5% step increase in the feedrate of the τ_{E_0} = 2.0 sec equilibrium state plus delayed shutoff of δS.
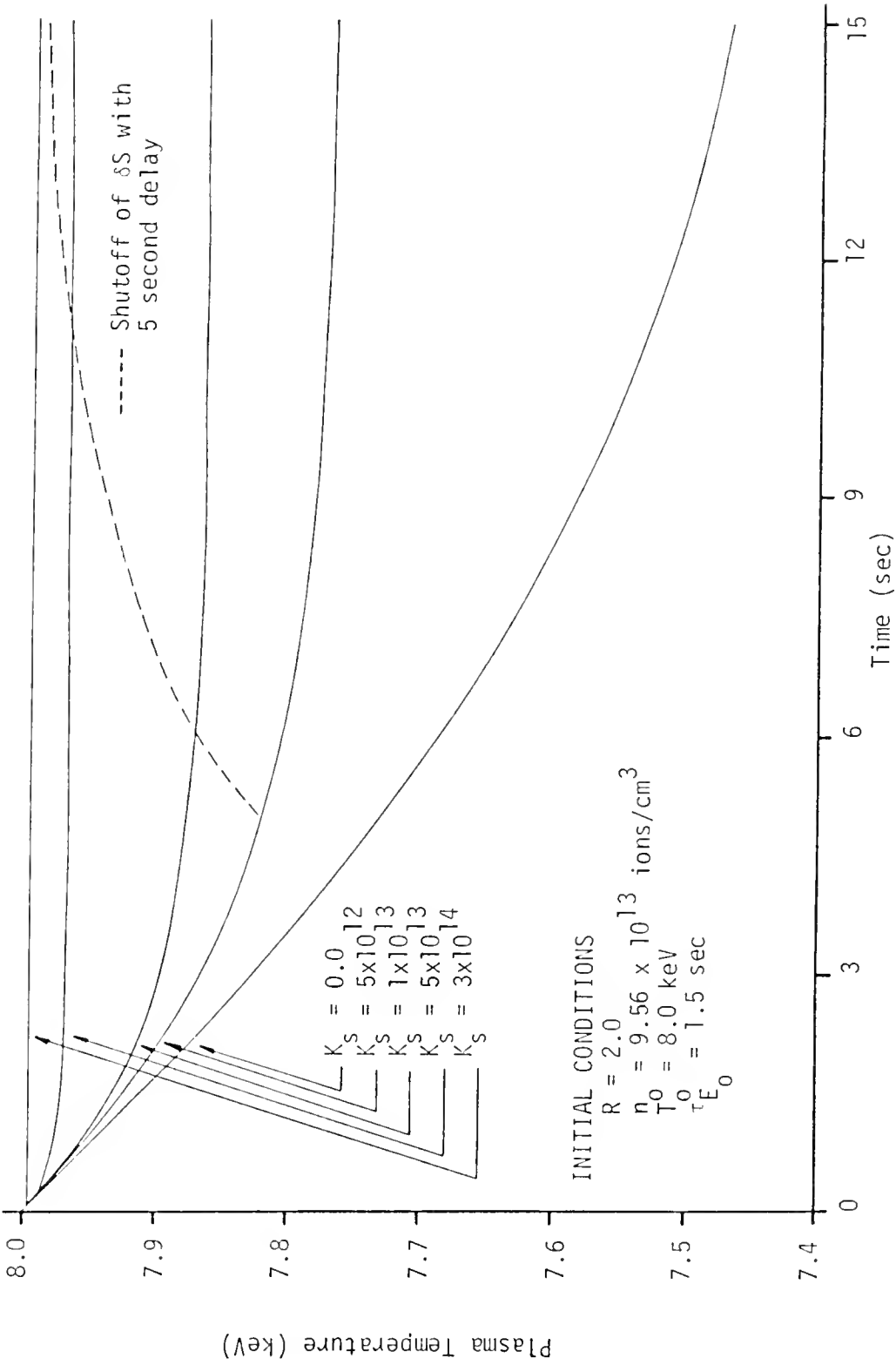
Figure 52. Variation of plasma temperature with temperature feedback following a 5% step decrease in the feedrate of the τ_{E_O} = 1.5 sec equilibrium state plus delayed shutoff of δS.
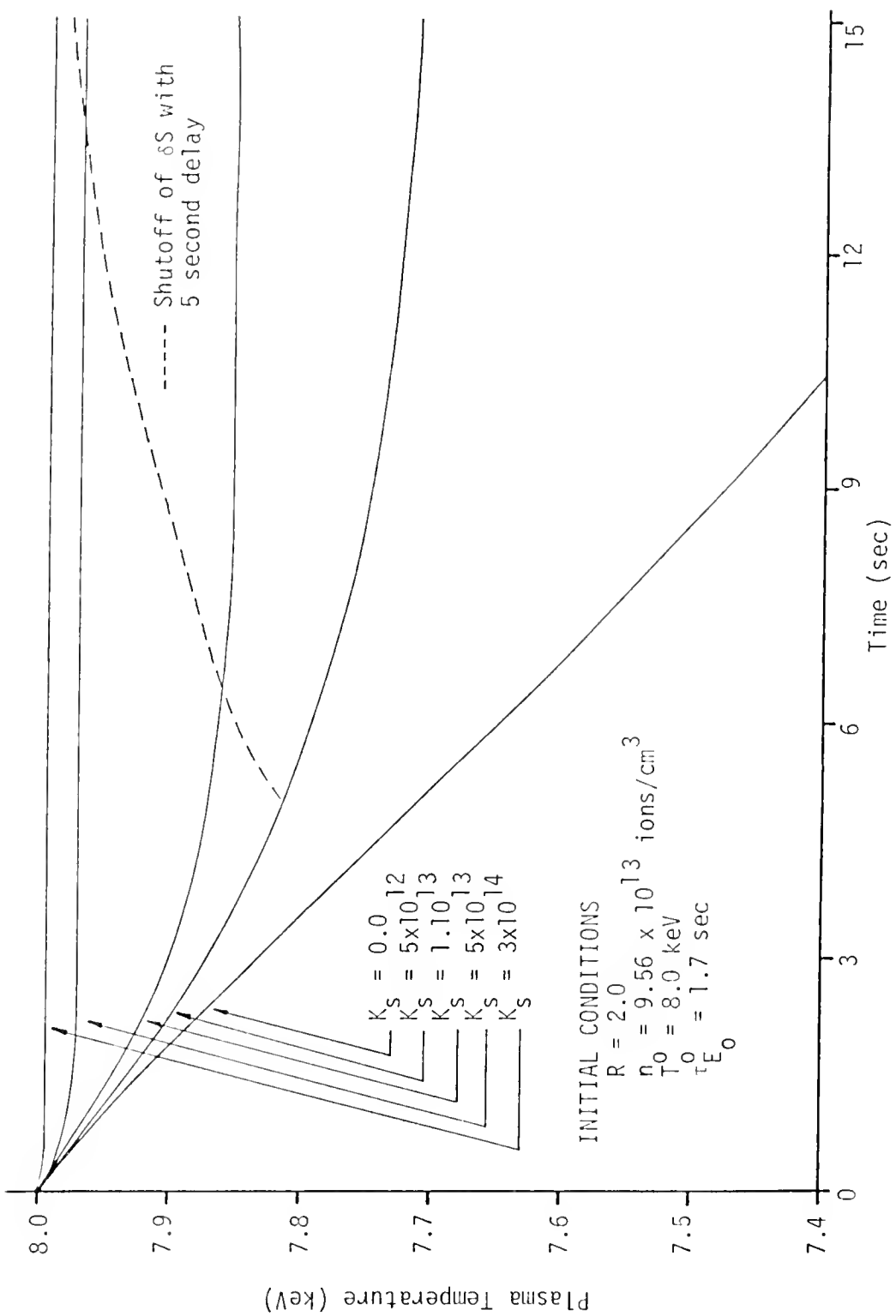
Figure 53. Variation of plasma temperature with temperature feedback following a 5% step decrease in the feedrate of the $\tau_{E_O} = 1.7$ sec equilibrium state plus delayed shutoff of δS.
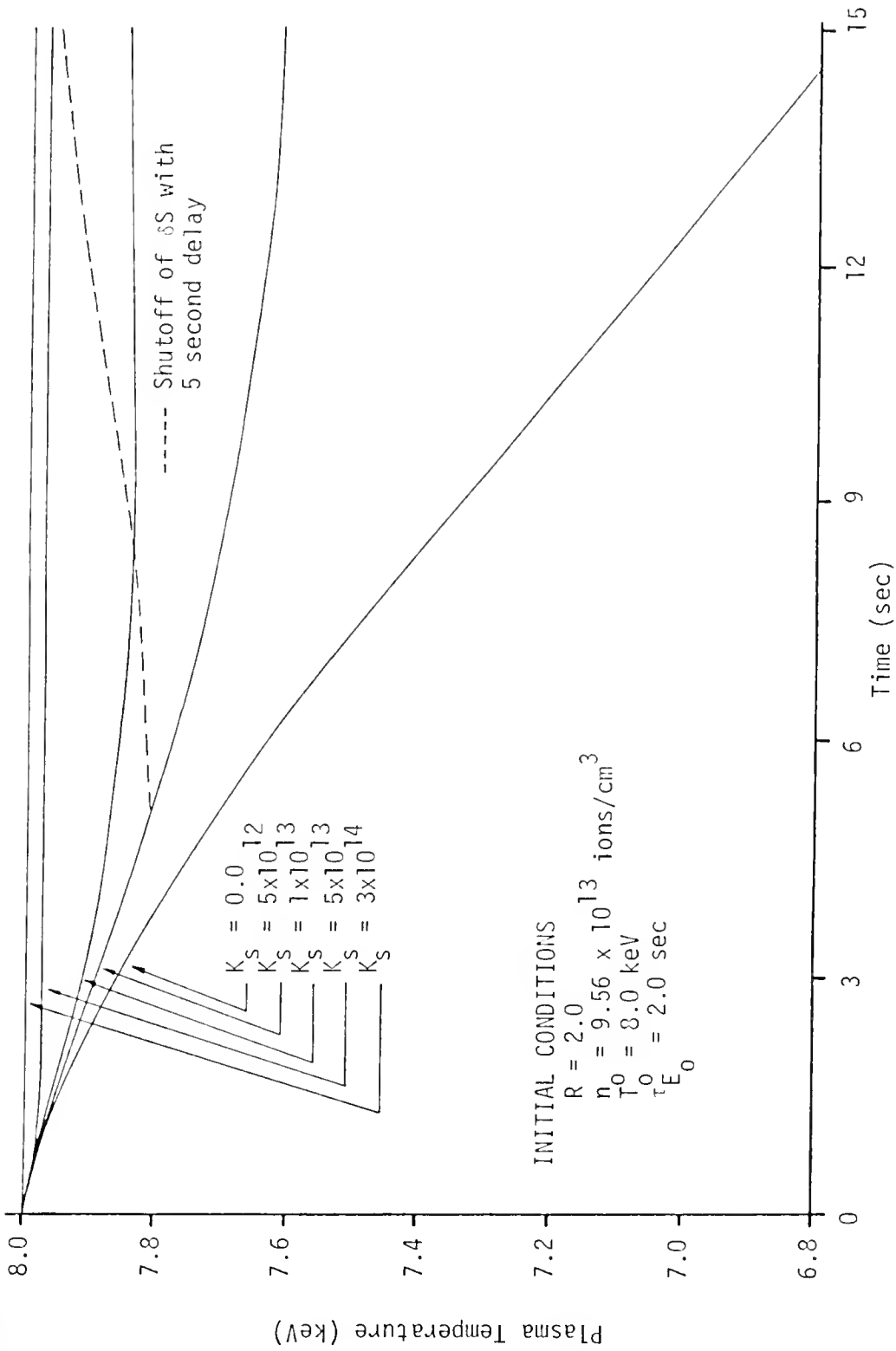
Figure 54. Variation of plasma temperature with temperature feedback following a 5% step decrease in the feedrate of the τ_{E_o} = 2.0 sec equilibrium state plus delayed shutoff of δS.

followed the temperature transients as shown previously. These figures
depicting transient development with feedback demonstrate that relatively
large feedback coefficients are required to compensate fully the per-
turbed feedrate driving effect especially for the larger confinement
case (τ_E = 2.0 sec) representing a more unstable plasma. This feedback
is effective at controlling the temperature while the feedrate is still
driving the transient because of the delay involved before feedrate
perturbations affect plasma temperature and neutron production levels
to any appreciable degree.

These transients of the form presented in Fig. 60 resulting from
simultaneous application of the step feedrate perturbations and tempera-
ture feedback support two general observations. First, the larger the
feedback coefficient the smaller the overall transient, as expected.
Second, up to a point, the larger the feedback coefficient, the more
quickly a steady state is reached although it will not be the original
steady-state equilibrium unless the feedback is very large. In the 15
second transients shown in Figs. 49-54, the plasma has reached or come
very close to reaching such a dynamic equilibrium. The steady state
consists of a dynamic equilibrium where the perturbed feedrate is trying
to drive the plasma away from the original equilibrium state and the
feedback is trying to pull the plasma back to its original state. The
size of the feedback coefficient governs its ability to control the
temperature at its original steady-state, 8.0 keV value. The larger the
feedback coefficient is, then the closer the temperature for the dynamic
equilibrium conforms to the desired 8.0 keV value. Unless the feedback
is sufficiently large, the plasma temperature and neutron production
rate at the dynamic equilibrium will not be the same as the value at the
initial steady state.

Although not shown in Figs. 55-60, too large values of feedback result in reaching the original neutron production rate but then severely overshooting. In design control of hybrid plasmas, such values should be avoided in favor of the larger values shown in Figs. 55-60 which do give good response. However, even for the most unstable plasma and the feedback coefficient set at K_s = 5 x 10^{12}/cm^3-sec-keV, the plasma temperature reached only 8.47 keV after 15 seconds. This value is less than a 6.0% total perturbation on the equilibrium temperature of 8.0 keV. The transients depicted in Figs. 49-54 further demonstrate that with sufficiently large feedback, the feedrate-perturbed plasma temperature can be controlled very close to the desired 8.0 keV level.

If the feedrate perturbation is turned off within a short time after the step change and the feedback based on temperature changes is incorporated, then very little transient development is expected. Little change is expected because of the controlling effect of the feedback combined with the slow growth of the uncontrolled temperature transient as previously demonstrated in Figs. 33-36. In addition, if the plasma has not developed too large a transient, then just eliminating the feedrate perturbation was found to be enough to return the plasma to the initial equilibrium 8.0 keV state on the same Mills-curve as noted previously.

These reduced transients are sketched in the dashed curves in Figs. 49-54 based on two feedback effects. First, the 5% perturbation in the feedrate was turned off with a 5 second delay time. Second, temperature feedback was applied through a small feedback coefficient value of K_s = 5 x 10^{12}/cm^3-sec-keV. Even for this small feedback coefficient, the dashed curves in Figs. 49-54 show uniform fast return of the plasma to its original equilibrium state in all cases.
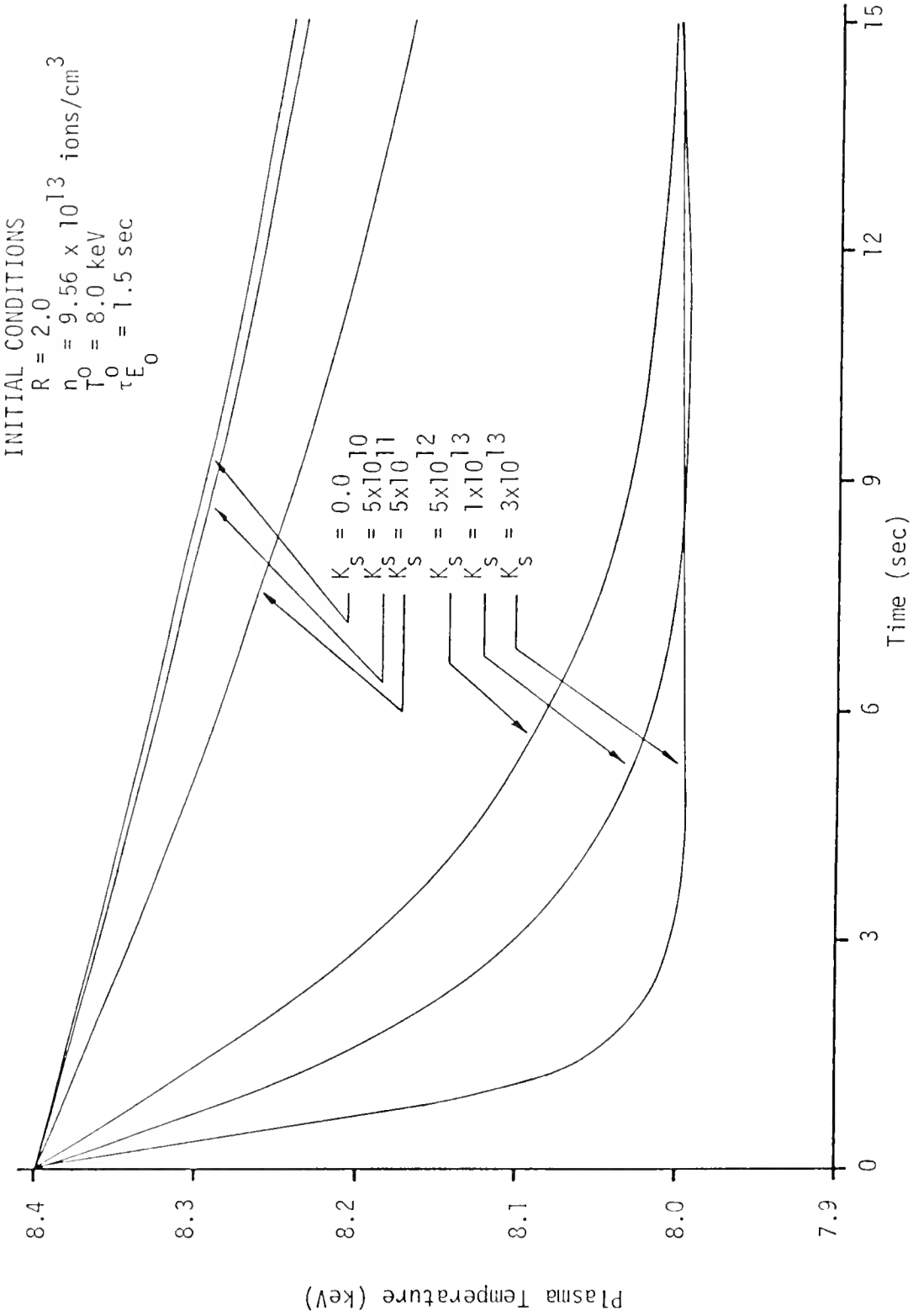
Figure 55. Variation of plasma temperature with temperature feedback following a 5% step decrease in the temperature of the τ_{E_0} = 1.5 sec equilibrium state.
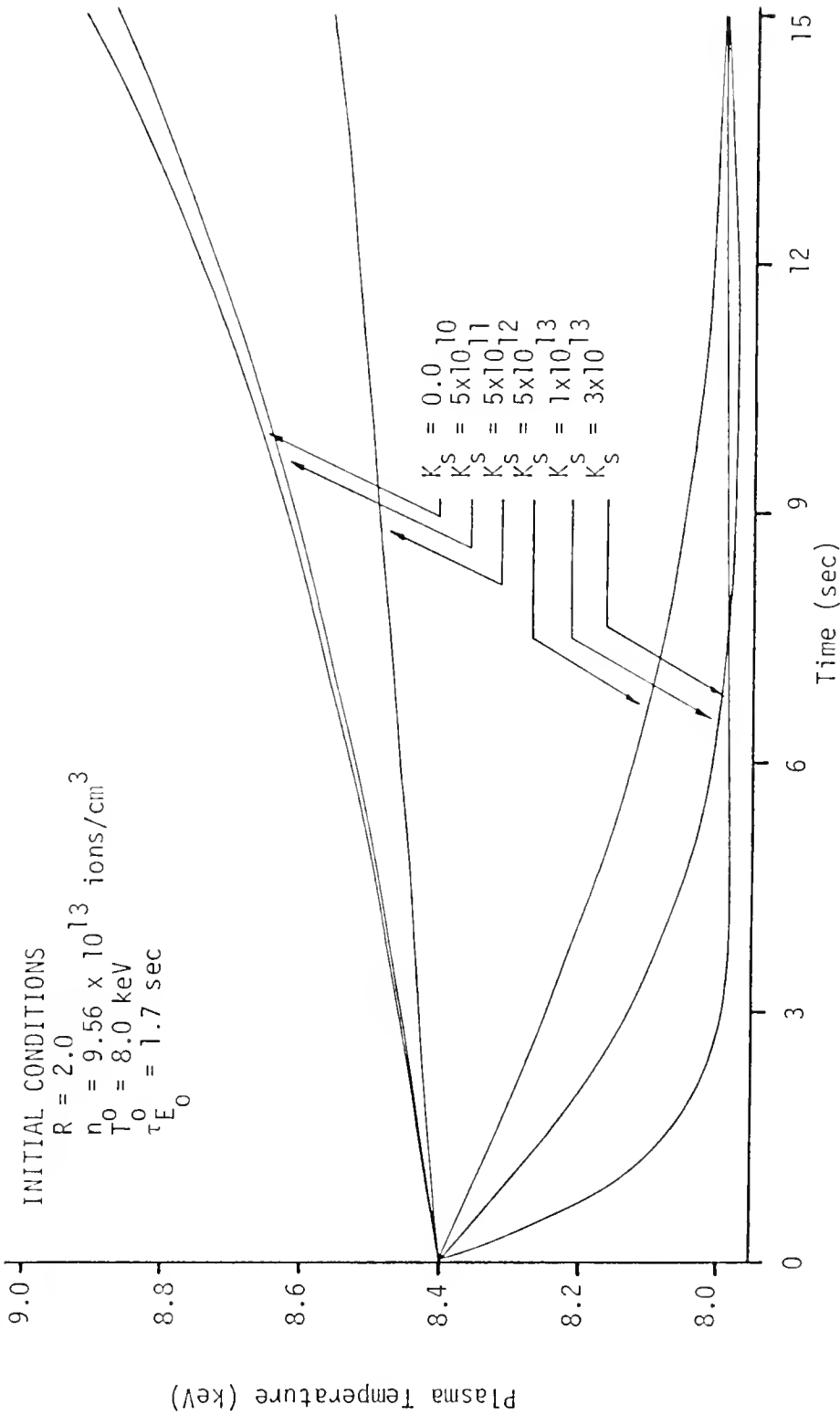
Figure 56. Variation of plasma temperature with temperature feedback following a 5% step increase in the temperature of the $\tau_{E_0} = 1.7$ sec equilibrium state.
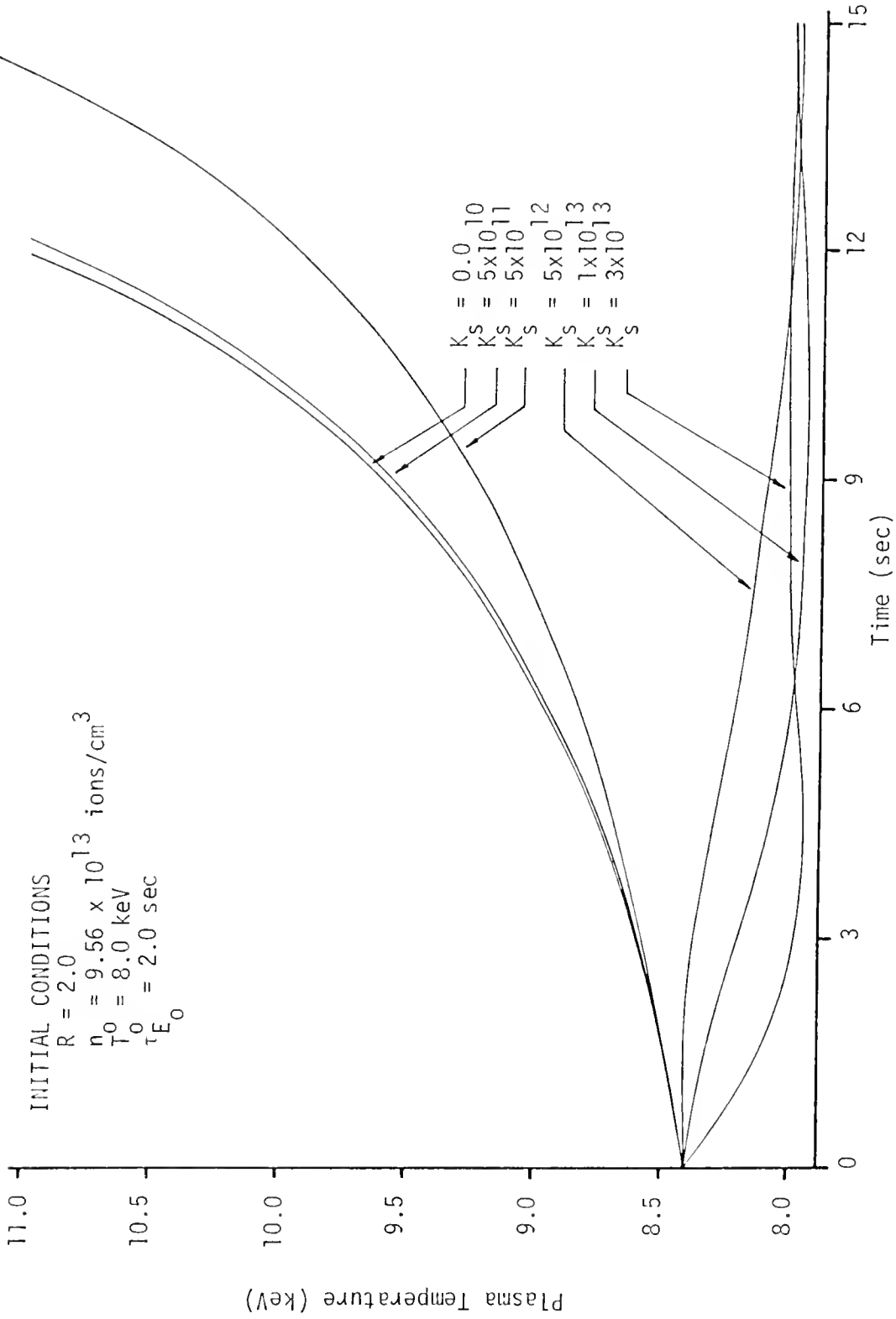
Figure 57. Variation of plasma temperature with temperature feedback following a 5% step increase in the temperature of the τ_{E_O} = 2.0 sec equilibrium state.
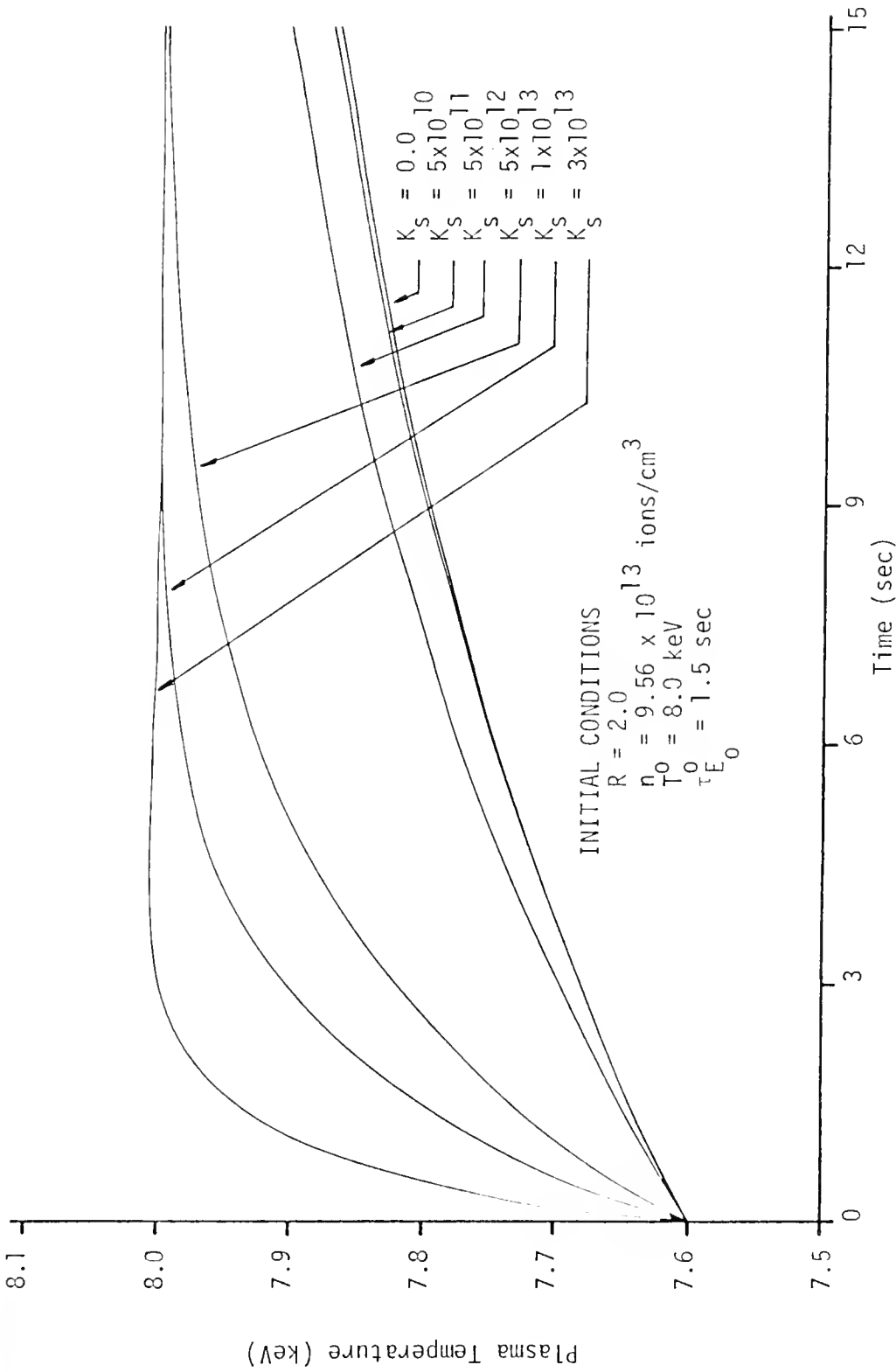
Figure 58. Variation of plasma temperature with temperature feedback following a 5% step decrease in the temperature of the τ_{E_o} = 1.5 sec equilibrium state.
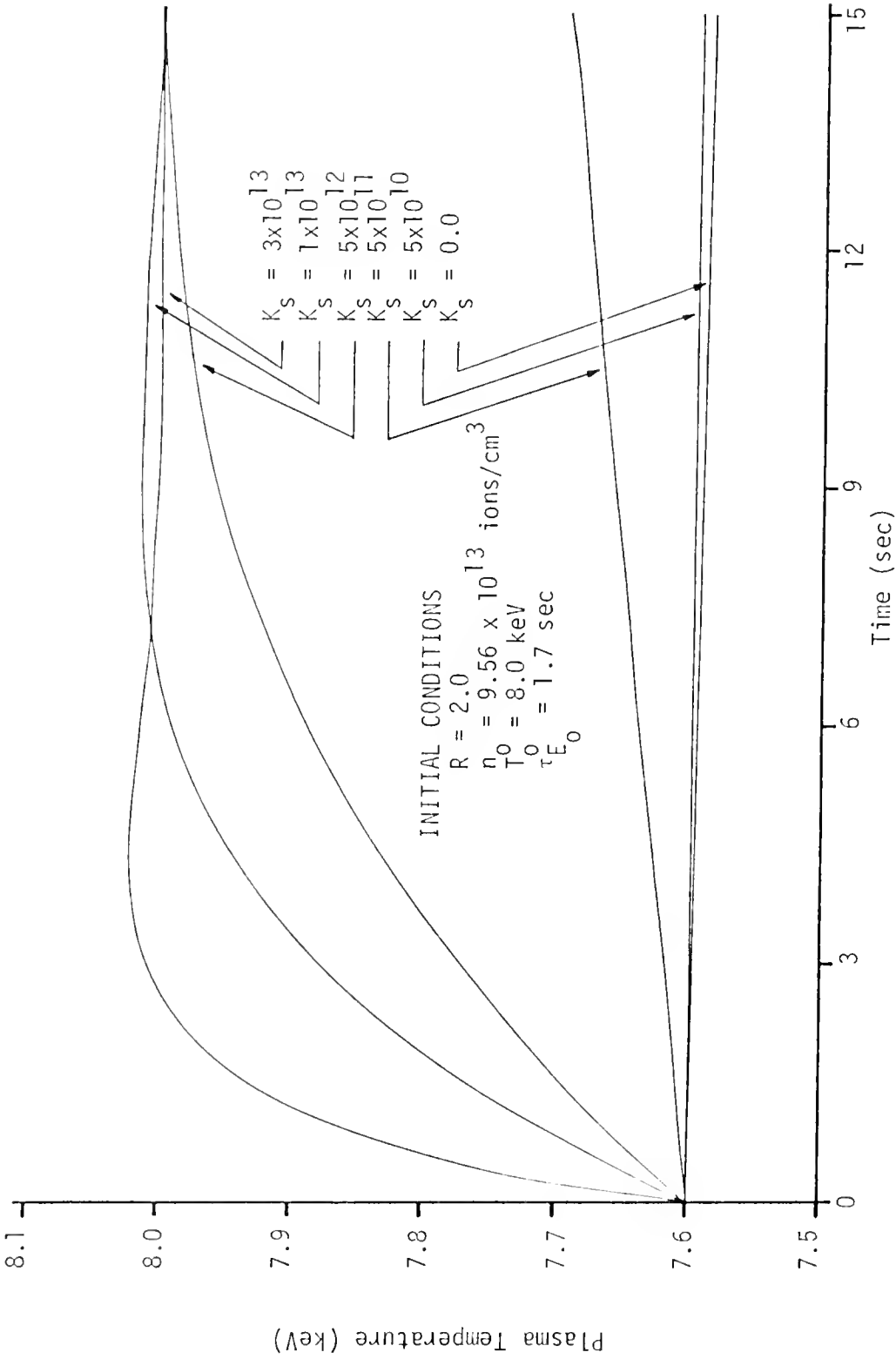
Figure 59. Variation of plasma temperature with temperature feedback following a 5% step decrease in the temperature of the τ_{E_O} = 1.7 sec equilibrium state.
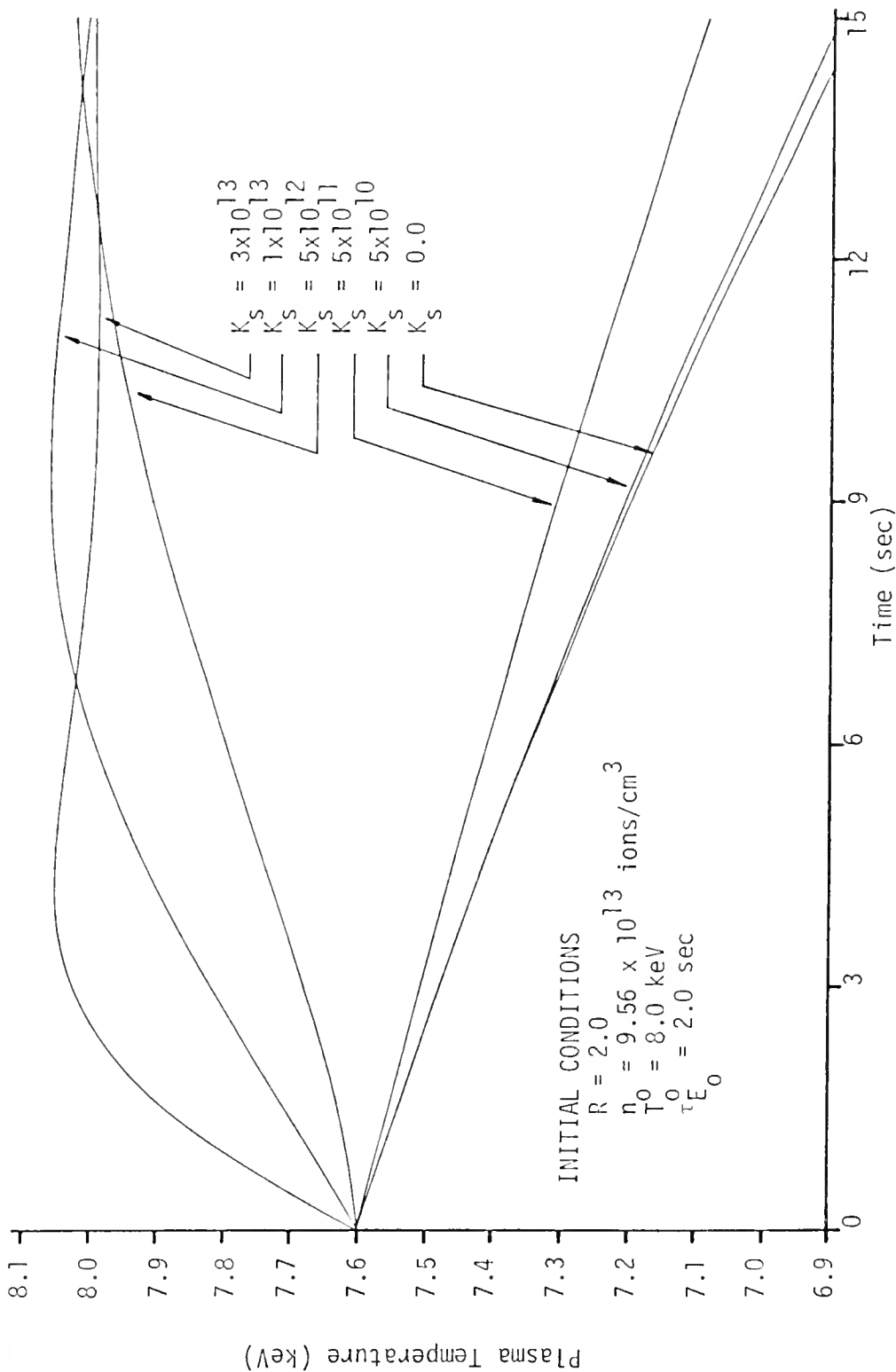
Figure 60. Variation of plasma temperature with temperature feedback following a 5% step decrease in the temperature of the τ_{E_0} = 2.0 sec equilibrium state.

Although not shown in the figures, similar runs made where the feedrate perturbation was zeroed after 1 second indicated practically no transient problems. In these cases the temperature did not undergo a sufficient transient in one second to be interesting.

The key to such effective control is application of dual control effects (delayed shutoff plus temperature-dependent feedback) to reduce the magnitude plasma temperature transients under source feedrate perturbations. With the perturbation shut off there was no driver to sustain the temperature transient so the temperature more or less quickly returned to the steady-state equilibrium. However, when the additional control of temperature feedback was added, then the temperature transient development was effectively controlled to prevent significant changes in the neutron source sustaining the hybrid blanket.

Finally, feedback control on the direct temperature perturbed cases was examined. The uncontrolled transient development following a step change perturbation in the temperature has been presented in Figs. 28-31. As noted, the prompt step changes contrast with the temperature transient development due to the source feedrate perturbation. For the source feedrate perturbation, the temperature changed in a continuous manner so that the neutron level was not perturbed to any great extent for some time. However, with the instantaneous 5% step increase in temperature, the neutron production rate jumped nearly 15% from 1.41×10^{11} nts/cm^3-sec to 1.62×10^{11} nts/cm^3-sec due to the sensitivity of the reactivity to temperature. Similarly, a 5% drop in temperature caused nearly 16% drop in the neutron production rate from 1.41×10^{11} nts/cm^3-sec to 1.213×10^{11} nts/cm^3-sec.

The transients represented in Figs. 55-60 demonstrate the effective-ness of temperature feedback in controlling the plasma temperature response following a step change in the steady-state, 8.0 keV temperature for different plasma confinement times corresponding to the required steady-state density and temperature conditions.· The temperature responses with feedback for step increases in temperature are shown in Figs. 55-57 while the responses with feedback for step decreases in temperature are shown in Figs. 58-60. As usual, the uncontrolled response determined for each case is presented for comparison. The limited transients depicted in Figs. 55-60 clearly demonstrate the effectiveness of the temperature-dependent feedback where the magnitude of the feedback coefficient, K_s, is noted on each curve as used in Eq. (189) which is repeated here:

$$S(t) = S_0 + K_s[T_0 - T(t)]$$ (190)

to emphasize that a negative feedback effect was used. Figures 55-60 show that rather large temperature perturbations can occur even with this feedback. In fact, the 15% instantaneous increase in neutron pro-duction for only a 5% increase in temperature is itself a significant factor, regardless of later controls. As shown in Figs. 55-60 these pergurbations in temperature following direct step changes in plasma temperature as the perturbing signal were much larger than the cor-responding perturbations resulting from the source feedrate perturbations. This difference can be attributed to the fact that the temperature perturbation directly alters the plasma temperature while the feedrate perturbation only indirectly affects the plasma temperature.

For purposes of examining large scale neutronic effects, the direct temperature perturbation is more interesting and more in need of control. As shown in Figs. 61-66, the volumetric neutron production rate in the plasma also showed significant changes for the direct temperature perturbation since this rate follows the temperature as previously discussed. As noted, the neutron production rate varies over a wider range than the plasma temperature.

Figures 61-66 demonstrate that small values of feedback are ineffective in the short term for control. Although all three plasma cases were controlled to be stable regardless of the step increase or decrease in temperature, this is not sufficient. A prompt return to the steady-state condition of a volumetric neutron production of 1.41×10^{11} nts/cm^3-sec corresponding to a temperature of 8.0 keV is needed. Thus, the feedback coefficient of $K_s = 5 \times 10^{12}$/cm^3-sec-keV in Figs. 61-66 is preferred of those feedback coefficients shown. Larger feedback coefficients were found to return the plasma to the required temperature or volumetric neutron production rate but not at a steady-state condition. The overshoot found with feedback coefficients above $K_s = 1 \times 10^{13}$/cm^3-sec-keV is an undesirable result. The effectively damped cases with $K_s = 5 \times 10^{12}$/cm^3-sec-keV were chosen as the preferred feedback effect since only three or four seconds longer was required for the system to return to a value near its original neutron production rate. In addition, the thermal cycling and mechanical problems can be minimized using the more efficient feedback values.

These neutron production rate responses with a temperature perturbation were examined as the limiting case for the plasma output under controlled conditions. The hybrid blanket must be capable of handling

such perturbations in plasma neutron production as part of its design basis; a 5% change in temperature during a plasma cycle is not unlikely.

The ranges of response found for the hybrid plasma have been presented in this chapter for point-model fusioning plasmas. These neutron production transients are the transients which are applicable as the fundamental basis for variations in the hybrid blanket system power level. In general, these changes are surprisingly slow to develop; the hybrid plasma is slow to respond to perturbing stimula due to the driving effect of the feedrate and injection energy. This is a fundamental difference in comparison with the development of time variations in fusioning but self-sustaining plasmas. This difference may be sufficiently important that hybrid plasmas will be deliberately derated in temperature to enhance controllability.
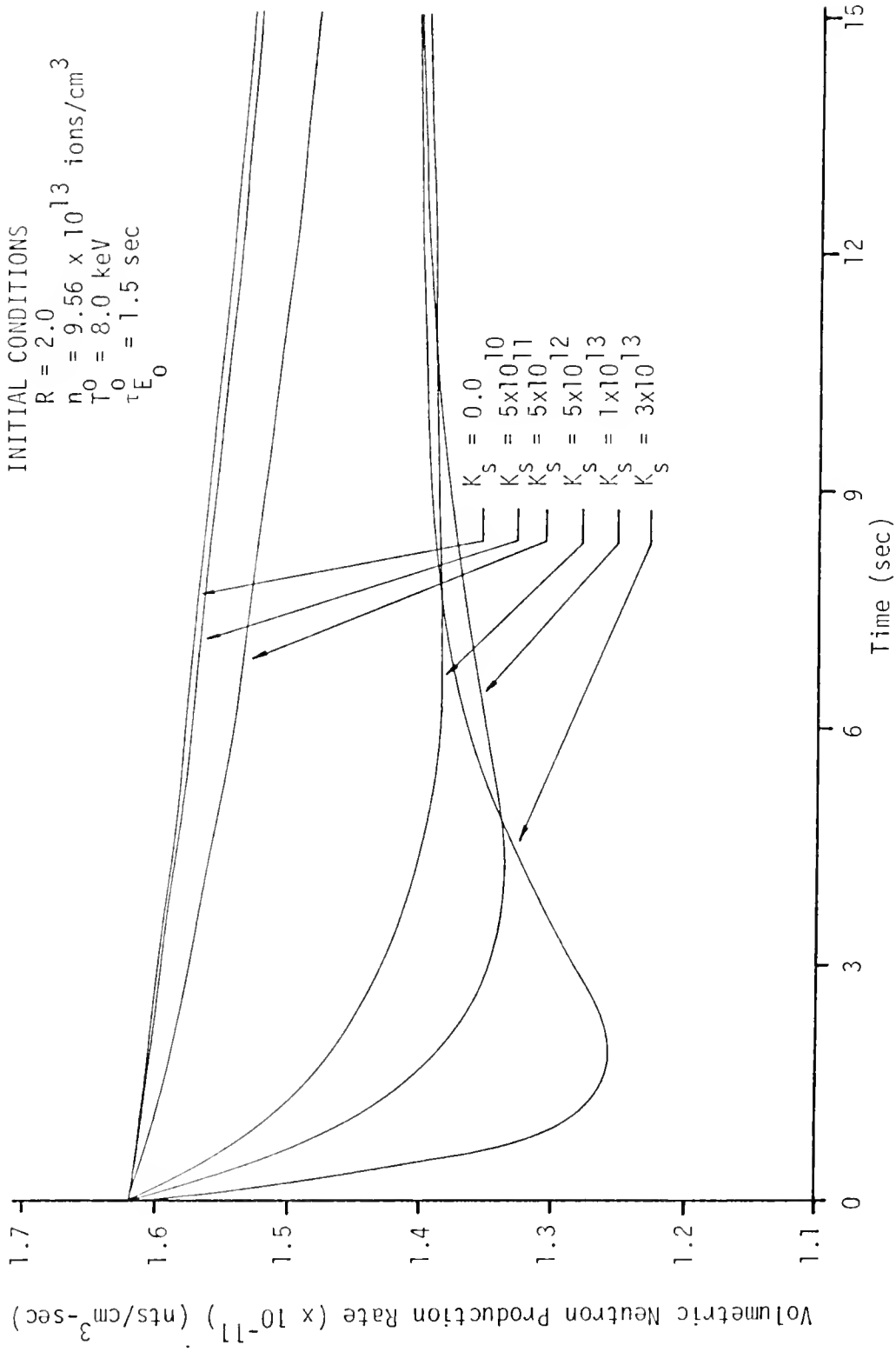
Figure 61. Variation of plasma volumetric neutron production rate with temperature feedback following a 5% step increase in temperature of the $\tau_{E_o} = 1.5$ sec equilibrium state.
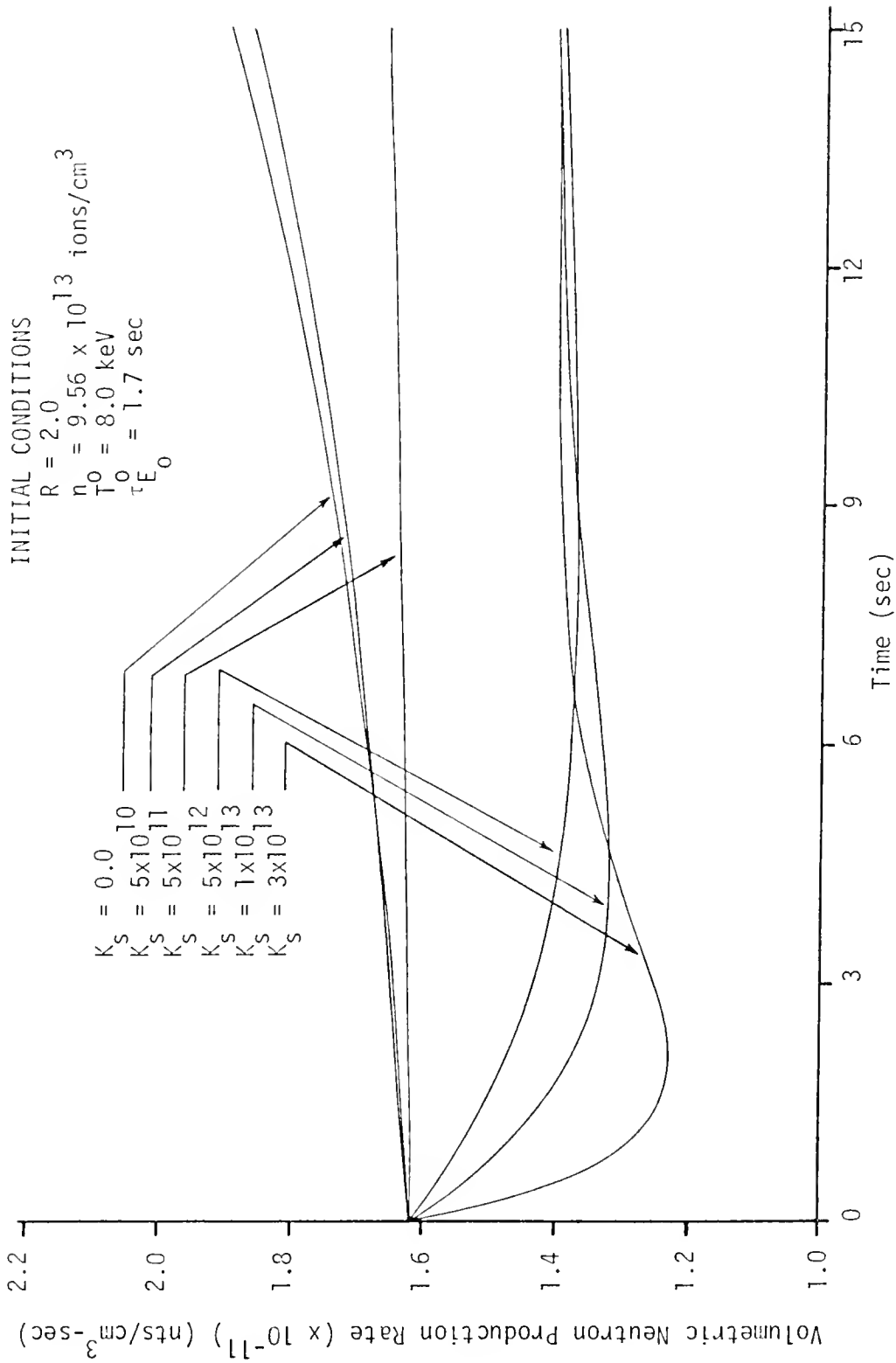
Figure 62. Variation of plasma volumetric neutron production rate with temperature feedback following a 5% step increase in temperature of the $\tau_{E_o} = 1.7$ sec equilibrium state.
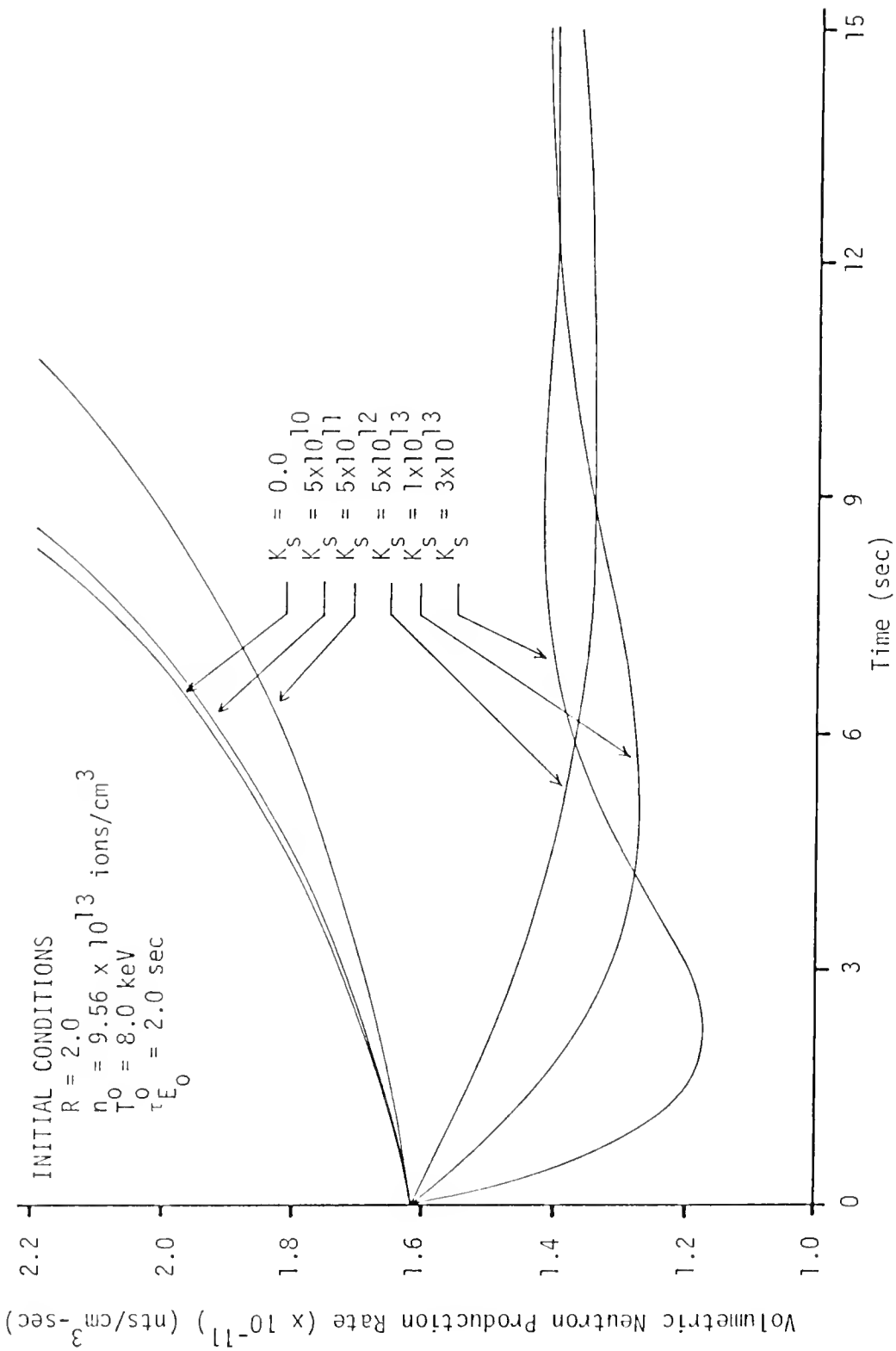
Figure 63. Variation of plasma volumetric neutron production rate with temperature feedback following a 5% step increase in temperature of the $\tau E_0 = 2.0$ sec equilibrium state.
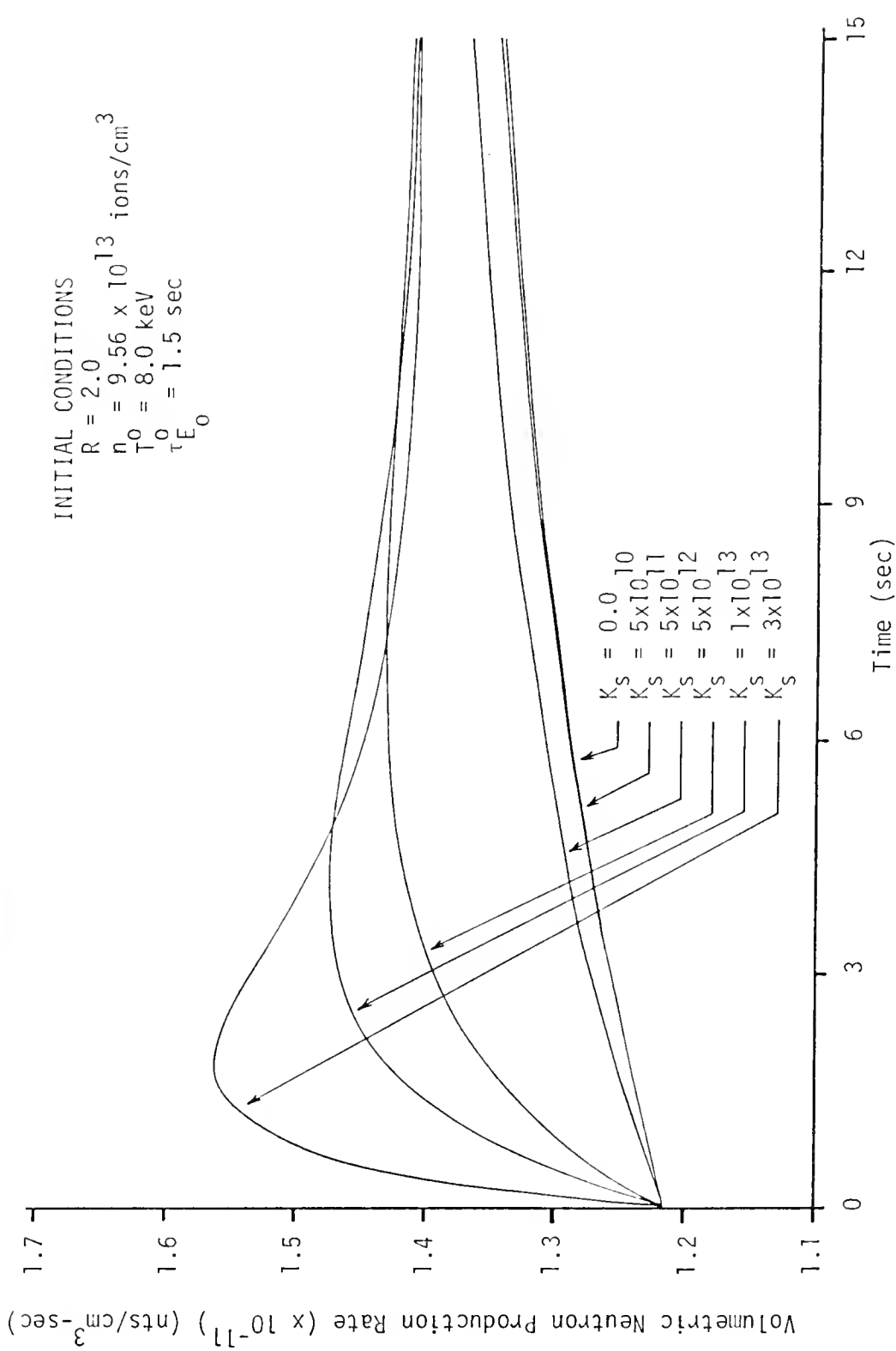
Figure 64. Variation of plasma volumetric neutron production rate with temperature feedback following a 5% step decrease in temperature of the τ_{E_o} = 1.5 sec equilibrium state.
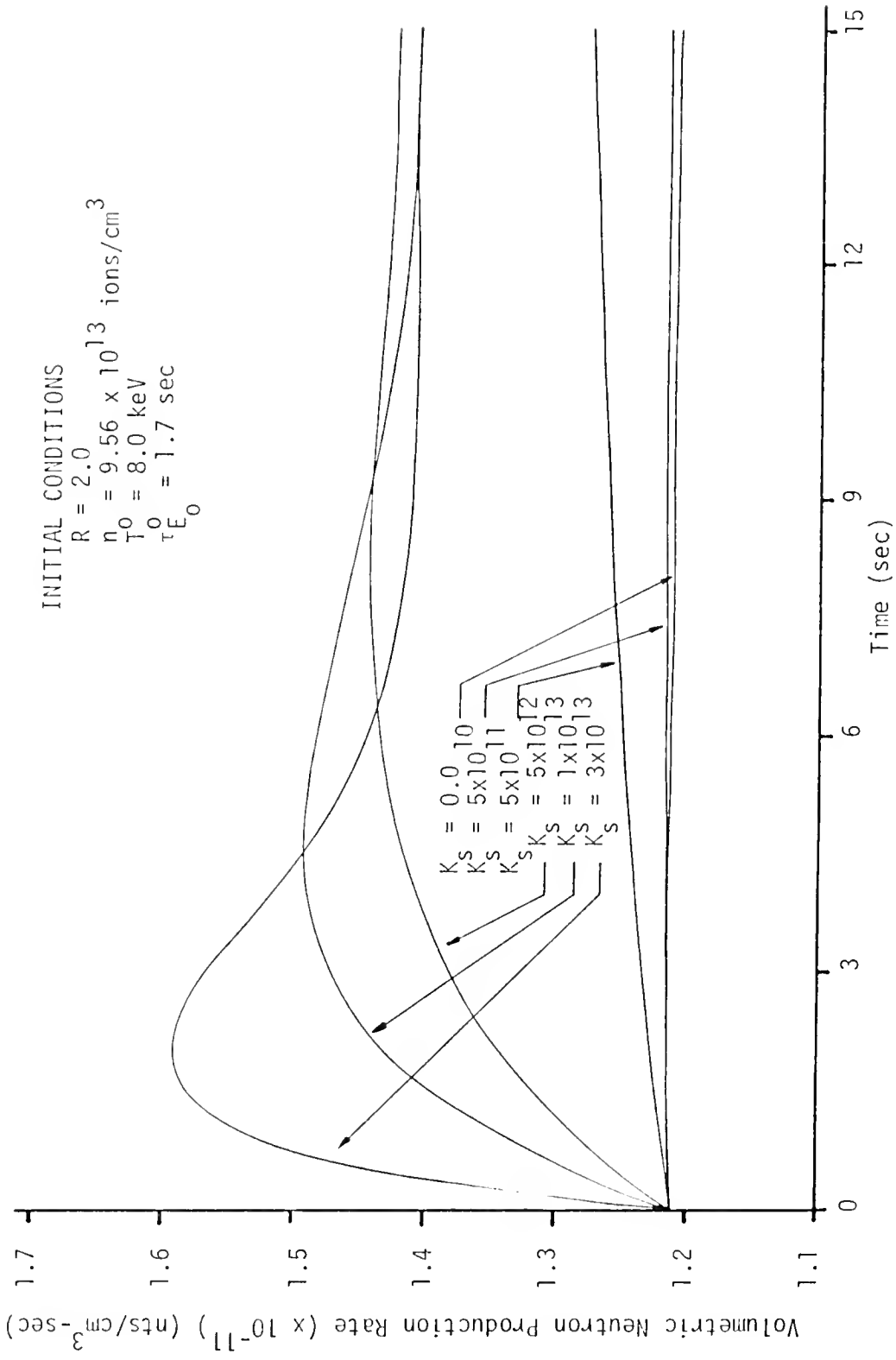
Figure 65. Variation of plasma volumetric neutron production rate with temperature feedback following a 5% step decrease in temperature of the $\tau_{E_0} = 1.7$ sec equilibrium state.
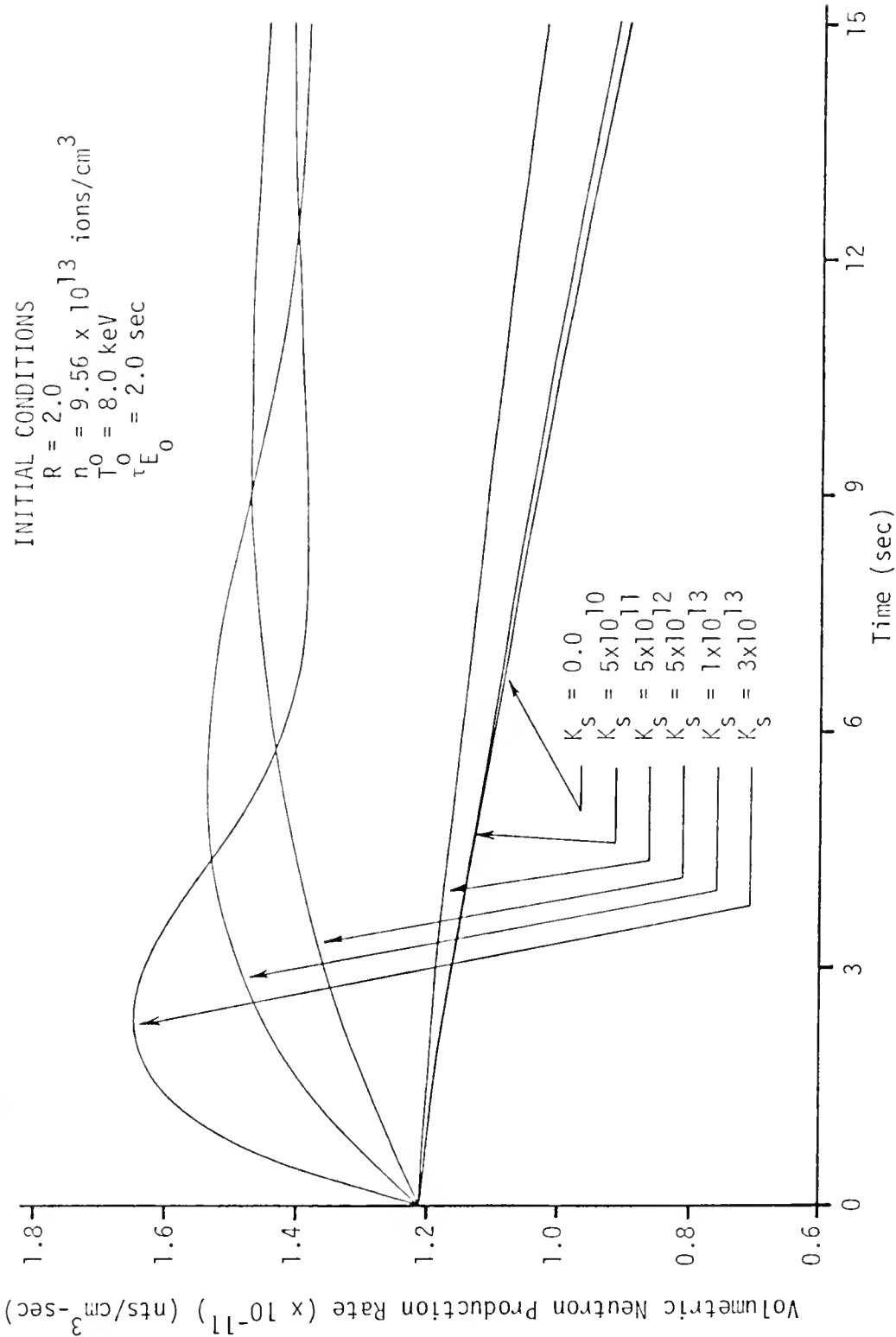
Figure 66. Variation of plasma volumetric neutron production rate with temperature feedback following a 5% step decrease in temperature of the $\tau_{E_o} = 2.0$ sec equilibrium state.

CHAPTER 5
HYBRID BLANKET ANALYSIS

Introduction

The plasma system was discussed in Chapter 4 incorporating time variation and control for perturbations of interest. At this point the hybrid blanket is considered. The research was aimed at analysis of the characteristics of a realistic hybrid as a possible alternative to the fast breeder for power production. The objective was not to invent an entirely new blanket, but to use and build on an existing design. Therefore, the most advanced hybrid blanket design available was chosen as the basis for the analysis. The geometric arrangement of the blanket along with the region and elemental constituents are summarized in Appendix B. As indicated, the blanket is designed to utilize a thermal fission lattice of low enrichment which is well-moderated with graphite and cooled with low absorption helium.

The blanket described in Appendix B is very similar to one of the systems developed in the PNL mirror hybrid studies.[64] This design was selected not only for its multiplicative capabilities but for its projected ability to breed both tritium and fissile fuel, as presented in Table 1-XV, Case 7. Since the design in Appendix B is specifically intended for use with a Tokamak fusion-fission hybrid to allow significant power production, the changes involved are basically those required for toroidal geometry.

First, scoping calculations were performed using diffusion theory to establish a range of viable values for the blanket effective neutron multiplication factor, k_{eff}, for various global blanket temperatures and fission lattice enrichments. Various calculational schemes were developed and tested using few group diffusion theory. The best scheme was then used to facilitate analysis of the blanket using 4-group diffusion theory. All diffusion theory calculations and later transport calculations treated the overall blanket as a slab. Because of the Tokamak plasma radius and distance to the first wall (calculated to be 230 cm in Appendix B), the assumption of slab geometry is not a great limitation for the neutronics calculations. In addition to values for k_{eff}, the diffusion theory calculations provided 4-group fundamental flux shapes for the slab hybrid blanket.

Next a series of inhomogeneous diffusion theory calculations were performed to mock up the effects of fusion neutrons using fission-like neutrons. Flux shapes as well as power density distributions were obtained for the enrichments and temperatures of interest. These calculations were used to analyze the worth of such neutrons as surface sources and volume sources in the hybrid lattice. By calculating the neutron source to produce the blanket design power of 6500 MWth, the results of the global formula for blanket energy deposition per entering neutron were compared with predictions. Since the formula should be most accurate for fission spectrum neutrons, this was an excellent test of the applicability of global analysis to the blanket.

At this point various parameters describing the kinetic properties of the blanket were evaluated to establish some of the blanket response to predicted perturbations in the neutron level entering from the

plasma. Such blanket characteristics as the negative inherent feedback coefficient with temperature increases as well as delayed neutron fractions and inhomogeneous source weighting factors were established using the diffusion theory calculations.

Essentially, the series of diffusion theory calculations and results were used to scope the variable enrichment and temperature parameters. The best enrichment and a reasonable temperature were then selected for further, more detailed and exact S_n transport theory analysis. The results of the diffusion theory predictions for k_{eff} were checked using an appropriate transport scheme of cross section evaluation and group-collapsing over the entire blanket. In addition, the 6-group fundamental mode flux shapes were obtained.

In the inhomogeneous transport theory calculations, the fusion neutron source energy was treated more nearly as a true 14 MeV source in a 6-group neutronic analysis. The magnitude of the surface source required to produce the 6500 MWth power level in the blanket was determined using an inhomogeneous S_n source calculation with 6 neutron groups. The results of the inhomogeneous S_n calculation were then used to establish the required plasma parameters needed to produce the blanket power level of 6500 MWth; the details of this calculation are given in Appendix B. In addition, the 6-group flux shapes and a breakdown of power generation in the inner convertor and the thermal fission lattice were obtained.

Finally, some consideration was given to the time-dependent behavior of the hybrid blanket under neutron source variations from the plasma. Kinetics calculations representing the effects of plasma-caused perturbations on the fusion neutron source driving the blanket were performed.

Changes in power level were examined for the usual slab geometry, 6 neutron flux groups and 6 groups of delayed neutrons. The resulting determination of the speed of response of the system was used to establish some characteristics for hybrid operational control.

Blanket Calculations Using Diffusion Theory

The first step in analyzing the hybrid blanket was to establish the ranges of effective neutron multiplication factors which are applicable. This was done by performing steady-state neutronic calculations on the basic blanket for a spectrum of reasonable enrichments. The enrichment range included natural uranium (0.711% enriched) at the lower end of the scale up to 1.50% enriched fuel at the upper end as summarized in Table B-III in Appendix B. Having selected a set of enrichments for which to evaluate k_{eff}, then an appropriate temperature was selected for the blanket. A broad range of global average temperatures was addressed based on the model of Chapter 3 to form a basis for future extended analyses of blanket thermal effects as well as to ascertain enrichment limits and temperature feedback effects.

The enrichment limits are related to the basic hybrid design requirement of $k_{eff} < 1$ on which this work is based. Although the effective neutron multiplication factor, k_{eff}, may be only 0.95 at an average global blanket temperature of 1000°K, the blanket itself is then very likely to be supercritical at room temperature because of the temperature defect. Such features imply the need for special reactivity control systems in the blanket at lower temperatures. To avoid this complexity, the decision was made to select the hybrid blanket to be subcritical

over the entire spectrum from operating temperatures when it would be least reactive down to room temperature where it would be most reactive.

In performing the necessary criticality studies on the hybrid blanket, slab geometry was assumed everywhere except in the unit cell. Preliminary calculations on a 600 cm long slab indicated that leakage is essentially negligible in the perpendicular direction; therefore, after the initial series of calculations, all perpendicular bucklings were assumed to be zero; that is, the perpendicular leakage was assumed negligible for a closed torus. All calculations were run over the blanket in the radial direction from the vacuum wall out to the shield region.

In doing the blanket criticality and other neutronics calculations a system was set up for calculating the necessary multigroup constants. The Battelle-Revised-THERMOS or BRT-1 code[63] was used to obtain thermal group constants and the PHROG code[79] was utilized to obtain fast group constants for input to a multigroup diffusion theory code. The more exact transport theory codes were used for the cross section evaluations as required in a consistent criticality calculation. Diffusion theory was only used for the final criticality calculation using the cross sections obtained using BRT-1 and PHROG.

A four-group criticality calculation was selected using the energy boundaries listed in TAble 5-I. For criticality calculations on fissile systems this set of group boundaries has been found to be reasonably accurate while affording the advantage of low price and fast computation times using one thermal group and three fast groups.

Table 5-I

Boundaries for Four-Group Criticality Calculation

Energy Group	Energy Range
1	0.853 MeV-10 MeV
2	5.30 keV-0.853 MeV
3	0.683 eV-5.3 keV
4	0.00 eV-0.683 eV

For these first criticality calculations, the BRT-1 code was used to obtain unit cell smeared thermal constants for the hybrid blanket thermal fission lattice described in Appendix B. The lattice was initially assumed to be an infinite repeating array of unit cells. The code was then run for the case of cylindrical geometry with two boundary conditions applied to all 30 energy groups; first, a boundary condition of zero current was applied at the centerline of the fuel pin, and second, a white albedo boundary condition was applied at the unit cell equivalent cylindrical boundary in the helium region shown in Fig. B4.

Some useful cell-smeared constants for the 1.35% enriched thermal fission lattice are presented in Table 5-II which lists the thermal cell-smeared inverse velocity, $1/v$, neutron energy, $\bar{E}$, diffusion coefficient, D, macroscopic absorption coefficient, Σ_a, as well as the macroscopic fission cross section, Σ_f, and its product with the neutrons per fission, $v\Sigma_f$. Constants for the 1.35% enrichment case are listed because it is the most applicable for later calculations. However, all cases for the enrichments calculated showed similar results in which all constants

decrease in value with increasing temperature. The values for the cell-smeared average neutron energies in the thermal group indicate the thermalized spectrum expected, especially at 290°K. Even the 970°K value of $\overline{E}$ = 0.116 eV is about the same as in a pressurized water reactor as found in other calculations.[118]

Table 5-II

BRT-1 Cell-Smeared Thermal Constants for 1.35% Enriched Fuel

Temperature (°K)	$\frac{1}{v}$ (sec/cm)	$\overline{E}$ (eV)	D (cm)	Σ_a (1/cm)	Σ_f (1/cm)	$v\Sigma_f$ (1/cm)
290	3.264×10^{-6}	.049	0.9049	3.11×10^{-3}	1.897×10^{-3}	4.610×10^{-3}
570	2.624×10^{-6}	.076	0.8966	2.476×10^{-3}	1.487×10^{-3}	3.614×10^{-3}
970	2.124×10^{-6}	.116	0.8867	2.004×10^{-3}	1.192×10^{-3}	2.897×10^{-3}

The radial variation of the BRT-1 generated thermal flux across the unit cell is shown in Fig. 67. Three relative flux profiles are shown for the 1.35% enrichment; one for each of the three lumped blanket temperatures at 290°K, 570°K, and 970°K. These fluxes are not the true thermal fluxes, but represent the BRT-1 flux in the unit-cell obtained when it was used to solve the integral transport equation for an infinite array of unit cells. These fluxes were used to obtain cell-averaged, flux-weighted cross sections for use in later calculations. The thermal flux profiles in Fig. 67 are noted to rise monotonically from the cell of the fuel column where it is significantly depressed out to near the edge of the unit cell where it is very slightly depressed (< 0.01%) due to the white albedo boundary condition. This boundary condition accounts for the fact that the graphite moderator is relatively thin.
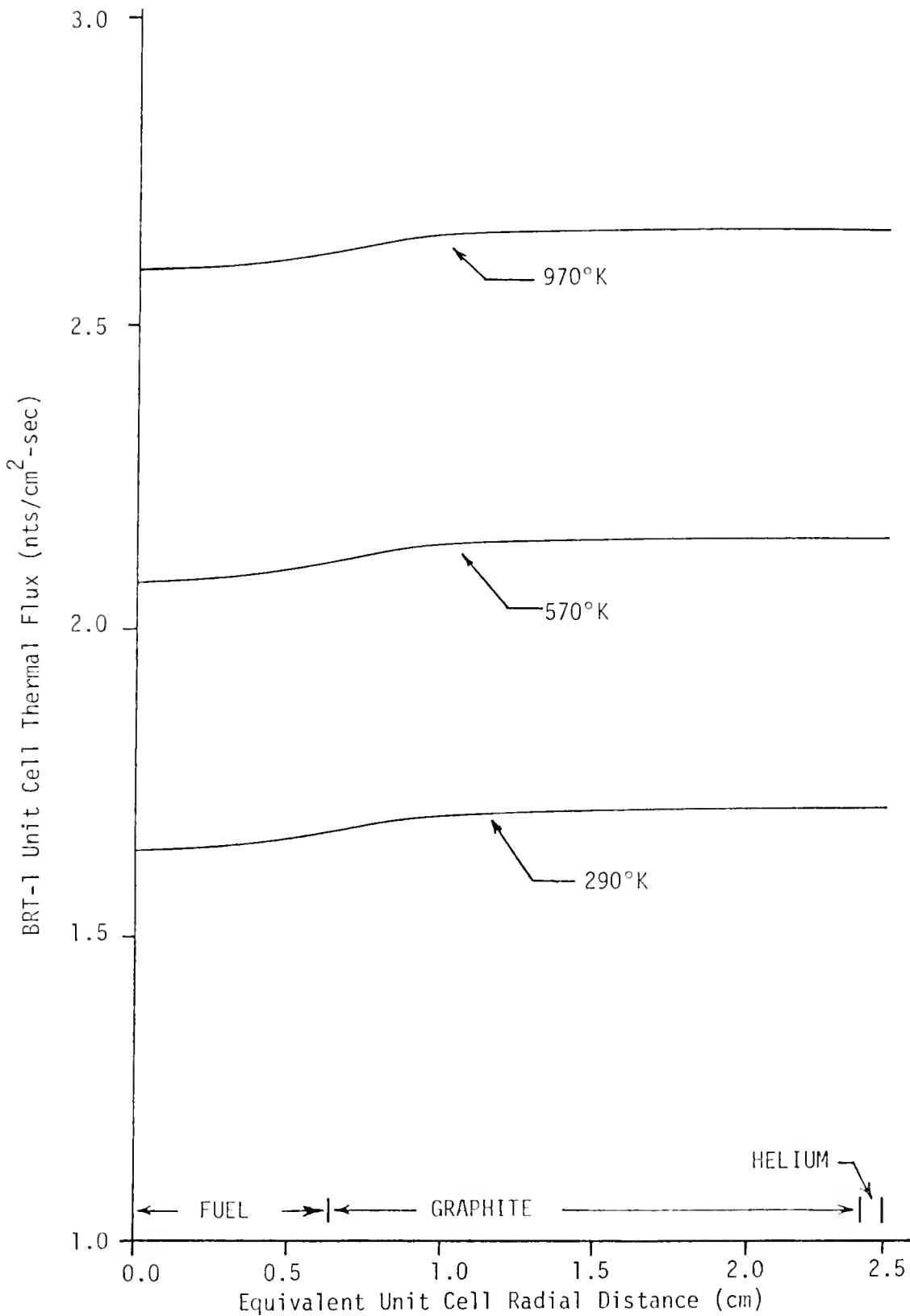
Figure 67. BRT-1 thermal flux profiles across the equivalent unit cell for 1.35% enrichment at 290°K, 570°K, and 970°K.

Reflecting boundary conditions are satisfactory when the moderator region is several neutron mean free paths in thickness. But when the moderator is thin, misleading results can be obtained due to effects illustrated in Fig. 68. In the cylindrical cell with reflecting boundary conditions, a neutron incident on the boundary is generally reflected so its path does not intersect the fuel element as in Fig. 68(a) unless the neutron is scattered in the moderator. However, in the actual cell shown in Fig. 68(b), neutrons "reflected" at the boundary are able to enter the fuel even without scattering. Therefore, the use of reflection boundary conditions is expected to make the flux too high in the moderator and calculations have shown such to be the case.[119]

For thin moderator regions, better accuracy is obtained when other boundary conditions are imposed that give a more diffuse reflection of the neutrons from the boundary of a cylindrical cell as opposed to the specular reflection in Fig. 68. The "white" albedo boundary condition is such a boundary condition in which the cell is modeled as surrounded by a purely scattering region at the outside of which reflecting boundary conditions are imposed.

For the three global temperatures, macroscopic graphite thermal scattering cross sections, Σ_s^C, in the graphite moderator region of the unit cell are listed in Table 5-III where the scattering mean free path, λ_s^C, is nearly 2.5 cm at all temperatures. Since the graphite region (at 1.74 cm thickness) is less than one mean free path thick, then the white albedo boundary condition is appropriate as demonstrated in Fig. 67 by the slight reduction in the flux profile at the edge of the unit cell. Neutrons reflected at the boundary of the cell can enter the fuel without scattering.
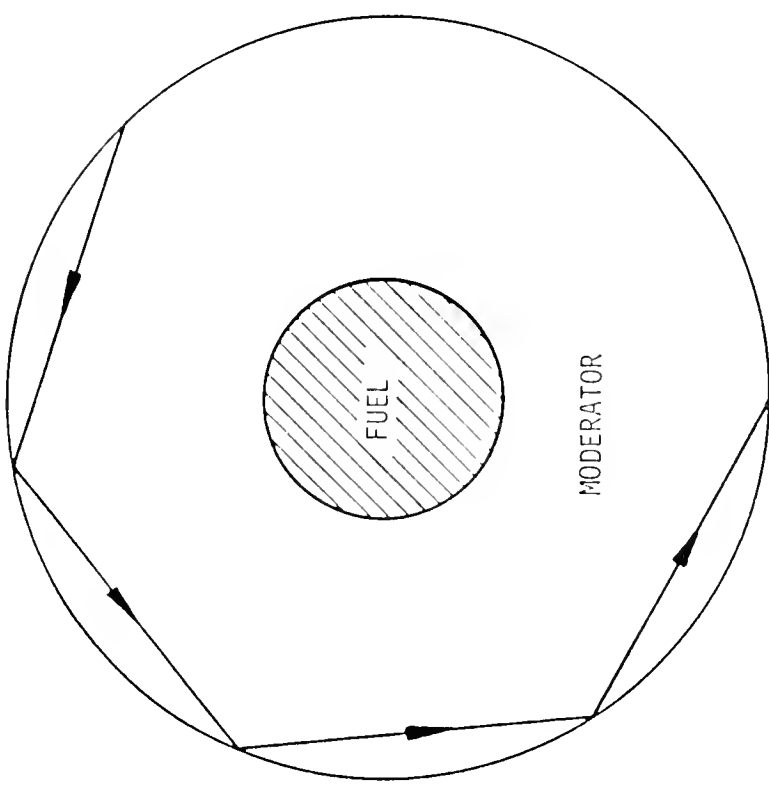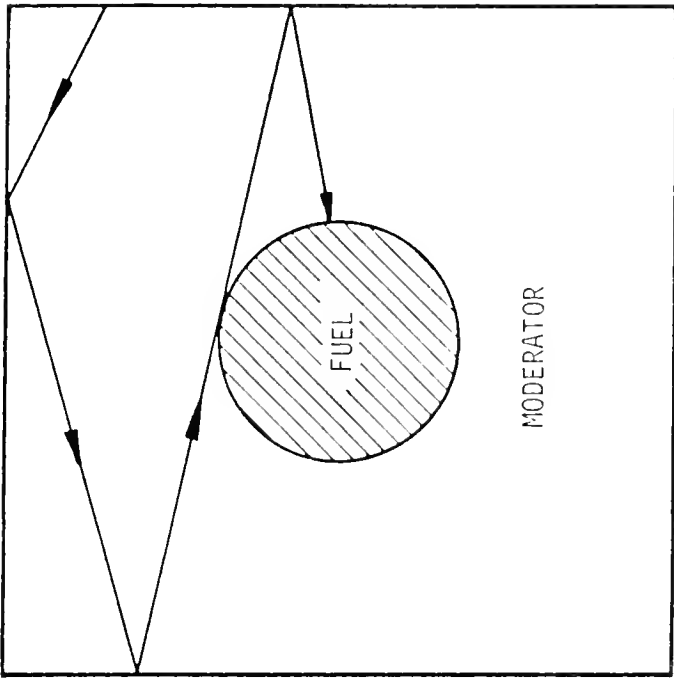
Figure 68. Typical paths for an unscattered neutron in (a) an equivalent unit cell and (b) an actual unit cell of a nuclear reactor.

Table 5-III

Graphite Moderator Region Scattering Properties

Temperature (°K)	Σ_s^C (1/cm)	λ_s^C (cm)
290	.402	2.49
570	.403	2.48
970	.408	2.45

Flux depression factors for the 1.35% enriched cases are listed in Table 5-IV for all three temperatures. The results listed in Table 5-IV indicate only slight depression in the fuel but significant increases in flux depression with temperature which accounts for a significant temperature defect in blanket reactivity with the blanket temperature change from 290°K to 970°K.

Table 5-IV

Flux Depression Factors for the 1.35% Enriched Lattices

Global Temperature	Fuel Column Flux Depression	Graphite Moderator Flux Depression	Helium Coolant Flux Depression
290°K	0.9707	1.0020	1.0042
570°K	0.9768	1.0016	1.0033
970°K	0.9812	1.0013	1.0027

Typical values for the average microscopic fission, $\bar{\sigma}_f$, and absorption, $\bar{\sigma}_a$, cross sections for ^{235}U and ^{238}U in the fuel column are listed

in Table 5-V. The variation of the capture-to-fission ratio in ^{235}U is particularly indicative of the expected blanket reactivity decrease with temperature.

Table 5-V

Average Cross Sections for ^{235}U and ^{238}U in the Fuel Column

Temperature (°K)	$\bar{\sigma}_f^{235}$ (b)	$\bar{\sigma}_a^{235}$ (b)	$\bar{\sigma}_a^{238}$ (b)	Capture-to-Fission Ratio in ^{235}U
290	380.8	337.6	1.89	0.174
570	298.5	351.9	1.54	0.179
970	239.3	283.4	1.27	0.184

Cell-smeared constants for the inner convertor region were not used because of unrealistic boundary condition assumptions made necessary by the restrictions on the number of regions accepted by BRT-1. This was found to be the case in an entire series of calculations which were performed to obtain "unit cell" constants for the inner convertor region. In addition, the inner convertor region is only 8.5 cm thick and is not really amenable to treatment as an infinite array of slab unit cells. The region is simply too thin to be treated any way except homogeneously, unless very costly and time consuming transport theory codes are used.

After the cell-smeared constants were obtained from BRT-1, these were input for the thermal fission lattice regions as part of the cross section data to run BRT-1 over the entire 260.25 cm thickness of blanket and shield described in Appendix B. Unfortunately, convergence over such a thickness was not possible using the BRT-1 code. The highly absorbing

convertor and breeder regions as well as the shield make convergence of the BRT-1 calculation impossible, particularly with the 30 space point limitation on the code. More could be added but even then, convergence would be slow resulting in costly computational schemes.

To overcome this deficiency the following scheme of cell calculations was developed and applied for running BRT-1 in multiple steps in slab geometry to obtain thermal constants for input to a diffusion theory calculation for the entire hybrid blanket for each of the temperatures involved. The specific case of 1.35% enrichment is outlined here.

First, a half-slab calculation was run over the blanket from the thermal fission lattice midpoint (90 cm into the lattice) out to the vacuum wall. Cross sections for all isotopes were either taken from the BRT-1 Direct Access Library or read in on cards during the calculation. All thermal lattice regions in this series were represented by the cell-smear constants output from the BRT-1 unit cell calculation whose resultant constants represent input parameters to describe the thermal lattice material as a homogeneous mixture.

A zero-current boundary condition was applied at the center of the fission lattice while two different conditions were applied at the vacuum wall; one required that the thermal flux in BRT-1 go to zero at the extrapolation distance while the other required that the current be zero at the vacuum wall as could be applicable in a 360° toroidal arrangement. Little difference was detected between the two cases because of the small size and low worth of the inner convertor region as well as the overall size of the blanket lattice. The placement of the 30 available BRT-1 space points was decided by pre-examination of other auxiliary calculations to establish those regions and positions where the BRT-1 flux

profile was expected to be most quickly varying. Regions such as the lithium breeder and inner convertor were then assigned more points which BRT-1 used to calculate thermal constants.

The 90 cm fission lattice region was subdivided into a 60 cm region closest to the center of the lattice and a 30 cm region nearer the absorbing inner breeder region where more space points were placed per unit thickness to facilitate spatial flux resolution where the flux was expected to be varying more quickly with position. The same closer placement of space points was utilized in the inner convertor in the 3.5 cm nearest the highly-absorbing lithium region. The placement of space points for this inner half blanket calculation is summarized in Table 5-VI. The flux profiles generated by BRT-1 for this 100 cm slab run are presented in Fig. 69 for three global temperature cases (290°K, 570°K, and 970°K) for the 1.35% enriched thermal lattice and zero flux vacuum wall boundary condition. These profiles represent the flux used to weight the thermal group cross sections for the hybrid blanket regions for which these BRT-1 calculations were run. These flux profiles do not represent the actual flux which can be obtained only from a criticality diffusion theory or transport theory calculation. The flux profiles do indicate that the proper boundary conditions are represented and the regions of high neutron multiplication have the highest relative flux. Although not presented here, the flux profile of Fig. 69 changed very little when the zero current vacuum wall boundary condition was used in BRT-1 because the inner convertor is a low worth region compared to the large thermal fission lattice. The low worth is depicted in Fig. 69 by the very low BRT-1 fluxes in the inner convertor compared to the fission lattice.
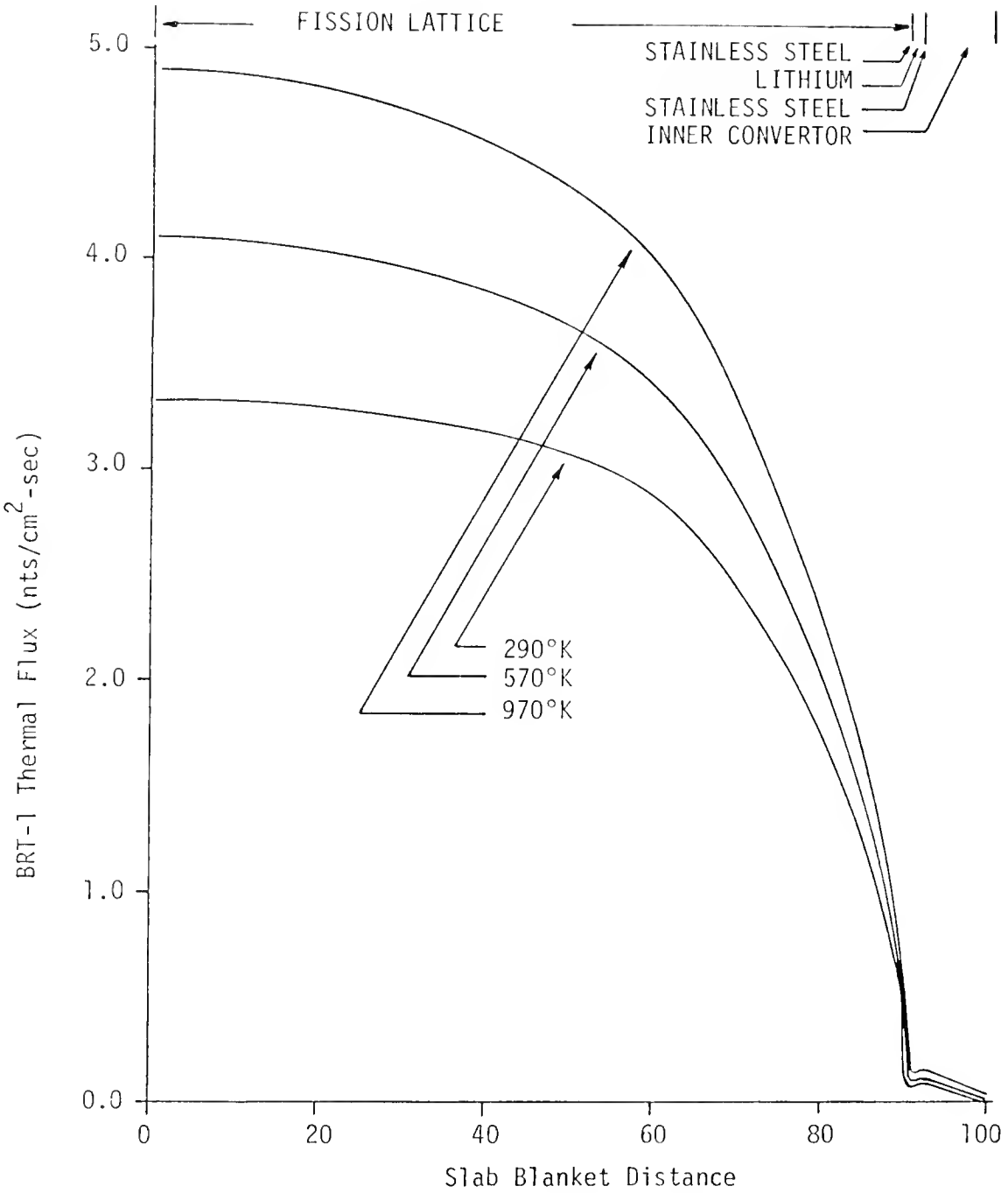
Figure 69. BRT-1 thermal flux profiles across the inner half of the
hybrid blanket for 1.35% enrichment at 290°K, 570°K, and
970°K with zero-flux vacuum wall boundary condition.

Table 5-VI

Space Point Placement for BRT-1 Calculation Over Inner
Half of the Hybrid Blanket

Region	Thickness (cm)	Space Points
Thermal Lattice	60.00	7
Thermal Lattice	30.00	7
Stainless Steel	0.25	2
Lithium Breeder	1.00	4
Stainless Steel	0.25	2
Inner Convertor	3.50	4
Inner Convertor	5.00	4

A similar but full-slab calculation was run over the outer 90 cm of the thermal lattice and extending 12 cm into the graphite reflector where previous diffusion theory calculations indicated the thermal flux peaked. In this calculation the zero-current boundary condition is applicable at both end points--one at the center of the thermal lattice, the other at the 12 cm point in the graphite reflector. This is where the term, full-slab calculation, is derived. The placement of space points is again important for the best possible spatial flux resolution as summarized in Table 5-VII.

Table 5-VII

Space Point Placement for BRT-1 Calculation Over Outer Half of the
Fission Lattice and into the Graphite Reflector

Region	Thickness (cm)	Space Points
Thermal Lattice	60.00	7
Thermal Lattice	30.00	5
Stainless Steel	0.25	2
Lithium Breeder	9.50	8
Stainless Steel	0.50	2
Graphite	12.00	6

Space points were again placed more closely in regions such as the outer 30 cm of the thermal lattice and the lithium breeder where the flux would be expected to vary most quickly with position. The flux profiles generated for this 112.5 cm slab run are presented in Fig. 70 for the three global temperatures at 1.35% fission lattice enrichment. These relative fluxes are again the fluxes used to generate weighted thermal group constants but do not represent the actual blanket fluxes. The flux profiles in Fig. 70 do indicate that the proper boundary conditions were applied as intended. The figure also indicates that the lithium outer breeder region is very well self-shielded and that the graphite is a reflector of neutrons back toward the fission lattice.

The third calculation in this series to obtain thermal constants is another half slab calculation covering the remaining 18 cm of the graphite reflector plus the 30 cm of shield material. There is no problem with placement of space points here with 6 points in the graphite, 6 points
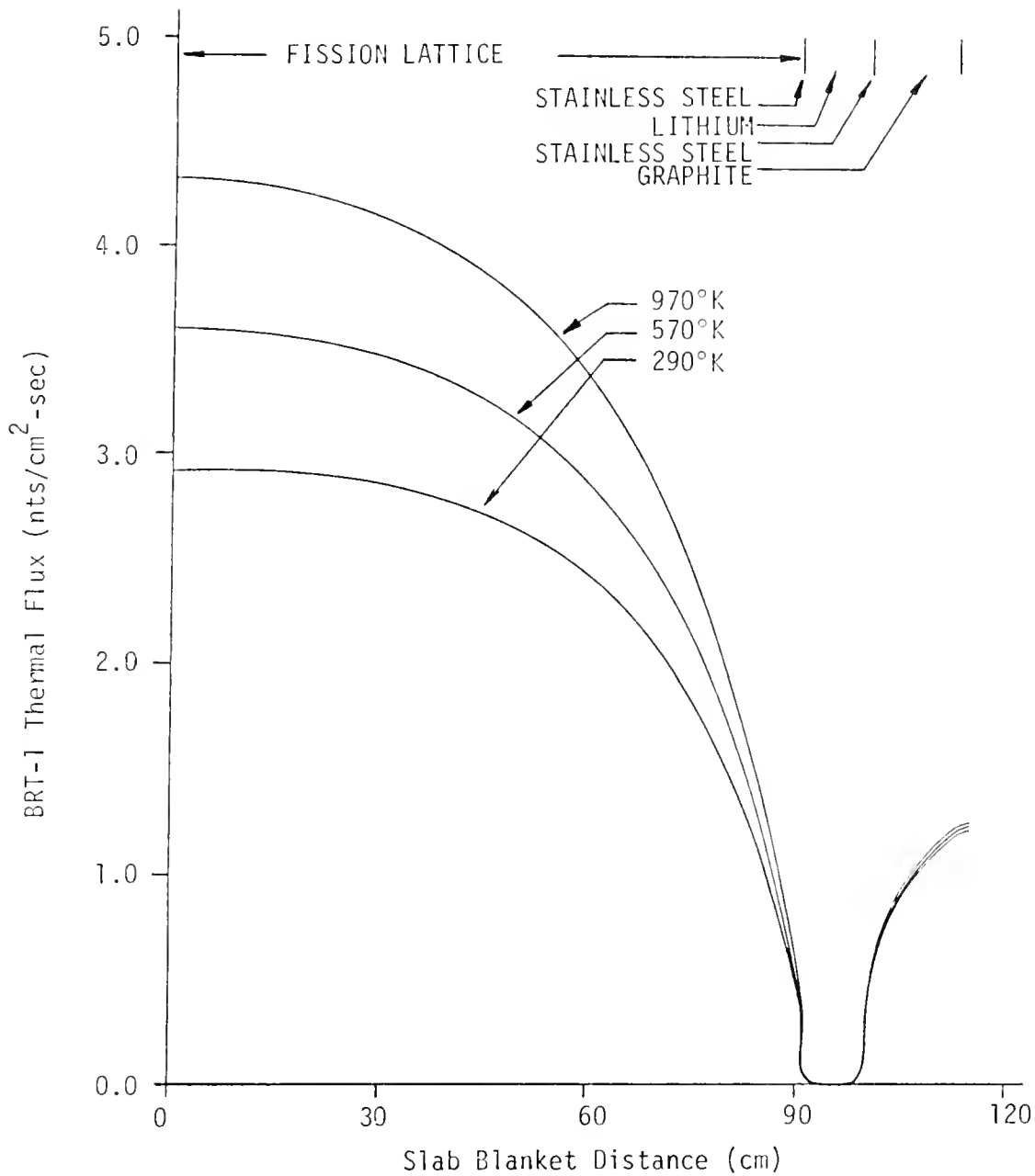
Figure 70.   BRT-1 thermal flux profiles across the outer half of the
fission lattice out to 12 cm of graphite reflector for
1.35% enrichment and 290°K, 570°K, and 970°K.

in the first 6 cm of the shield, and the remaining 18 points in the final 24 cm of the shield. The BRT-1 would not converge or even run for larger thicknesses of the highly-absorbing shield region; however, later calculations indicated that the 30 cm is sufficient for neutronic results. For this third calculation a zero-current boundary condition was applied in the graphite while the thermal flux in the shield was required to approach zero. The flux profiles generated by BRT-1 in this case are presented in Fig. 71 and indicate agreement with required boundary conditions.

The series of three cell calculations discussed above supplied the thermal group constants for all regions in the hybrid blanket for the 1.35% enriched thermal lattice at each of the three global temperatures of interest. The same procedure was repeated for the other enrichments. Note that there are a total of 10 distinct regions in the resultant calculations for which thermal constants were produced. Indeed, separate constants were maintained for the thermal lattice for calculations which require the four separate unit cell regions of 30, 60, 60, and 30 cm, respectively, to account more accurately for flux variations near region boundaries. Therefore, a total of 13 distinct regions was maintained.

Next, the PHROG code was used to generate fast neutron spectra and average multigroup constants. PHROG, with 68 fine fast groups, is an improvement of the GAM-1 code[120] primarily due to the inclusion of the Chernick-Nordheim resonance treatment for the ^{238}U and ^{235}U isotopes. PHROG constants can be edited over the entire range from 10 MeV to 0.414 eV, but were edited for the hybrid calculations over the range from 10 MeV to 0.683 eV. Since BRT-1 was used for the thermal energy range up to 0.683 eV, exact coverage of the entire range from 10 MeV down to near zero was obtained.
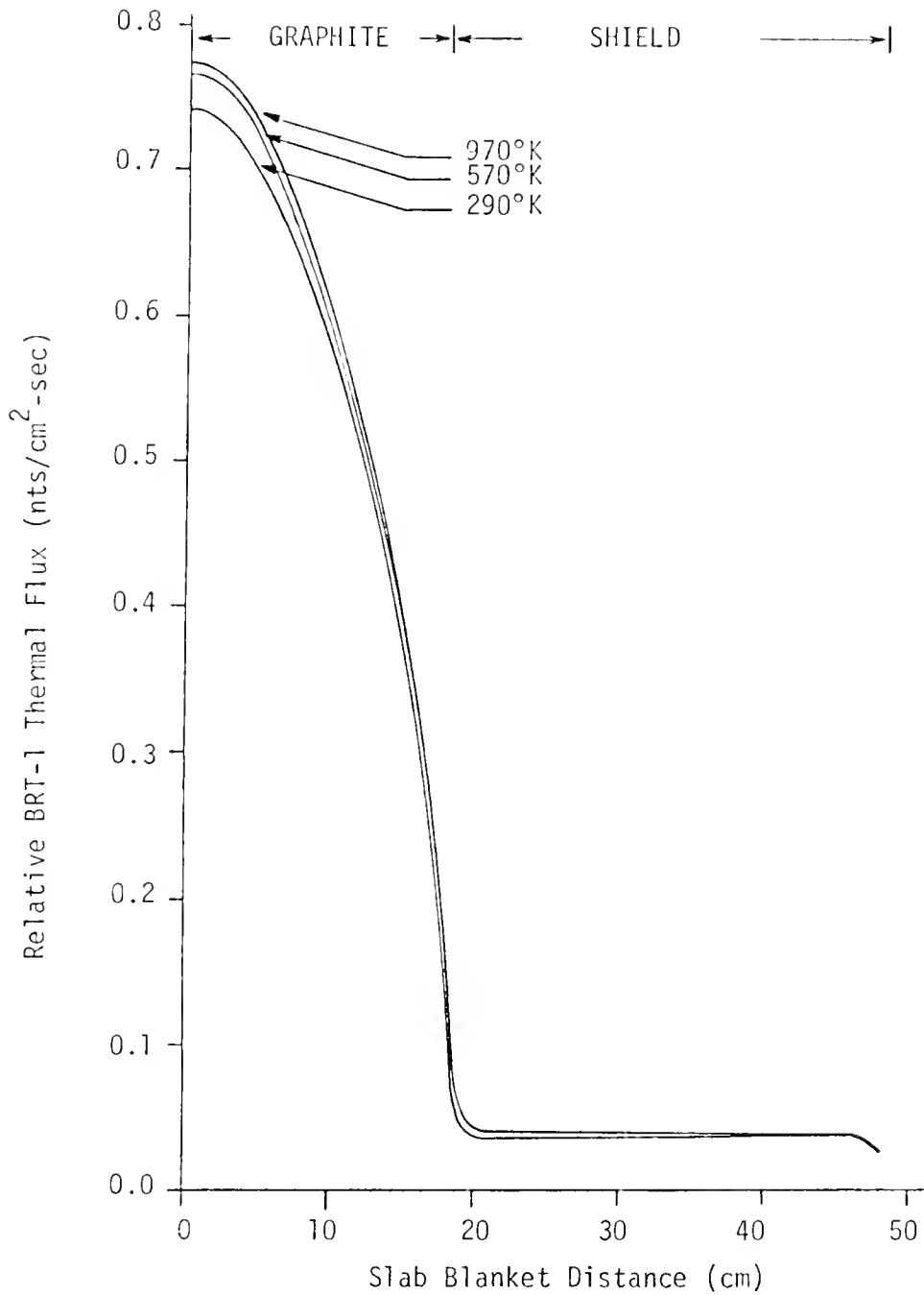
Figure 71. Thermal flux profiles from BRT-1 calculations across the outer 18 cm of graphite reflector and 30 cm of shield for 290°K, 570°K, and 970°K.

Energy dependent fast neutron spectra for this work were generated by PHROG utilizing the B_n approximation to the time-independent transport equation. The B_1 approximation is superior to P_1 theory due to speedier convergence and higher accuracy. However, for finite systems, B_1 theory is applicable only if the medium can be homogenized and if the space and energy variables are separable to allow the flux, $\phi(x,\mu,E)$, to be written as follows:

$$\phi(x,\mu,E) = e^{iBx}\psi(B,\mu,E) \tag{191}$$

where x, μ, and E are the position, neutron scattering angle cosine, and neutron energy variables, respectively, while B^2 represents the geometric buckling of the fundamental mode and i represents the square root of -1. These conditions of separability imply buckling of the flux which the hybrid meets. The homogenization condition was met by running PHROG over separate and homogenized regions of the blanket.

Here again a scheme was devised for calculating all the necessary fast neutron group constants for 10 distinct hybrid regions. First, a B_1 calculation was used to generate 68 fine group fluxes and currents for the thermal fission lattice region. These fluxes and currents were used for weighting cross sections, diffusion coefficients, and other region-dependent constants to obtain three broad group constants for the thermal fission lattice region. The B_1 calculation was performed on the homogenized thermal lattice region taking account of unit cell geometry for resonance effects and interactions between cells for the 4.66 cm hexagonal pitch and 0.635 cm radius fuel column. This geometry is described in detail in Appendix B. The geometric buckling factor, as input to the code, corresponded to the thermal fission lattice region thickness: $B = \pi/180$

cm = 0.01745/cm. The thermal lattice was not subdivided for the fast

group calculations because to do so would mean artificially and arbi-

trarily increasing the leakages.[121] This fact was verified in separate

calculations not reported here.

In addition, a B_1 type calculation was performed on the homogenized

inner convertor region using a geometric buckling of $B = \pi/8.5$ cm =

0.3696/cm and also assuming the three, 2 cm thick, depleted uranium

plates constituted a large array of identical unit cells. Such B_1 cal-

culations were also performed for the 9.5 cm thick outer lithium region,

the 30 cm thick graphite reflector, and the 30 cm thick shield region.

Cell type calculations were performed on all other regions which included

the inner 1.0 cm thick lithium region plus the stainless steel liners on

the lithium regions and the thermal lattice. The cell option calculation

in each case used fluxes and currents generated in a B_1 calculation on

an adjacent region so that PHROG in these cases was used only to perform

the cross section weighting. The applicable PHROG option and the source

of fluxes and currents in cell calculations are listed in Table 5-VIII.

Essentially, B_1 calculations were performed for all regions which

were thick enough to preclude assuming the fluxes and currents present

would be characteristic of an adjacent region; that is, thick enough to

contain characteristic neutron spectra. In addition, only the thermal

fission lattice and the 8.5 cm inner convertor regions have positive

buckling values to account for the net leakage of fast neutrons. All

other regions have a net gain of fast neutrons since none are born there.

Since complex numbers are not possible, extremely small buckling values

close to zero (1.00 x 10^{-8}) were input in all PHROG runs involving regions

with a net gain of fast neutrons. This series of fast spectrum

calculations at the three temperatures (290°K, 570°K, 970°K) was repeated

for all the reference enrichments from 0.711% to 1.50%. Little change

was noted in individual constants as these parameters were changed but

significant changes were expected in the subsequently calculated effective

neutron multiplication factors (k_{eff}) of the blanket for the various

cases.

Table 5-VIII

Summary of PHROG Calculations by Region

Region	Width (cm)	Calculation Type	Source of Fluxes and Currents
Inner Convertor	8.50	B_1	Region Generated
Stainless Steel	0.25	Cell	Inner Convertor
Lithium Breeder	1.00	Cell	Inner Convertor
Stainless Steel	0.25	Cell	Fission Lattice
Thermal Fission Lattice	180.00	B_1	Region Generated
Stainless Steel	0.25	Cell	Fission Lattice
Outer Lithium Breeder	9.50	B_1	Region Generated
Stainless Steel	0.50	Cell	Outer Lithium Breeder
Graphite Reflector	30.00	B_1	Region Generated
Outer Shield	30.00	B_1	Region Generated

Resonance region microscopic scattering cross section values for

resonance calculations were used in the various PHROG runs.[122] These

cross section values are listed for reference in Table 5-IX for all
nuclides included in the blanket.

Table 5-IX

Resonance Region Scattering Cross Sections for Blanket Nuclides

Nuclide	Resonance Region Scattering Cross Section (b)
^{235}U	10.45
^{238}U	10.7
O	3.656
H	20.22
Fe	11.155
Ni	17.57
Cr	4.35
Mn	3.00
He	0.75
C	4.53

The results of these BRT-1 and PHROG calculations for the 1.35% en-
riched, 570°K case are presented in Tables 5-X and 5-XI. The four-group
diffusion coefficients, macroscopic absorption and fission cross sections
as well as the product, $\nu\Sigma_f$, and the average inverse velocity are pre-
sented in Table 5-X. the macroscopic downscattering cross sections are
presented in Table 5-XI. These constants were all input to the CORA
diffusion theory code.[80] There was no consideration for upscattering in
these calculations since CORA does not utilize upscattering--hence, the

choice of the 0.683 eV cutoff in BRT-1 for the thermal group. This
relatively high cutoff was selected to preclude concern with upscattering.
Similar results are shown in Tables 5-XII and 5-XIII for the 970°K
blanket. Calculations of the average thermal group neutron energy in
the fission lattice yielded 0.079 eV for the 570°K case and 0.118 eV for
the 970°K case with 1.35% enrichment. These values indicate reasonably
good thermalization and little need for upscattering to be of concern
above the 0.683 eV thermal cutoff.

The four-group constants for the 1.35% enriched case as well as
results for the other enrichments, were input to CORA which is a one-
dimensional, few group diffusion theory code used to perform detailed
neutron balances for each different system. CORA uses fission source
iteration to solve the set of difference equations as follows:

$$[A][\phi] + [S] = 0 \tag{192}$$

where [A] is the matrix containing leakage, removal, absorption, and
scattering properties, [φ] is the flux vector, and [S] is the source
vector accounting for the total neutron source including external, fission,
and inscattering sources. By assuming a known source and iterating, the
flux distribution was determined along with the system eigenvalue or
effective neutron multiplication factor, k_{eff}.

Typical four-group flux profiles obtained from CORA are presented
in Figs. 72, 73, and 74 for the 290°K, 570°K, and 970°K blankets and 1.35%
enrichment. These figures show the fundamental mode flux shapes for all
four groups subject to the zero current vacuum wall boundary conditions.
As the temperature was raised, the higher energy groups became more
depressed compared to the thermal groups which is caused by the increased

Table 5-X

Four-Group, 13-Region Constants for 1.35% Enrichment at 570°K from BRT-1 and PHROG

Region	Group	D (cm)	Σ_a (1/cm)	$\nu\Sigma_f$ (1/cm)	Σ_f (1/cm)	$(\frac{1}{v})$ (sec/cm)
Inner Convertor (8.5 cm)	1	1.123	7.731×10^{-3}	1.605×10^{-2}	5.963×10^{-3}	5.343×10^{-10}
	2	0.8504	3.139×10^{-3}	1.312×10^{-4}	5.335×10^{-5}	1.614×10^{-9}
	3	0.6167	1.545×10^{-2}	4.064×10^{-4}	4.064×10^{-4}	1.232×10^{-8}
	4	0.8510	3.665×10^{-2}	1.076×10^{-2}	4.428×10^{-3}	1.305×10^{-6}
Stainless Steel (0.25 cm)	1	1.719	1.775×10^{-3}	0.0	0.0	5.343×10^{-10}
	2	1.132	6.173×10^{-4}	0.0	0.0	1.614×10^{-9}
	3	0.3464	6.429×10^{-3}	0.0	0.0	1.292×10^{-8}
	4	0.3100	8.191×10^{-2}	0.0	0.0	1.466×10^{-6}
Inner Lithium (1.00 cm)	1	4.875	6.757×10^{-4}	0.0	0.0	5.343×10^{-10}
	2	4.320	2.126×10^{-3}	0.0	0.0	1.614×10^{-9}
	3	5.248	8.576×10^{-3}	0.0	0.0	1.282×10^{-8}
	4	0.2265	1.244×10^{0}	0.0	0.0	1.847×10^{-6}
Stainless Steel (0.25 cm)	1	1.725	1.355×10^{-3}	0.0	0.0	5.662×10^{-10}
	2	0.7233	9.782×10^{-4}	0.0	0.0	3.394×10^{-9}
	3	0.3471	1.261×10^{-2}	0.0	0.0	1.704×10^{-7}
	4	0.2991	1.274×10^{-1}	0.0	0.0	2.281×10^{-6}
Fission Lattice (30 cm)	1	2.390	1.561×10^{-4}	3.135×10^{-4}	1.182×10^{-4}	5.662×10^{-10}
	2	1.098	1.446×10^{-4}	2.494×10^{-5}	1.020×10^{-5}	3.394×10^{-9}
	3	0.9472	1.714×10^{-3}	2.933×10^{-4}	1.207×10^{-4}	1.704×10^{-7}
	4	0.9433	2.359×10^{-3}	3.437×10^{-3}	1.414×10^{-3}	2.504×10^{-6}
Fission Lattice (60 cm)	1	2.389	1.561×10^{-4}	3.135×10^{-4}	1.182×10^{-4}	5.662×10^{-10}
	2	1.093	1.446×10^{-4}	2.494×10^{-5}	1.020×10^{-5}	3.394×10^{-9}
	3	0.9472	1.714×10^{-4}	2.933×10^{-4}	1.207×10^{-4}	1.704×10^{-7}
	4	0.9441	2.455×10^{-3}	3.582×10^{-3}	1.474×10^{-3}	2.602×10^{-6}

Table 5-X

(continued)

Region	Group	D (cm)	Σ_a (1/cm)	$\nu\Sigma_f$ (1/cm)	Σ_f (1/cm)	$(\frac{1}{v})$ (sec/cm)
Fission Lattice (60 cm)	1	2.389	1.561×10^{-4}	3.135×10^{-4}	1.182×10^{-4}	5.662×10^{-10}
	2	1.098	1.446×10^{-4}	2.494×10^{-5}	1.020×10^{-5}	3.394×10^{-9}
	3	0.9472	1.714×10^{-3}	2.933×10^{-4}	1.207×10^{-4}	1.704×10^{-7}
	4	0.9439	2.452×10^{-3}	3.577×10^{-3}	1.472×10^{-3}	2.599×10^{-6}
Fission Lattice (30 cm)	1	2.389	1.561×10^{-4}	3.135×10^{-4}	1.182×10^{-4}	5.662×10^{-10}
	2	1.098	1.446×10^{-4}	2.494×10^{-5}	1.020×10^{-5}	3.394×10^{-9}
	3	0.9472	1.714×10^{-3}	2.933×10^{-4}	1.207×10^{-4}	1.704×10^{-7}
	4	0.9429	2.352×10^{-3}	3.426×10^{-3}	1.410×10^{-3}	2.497×10^{-6}
Stainless Steel (0.25 cm)	1	1.725	1.350×10^{-3}	0.0	0.0	5.662×10^{-10}
	2	0.7238	9.782×10^{-4}	0.0	0.0	3.394×10^{-9}
	3	0.3471	1.261×10^{-2}	0.0	0.0	1.704×10^{-7}
	4	0.2992	1.308×10^{-1}	0.0	0.0	2.328×10^{-6}
Outer Lithium (9.5 cm)	1	5.458	7.6325×10^{-3}	0.0	0.0	5.911×10^{-10}
	2	7.592	2.597×10^{-3}	0.0	0.0	3.197×10^{-9}
	3	5.779	1.135×10^{-2}	0.0	0.0	1.699×10^{-7}
	4	0.2329	1.171×10^{0}	0.0	0.0	1.739×10^{-6}
Stainless Steel (0.50 cm)	1	1.741	1.136×10^{-3}	0.0	0.0	5.911×10^{-10}
	2	0.706	9.306×10^{-4}	0.0	0.0	3.197×10^{-9}
	3	0.3511	5.622×10^{-3}	0.0	0.0	1.699×10^{-8}
	4	0.3022	1.183×10^{-1}	0.0	0.0	1.739×10^{-6}
Graphite (30 cm)	1	2.238	0.0	0.0	0.0	5.670×10^{-10}
	2	1.013	0.0	0.0	0.0	3.396×10^{-9}
	3	0.8787	0.0	0.0	0.0	1.922×10^{-7}
	4	0.8724	1.507×10^{-4}	0.0	0.0	2.361×10^{-6}

Table 5-X

(continued)

Region	Group	D (cm)	Σ_a (1/cm)	$\nu\Sigma_f$ (1/cm)	Σ_f (1/cm)	$(\frac{1}{v})$ (sec/cm)
Shield	1	1.575	8.579×10^{-4}	0.0	0.0	5.559×10^{-10}
	2	0.8639	1.798×10^{-3}	0.0	0.0	2.651×10^{-9}
	3	0.4493	6.448×10^{-2}	0.0	0.0	1.081×10^{-7}
	4	0.1466	8.207×10^{-1}	0.0	0.0	1.427×10^{-6}

Table 5-XI

PHROG-Generated Macroscopic Downscattering Cross Sections for 1.35%
Enrichment, 570°K, and 13 Regions

Region	$\Sigma_{s_{1\to2,3,4}}$ (1/cm)	$\Sigma_{s_{2\to3,4}}$ (1/cm)	$\Sigma_{s_{3\to4}}$ (1/cm)
Inner Convertor	4.322×10^{-2} 1.213×10^{-5} 0.0	9.248×10^{-5} 0.0	1.027×10^{-13}
Stainless Steel	2.342×10^{-2} 2.392×10^{-5} 0.0	8.822×10^{-5} 0.0	1.697×10^{-13}
Inner Lithium Breeder	1.065×10^{-2} 0.0 0.0	4.550×10^{-5} 6.222×10^{-10}	1.272×10^{-3}
Stainless Steel Liners on Fission Lattice (2)	2.475×10^{-2} 2.909×10^{-5} 0.0	5.876×10^{-3} 0.0	2.922×10^{-3}
Thermal Fission Lattice Regions (4)	2.428×10^{-2} 3.123×10^{-7} 9.993×10^{-12}	1.044×10^{-2} 0.0	5.334×10^{-4}
Outer Lithium Breeder	1.656×10^{-2} 0.0 0.0	1.448×10^{-3} 2.794×10^{-10}	8.910×10^{-11}
Outer Stainless Steel	2.732×10^{-2} 3.853×10^{-5} 0.0	3.609×10^{-3} 0.0	1.529×10^{-10}
Graphite Reflector	2.588×10^{-2} 0.0 1.159×10^{-2}	0.0 0.0	7.041×10^{-3}
Shield	6.375×10^{-2} 3.035×10^{-4} 3.610×10^{-8}	5.538×10^{-2} 6.374×10^{-6}	2.171×10^{-2}

Table 5-XII

Four-Group, 13-Region Constants for 1.35% Enrichment at 970°K from BRT-1 and PHROG

Region	Group	D (cm)	Σ_a (1/cm)	$\nu\Sigma_f$ (1/cm)	Σ_f (1/cm)	$(\frac{1}{v})$ (sec/cm)
Inner Convertor (8.5 cm)	1	1.123	7.731×10^{-3}	1.605×10^{-2}	5.964×10^{-3}	5.343×10^{-10}
	2	0.8505	3.139×10^{-3}	1.312×10^{-4}	5.335×10^{-5}	1.614×10^{-9}
	3	0.6163	1.569×10^{-2}	4.098×10^{-4}	1.686×10^{-4}	1.280×10^{-8}
	4	0.8523	2.725×10^{-2}	1.122×10^{-2}	4.617×10^{-3}	1.329×10^{-6}
Stainless Steel (0.25 cm)	1	1.719	1.775×10^{-3}	0.0	0.0	5.343×10^{-10}
	2	1.132	6.173×10^{-4}	0.0	0.0	1.614×10^{-9}
	3	0.3464	6.431×10^{-3}	0.0	0.0	1.280×10^{-8}
	4	0.3114	8.022×10^{-2}	0.0	0.0	1.436×10^{-6}
Inner Lithium (1.00 cm)	1	5.244	6.282×10^{-4}	0.0	0.0	5.343×10^{-10}
	2	4.647	2.060×10^{-3}	0.0	0.0	1.614×10^{-9}
	3	5.644	7.962×10^{-3}	0.0	0.0	1.280×10^{-8}
	4	0.2810	1.034×10^{0}	0.0	0.0	1.652×10^{-6}
Stainless Steel (0.25 cm)	1	1.725	1.354×10^{-3}	0.0	0.0	5.662×10^{-10}
	2	0.7238	9.782×10^{-4}	0.0	0.0	3.394×10^{-9}
	3	0.3470	1.255×10^{-2}	0.0	0.0	1.691×10^{-7}
	4	0.3050	1.080×10^{-1}	0.0	0.0	1.933×10^{-6}
Fission Lattice (30 cm)	1	2.390	1.561×10^{-4}	3.135×10^{-4}	1.182×10^{-4}	5.662×10^{-10}
	2	1.098	1.446×10^{-4}	2.494×10^{-5}	1.020×10^{-5}	3.394×10^{-9}
	3	0.9468	1.830×10^{-3}	2.970×10^{-4}	1.222×10^{-4}	1.691×10^{-7}
	4	0.9360	1.945×10^{-3}	2.808×10^{-3}	1.156×10^{-3}	2.065×10^{-6}
Fission Lattice (60 cm)	1	2.390	1.561×10^{-4}	3.135×10^{-4}	1.182×10^{-4}	5.662×10^{-10}
	2	1.098	1.446×10^{-4}	2.494×10^{-5}	1.020×10^{-5}	3.394×10^{-9}
	3	0.9468	1.830×10^{-3}	2.970×10^{-4}	1.222×10^{-4}	1.691×10^{-7}
	4	0.9360	1.992×10^{-3}	2.880×10^{-3}	1.185×10^{-3}	2.112×10^{-6}

Table 5-XII

(continued)

Region	Group	D (cm)	Σ_a (1/cm)	$\nu\Sigma_f$ (1/cm)	Σ_f (1/cm)	$(\frac{1}{v})$ (sec/cm)
Fission Lattice (60 cm)	1	2.390	1.561×10^{-4}	3.135×10^{-4}	1.182×10^{-4}	5.662×10^{-10}
	2	1.098	1.446×10^{-4}	2.494×10^{-5}	1.020×10^{-5}	3.394×10^{-9}
	3	0.9468	1.830×10^{-3}	2.970×10^{-4}	1.222×10^{-4}	1.691×10^{-7}
	4	0.9359	1.991×10^{-3}	2.878×10^{-3}	1.184×10^{-3}	2.111×10^{-6}
Fission Lattice (30 cm)	1	2.390	1.561×10^{-4}	3.135×10^{-4}	1.182×10^{-4}	5.662×10^{-10}
	2	1.098	1.446×10^{-4}	2.494×10^{-5}	1.020×10^{-5}	3.394×10^{-9}
	3	0.9468	1.830×10^{-3}	2.970×10^{-4}	1.222×10^{-4}	1.691×10^{-7}
	4	0.9359	1.941×10^{-3}	2.803×10^{-3}	1.153×10^{-3}	2.061×10^{-6}
Stainless Steel (0.25 cm)	1	1.725	1.354×10^{-3}	0.0	0.0	5.662×10^{-10}
	2	0.7238	9.782×10^{-4}	0.0	0.0	3.394×10^{-9}
	3	0.3470	1.255×10^{-2}	0.0	0.0	1.691×10^{-7}
	4	0.3052	1.099×10^{-1}	0.0	0.0	1.967×10^{-6}
Outer Lithium (9.50 cm)	1	5.870	7.096×10^{-4}	0.0	0.0	5.911×10^{-10}
	2	8.167	2.414×10^{-3}	0.0	0.0	3.197×10^{-9}
	3	6.216	1.056×10^{-2}	0.0	0.0	1.699×10^{-8}
	4	0.2922	9.826×10^{-1}	0.0	0.0	1.570×10^{-6}
Stainless Steel (0.50 cm)	1	1.741	1.136×10^{-3}	0.0	0.0	5.911×10^{-10}
	2	0.7065	9.306×10^{-4}	0.0	0.0	3.197×10^{-9}
	3	0.3511	6.622×10^{-3}	0.0	0.0	1.699×10^{-8}
	4	0.3072	1.021×10^{-1}	0.0	0.0	1.828×10^{-6}
Graphite (30 cm)	1	2.238	0.0	0.0	0.0	5.670×10^{-10}
	2	1.018	0.0	0.0	0.0	3.396×10^{-9}
	3	0.8787	0.0	0.0	0.0	1.922×10^{-7}
	4	0.8649	1.258×10^{-4}	0.0	0.0	1.971×10^{-6}

Table 5-XII

(continued)

Region	Group	D (cm)	Σ_a (1/cm)	$\nu\Sigma_f$ (1/cm)	Σ_f (1/cm)	$(\frac{1}{v})$ (sec/cm)
Shield (30 cm)	1	1.575	8.579×10^{-4}	0.0	0.0	5.559×10^{-10}
	2	0.8639	1.798×10^{-3}	0.0	0.0	2.651×10^{-9}
	3	0.4493	6.443×10^{-2}	0.0	0.0	1.081×10^{-7}
	4	0.1674	8.142×10^{-1}	0.0	0.0	1.416×10^{-6}

Table 5-XIII

PHROG-Generated Macroscopic Downscattering Cross Sections for 1.35%
Enrichment, 970°K, and 13 Regions

Region	$\Sigma_{s_{1 \to 2,3,4}}$ (1/cm)	$\Sigma_{s_{2 \to 3,4}}$ (1/cm)	$\Sigma_{s_{3 \to 4}}$ (1/cm)
Inner Convertor	4.318×10^{-2} 1.213×10^{-5} 0.0	9.243×10^{-5} 0.0	9.627×10^{-14}
Stainless Steel	2.342×10^{-2} 2.392×10^{-5} 0.0	8.819×10^{-5} 0.0	1.592×10^{-13}
Inner Lithium	9.896×10^{-3} 0.0 0.0	4.228×10^{-5} 5.783×10^{-10}	1.109×10^{-13}
Stainless Steel Liners on Fusion Lattice (2)	2.475×10^{-2} 2.910×10^{-5} 0.0	5.826×10^{-3} 0.0	2.890×10^{-3}
Thermal Fission Lattice Regions (4)	2.427×10^{-2} 3.123×10^{-7} 9.993×10^{-12}	1.044×10^{-2} 0.0	5.275×10^{-3}
Outer Lithium	1.539×10^{-2} 0.0 0.0	1.347×10^{-3} 2.597×10^{-10}	8.283×10^{-11}
Outer Stainless Steel	2.732×10^{-2} 3.853×10^{-5} 0.0	3.609×10^{-3} 0.0	1.529×10^{-10}
Graphite Reflector	2.588×10^{-2} 0.0 0.0	1.159×10^{-2} 0.0	7.041×10^{-3}
Shield	6.375×10^{-2} 3.035×10^{-4} 3.610×10^{-8}	5.538×10^{-2} 6.374×10^{-6}	2.171×10^{-2}

resonance absorption of neutrons in higher energy groups at higher temperatures. This fact is particularly evident in the hybrid system where the fuel is only slightly enriched and fertile isotopes are prevalent.

The 970°K case with zero-flux, vacuum wall boundary condition is included as Fig. 75 to illustrate further the essential indifference of the blanket to the boundary conditions except very near the wall. All other enrichments show similar results with symmetric flux shapes in the thermal fission lattice and peaking of the thermal flux in the graphite reflector.

The results of the diffusion theory criticality calculations using four neutron energy groups and thirteen regions in the blanket are listed in Table 5-XIV. The range of enrichments considered extends from natural uranium up to 1.50% enrichment which is a cutoff selected on the basis that higher enrichments begin to defeat significantly the hybrids' advantages in a fuel short economy. If significantly enriched fuel is needed, then the complexity of the hybrid will override its reduction of fuel requirements. In addition, higher enrichments begin to give criticality or $k_{eff} \geq 1.0$ at significantly elevated temperatures resulting in a loss of inherent safety in operating the hybrid device.

Table 5-XIV contains several important pieces of information. First, the use of different inner hybrid vacuum wall boundary conditions has little effect on the magnitude of the blanket neutron multiplication factor. For example, the 1.35% enriched case at room temperature shows $k_{eff} = 1.0014$ for a zero current ($J \to 0$) inner boundary condition on all four groups. For the same case run with a zero flux ($\phi \to 0$) inner boundary condition on all four groups, $k_{eff} = 0.9975$. Although one is

Table 5-XIV

Results of Diffusion Theory Criticality Calculations

^{235}U Enrichment	k_{eff} $(J \to 0)$*	k_{eff} $(\phi \to 0)$
Temperature Series 1: 290°K		
0.711%	0.7757	0.7726
0.80%	0.8189	0.8157
0.90%	0.8616	0.8583
1.00%	0.8992	0.8957
1.20%	0.9623	0.9585
1.35%	1.0014	0.9975
1.50%	1.0350	1.0310
Temperature Series 2: 570°K		
0.711%	0.7285	0.7255
0.30%	0.7716	0.7685
0.90%	0.8145	0.8112
1.00%	0.8524	0.8489
1.20%	0.9164	0.9128
1.35%	0.9564	0.9526
1.50%	0.9910	0.9871
Temperature Series 3: 970°K		
0.711%	0.6860	0.6831
0.80%	0.7288	0.7256
0.90%	0.7714	0.7680
1.00%	0.8080	0.8046
1.20%	0.8721	0.8685
1.35%	0.9124	0.908
1.50%	0.9474	0.9436

*Note that the blanket multiplication factor is strongly dependent on temperature but only weakly dependent on the choice of boundary condition for the plasma vacuum wall.
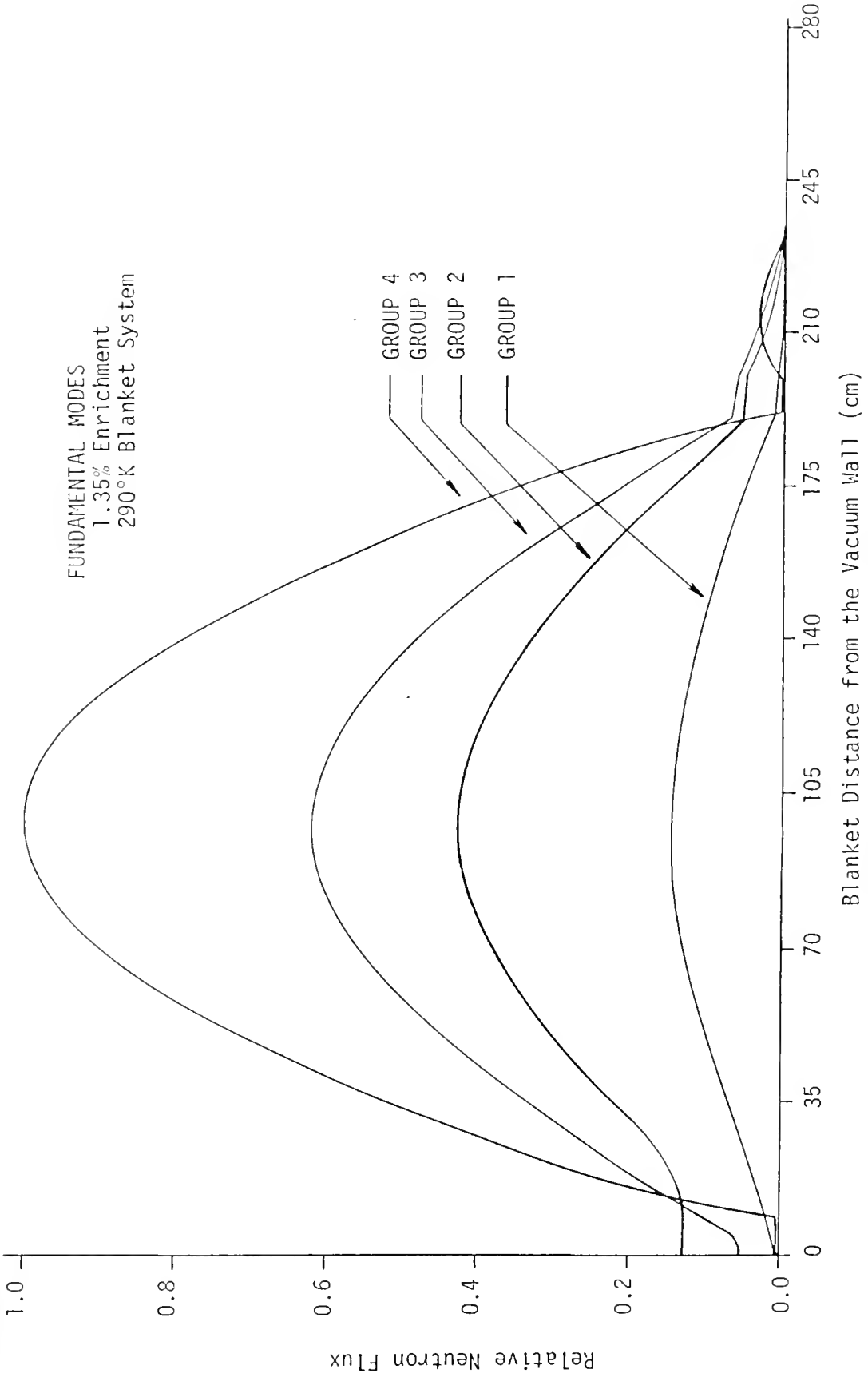
Figure 72.   Four-group fundamental mode flux profiles from CORA for the 1.35% enrichment at 290°K with zero-current vacuum wall boundary condition.
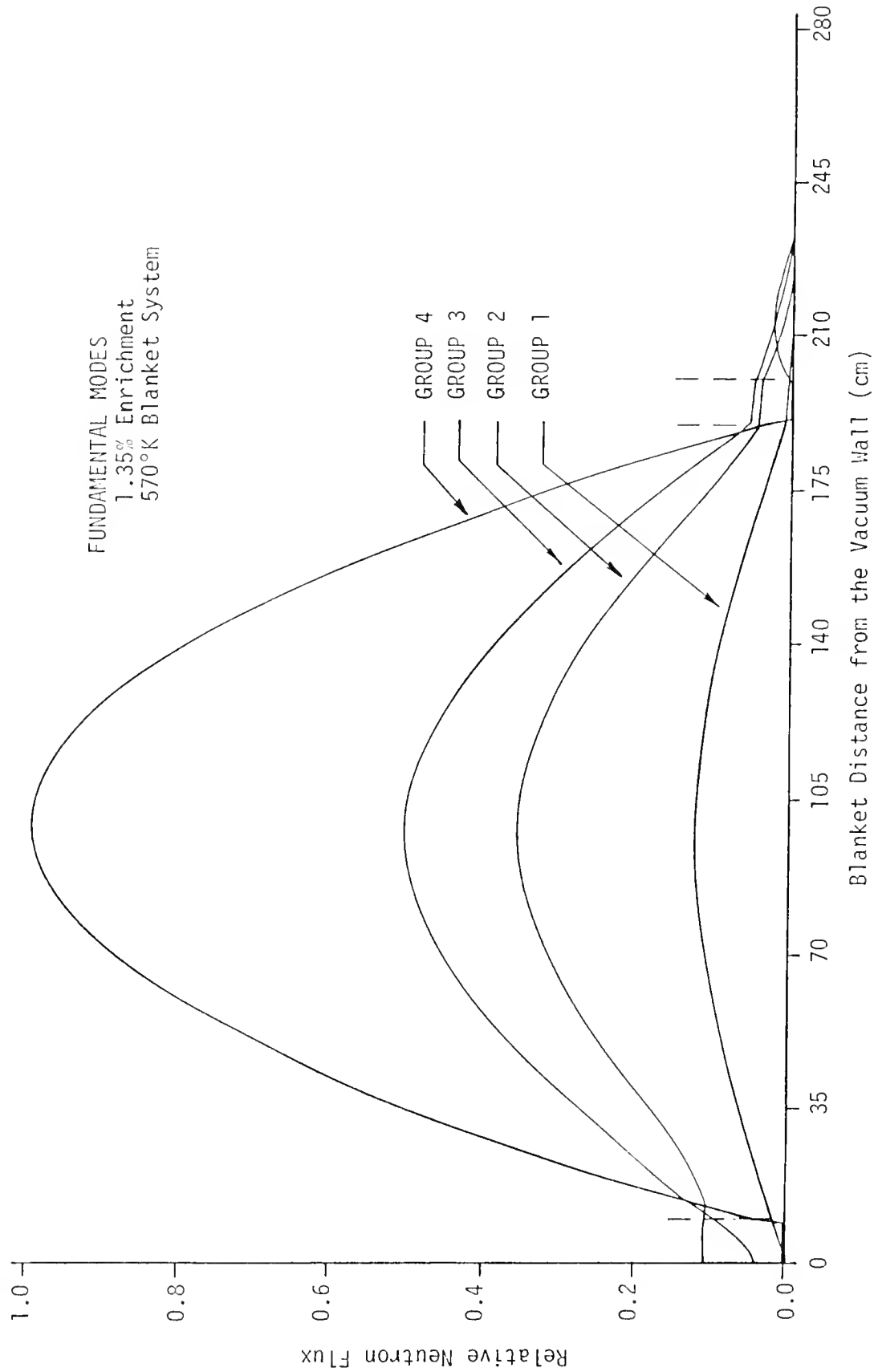
Figure 73. Four-group fundamental mode flux profiles from CORA for the 1.35% enrichment at 570°K with zero-current vacuum wall boundary condition.
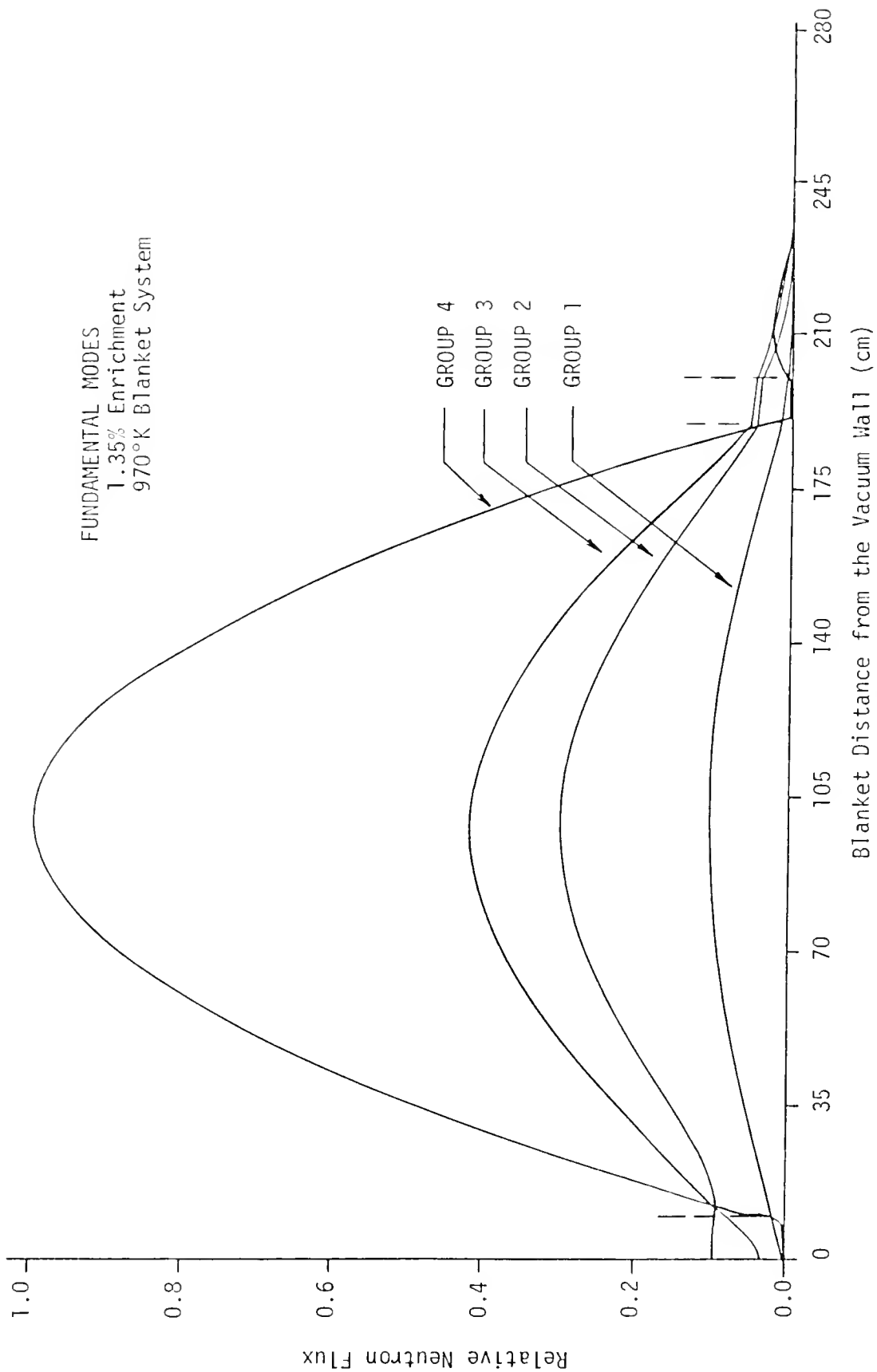
Figure 74. Four-group fundamental mode flux profiles from CORA for the 1.35% enrichment at 970°K with zero-current vacuum wall boundary condition.
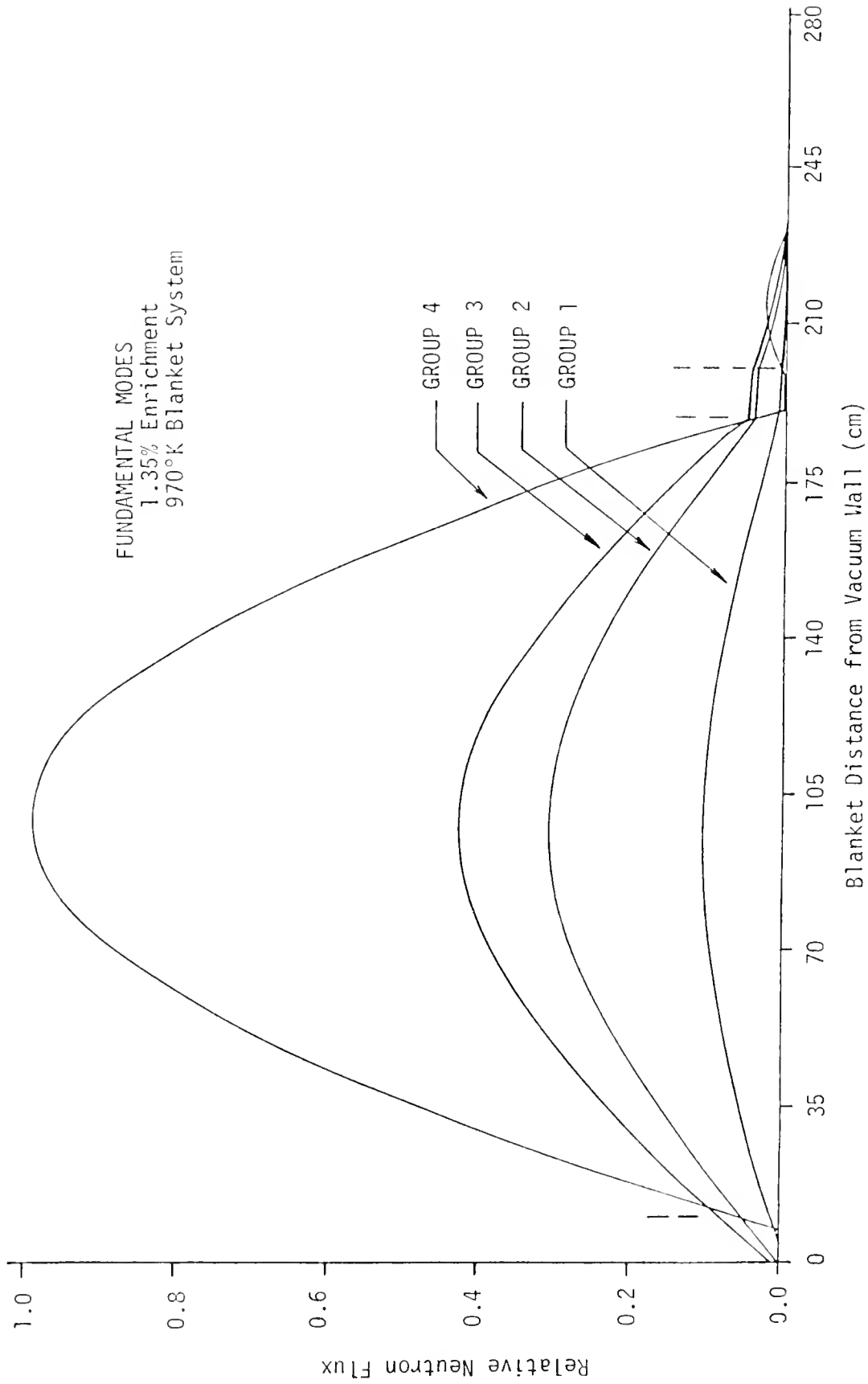
Figure 75. Four-group fundamental mode flux profiles from CORA for the 1.35% enrichment at 970°K with zero-flux vacuum wall boundary condition.

supercritical and the other subcritical, the difference in the computed

values of k_{eff} for these two cases is meaningless since cross section

data is usually not reliable enough to justify this difference. Such

uncertainties in criticality calculations account for the extreme care

and attention to procedures used in the startup of power reactors.[123]

Similarly, the other entries for k_{eff} in Table 5-XIV show very small

differences of less than 0.4% for the change in boundary condition.

Such differences in the computed values of k_{eff} could be important

during startup at room temperature as in the 1.35% enriched case if these

values were fortuitously accurate enough. The difference between super-

criticality ($k_{eff} > 1$) and subcriticality ($k_{eff} < 1$) at room temperature

is significant if accurate. However, at an operating temperature of

970°K, there is not much difference between $k_{eff} = 0.9124$ and $k_{eff} =$

0.9087. Both are far subcritical and very safe, as far as criticality

considerations are concerned. Decay heat after shutdown can supply suf-

ficient elevation in temperature to assure that, once operation is begun,

there is no problem with maintaining an elevated blanket temperature to

prevent a criticality accident.

In addition to giving the range of enrichments utilized and the

boundary condition differences, Table 5-XIV also indicates the large

defect in blanket reactivity due to temperature increases. The 1.35%

enriched case is typical; the blanket with this enrichment in the thermal

fission lattice was predicted to have a room temperature effective neutron

multiplication factor (k_{eff}) of approximately unity depending on the

applicable inner wall boundary condition. The 970°K system is nearly

critical; however, at 570°K which is far below anticipated blanket

thermal operating temperatures, the effective multiplication factor is

reduced to $k_{eff} \approx 0.95$. In fact, at the possible operating temperature of 970°K, the k_{eff} value is reduced to about 0.91 due to the temperature defect.

This large temperature defect is a major drawback to the hybrid design because it causes such low k_{eff} values at operating conditions if subcriticality of design is to be maintained at room temperature. Of course, considerations of other reductions in k_{eff} due to fuel burnup and fission product poison production have been omitted.

The variation of k_{eff} with temperature for the 1.35% enrichment is graphed in Fig. 76. The temperature coefficient of reactivity is defined by the relation:[124]

$$\alpha_T = \frac{1}{k_{eff}^2} \frac{dk_{eff}}{dT_B} \tag{193}$$

where k_{eff} and the derivative term were evaluated at the global blanket temperature, T_B. The derivative term can be calculated from Fig. 76 so that graphs like Fig. 76 can be constructed from the data in Table 5-XIV for any of the hybrid blankets whose criticality calculations are summarized in Table 5-XIV. Note that the two curves for the two different boundary conditions at the vacuum wall closely parallel each other so the temperature feedback coefficient is essentially independent of the boundary condition. Later transport calculations were run to show that $k_{eff} = 0.919$ at 900°K for the 1.35% enriched blanket. Such a value of k_{eff} is compatible with the curves in Fig. 76. The blanket feedback temperature coefficient calculated from Fig. 76 at 900°K is $\alpha_T = -1.05 \times 10^{-4}$ $\Delta k/k/°F$ which represents a strong, negative, temperature feedback effect. This is a quantity which is very useful in characterizing
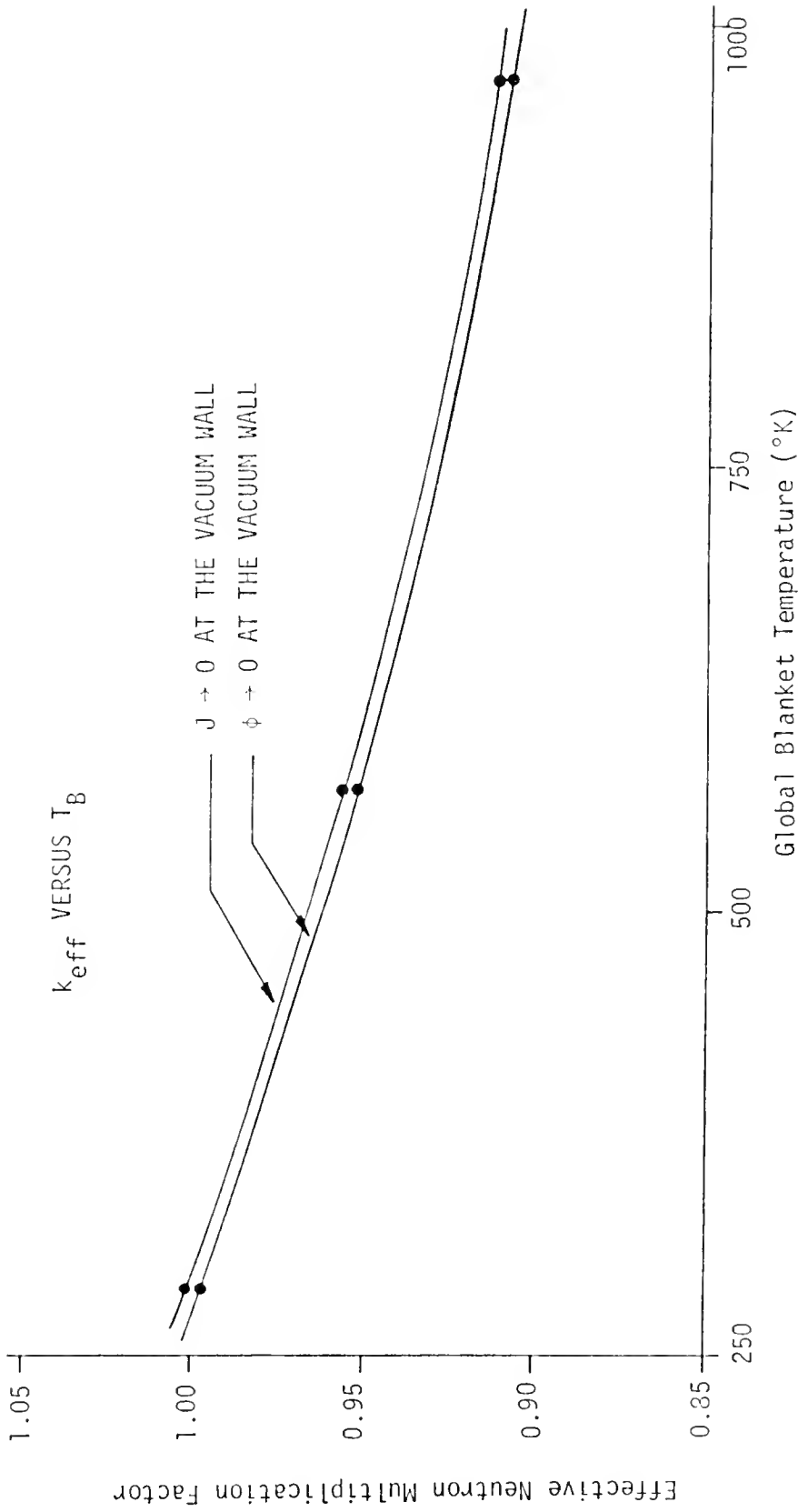
Figure 76. Variation of blanket effective neutron multiplication factor with temperature for the 1.35% enrichment using four-group diffusion theory.

the kinetic properties of multiplying systems such as hybrid blankets. As shown in Fig. 76, this negative feedback effect changes most quickly with temperature at low temperatures and gradually begins to saturate at higher temperatures where the curve has a smaller negative slope. This effect can be attributed to saturation of the absorber resonances at higher temperatures. This negative feedback guarantees stability of the blanket model of Chapter 3 and will help to control power excursions.

The extensive criticality calculations with the four-group CORA code were checked using the MONA code.[125] To do this, selected PHROG calculations were re-run to get 20 fast energy groups for use in the MONA code. Although much more costly to obtain, the criticality results for 21 total groups for selected cases compared (all three temperatures at both 1% and 1.35% enrichments) showed less than 0.1% difference in the blanket effective neutron multiplication factor between CORA and MONA results. When constants were coalesced to four groups, the resultant four-group fundamental mode flux shapes and k_{eff} values were essentially the same as those obtained using CORA.

Inhomogeneous Diffusion Theory Calculations

Consideration was next turned to the driven blanket and attempts were made to investigate the applicability of the global parameter formula for energy deposition per fusion neutron entering the blanket. The PNL studies[1,64] and others[60] described in Chapter 1 refer to the blanket power in terms of Q_B. The point-model formula for Q_B, derived in Appendix A, is repeated here:

$$Q_B = \frac{G_f}{\bar{\nu}} \left[\frac{k_{eff}}{1 - k_{eff}} \right] + E_n + \delta_E \tag{194}$$

where E_n for these first cases was chosen as the average neutron energy
in the first group of the CORA calculations. Therefore, E_n = 2.92 MeV
which is somewhat above the average energy of 2 MeV for a neutron pro-
duced in a ^{235}U fission reaction. If the global relationship in Eq. (194)
were valid for estimating blanket power production, then it was expected
that the blanket energy production could be predicted on the basis of a
known magnitude surface source in the first group of CORA. Therefore,
a number of inhomogeneous calculations were run concentrating on the most
reactive blankets at 1.35% and 1.50% thermal lattice enrichments.
Certainly, if Eq. (194) is valid, then using 2.92 MeV neutrons, which is
near the average fission energy, would be expected to result in order of
magnitude agreement with the predictions of the global energy deposition
equation.

The method used to input an inhomogeneous source into the CORA code
involves the boundary condition relationship:

$$\alpha\phi - \beta J + \gamma = 0 \tag{195}$$

where ϕ is the flux and J is the current in the group in question at the
boundary of interest and α, β, and γ are coefficients which must be input
for each group at each surface for which a boundary condition is required.

To put an inhomogeneous surface source at the vacuum wall, the
α-coefficient was set to zero to yield Eq. (196):

$$J = \gamma/\beta \ (nts/cm^2\text{-sec}) \ . \tag{196}$$

As usual, the β-coefficient was set to unity so the problem involved
selecting the appropriate γ-coefficient for each of the blankets involved

to model a source expected to produce the blanket design power of 6500 MWth.

First, the blanket energy multiplication, Q_B, was calculated. The average value of $\bar{\nu}$, the neutrons per fission, was calculated for each case using the following volume weighting formula based on fluxes from previous scoping CORA inhomogeneous calculations:

$$\bar{\nu} = \frac{\sum\limits_{M} V_M \sum\limits_{G=1}^{4} (\nu\Sigma_f)_{G,M} \; \bar{\phi}_{G,M}}{\sum\limits_{M} V_M \sum\limits_{G=1}^{4} \Sigma_{f_{G,M}} \; \bar{\phi}_{G,M}} \tag{197}$$

where

$\bar{\phi}_{G,M}$ = the average flux in broad group G and region M

$\Sigma_{f_{G,M}}$ = the average macroscopic fission cross section in group G and region M

$(\nu\Sigma_f)_{G,M}$ = the average product of Σ_f and the neutrons per fission in group G and region M

V_M = the volume of the fissile regions in which fissions can occur

M = total number of regions containing fissile material which is two (2) when the thermal lattice is treated as a single region and five (5) when the thermal lattice is subdivided as for the 13-region CORA calculations.

The scoping inhomogeneous calculations did not require the exact source value for providing 6500 MWth because $\bar{\nu}$ can even be calculated from a unit neutron source. The effects of increasing the wall source are additive unless feedback effects are included due to temperature changes.

The required wall surface source, γ, or current of 2.92 MeV neutrons was predicted on the basis of the following equation:

$$\gamma = \frac{P_{TOT}}{Q_B A_s} \tag{198}$$

where A_s is the equivalent vacuum wall surface area bordering the hybrid inner convertor region and P_{TOT} is the total blanket power generation.

These blanket calculations were based on a volume equivalence between the actual toroidal blanket volume and the slab blanket volume modeled for all the computer code calculations using inhomogeneous sources. With the vacuum wall radius, r_i, at 230 cm and the fissile, power-producing volume extending essentially to a radius of $r_o = r_i + 190$ cm excluding the outer lithium convertor, the actual toroidal fissile blanket volume was calculated using Eq. (199):

$$V_{fissile} = \pi(r_o^2 - r_i^2) \cdot 2\pi R_T \tag{199}$$

where the major radius R_T was set to $R_T = 3r_i$ for a safety factor of 3. These calculations and equations assumed the inner lithium region to be part of the power-producing volume. Similarly, the formula for fissile volume in slab blanket geometry is given by Eq. (200):

$$V_{fissile} = A_s \cdot (r_o - r_i) \quad . \tag{200}$$

Therefore, the equivalent slab surface area used in the inhomogeneous CORA calculations is given by Eq. (201):

$$A_s = \pi(r_o + r_i) \cdot 2\pi \cdot 3r_i = 8.86 \times 10^6 \text{ cm}^2 \quad . \tag{201}$$

This equivalent slab surface area is considerably larger ($\sim 40\%$) than the actual surface area of the toroidal vacuum wall, A_T, which is given by

Eq. (199):

$$A_T = 2\pi R \cdot 2\pi \cdot r_i = 6.265 \times 19^6 \text{ cm}^2 . \tag{202}$$

Estimated values of the driving source were found to be six to ten times smaller than predicted to produce the design blanket power of 6500 MWth which is based on the requirement that the average blanket power density, $\bar{p}$, be about 2.9 W/cm^3. These results are summarized in Table 5-XV where the estimated inhomogeneous source values (γ_{EST}) and the actual source values (γ_{ACT}) required by CORA to produce 6500 MWth are listed together with the ratio

$$\zeta_1 = \frac{\gamma_{EST}}{\gamma_{ACT}} \tag{203}$$

which is simply the surface conversion coefficient defined in the hybrid analytical model developed in Chapter 3. The coefficient is the same except that here it is defined in terms of the sources required to pro-duce the specified design power. The fact that the conversion coefficient, ζ_1, is so far from unity in all these calculations is surprising especially based on its extensive use in some hybrid work. The results quoted in Table 5-XV demonstrate that the global formula for the blanket energy deposition per entering neutron is not really applicable to hybrid blankets for cases where neutrons similar to fission neutrons are being introduced. The derivation of the relationship for Q_B in Appendix A is specifically based on fission spectrum neutrons but using neutrons of average energy 2.92 MeV should yield at least rough estimates of the source strength required if the global formalization is to be useful.

Table 5-XV

Summary of Inhomogeneous CORA Calculations for Variations
in Enrichment and Temperature

Blanket Case*	k_{eff}	$\bar{\nu}$	Q_B (MeV)	Y_{EST} (nts/cm^2-sec)	Y_{ACT} (nts/cm^2-sec)	ζ_1
290°K/1.35%	0.9975	2.434	31323.0	1.462×10^{11}	1.237×10^{12}	0.118
570°K/1.35%	0.9526	2.459	1584.3	2.890×10^{12}	1.982×10^{13}	0.146
970°K/1.35%	0.9087	2.480	781.9	5.855×10^{12}	3.574×10^{13}	0.164
570°K/1.50%	0.9871	2.441	6054.7	7.561×10^{11}	5.810×10^{12}	0.130
970°K/1.50%	0.9436	2.464	1317.5	3.475×10^{12}	2.346×10^{13}	0.148

*All values listed were obtained using group 1 source neutrons in the 4-group, 13-region, inhomogeneous CORA calculations to produce 6500 MWth of blanket power.

In fact, using 2.92 MeV neutrons should yield more power than predicted, since the neutrons are more energetic than fission spectra neutrons. The surface entry of neutrons is obviously less useful for power production than expected.

The 4-group flux profiles for the 570°K and 970°K blankets with 1.35% and 1.50% enrichments are presented in Figs. 77-80 where the thermal group flux is dominant. There is significant asymmetry of the neutron flux shape with skewing toward the vacuum wall in all groups except the thermal group. The thermal group, where most neutrons are located, shows a distinctly symmetric shape similar to the fundamental mode shapes presented in Figs. 72-75. These shapes are vastly different from the monotonically decreasing fluxes associated with pure fusion systems.

As shown in Figs. 81 and 82, the power density is considerably peaked at the first wall but much less than for pure fusion systems since the entire 190 cm fissile blanket is energy productive. As the system k_{eff} is increased, the resultant power density distribution becomes increasingly less peaked in the first wall for the same 3.89 W/cm^3 average power density. Therefore, when fusion neutrons are introduced, k_{eff} must be relatively high to prevent excessive power density in the inner convertor. However, this is not possible beyond a point, as demonstrated by the diffusion theory calculations with CORA. If k_{eff} is actually close to unity, as in the 570°K, 1.50% enriched case, then it will be supercritical at room temperatures, requiring the added complication of poisons and control rods. Choosing the higher k_{eff} blanket would also defeat the basic enrichment savings of the hybrid if larger enrichments are needed to maintain significant k_{eff} values at elevated operating temperatures.
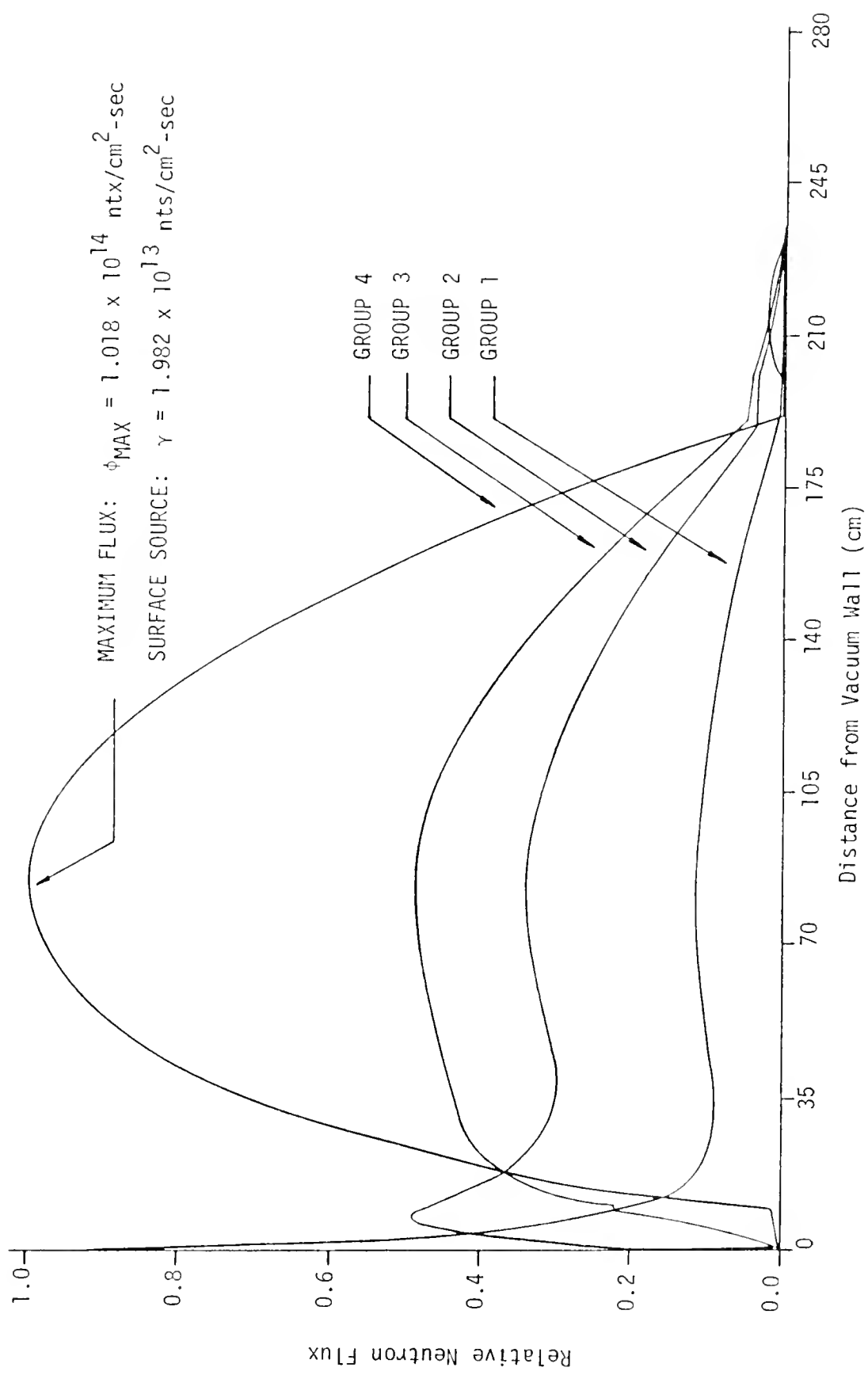
Figure 77. Four-group flux profiles from inhomogeneous CORA run using group 1 surface source to generate 6500 MWth for 1.35% enrichment at 570°K.
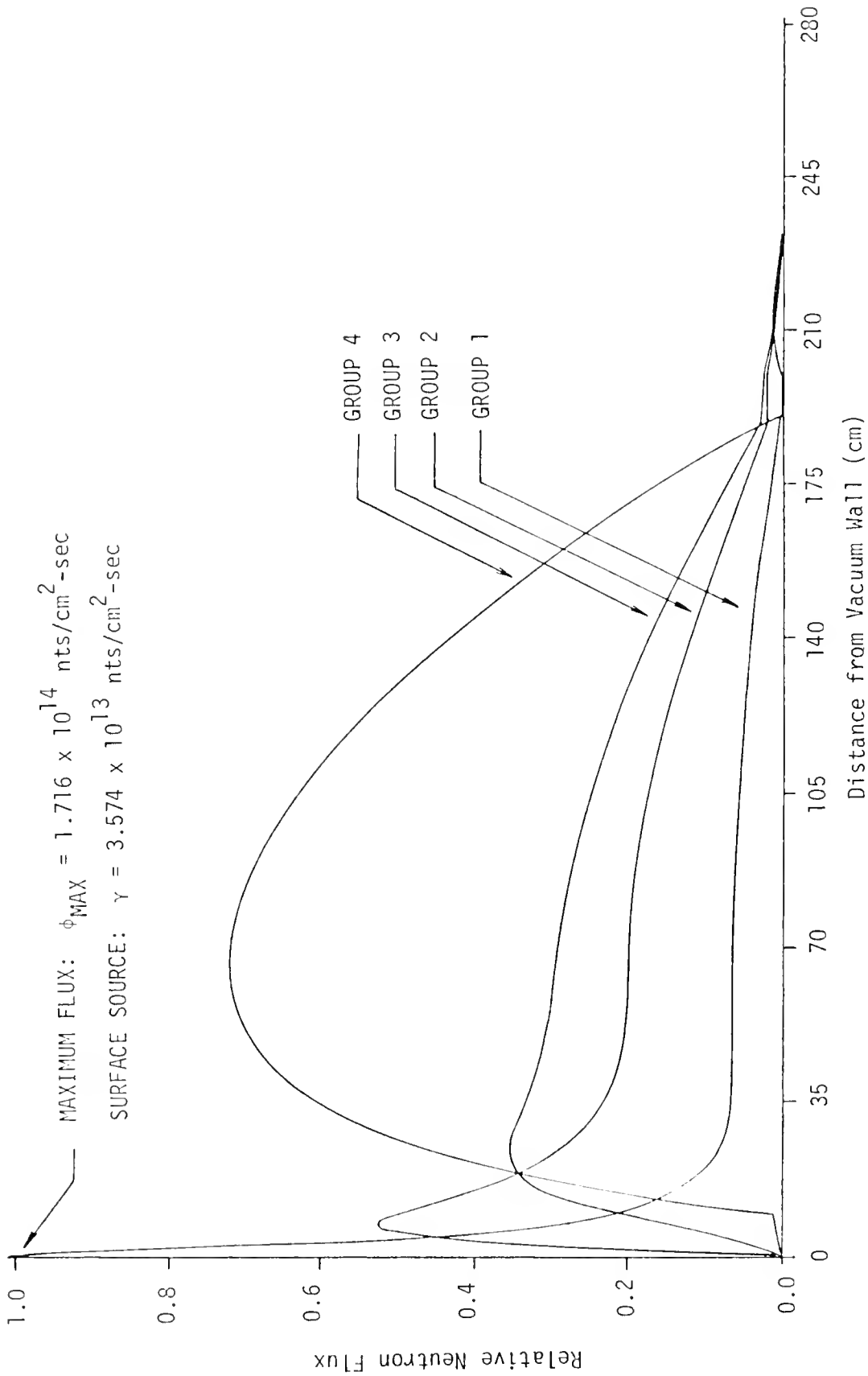
Figure 78. Four-group flux profiles from inhomogeneous CORA run using group 1 surface source to generate 6500 MWth for 1.35% enrichment at 970°K.
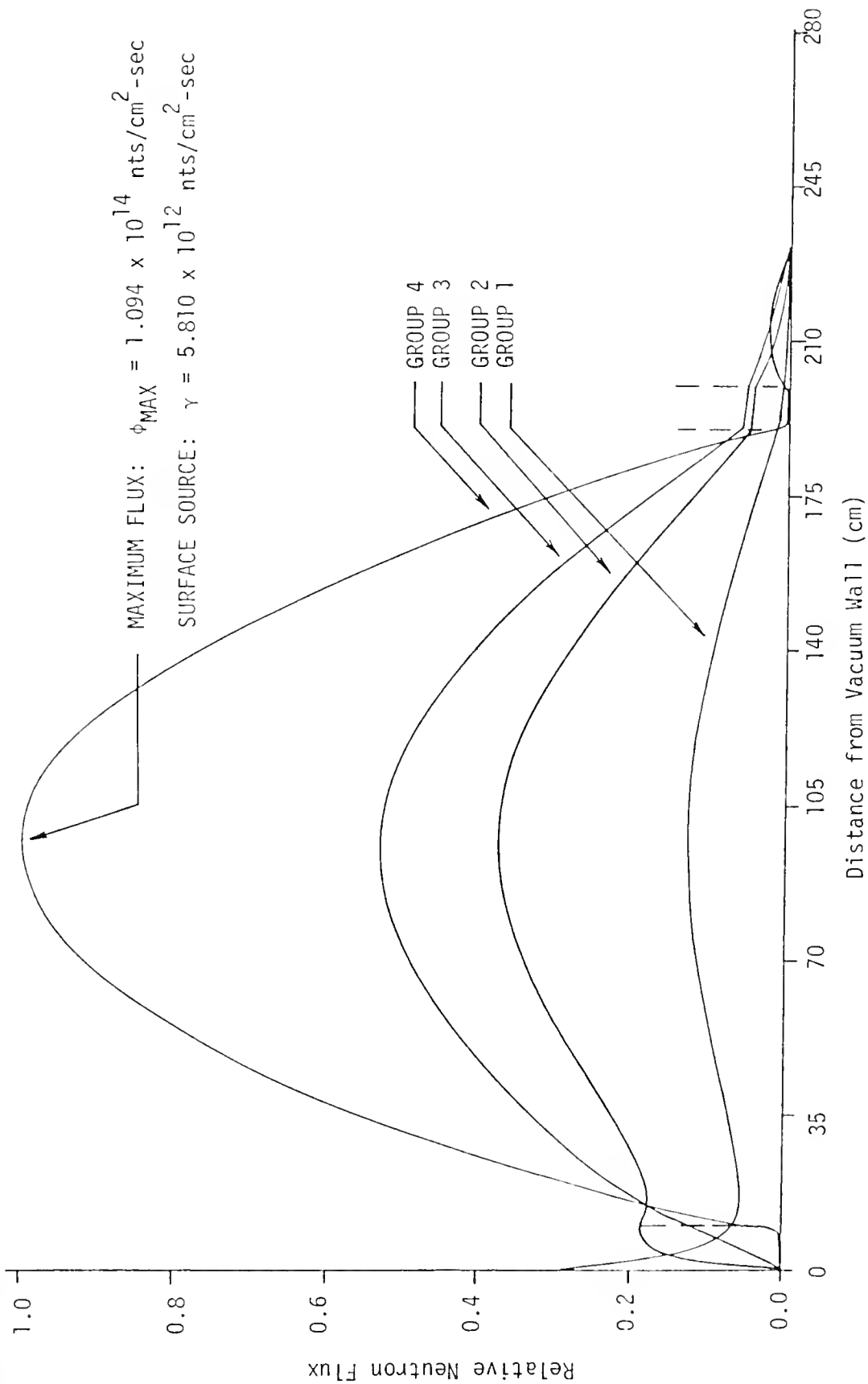
Figure 79.   Four-group flux profiles from inhomogeneous CORA run using group 1 surface source to generate 6500 MWth for 1.50% enrichment at 570°K.
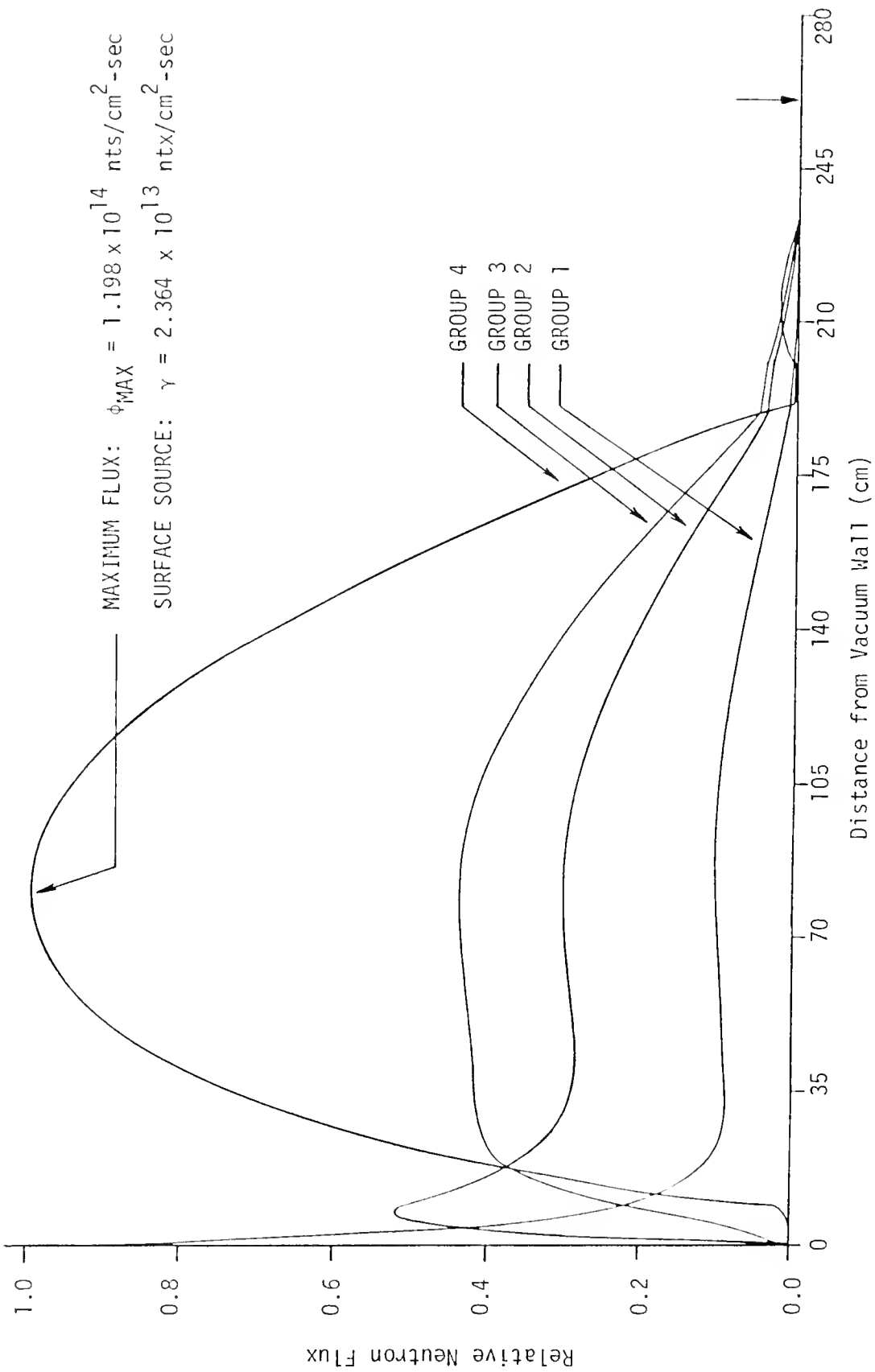
Figure 80. Four-group flux profiles from inhomogeneous CORA run using group 1 surface source to generate 6500 MWth for 1.50% enrichment at 970°K.
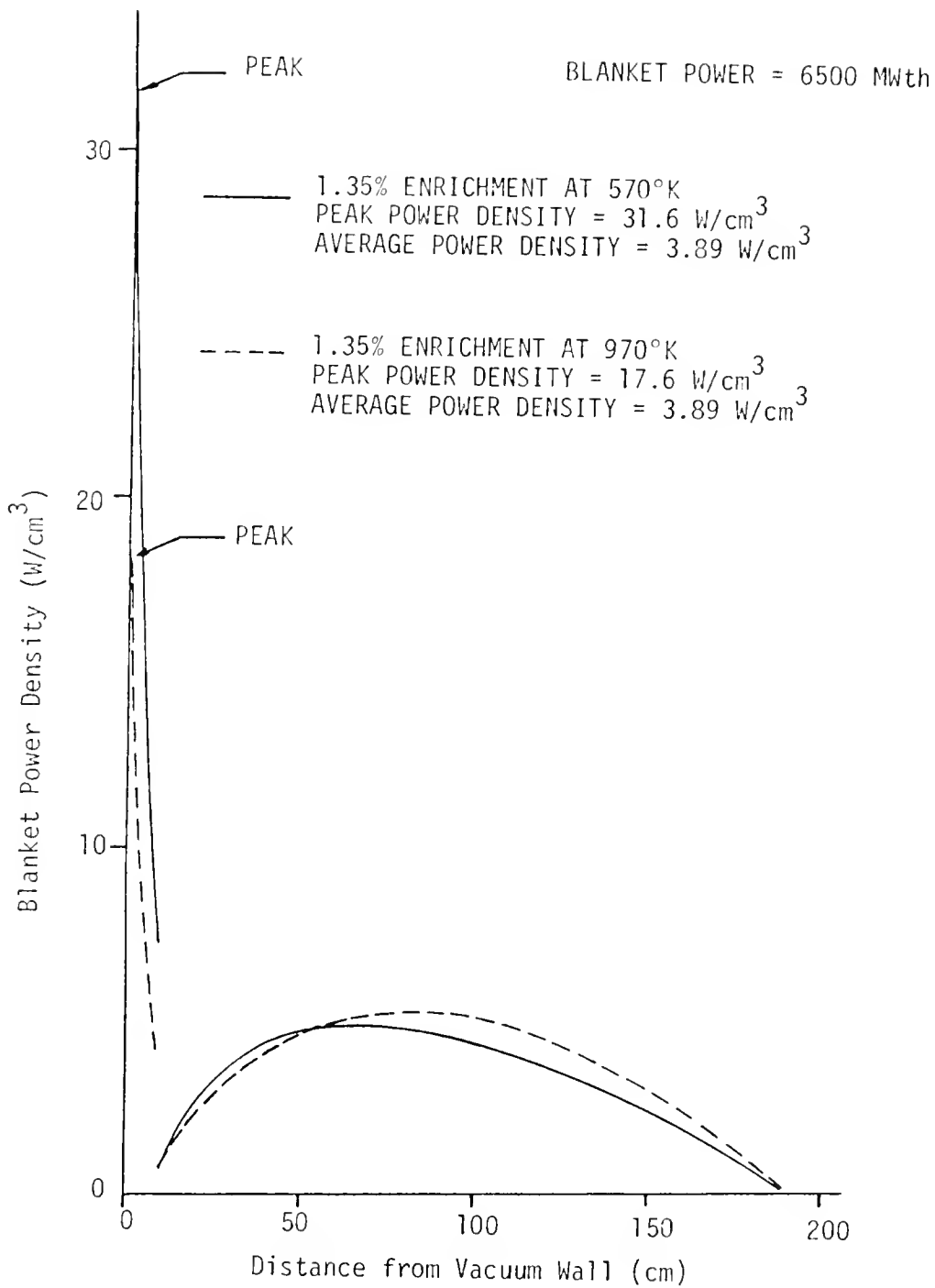
Figure 81. Blanket power density variation for 6500 MWth for 1.35% enrichment at 570°K and 970°K.
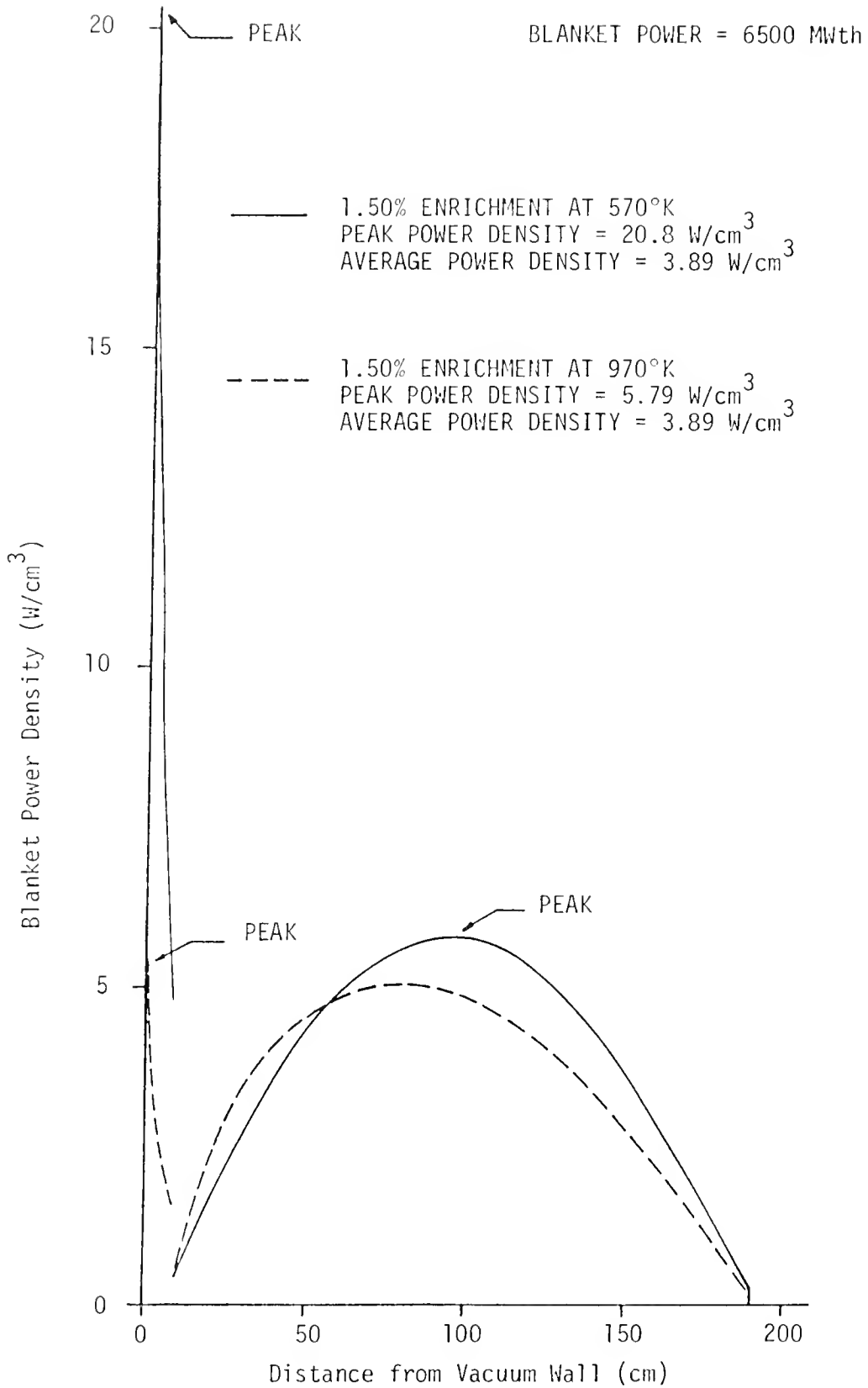
Figure 82.   Blanket power density variation for 6500 MWth for 1.50%
enrichment at 570°K and 970°K.

Kinetic Parameters

Certain kinetic parameters were also evaluated for the hybrid blanket using CORA diffusion theory calculations. Since the 1.35% enriched blanket is the best system design to prevent criticality and yet maintain reasonable k_{eff} at high temperature, the calculations of kinetic parameters were specifically directed to this blanket plus the 1.50% enriched blanket. The 1.50% enrichment will be possible provided controls are made available to prevent criticality at room temperature.

The overall temperature feedback coefficient was determined from the variation of k_{eff} with the global blanket temperature. However, certain other parameters are characteristic of these blankets and were obtained using the adjoint calculation option in the CORA code. Specifically, the prompt neutron generation time, Λ, the effective delayed neutron fraction, β_{eff}, and the inhomogeneous source weighting factors, ς_2, were calculated for a number of the blanket cases to characterize their kinetic properties.

The prompt neutron generation time was calculated based on the following volume integral:[80]

$$\Omega = \sum_{G=1}^{4} \frac{1}{U} \int_V \left(\frac{1}{v}\right)_{G,M} \phi_G(\vec{r}) \phi_G^+(\vec{r}) d\vec{r} \tag{204}$$

where

$\phi_G(r)$ = actual neutron flux generated by CORA forward calculation in broad group G

$\phi_G^+(r)$ = adjoint flux generated by CORA adjoint calculation for a critical reference state

$\left(\frac{1}{v}\right)_{G,M}$ = average inverse velocity in group G and region M

U = adjoint weighted production term.

Typical inverse velocities needed for this calculation are listed in Tables 5-X and 5-XII for the 570°K and 970°K blankets at 1.35% enrichments. The adjoint weighted production term was calculated in the CORA code using the following volume integral ($\int\limits_{V}$) relation:

$$U = \int\limits_{V} d\vec{r} \sum_{G} \sum_{G'} \chi_{G'} \nu\Sigma_{f_G}(\vec{r})\phi_G(\vec{r})\phi_{G'}^{+}(\vec{r}) \tag{205}$$

where the fission spectrum yield fractions, $\chi_{G'}$, for prompt fissions for the four broad group CORA calculations are needed to calculate the production term. The necessary spectrum yield fractions were obtained using the PHROG code[79] whose data were generated from the Evaluated Nuclear Data Files (ENDF/B)[126] to yield the fractions: $\chi_1 = 0.7536$, $\chi_2 = 0.2464$, $\chi_3 = \chi_4 = 0$. Resultant values for the prompt neutron lifetime ($\ell_p = \Omega k_{eff}$) and the generation times for the 1.35% and 1.50% blankets at elevated temperatures are listed in Table 5-XVIII. These relatively long times up to nearly a millisecond are indicative of a thermalized system with low absorption since most of a neutron's lifetime is spent diffusing at thermal energies.

Values for the average effective delayed neutron fraction, $\overline{\beta}_{eff}$, were calculated using the following standard formula for the contribution from each of six (6) delayed neutron groups:[127]

$$\overline{\beta}_{i_{eff}} = \frac{\beta_i}{U} [\sum_{G=1}^{4} \chi_{i_G}^{D} \int\limits_{V} \int\limits_{E'} (\nu\Sigma_f)_{G'}\phi_{G'}(\vec{r})\phi_G^{+}(\vec{r})d\vec{r} \, dE'] \tag{206}$$

where the subscript, i, denotes one of six delayed neutron groups and the subscript, G, denotes one of the four broad neutron groups for which the CORA code was run. The actual yield fractions, β_i, for the six delayed neutron groups are listed in Table 5-XVI.[128]

Table 5-XVI

Yield Fractions for Six Delayed Neutron Precursor Groups

Delayed Neutron Group	Delayed Neutron Yield Fraction (β_i)
1	.000215
2	.001424
3	.001274
4	.002568
5	.000748
6	.000273
Total Actual Delayed Neutron Fraction	β = 0.006502

The required fission spectrum yield fractions for the delayed neutrons are given by the term, $\chi^D_{i_G}$, for delayed group, i, and neutron energy group, G; values used in this work were calculated from data reported by Shalev and Cuttler.[129] The values used are presented in Table 5-XVII.

Table 5-XVII

Delayed Neutron Energy Spectrum Yield Fractions for 4-Group CORA Calculations

Group 1	Group 2	Group 3	Group 4
0.15	0.85	0.0	0.0
0.25	0.75	0.0	0.0
0.25	0.75	0.0	0.0
0.27	0.73	0.0	0.0
0.23	0.77	0.0	0.0
0.23	0.77	0.0	0.0

The resultant $\bar{\beta}_{eff}$ characteristic of the blanket in question is given by the simple summation of the $\bar{\beta}_{i_{eff}}$ values over the six delayed groups:

$$\bar{\beta}_{eff} = \sum_{i=1}^{6} \bar{\beta}_{i_{eff}} \qquad (207)$$

Values of $\bar{\beta}_{eff}$ for four blanket cases of interest are listed in Table 5-XVIII where the $\bar{\beta}_{eff}$ values are somewhat higher than the total actual fraction listed in Table 5-XVII because of the reduced energy spectrum of the delayed neutrons as well as a very small preferential leakage of fast neutrons. There is little variation with temperature or enrichment in the ranges listed.

Table 5-XVIII

Blanket Kinetic Parameters

Case	k_{eff}	ℓ_p (sec)	Ω (sec)	$\bar{\beta}_{eff}$
570°K/1.35%	0.9526	9.19 x 10^{-4}	9.65 x 10^{-4}	0.006537
970°K/1.35%	0.9086	8.90 x 10^{-4}	9.79 x 10^{-4}	0.006521
570°K/1.50%	0.9871	8.65 x 10^{-4}	8.76 x 10^{-4}	0.006549
970°K/1.50%	0.9436	8.39 x 10^{-4}	8.89 x 10^{-4}	0.006534

Inhomogeneous source weighting factors were also calculated from the CORA adjoint problem using only 10 distinct regions by treating the fission lattice as a single region. The effective inhomogeneous source

in group, G, and region, M, is defined by a volume integral over the region as follows:

$$Q_{G,M} = \frac{n_c}{\Omega} \left[\frac{1}{U} \int_{V_M} S_G(\vec{r}) \phi_G^+(\vec{r}) d\vec{r} \right] \tag{208}$$

where $S_G(\vec{r})$ is the actual inhomogeneous source variation with position $\vec{r}$ in the volume, V_M, in group, G, and n_c is the average neutron density in the blanket for consistency in this investigation. The average neutron density can be defined alternatively as the power, power density, or total neutrons in the reactor similar to the same variable in the point-model kinetics equations. Therefore, the inhomogeneous source weighting factors are defined for each group, G, and region, M, as follows:

$$\zeta_{2_{G,M}} = \frac{Q_{G,M}}{S_{G,M}} = \frac{n_c}{\Omega U} \int_{V_M} \phi_G^+(\vec{r}) d\vec{r} \quad . \tag{209}$$

The source weighting factors, $\zeta_{2_{G,M}}$, give the equivalent value of a volume source for a region, M, and a group, G, based on the inhomogeneous source distribution, $S_G(\vec{r})$, given in Eq. (208). Typical values for these source weighting factors in blankets subjected to 2.92 MeV neutrons are presented in Table 5-XIX for the 1.35% and 1.50% enriched blankets at elevated global temperatures of 570°K and 970°K.

In general, the values presented in Table 5-XIX indicate that neutrons introduced into the thermal fission lattice have a much larger worth or effectiveness at producing further fissions. This was expected and verified by the inhomogeneous calculations to determine the source weighting factors.

Table 5-XIX

Source Weighting Factors in Four Groups and Ten Regions

Region	Group 1	Group 2	Group 3	Group 4
	Case 1: 1.35% Enrichment and 570°K			
Inner Convertor (8.5 cm)	6.799×10^{-3}	5.051×10^{-3}	3.218×10^{-3}	9.829×10^{-4}
Stainless Steel (0.25 cm)	$.3.416 \times 10^{-4}$	2.629×10^{-4}	2.042×10^{-4}	2.730×10^{-5}
Lithium (1.0 cm)	1.394×10^{-3}	1.073×10^{-3}	8.550×10^{-4}	1.543×10^{-4}
Stainless Steel (0.25 cm)	3.557×10^{-4}	2.754×10^{-4}	2.242×10^{-4}	1.086×10^{-4}
Thermal Lattice (180 cm)	9.162×10^{-1}	9.241×10^{-1}	9.533×10^{-1}	1.247×10^{0}
Stainless Steel (0.25 cm)	3.278×10^{-2}	2.458×10^{-4}	1.747×10^{-4}	1.032×10^{-4}
Lithium (9.50 cm)	1.108×10^{-4}	9.027×10^{-3}	5.643×10^{-3}	1.553×10^{-4}
Stainless Steel (0.50 cm)	5.139×10^{-2}	4.400×10^{-4}	2.581×10^{-4}	2.031×10^{-13}
Graphite (30 cm)	1.345×10^{-4}	9.724×10^{-3}	4.946×10^{-3}	6.045×10^{-12}
Shield (30 cm)	6.198×10^{-4}	2.059×10^{-4}	4.387×10^{-5}	1.270×10^{-14}
	Case 2: 1.35% Enrichment and 970°K			
Inner Convertor (8.5 cm)	7.302×10^{-3}	5.410×10^{-3}	3.420×10^{-3}	1.188×10^{-3}
Stainless Steel (0.25 cm)	3.670×10^{-4}	2.819×10^{-4}	2.189×10^{-4}	3.684×10^{-5}
Lithium (1.0 cm)	1.499×10^{-3}	1.150×10^{-3}	9.127×10^{-4}	2.082×10^{-4}
Stainless Steel (0.25 cm)	3.815×10^{-4}	2.949×10^{-4}	2.391×10^{-4}	1.180×10^{-4}
Thermal Lattice (180 cm)	9.892×10^{-1}	9.976×10^{-1}	1.029×10^{0}	1.371×10^{0}
Stainless Steel (0.25 cm)	3.542×10^{-4}	2.768×10^{-4}	1.901×10^{-4}	1.100×10^{-4}
Lithium (9.50 cm)	1.207×10^{-2}	9.844×10^{-3}	6.212×10^{-3}	2.002×10^{-4}
Stainless Steel (0.50 cm)	5.641×10^{-4}	4.820×10^{-4}	2.863×10^{-3}	9.463×10^{-12}
Graphite (30 cm)	1.477×10^{-2}	1.068×10^{-2}	5.488×10^{-3}	2.838×10^{-10}
Shield (30 cm)	6.812×10^{-4}	2.272×10^{-4}	4.868×10^{-5}	5.992×10^{-13}

Table 5-XIX

(continued)

Case 3: 1.50% Enrichment and 570°K

Region	Group 1	Group 2	Group 3	Group 4
Inner Convertor (8.5 cm)	6.175×10^{-3}	4.991×10^{-3}	3.186×10^{-3}	9.717×10^{-4}
Stainless Steel (0.25 cm)	3.373×10^{-4}	2.598×10^{-4}	2.022×10^{-4}	2.724×10^{-5}
Lithium (1.0 cm)	1.377×10^{-3}	1.061×10^{-3}	8.467×10^{-4}	1.646×10^{-4}
Stainless Steel (0.25 cm)	3.512×10^{-4}	2.722×10^{-4}	2.220×10^{-1}	1.083×10^{0}
Thermal Lattice (180 cm)	9.013×10^{-1}	9.091×10^{-1}	9.378×10^{-1}	1.225×10^{-4}
Stainless Steel (0.25 cm)	3.234×10^{-4}	2.516×10^{-4}	1.728×10^{-4}	1.026×10^{-4}
Lithium (9.50 cm)	1.093×10^{-2}	8.913×10^{-3}	5.581×10^{-3}	1.553×10^{-3}
Stainless Steel (0.50 cm)	5.072×10^{-2}	4.345×10^{-4}	2.552×10^{-4}	2.293×10^{-13}
Graphite (30 cm)	1.328×10^{-2}	9.605×10^{-3}	4.892×10^{-3}	6.852×10^{-2}
Shield (30 cm)	6.122×10^{-4}	2.035×10^{-4}	4.339×10^{-5}	1.440×10^{-14}

Case 4: 1.50% Enrichment and 970°K

Region	Group 1	Group 2	Group 3	Group 4
Inner Convertor (8.5 cm)	7.226×10^{-3}	5.364×10^{-3}	3.401×10^{-3}	1.176×10^{-3}
Stainless Steel (0.25 cm)	3.631×10^{-4}	2.791×10^{-4}	2.164×10^{-4}	3.671×10^{-5}
Lithium (1.0 cm)	1.431×10^{-3}	1.139×10^{-3}	9.056×10^{-4}	2.082×10^{-4}
Stainless Steel (0.25 cm)	3.775×10^{-4}	2.921×10^{-4}	2.373×10^{0}	1.176×10^{0}
Thermal Lattice (180 cm)	9.754×10^{-1}	9.838×10^{-1}	1.015×10^{0}	1.350×10^{0}
Stainless Steel (0.25 cm)	3.503×10^{-4}	2.737×10^{-4}	1.884×10^{-4}	1.094×10^{-4}
Lithium (9.50 cm)	1.193×10^{-2}	9.741×10^{-4}	6.156×10^{-3}	2.000×10^{-4}
Stainless Steel (0.50 cm)	5.579×10^{-4}	4.769×10^{-4}	2.838×10^{-4}	1.008×10^{-11}
Graphite (30 cm)	1.462×10^{-4}	2.250×10^{-4}	4.824×10^{-4}	6.385×10^{-13}

Calculations were also performed to determine the size of constant but distributed volume sources which would be needed to produce 6500 MWth in the blanket. To do this, the current, determined by the inhomogeneous surface source calculations, was converted to an equivalent volume source, s_V, in one-dimensional CORA calculations by the volume-conserving relation given in Eq. (210):

$$s_V = \frac{\gamma}{\Delta x} \tag{210}$$

where Δx is the blanket thickness into which the constant volume source, s_V, was distributed.

Cases were run for equivalent volume sources where the source was confined to only the 8.5 cm inner convertor, $s_{8.5}$, and then to the 188.5 cm total fissile thickness (inner convertor plus thermal lattice), $s_{188.5}$. The source weighting factors presented in Table 5-XIX indicate very low worth for neutrons inserted into the inner convertor region in group 1 contrasted with high worth for neutrons inserted into the thermal lattice in qualitative support of the inhomogeneous surface source results.

This situation is confirmed by the results presented in Table 5-XX for the two highest enrichment blankets at elevated temperatures. For neutrons introduced into the inner convertor only, the source strength required for 6500 MWth was greatly underpredicted as shown by the volume source conversion coefficient, $\zeta_2^{8.5}$, for all cases. When the source was distributed uniformly throughout both fissile regions then the predicted source size requirements approached those actually required. For the cases listed in Table 5-XX, values for the volume source conversion coefficient, $\zeta_2^{188.5}$, are in the range 0.81 to 0.84. Such values are in

Table 5-XX

Effectiveness of Uniform Volume Sources for Design Power Level

Case 1:   Inner Convertor (8.5 cm) Source

Blanket	Predicted s_V $(nts/cm^3\text{-}sec)$	Actual s_V $(nts/cm^3\text{-}sec)$	$\zeta_2^{8.5}$
570°K/1.35%	3.40×10^{11}	2.325×10^{12}	0.146
970°K/1.35%	6.92×10^{11}	4.371×10^{12}	0.158
570°K/1.50%	8.90×10^{10}	6.25×10^{11}	0.142
970°K/1.50%	4.09×10^{11}	2.77×10^{12}	0.147

Case 2:   Inner Convertor/Thermal Lattice (188.5 cm) Source

Blanket	Predicted s_V $(nts/cm^3\text{-}sec)$	Actual s_V $(nts/cm^3\text{-}sec)$	$\zeta_2^{188.5}$
570°K/1.35%	1.53×10^{10}	1.86×10^{10}	0.823
970°K/1.35%	3.11×10^{10}	3.72×10^{10}	0.887
570°K/1.50%	4.01×10^{9}	4.92×10^{9}	0.815
970°K/1.50%	1.84×10^{10}	2.24×10^{10}	0.823

qualitative agreement with the source weighting factors of Table 5-XIX for neutrons inserted into both fissile regions.

A simple volume weighting of the fissile region group 1 source weighting factors in Table 5-XX for each case indicates expected $\zeta_2^{188.5}$ values of .875, .945, .861, and .932 for the 1.35% enriched blanket at 570°K and 970°K and the 1.50% enriched blanket at 570°K and 970°K, respectively. In both cases qualitative verification of neutron source worth was obtained as expected. Since leakage from the inner convertor was not removed and since the actual fundamental mode was not followed in uniformly introducing the volume sources in either case, quantitative agreement was not expected. However, the neutronic interaction of planar source neutrons with the blanket is better delineated and explained in anticipation of eventual utilization of fusion neutrons to drive the blanket for power production.

Transport Theory Calculations

Previous calculations addressed fission energy source neutrons. The 14.06 MeV fusion neutrons were specifically addressed using the newly-released AMPX modular code system[81] described in Appendix D. The AMPX system was used to produce and manipulate the required cross section data and to perform the necessary eigenvalue and inhomogeneous source calculations on the hybrid blanket. No other work has been reported in this area using the AMPX package.

The basic cross section information for blanket nuclides was taken from the Evaluated Nuclear Data Files (ENDF/B-III and IV).[126,130] These ENDF/B data are specified in files for practically any nuclear process.[130]

The XLACS modular code[131] is part of the AMPX system as described in Appendix D and is designed to produce full energy range, neutron cross section libraries.

The XLACS module within the AMPX system as well as the "old" XLAC code[132] has been used previously to produce and store libraries of weighted multigroup neutron cross sections from ENDF/B-III and ENDF/B-IV data for many different nuclides at selected temperatures. The libraries exist in standard 123-group fine structure covering the neutron energy spectrum from 14.92 MeV at the upper limit down to 0.00474 eV (essentially zero) at the lower end of the energy spectrum. The AMPX Master Library energy boundaries for the 123-group neutron cross section data are listed in Table 5-XXI.

The NITAWL module[133] described in Appendix D was used to select the nuclides from the XLACS-produced AMPX Master Library for a P_2-S_4, discrete ordinate calculation; blanket nuclides were selected based on an assumed global hybrid blanket temperature of 900°K. This temperature was selected because of the availability of nearly complete nuclide data in the existing AMPX Master Library at this thermal temperature. In addition, the temperature is within the range of temperatures considered in the diffusion theory calculations and is not an unreasonable effective operating temperature for a demonstration hybrid blanket system. Nuclides selected together with AMPX Library ID Numbers and thermal temperatures are listed in Table 5-XXII. The nuclides listed were used to analyze the 1.35% enriched hybrid blanket at 900°K.

All of the nuclides stored in the XLACS-produced AMPX Master Library, used as input for the hybrid transport calculations, were checked for internal consistency using the RADE module[134] within the AMPX

Table 5-XXI

AMPX Master Library 123-Group Energy Boundaries

Group	Upper Energy Boundary (eV)	Group	Upper Energy Boundary (eV)	Group	Upper Energy Boundary (eV)
1	1.492×10^7	42	2.472×10^5	83	2.904×10^1
2	1.350×10^7	43	2.237×10^5	84	2.260×10^1
3	1.221×10^7	44	2.024×10^5	85	1.760×10^1
4	1.105×10^7	45	1.832×10^5	86	1.371×10^1
5	1.000×10^7	46	1.657×10^5	87	1.068×10^1
6	9.048×10^6	47	1.500×10^5	88	8.315×10^0
7	8.187×10^6	48	1.357×10^5	89	6.477×10^0
8	7.408×10^6	49	1.228×10^5	90	5.043×10^0
9	6.703×10^6	50	1.111×10^5	91	3.928×10^0
10	6.065×10^6	51	8.652×10^4	92	3.059×10^0
11	5.488×10^6	52	6.738×10^4	93	2.382×10^0
12	4.966×10^6	53	5.248×10^4	94*	1.859×10^0
13	4.493×10^6	54	4.087×10^4	95	1.709×10^0
14	4.066×10^6	55	3.183×10^4	96	1.567×10^0
15	3.679×10^6	56	2.479×10^4	97	1.432×10^0
16	3.329×10^6	57	1.930×10^4	98	1.285×10^0
17	3.012×10^6	58	1.503×10^4	99	1.134×10^0
18	2.725×10^6	59	1.171×10^4	100	9.992×10^{-1}
19	2.466×10^6	60	9.119×10^3	101	8.810×10^{-1}
20	2.231×10^6	61	7.102×10^3	102	7.684×10^{-1}
21	2.019×10^6	62	5.531×10^3	103	6.552×10^{-1}
22	1.827×10^6	63	4.307×10^3	104	5.488×10^{-1}
23	1.653×10^6	64	3.355×10^3	105	4.485×10^{-1}
24	1.496×10^6	65	2.612×10^3	106	3.614×10^{-1}
25	1.353×10^6	66	2.035×10^3	107	2.994×10^{-1}
26	1.225×10^6	67	1.585×10^3	108	2.493×10^{-1}
27	1.108×10^6	68	1.234×10^3	109	2.071×10^{-1}
28	1.003×10^6	69	9.611×10^2	110	1.798×10^{-1}
29	9.072×10^5	70	7.485×10^2	111	1.598×10^{-1}
30	8.209×10^5	71	5.829×10^2	112	1.398×10^{-1}
31	7.247×10^5	72	4.540×10^2	113	1.198×10^{-1}
32	6.721×10^5	73	3.536×10^2	114	9.974×10^{-2}
33	6.081×10^5	74	2.754×10^2	115	8.231×10^{-2}
34	5.502×10^5	75	2.145×10^2	116	6.990×10^{-2}
35	4.979×10^5	76	1.670×10^2	117	5.989×10^{-2}
36	4.505×10^5	77	1.301×10^2	118	4.987×10^{-2}
37	4.076×10^5	78	1.013×10^2	119	2.984×10^{-2}
38	3.688×10^5	79	7.889×10^1	120	2.978×10^{-2}
39	3.337×10^5	80	6.144×10^1	121	2.108×10^{-2}
40	3.020×10^5	81	4.785×10^1	122	1.489×10^{-2}
41	2.732×10^5	82	3.727×10^1	123	9.829×10^{-3}
					4.742×10^{-3}

*Group 94 is the first thermal group.

system prior to their utilization. Those found to be defective were replaced.

Table 5-XXII

Nuclides Selected from the AMPX Library

Nuclide	ID Number	Temperature (°K)
^{235}U	922358	900
^{238}U	922388	900
^{16}O	80005	900
^{12}C	60005	900
Si	140005	900
He	20080	800
^{6}Li	30065	900
^{7}Li	30075	900
Cr	240005	900
Mn	250005	900
Fe	260005	900
Ni	280005	900
Zr	400005	900
H	100046	627

The only hydrogen available was in the ZrH_2 combined form and at a temperature of 627°K. This hydrogen was used because hydrogen is only present in the shield which has little neutronic effect on the power-producing sections of the blanket as indicated by the reported source

weighting factors. The helium nuclide was selected at 800°K as the closest available temperature to 900°K. In addition, even if the blanket is at some global temperature, such as 900°K, then the helium coolant would be at a lower temperature.

The NITAWL code was used to read the AMPX library data and then to perform resonance self-shielding calculations on the nuclides for which resonance data were stored. The Nordheim Integral Treatment[135] was employed for the actual neutron resonance self-shielding calculation in NITAWL.

NITAWL also has the ability to create duplicate sets of data for designated nuclides just as the older XSDRN[136] code does. For example, the ^{235}U and ^{238}U resonance nuclides occur within two different compositions--the unmoderated inner convertor and the moderated thermal lattice. In addition, the remainder of the inner convertor is stainless steel and helium while that of the thermal lattice is primarily graphite moderator as indicated in Appendix B. Therefore, different resonance calculations were required for the uranium nuclides in each region. For example, the values input for the effective moderator cross section per absorber atom, $(\sigma_m)_{eff}$, for ^{235}U and ^{238}U in the fuel lumps within the two regions are very different as indicated by Eq. (211):[136]

$$(\sigma_m)_{eff} = \sigma_{p_0} + \sigma_m + \sigma_e \qquad (211)$$

where

σ_{p_0} = the absorber potential scattering cross section

σ_m = the moderator scattering cross section per absorber term

σ_e = the effective escape cross section.

The effective escape cross section for the fuel lump is given by Eq. (212):

$$\sigma_e = 1/\overline{\ell} \, N_a \qquad (212)$$

where

N_a = number density of the absorber in the fuel lump

$\overline{\ell}$ = mean chord length in the fuel lump.

Values of $(\sigma_m)_{eff}$ for the two applicable types of hybrid fuel lumps are summarized in Table 5-XXIII.

Table 5-XXIII

Effective Moderator Scattering Cross Sections per Absorber Atom

Fuel Lump Type	$(\sigma_m)^{235}_{eff}$ (b)	$(\sigma_m)^{238}_{eff}$ (b)
Inner Convertor Fuel Plates	1416	28.75
Thermal Lattice Fuel Columns	1328	194.6

In contrast to the previous XSDRN libraries which did not treat ^{235}U as a resonance nuclide, the AMPX system contains resonance data for ^{235}U as well as ^{238}U. With the two duplicate nuclides required for mocking up resonance nuclides in both the thermal lattice and the inner convertor, the resonance calculation in NITAWL included four nuclides. As a result, the NITAWL resonance calculations were very expensive and time consuming despite the segregation into a separate modular code.

The NITAWL resonance calculations are summarized in Table 5-XXIV where the isotopic resonance integrals, I_{235} for ^{235}U and I_{238} for ^{238}U, in both the inner convertor and the thermal lattice are presented. The absorption resonance integrals and the separate fission contributions are presented for all four (4) cases in Table 5-XXIV; the disparity in the values justified and indicates the necessity for treating nuclides in separate regions distinctly, especially if they are resonance nuclides or moderating nuclides with cross sections which are sensitive to changes in neutron flux spectra.

Table 5-XXIV

Isotopic Resonance Integral Values Obtained from NITAWL

Region	I_{235} (b)		I_{238} (b)	
	Absorption	Fission	Absorption	Fission
Inner Convertor	222.5	131.2	11.57	0.00048
Thermal Lattice	230.3	135.7	40.55	0.00052

The results of Table 5-XXIV demonstrate the increasing absorption effects with a softened spectrum as expected in the thermal lattice.

In addition, other duplicate nuclides were designated in NITAWL for oxygen and helium which appear in both the inner convertor and the thermal lattice cells as well as for graphite which appears in the thermal lattice and the reflector. Essentially, these are all isotopes which are subjected to much different spectra in different regions and/or resonance nuclides which are very sensitive to neutron spectrum changes.

The AMPX library, through the XLACS processing, also includes the (n,3n) reaction in ^{238}U which can be significant for blanket systems of low enrichment driven by fusion neutrons.[12]

The output obtained from NITAWL consisted of a working library of cross sections as prospective input for the XSDRNPM module.[82] The working library from NITAWL contained cross section data in the standard, 123-group structure produced using XLACS, essentially with the resonance data processed.

In essence, NITAWL was used to perform the resonance data processing and to select and label those nuclides required in further applications of the S_n transport calculation, XSDRNPM, to produce broad group cross section libraries and to perform criticality calculations.

After the so-called working library of cross section data was produced by NITAWL, the XSDRNPM code, which is also part of the AMPX package, was used to obtain cell-weighted constants from the NITAWL library. The method of discrete ordinates transport theory is employed by XSDRNPM. A P_2-S_4 XSDRNPM unit cell calculation was run to produce a cell-averaged set of cross sections for each nuclide in a reduced 43-group cross section structure.

For discrete ordinates calculations with XSDRNPM, the S_n quadrature sets chosen must satisfy the following two equations:[136]

$$\sum_{m=1}^{MM} w_m = 1.0 \tag{213a}$$

$$\sum_{m=1}^{MM} \mu_m w_m = 0.0 \tag{213b}$$

where MM is the number of directions, the w_m are the direction weights,

and the μ_m are the direction cosines. The values chosen for the P_2-S_4 calculations are presented in Table 5-XXV. These were used as the default values in XSDRNPM and they satisfy Eqs. (213a) and (213b).

Table 5-XXV

Hybrid Blanket Analysis S_4 Quadrature Constants

Direction Weights (w_m)	Direction Cosines (μ_m)	Product ($\mu_m w_m$)
0.00	-1.000000	0.0000000
0.25	-0.788675	-0.1971688
0.25	-0.211325	-0.0528313
0.25	+0.211325	+0.0528313
0.25	+0.788675	+0.1971688

The cross section data used by the XSDRNPM calculations for each process is defined by the following equation:

$$\bar{N} \, \bar{\sigma}_g^{cell} \, \bar{\phi}_g \, V_{cell} = \int_{cell} d\vec{r}[N(\vec{r}) \int_{E \epsilon g} dE \, \phi(\vec{r},E)\sigma(\vec{r},E)] \tag{214}$$

where the following definitions apply:

$N(r)$ = the nuclide density at position, $\vec{r}$

V_{cell} = cell volume

$\sigma(\vec{r},E)$ = nuclide cross section from the process at position, $\vec{r}$, and energy, E

$\phi(\vec{r},E)$ = neutron flux per unit energy and volume at $\vec{r}$ and E

N_{cell} = homogeneous cell number density

$\bar{\sigma}_g^{cell}$ = the cell average cross section

$$\overline{\phi}_g = \text{the cell average flux in group, } g$$

and

$$\overline{\phi}_g = \int_{E\varepsilon g} dE[\int_{cell} d\vec{r}\ \phi(\vec{r},E)]/\int_{cell} d\vec{r} \ . \qquad (215)$$

So the cross sections in XSDRNPM are cell "averaged" values across a group to yield the 123 fine-group values used here. The fluxes calculated by XSDRNPM are energy-integrated values. Therefore, the definition for a cell-averaged cross section in XSDRNPM is

$$\overline{N}\ \overline{\sigma}_G^{cell}\ \overline{\phi}_G\ V = \sum_{j=1}^{Z} N_j \sum_{i\varepsilon j} \Delta V_i \sum_{g\varepsilon G} \phi_g(i)\sigma_g(j) \qquad (216)$$

where the following definitions apply for the discretization:

Z = total number of zones in the system

j = zone index

N_j = number density in zone, j

i = spatial interval index

ΔV_i = volume of interval, i

g = fine group index

G = broad group index

$\sigma_g(j)$ = group, g, value of the microscopic cross section.

Additional required terms are

$$V = \sum_{i=1}^{I} \Delta V_i \qquad (217a)$$

where I = total number of spatial intervals and

$$\phi_g(i) = \int_{E \varepsilon g} \phi(\vec{r}, E) dE \tag{217b}$$

$$\overline{\phi}_G = \frac{1}{V} \sum_{i=1}^{I} \Delta V_i \sum_{g \varepsilon G} \phi_g(i) \tag{217c}$$

$$\overline{N} = \frac{1}{V} \sum_{j=1}^{Z} N_j \sum_{i \varepsilon j} \Delta V_i . \tag{217d}$$

This cell-averaging scheme was used to produce one set of cross sections per nuclide. However, the XSDRNPM calculation utilized additional iso-tope numbers with very small number densities, essentially to mock-up the nuclides not present in the unit cell which were located in one of the other nine regions of the hybrid blanket system. Since these nuclides are subject to different spectra, they were retained as distinct nuclides.

The P_2-S_4 calculation to obtain a collapsed set of cell-averaged cross sections utilized a zero-current or reflected boundary condition at the cell center and the usual white albedo condition at the cell edge. The 43-group structure designated by G in Eqs. (216) and (217c) above is presented in Table 5-XXVI. The same boundaries at 13.50 MeV-14.92 MeV were maintained on group 1 to facilitate eventual introduction of an inhomo-geneous source into this group to simulate the 14.06 MeV fusion source as nearly as possible within the limits of the AMPX Master Library.

Note that, since the 43-group structure is the broader group struc-ture, its group designation uses the symbol, "G," versus the symbol, "g," for the fine-group structure. This same methodology was utilized for all group structures obtained from more-detailed (fine) structures.

Table 5-XXVI

XSDRNPM 43-Group Energy Boundaries

Group	Upper Energy Boundary (eV)	Group	Upper Energy Boundary (eV)
1	1.492×10^7	23	1.585×10^3
2	1.350×10^7	24	9.611×10^2
3	1.221×10^7	25	4.540×10^2
4	1.000×10^7	26	2.754×10^2
5	7.408×10^6	27	1.301×10^2
6	5.488×10^6	28	6.144×10^1
7	4.066×10^6	29	2.260×10^1
8	3.012×10^6	30	8.315×10^0
9	2.231×10^6	31	3.928×10^0
10	1.653×10^6	32	1.859×10^0
11	1.225×10^6	33	1.432×10^0
12	8.209×10^5	34	9.992×10^{-1}
13	6.081×10^5	35	6.552×10^{-1}
14	3.688×10^5	36	4.485×10^{-1}
15	2.732×10^5	37	2.994×10^{-1}
16	1.832×10^5	38	2.071×10^{-1}
17	1.228×10^5	39	1.398×10^{-1}
18	5.248×10^4	40	9.974×10^{-2}
19	2.479×10^4	41	5.989×10^{-2}
20	1.171×10^4	42	3.984×10^{-2}
21	5.531×10^3	43	1.489×10^{-2}
22	3.355×10^3		4.742×10^{-3}

Next the cell-averaged set of cross sections produced for 43 groups
was input to a P_2-S_4 transport theory calculation in the XSDRNPM code
which was run across the entire 260.25 cm thick hybrid blanket model in
which all 10 regions were maintained distinct. In this calculation, the
cross sections were region-averaged over those regions containing the
nuclide identified in the previous cell transport calculation. The
region-averaged cross sections were produced by XSDRNPM using the
following relation:

$$\bar{\sigma}_G^{\text{region}} = \frac{\sum\limits_{\text{cell}} N(\vec{r})[\int\limits_{E\epsilon G} \phi(\vec{r},E)\ \sigma(\vec{r},E)dE]d\vec{r}}{\int\limits_{\text{cell}} N(\vec{r})\ [\int\limits_{E\epsilon G} \phi(\vec{r},E)dE]d\vec{r}} \quad , \tag{218}$$

or, using previous identities from Eqs. (217a)-(217d):

$$\bar{\sigma}_G^{\text{region}} = \frac{\sum\limits_{j=1}^{Z} N_j \sum\limits_{i\epsilon j} \Delta V_i \sum\limits_{g\epsilon G} \phi_g(i)\ \sigma_g(j)}{\sum\limits_{j=1}^{Z} N_j \sum\limits_{i\epsilon j} \Delta V_i \sum\limits_{g\epsilon G} \phi_g(i)} \tag{219}$$

where the symbol, "G," designates the broad groups and the symbol, "g," designates the finer groups.

This region-averaging scheme was used to produce one set of cross sections per nuclide identified in the earlier 123-43 group calculation. However, each element appearing in a different one of the 10 basic regions was treated as a distinct separate nuclide through the XSDRNPM nuclide identification system and energy-dependent flux seen by a nuclide will vary depending on the region in which it is located.

The first region-weighting calculation was performed to collapse the 43-group cross section set to the 26 groups listed in Table 5-XXVII. The boundary conditions applied included a zero-flux condition at the edge of the shield for all groups and a zero-current condition at the plasma vacuum wall.

Table 5-XXVII

XSDRNPM 26-Group and 11-Group Energy Boundaries

Group	Upper Energy Boundary (eV)	Group	Upper Energy Boundary (eV)
1	1.492×10^7	1	1.492×10^7
2	1.350×10^7	2	1.350×10^7
3	1.000×10^7	3	1.000×10^7
4	7.408×10^6		
5	5.438×10^6		
6	3.012×10^6	4	3.012×10^6
7	1.653×10^6		
8	8.209×10^5	5	8.209×10^5
9	3.688×10^5		
10	1.832×10^5	6	1.832×10^5
11	5.348×10^4		
12	1.171×10^4		
13	5.531×10^3	7	5.531×10^3
14	1.585×10^3		
15	4.540×10^2		
16	1.301×10^2	8	1.301×10^2
17	2.260×10^1		
18	8.315×10^0		
19	3.928×10^0		
20	1.859×10^{-1}	9	1.859×10^0
21	9.992×10^{-1}		
22	6.552×10^{-1}	10	6.552×10^{-1}
23	4.485×10^{-1}		
24	2.071×10^{-1}		
25	9.974×10^{-2}	11	9.974×10^{-2}
26	3.984×10^{-2}		
	4.742×10^{-3}		4.742×10^{-3}

Similar calculations were also run for a zero-flux vacuum wall condition but the zero current condition was the option selected to model most closely the actual blanket condition at the vacuum wall. The zero current condition essentially accounts for leakage into the toroidal plasma which, for a closed torus, may be partly balanced by the returning neutrons.

As noted in the diffusion theory calculations and again with the transport calculations, the blanket effective neutron multiplication, k_{eff}, is not affected by the vacuum wall boundary conditions. For the P_2-S_4, 43-group to 26-group XSDRNPM calculation, values of k_{eff} = 0.921 with the zero-current condition and k_{eff} = 0.919 with the zero-flux boundary condition at the vacuum wall were obtained.

Attempts to run an inhomogeneous source calculation for the 26-group case were unsuccessful because of excessive running times and lack of convergence. Such results are to be expected since XSDRNPM has no special features to speed or aid convergence of inhomogeneous source problems which are more difficult to converge than eigenvalue calculations.[137]

The decision was made at this point to continue the group-collapsing procedures to obtain a few-group set with which further calculations would be possible for inhomogeneous sources. All further calculations were performed for a zero-flux condition at both the vacuum wall and the outer shield regions of the hybrid blanket. Therefore, the same P_2-S_4 calculation was repeated to reduce the 26-group cross section set to 11 groups whose boundaries are also presented in Table 5-XXVII. Finally, the 11-group cross sections were used to run a P_2-S_4 XSDRNPM transport calculation and obtain the necessary fluxes and currents to reduce the set to 6 energy groups whose boundaries are listed in Table 5-XXVIII.

The boundaries of the highest energy group were retained in all these calculations in anticipation of implementation of an inhomogeneous fusion neutron source. The results for k_{eff} for each transport calculation across the entire blanket from 43 groups down to 6 groups are presented in Table XXIX.

Table 5-XXVIII

XSDRNPM 6-Group Cross Section Energy Boundaries

Group	Upper Energy Boundary (eV)
1	1.491×10^{7}
2	1.350×10^{7}
3	3.012×10^{6}
4	8.209×10^{5}
5	5.521×10^{3}
6	6.552×10^{-1}
	4.742×10^{-3}

Table 5-XXIX

XSDRNPM k_{eff} Results for a Zero-Flux Boundary Condition
at the Vacuum Wall

Number of Groups	k_{eff}
43	0.9191
36	0.9192
11	0.9193
6	0.9193

The values for k_{eff} in Table 5-XXIX are essentially identical and indicate the six group structure should be adequate to describe the gross neutronic properties of the blanket.

Only the lowest group in Table 5-XXVIII is retained as a thermal group in the 6-group structure from the 30 original thermal groups in the 123-group structure. The results presented in Fig. 76 for the variation of k_{eff} with global blanket temperature were used to predict a global value of k_{eff} = 0.915 on the basis of diffusion theory calculations for the global blanket temperature of 900°K used in the discrete ordinate P_2-S_4 analysis of the hybrid blanket. The close agreement of the predicted value with the actual calculated value of k_{eff} = 0.919 is a further indication of the basic validity of the XSDRNPM calculational scheme for the blanket. Although the k_{eff} value predicted by diffusion theory is somewhat lower than that predicted by the S_n discrete ordinates theory, the difference is less than 1/2%, and indicates the values are essentially identical. The small difference can easily be accounted for on the basis of the different cross section libraries utilized; however, the degree of agreement is encouraging for future calculations of either type on such hybrid blankets. The fundamental mode flux shapes for all six groups are graphed in Fig. 83 where group 1 does not register on the linear plot due to fission neutrons occurring predominantly in the energy range below 10 MeV. The flux shapes are very similar to those presented for the diffusion theory, four-group calculations where the thermal group is predominant and groups become less predominant with increased group energy. Again, the basic symmetry of the flux profiles in Fig. 83 is apparent. The same plots are presented on a semi-logarithmic scale in Fig. 84 to demonstrate the large thermal flux depression in the outer
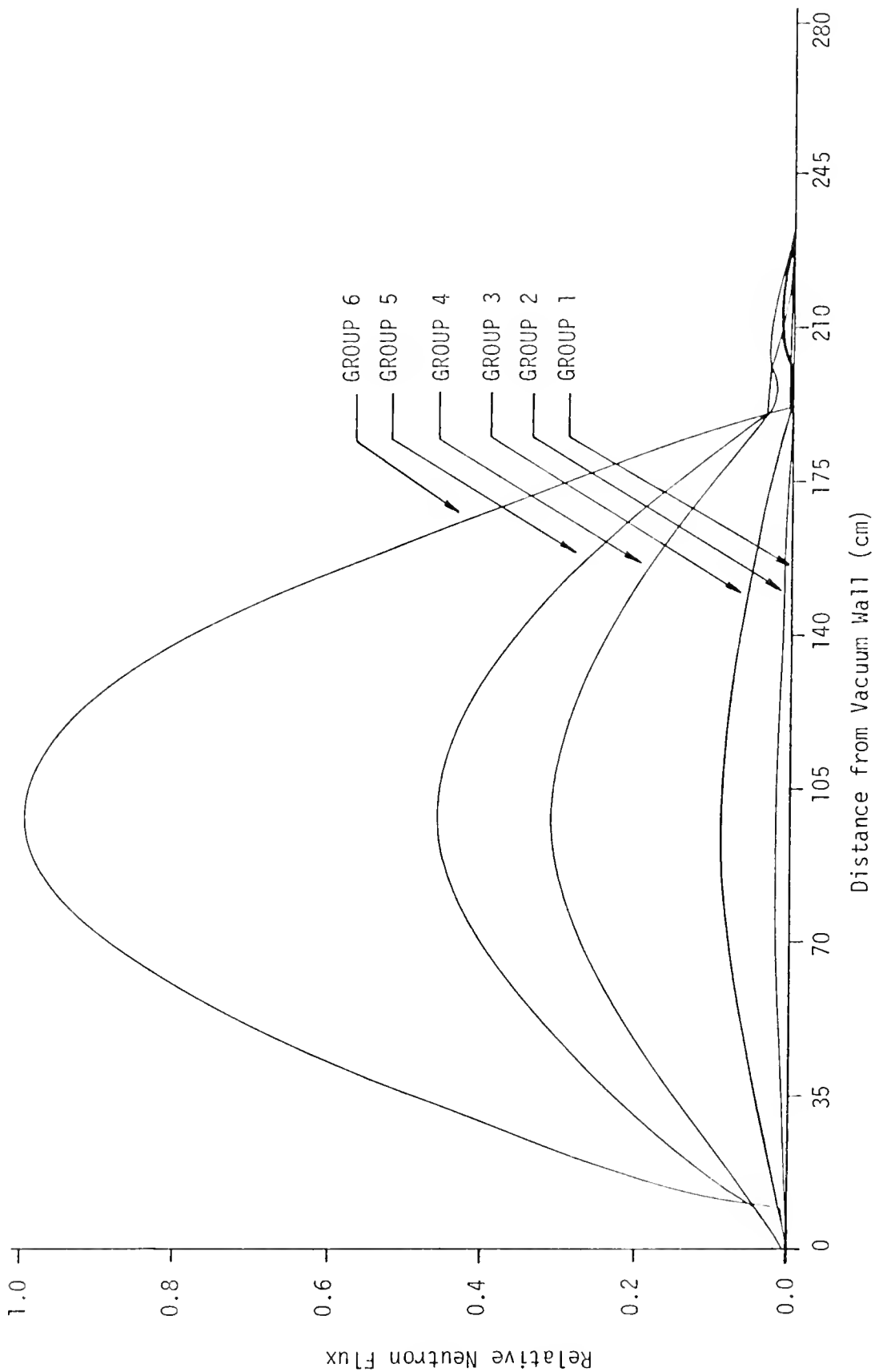
Figure 83. Six-group fundamental mode flux profiles from XSDRNPM for 1.35% enrichment at 900°K with zero-flux vacuum wall boundary condition.

Figure 84. Six-group fundamental mode flux profiles from XSDRNPM for 1.35% enrichment at 900°K with zero-flux vacuum wall boundary condition.

GROUP 6
GROUP 5
GROUP 4
GROUP 3
GROUP 2
GROUP 1

Distance from the Vacuum Wall (cm)

Relative Neutron Flux

lithium breeder region as well as the many orders of magnitude decrease
of all flux groups at 30 cm into the shield region. The large decrease
supplies the justification for neutronically treating only 30 cm of the
shield for flux and power calculations.

Inhomogeneous Transport Theory Calculations

The 6-group cross section library data generated by the series of
XSDRNPM calculations was used in an inhomogeneous calculation to determine
the size of the source necessary to produce 6500 MWth of blanket power.
Since k_{eff} = 0.9193, preliminary inhomogeneous calculations were run to
evaluate the average value of the neutrons per fission parameter as
follows:

$$\bar{\nu} = \frac{\sum\limits_{M=1,5} \sum\limits_{G=1}^{6} (\nu\Sigma_f)_{G,M} \; \phi_{T_{G,M}}}{\sum\limits_{M=1,5} \sum\limits_{G=1}^{6} (\Sigma_f)_{G,M} \; \phi_{T_{G,M}}} \tag{220}$$

where $\phi_{T_{G,M}}$ is the total flux in broad group, G, and fissioning region, M.
The resultant value of the average neutrons per fission, $\bar{\nu}$, for the 900°K,
1.35% enriched blanket is $\bar{\nu}$ = 2.607 which is relatively high versus the
usual thermal fission value of $\bar{\nu}$ = 2.433 calculated using the fundamental
mode flux shapes presented in graphical form in Figs. 83 and 84. For these
shapes, ∿ 44% of the inner convertor fissions were found to occur in
groups 1, 2, and 3, while only 1.15% of all fissions in the thermal
lattice occur in groups 1, 2, and 3. Overall for the fundamental mode
flux shapes, only 1.3% of all fissions occur in the top three groups which
contrasts markedly with the 13.4% in the top three groups when driven by

14 MeV neutrons entering from the vacuum wall. The increase is due to the effect of fissions induced by the 14.06 MeV fusion neutron source which produces about 4.47 neutrons per fission on the average in group 1 between 14.92 MeV and 13.50 MeV. The $\bar{\nu}$-value of 2.607 is elevated about 7% above thermal values showing the effect of energetic fission caused by fusion neutrons.

Further calculations on the inhomogeneous source problem using Eq. (220) indicated that $\sim$ 95.6% of all fissions in the inner convertor occur due to neutrons in groups 1, 2, and 3 above 0.82 MeV. In contrast, $\sim$ 1.63% of all fissions in the thermal lattice occur due to neutrons in these three highest energy groups.

At this point, the global blanket energy deposition relationship in Eq. (194) was utilized to estimate the size of the fusion neutron source required to produce 6500 MWth of blanket fission plus fusion neutron energy.

Since k_{eff} = 0.9193 and $\bar{\nu}$ = 2.607, Q_B = 857.0 MeV deposited in the blanket per entering fusion neutron, the vacuum wall source estimated was 5.342 x 10^{12} nts/cm^2 sec using the equivalent slab current relationship:

$$J_{14} = P_{TOT}/A_s \, Q_B \tag{221}$$

where J_{14} is the fusion neutron surface source at the vacuum wall and A_s is the previously defined equivalent slab wall area (A_s = 8.863 x 10^6 cm^2). The XSDRNPM-based prediction for the current source at 5.342 x 10^{12} nts/cm^2 sec was womewhat larger than expected because of the decrease in Q_B caused by the elevated value of $\bar{\nu}$ used to calculate Q_B. Nevertheless,

the fusion neutrons are much higher in energy than fission spectrum neutrons on which the global energy production formula is based. Instead of the large discrepancy between the expected source size requirement versus the much larger actual source required, it was expected that the source required to produce 6500 MWth should be very close or even smaller than the predicted value of 5.342×10^{12} fusion nts/cm^2 sec. Of course, the average energy in group 1 is ~ 13.8 MeV which is somewhat less than 14.06 MeV but still much above the 2 MeV average for fission spectrum neutrons.

The 6-group inhomogeneous source calculation in XSDRNPM indicates that, to get 6500 MWth of power produced in the blanket, the 14 MeV neutron current must be $J_s = 1.336 \times 10^{13}$ nts/cm^2 sec based on the XSDRNPM quoted average product of the macroscopic fission cross section and the total flux ($\Sigma_f \phi_T$) for each slab type fissile region. The flux shapes and magnitudes for this fusion source to produce 6500 MW are presented in Fig. 85, where the characteristic asymmetry is noted on the semi-logarithmic plots in all the epithermal groups. The group 1 flux is monotonically decreasing across the blanket because less than 0.01% of all fissions give neutrons in this top group ($\chi_1 = 9.14 \times 10^{-5}$); essentially all such neutrons originate in the fusioning plasma.

The resultant surface source conversion coefficient, ζ_1^{14}, is again given by

$$\zeta_1^{14} = \frac{J14_{EST}}{J14_{ACT}} \tag{222}$$

which yields, $\zeta_1^{14} = 0.400$, which still indicates that the fusion neutrons are not nearly as productive as the global energy deposition equation
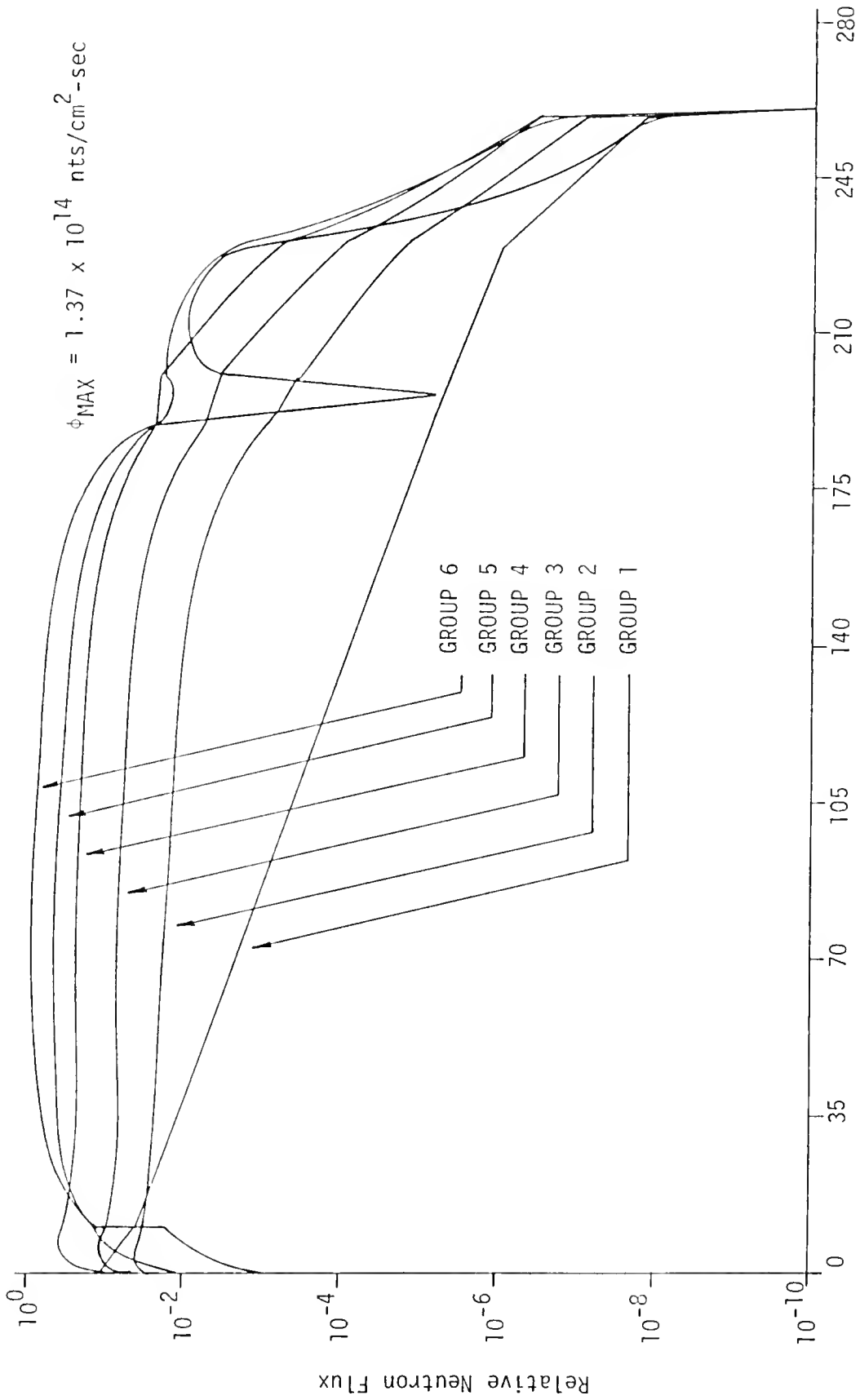
Figure 85. Six-group flux profiles for a surface source of 1.336×10^{13} nts/cm^2-sec in group 1 to generate 6500 MWth at 1.35% enrichment and 900°K.

implies. Even for 14 MeV neutrons, the coefficient, ς_1^{14}, is still considerably below unity. A further inhomogeneous calculation was performed to justify the reduced worth of 14 MeV neutrons.

A unit source of 14 MeV neutrons was input at the vacuum wall in group 1. By specifying a unity normalization factor, the transmission ratio for the group 1 neutrons was output as the region leakages in the XSDRNPM balance tables for the problem. These leakages or transmission ratios are presented in Table 5-XXX. Because less than 0.01% of fission neutrons are born into the first group, there is no problem with fission neutrons clouding the transmission properties of the blanket for the 14 MeV neutrons.

Table 5-XXX

Transmission Ratio for 14 MeV Neutrons Through the Hybrid Blanket

Region	Thickness (cm)	Fractional Transmission of Group 1 Neutrons
Inner Convertor	8.50	6.962×10^{-2}
Stainless Steel	0.25	6.651×10^{-2}
Lithium Breeder	1.00	6.315×10^{-2}
Stainless Steel	0.25	6.033×10^{-2}
Thermal Lattice	180.00	1.019×10^{-5}
Stainless Steel	0.25	9.722×10^{-6}
Lithium Breeder	9.50	5.939×10^{-6}
Stainless Steel	0.50	5.423×10^{-6}
Graphite	30.00	1.189×10^{-6}
Shield	30.00	1.547×10^{-8}

The transmission results of Table 5-XXX are plotted in Fig. 86 where the dramatic drop in 14 MeV neutrons after only 8.5 cm of the inner convertor is apparent. Only about 6% of the incoming 14 MeV neutrons ever
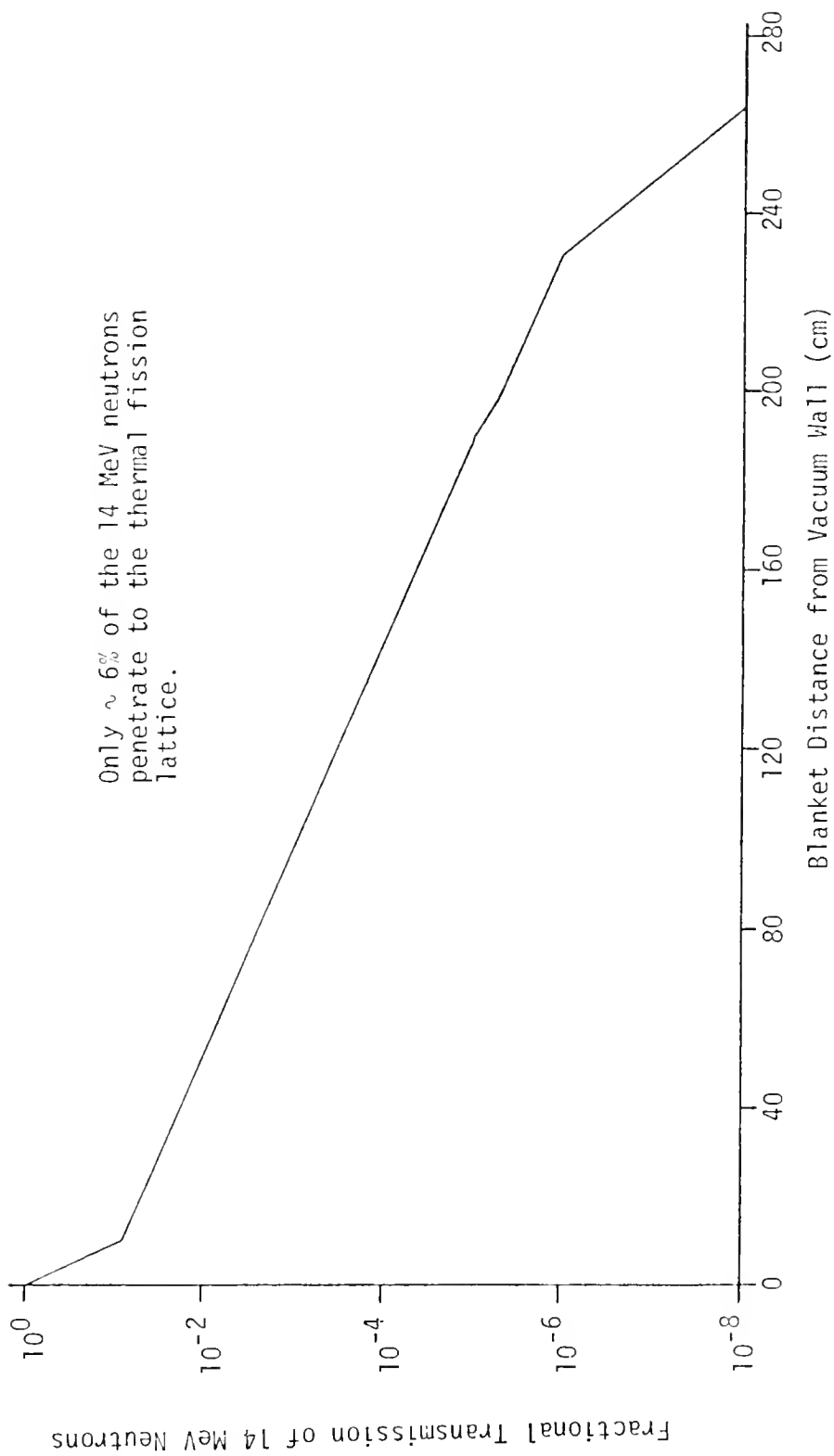
Figure 85.   Fractional transmission of 14 MeV neutrons through the hybrid blanket.

get to the thermal lattice where their high energy can be most effective at producing fissions and thermal energy. Based on the results of the transport calculation, the fusion neutron vacuum wall source was set at 1.336×10^{13} fusion nets/cm^2 sec.

Although much larger than the predicted value of 5.34×10^{12} nts/cm^2-sec, the current of 1.336×10^{13} nts/cm^2-sec corresponds to a fusion neutron wall loading of only 0.30 MW/m^2 as calculated in Appendix B. Such a wall loading is an order of magnitude or more below the wall loadings predicted for pure fusion systems.[33] The outage time and cost to replace the vacuum wall are predicted to be a primary problem in the implementation of pure fusion power. By using a Tokamak hybrid with such low wall loading, the problem with loss of vacuum wall integrity can be greatly reduced.

Time-Dependent Blanket Considerations

Since the 14 MeV neutrons are the power source for the hybrid blanket, the time-dependent analysis of the fission blanket was directed to account for the 14 MeV neutrons as accurately as possible. There were no point-model codes available for treating 14 MeV neutrons distinctly without subsuming them in inhomogeneous weighting factors. Therefore, the GAKIN II code[83] was used to obtain some useful information about the time-dependent characteristics of the blanket while retaining the spatial-dependence of the flux shapes.

The GAKIN II code was used since the most accurate data for the blanket was available from the P_2-S_4, 6-group XSDRNPM results. The constants from the XSDRNPM calculations were input to GAKIN II which is a

one-dimensional, multigroup diffusion theory kinetics code. The slab

geometry was again utilized and the source of 14 MeV neutrons was in-

corporated into a 0.23 cm thick volume element of equivalent intensity

at the vacuum surface, since GAKIN II cannot treat surface surfaces as

such. The objective of the GAKIN calculation was to examine blanket

time-dependent response times so the exact size of the source is not of

any concern. The relative behavior of the blanket and the time for

transients to occur is the primary interest.

The GAKIN II code uses a forced-critical system for all cases where

the values of $\bar{\nu}$ are adjusted by the code to establish a critical system

for which the fundamental mode flux shapes are calculated, but a series

of runs were made to determine the kinetic response of the hybrid blanket.

In general, it was found that the time for the fundamental mode fluxes to

evolve under an input of 14 MeV neutron source was $\lesssim 0.5$ seconds. In

other words, the blanket responds very quickly to plasma neutron pro-

duction rate changes.

For the forced-critical configuration, a relative unit source

($Q_u = 1.00$), inserted at time zero, yielded the blanket relative power

response shown in the lower curve in Fig. 87. The response consists of

the initial fast rise to a certain level followed by continued linear

growth of the power due to the source, given by a term proportional to the

product, $Q_u \cdot t$. In other words, the power in a forced-critical system

with a pure source inserted has the following power response at some time

after the initial transients have died away:[138]

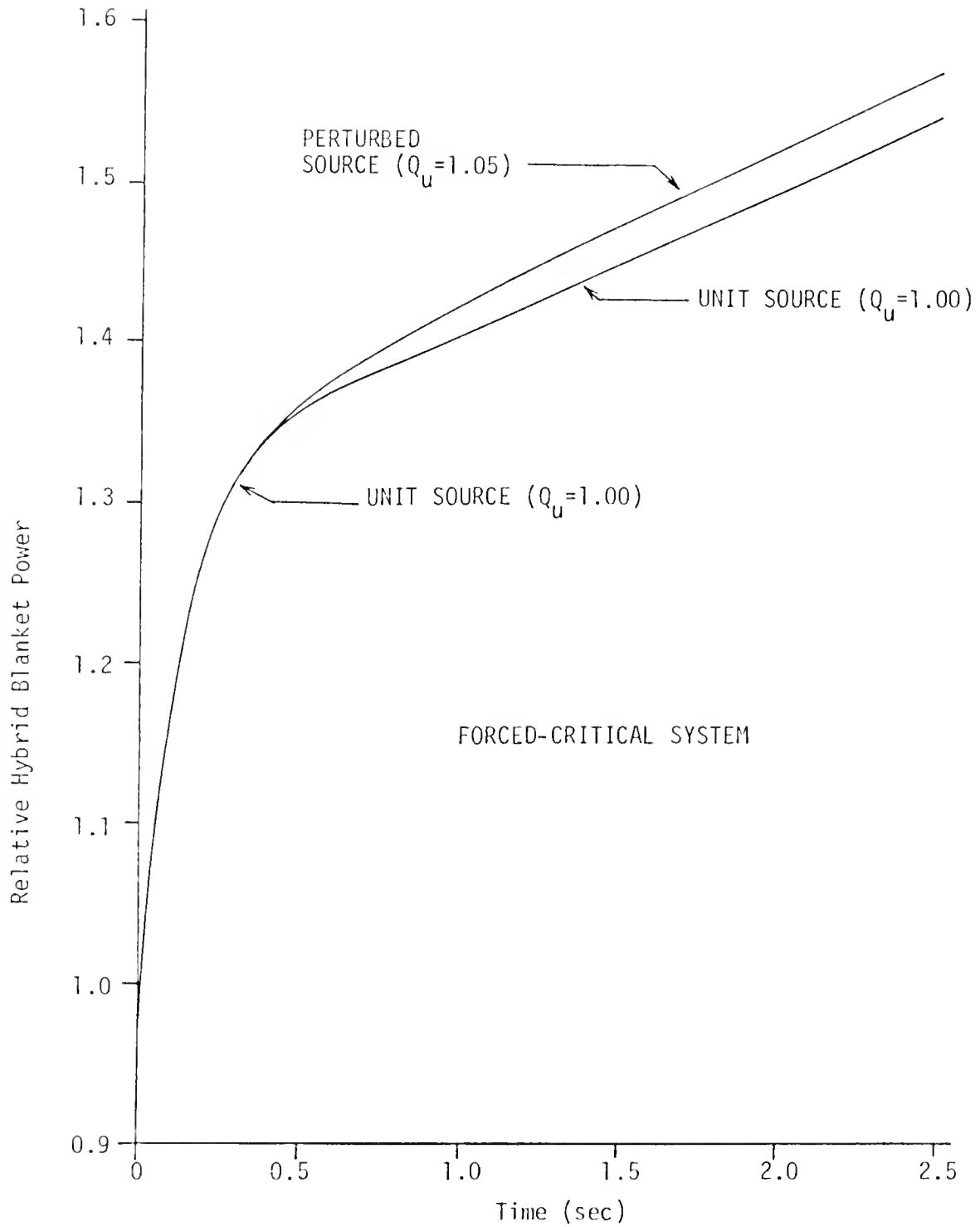$$P(t) = P_i + \kappa \cdot Q_u \cdot t \tag{223}$$

where

Figure 87.   Power transient in the hybrid blanket following a 5% step
increase in the neutron source for a forced-critical system.

$P(t)$ = power at time, t

P_i = power after initial transients have died away

κ = conversion coefficient

Q_u = relative unit source.

Of interest is the fact that the system requires approximately 0.5 second to reach an equilibrium-like condition where additional power growth is due solely to additional neutrons from the source adding to the power level through fissions, and not due to the initial multiplication and distribution of neutrons in the system. In other words, $\sim$ 0.5 seconds is required for the power to readjust to the source and continue growth at a reduced linear rate.

The initial jump is due to prompt neutrons generated by fission which make the system rise on a fast period due to prompt neutron multiplication on the time scale of the prompt neutron lifetime ($\ell_p \sim 10^{-3}$ sec) as presented in Table 5-XVIII. However, the system is exactly forced-critical so eventually, at $\sim$ 0.5 seconds, the delayed neutrons begin to hold the system back significantly.

Under the assumption that response times in the forced-critical blanket will be close to those for the actual blanket, the responses in Fig. 87 were separated to obtain those in Fig. 88. This was considered to be a reasonable assumption based on the value of k_{eff} = 0.919 for this blanket which means it is highly multiplying.[118] Therefore, its inhomogeneous flux shapes are not too different from those for a linear critical reactor such as analyzed by Fig. 87.

The curves in Fig. 88 represent the types of curves that are expected in subcritical systems which are driven by a neutron source. The curves
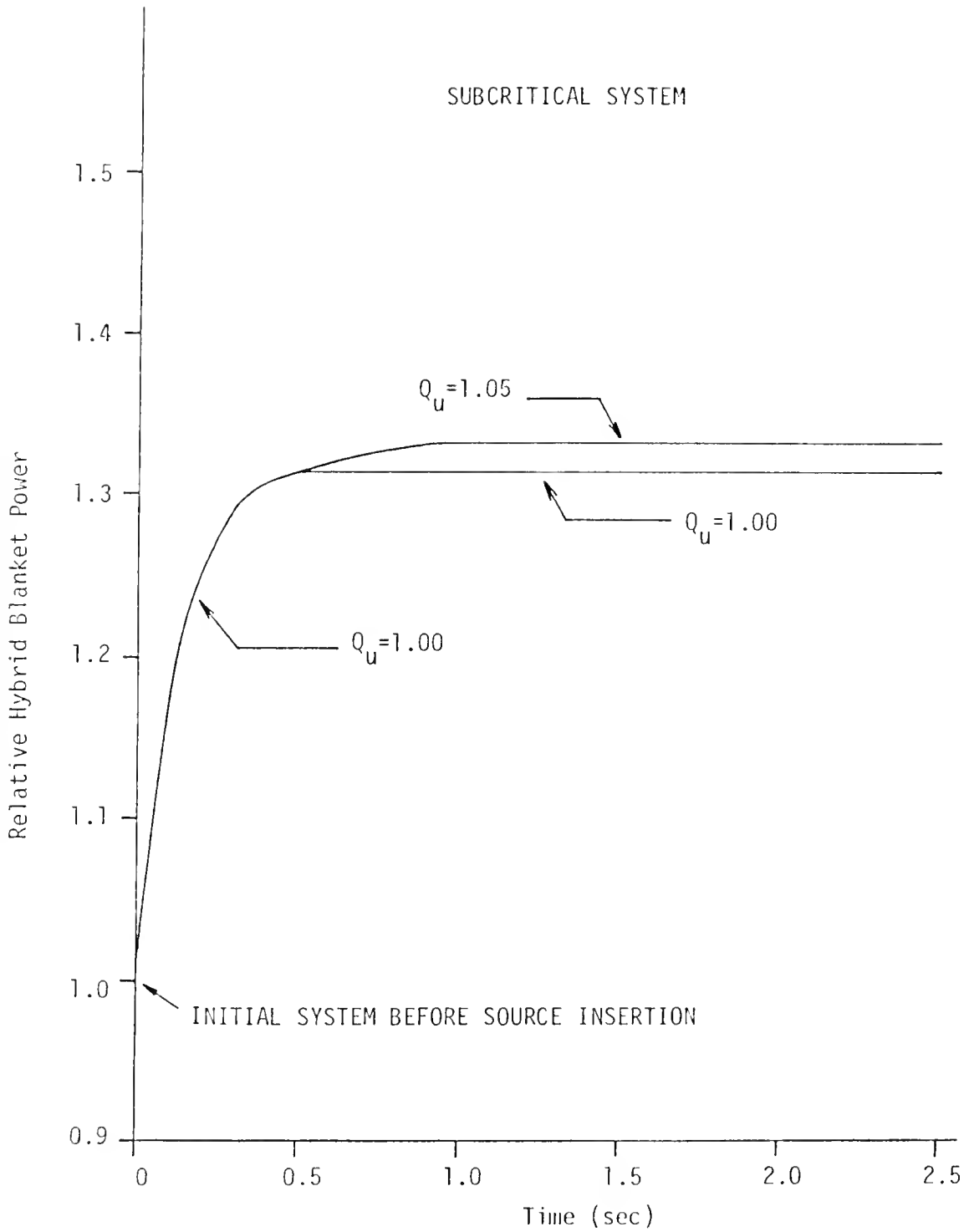
Figure 88. Hybrid blanket power transient derived for a subcritical system.

in Fig. 88 were derived by extrapolating the linear portions of the curves
in Fig. 87 back to time zero and subtracting the difference between the
extrapolated straight line and the actual curve. The steady-state value
was set at the relative power value where the transient power response
becomes negligible: $t = 0.5$ sec.

Because the blanket responds so quickly to neutron production rates,
the strong negative temperature coefficient can be used to control power
increases inherently. Monitoring of the blanket behavior in the form of
fuel temperature (or more directly, neutron density) can be expected to
allow feedback control of the plasma because the time for the plasma to
respond significantly to perturbations in feedrate is relatively long as
shown on Figs. 33-36 in Chapter 4. Even for direct 5% temperature per-
turbations, the initial instantaneous change, $\sim 15\%$, in neutron production
rates is followed by relatively slow changes in temperature and neutron
production rates as shown in Figs. 28-31 of Chapter 4. In fact, in some
cases examined in the time-dependent plasma calculations of Chapter 4,
the time for the plasma neutron production to change by more than 20%
was found to be on the order of 6-10 seconds. Therefore, the time should
exist for the final artificial safety or "emergency" feedback control of
the fusion-fission, point-model diagram in Fig. 19 of Chapter 3 to be
effective--at least, in forestalling significant overpower conditions in
the hybrid system.

The 6-group flux shapes presented in Fig. 85 for the 14 MeV neutron
driven blanket are still applicable for the small perturbations considered
here. Although perhaps not expected to be a safety-significant concern
for plasmas, the public and regulatory attitude toward nuclear energy

after the Three Mile Island Incident will necessitate such ultraconservative considerations for the hybrid or any other nuclear power system.

Even for decreases in plasma neutron production, the same feedback effect, either from the blanket temperature or neutron density, could be used to prevent significant decreases in plasma power production. Since the sensitivity of plasma neutron production to temperature changes is approximately 3 to 1 at hybrid temperatures of ~ 8.0 keV, as shown in Fig. C1 of Appendix C, the design overpower settings for hybrids may have to be large for initial jumps such as those associated with the +5% δT perturbations examined in Chapter 4 leading to 15% instantaneous increases in neutron production and thus blanket power. This overpower result assumes no doppler temperature feedback is effective in the blanket. However, beyond the initial hypothesized changes, the plasma responds slowly, particularly for lower confinement times such as 1.5-1.8 seconds, where the states with lower confinement times are stable. Even the unstable states undergo transients slowly enough to allow blanket feedback to implement control. Such states will undoubtedly be chosen for hybrid operation if possible.

The negative inherent blanket temperature feedback depicted in Fig. 76 can contribute to control power changes while preventing significant power increases over 115% of design power. The negative temperature coefficient ($\alpha_T \simeq 1.05 \times 10^{-4}$ $\Delta k/k/°F$), at 900°F indicates the potential for strong inherent feedback control.

One other point of time-dependent interest is hybrid reactor startup. The plasma must be heated from below neutron producing temperatures ($T \lesssim 1.0$ keV) up to plasma power conditions ($T \approx 8.0$ keV) in a very short time of less than a second because of plasma physics considerations.

Since the time response of the blanket is so fast, the blanket may have to go from essentially zero power to something over 30-50% power in no more than a few seconds. This could present significant material aging problems especially for load-bearing structures such as the magnet supports and the stainless steel blanket liners. There may be no definitive way to prevent such problems without periodic replacement of structures.

CHAPTER 6
CONCLUDING COMMENTS

Discussion and Conclusions

The investigation of neutrons and their associated energy multipli-
cation in the hybrid blanket of this study was very instructive. The
global equation currently used by some researchers to relate the blanket
energy multiplication to the blanket effective neutron multiplication
factor was investigated; the results obtained indicate the global approach
supplies a poor estimate of blanket energy multiplication for a fusion
neutron source and an even poorer estimate for fission energy neutrons.

Diffusion theory and discrete ordinates transport theory analysis
were both applied to establish the relative importance of the inner con-
vertor region for power generation. Although results indicate the blanket
energy deposition per fusion neutron to be some 60% below point-model
predictions, the selected blanket is still a significant multiplier, by
a factor of 25 or more, of the neutron energy entering the blanket via
fusion neutrons. The documentation of the reduced worth of fusion
neutrons, entering the blanket through a convertor region, may be a
significant factor in redesigning vacuum walls of hybrid reactors despite
the advantages of reduced 14 MeV wall loadings. There is obviously con-
siderable room for reevaluating the application of global values of k_{eff}
to estimate blanket energy deposition in hybrids.

The results of an S_n transport calculation showed that a 14 MeV source of 1.336×10^{13} nts/cm^2-sec is required by volume equivalence of a slab with the Tokamak geometry to produce 6500 MWth in the blanket. The source value was used to establish the steady-state requirements on plasma temperature and density from geometric considerations of the Tokamak hybrid plasma volume involved. In addition, the S_n calculation was used to show that only about 6% of the 14 MeV fusion neutrons reach the thermal fission lattice without a collision. These transmission results indicate graphically why the blanket is less effective at energy multiplication than expected from previous reports. These results also indicate why such very low energy multiplication values were found for fission energy neutrons.

The results of this work on fusion-fission hybrid reactors demonstrate that stability predictions for plasmas can be based on engineering considerations of linearized models. Arbitrary perturbations in the plasma feedrate were used to analyze the plasma in the frequency domain using transfer function analysis. Since the results of this method of analysis agree with previous work, the primary usefulness of the concept is its point-model application to the combined hybrid plasma blanket to demonstrate their reactive interdependence. The overall linearized hybrid model was developed and its stability was found to depend essentially on the plasma characteristics because of the inherent negative temperature feedback coefficient and subcriticality of the blanket. The model is interesting in that both the source and reactivity perturbations are retained in the blanket part of the model. Because of the unique characteristics of the hybrid system, the fissile blanket is both subcritical and power-producing. This model representation with both

perturbations retained is unique to the current hybrid study showing the hybrid component variable interdependence.

Since the blanket was found to depend inherently only on the plasma neutron production rate for the point-model plasma used in this study, artificial temperature feedback on the plasma feedrate was postulated using both the global plasma temperature and the global blanket temperature. Although plasma feedrate control using a signal from the plasma temperature will probably be used to control the power level in hybrid devices, re-dundant feedback may be needed. Although posutulated in Chapter 3, the blanket temperature may be too long acting for effective control. As pre-sented in Chapter 5, the neutron flux or power level was found to respond very quickly in less than 0.5 seconds to variations in plasma neutron production. Therefore, the results of this study indicate that the neutron density near the first wall could be used as a sensor for initi-ating the additional control on plasma transient response.

The Tokamak fusion-fission hybrid design was selected for further, more specific analysis. As indicated, more power was found to be possible at lower power density with the Tokamak fusion-fission hybrid reactor than with the PNL spherical system from which the model was derived. The emphasis was placed on total power production, not fuel production, which has turned out to agree with current recommendations for hybrid develop-ment.

The hybrid plasma selected was relatively nonreactive at a tempera-ture of only 8.0 keV and a density of 9.56×10^{13} ions/cm^3. The Tokamak plasma equilibrium conditions were reasonably chosen on the basis that a surface source of 1.336×10^{13} nts/cm^2-sec was required at the vacuum wall to produce the design power of 6500 MWth for a volume-conserved slab blanket.

The time-dependent analysis of the hybrid plasma, when subjected to small but significant ± 5% variations in state variables, does indicate a surprisingly slow response by the plasma. Previous analysis of transients in point-model plasmas has ignored the low-reactivity plasmas associated with hybrid systems. This work found that the plasma response to reasonable engineering perturbations in feedrate and temperature may be much slower than expected. Since plasma density variations are minimal, neutron production rates were found to follow temperature changes very closely. However, analysis indicated that relatively long intervals of 6-10 seconds were required for significant variation of neutron production rates beyond the equilibrium state in the case of a 5% feedrate perturbation or beyond the 15% change in neutron production level associated with direct 5% temperature perturbations. From such point-model hybrid plasma behavior, in contrast to highly-reactive pure fusion plasmas, the conclusion is drawn that control may be easier since more time is available for establishing control. Hybrid systems will always have to be designed for the initial transients associated with feedrate, temperature, or other perturbations. Control systems will never be able to prevent the immediate consequences of so-called design perturbations. However, as with LWR safety and control systems, the control systems from the hybrid plasma can be set up to prevent the continued growth of the transient with some delay time. Since the transients are slow growing and the blanket has a negative temperature coefficient, the design overpower condition can be much lower allowing steady-state operation at higher power densities than expected prior to the work discussed here.

Since the stability was found to depend strongly on the confinement time, the best possibility for control of hybrid reactor plasmas, and hence the entire blanket-plasma system, may be by control of the magnetic field. Therefore, the most important conclusion drawn from the results of this work is that the hybrid system can be controlled more easily than either of its derived components--pure fusion systems or fission reactors. This conclusion leads to the logical extension of the hybrid model to include magnetic effects on the plasma.

In the hybrid, the subcritical blanket depends on the plasma neutron production rate to produce power. Reasonably expected 5% perturbations in plasma state variables such as temperature have indicated the neutron production rates will vary no more than $\pm$ 15% instantaneously. For the plasma feedrate perturbation, the neutron production change is delayed. For either case, the variation for times following the perturbation was very slow for confinement times in the range from 1.5-1.8 seconds. Since larger confinement times resulted in fast plasma transients, the use of lower confinement times is recommended so that the plasma can be controlled, as indicated in Chapter 4, by artificial plasma temperature feedback on the feedrate.

The blanket was found to have the same steady-state flux distributions and power distributions regardless of the neutron-source intensity. Although this relative constancy of flux shape does not account for temperature effects, this does indicate very little flux shape change during the $\pm$ 15% instantaneous source perturbations expected for $\pm$ 5% perturbations in plasma temperature. During the subsequent slow variations in neutron production rate, the shape functions would be nearly constant. The space-time kinetics calculations demonstrated clearly the fast

response of the blanket in keeping with its millisecond prompt neutron lifetime and its subcriticality.

Provided the blanket system is designed for the initial 115% overpower condition (perhaps 120%), there should be no problem. As indicated in Chapter 5, current LWR's are usually designed for 110-114% overpower conditions. Therefore a small fractional increase should present no technological problems other than the possible loss in overall plant economics. Also, the negative temperature coefficient of the blanket is expected to further limit overpower transients as well as reductions in power.

Further investigations will determine exactly how much control is exerted by the negative temperature coefficient. Certainly, future extensions of this work should deal with setting up a multi-node blanket system so that the fuel, graphite, and helium regions of the unit cell can have separate temperatures. This will allow more realistic calculations of the feedback coefficient which were not warranted at this point. Although no time-dependent feedback effects were examined in the current effort, the speed of response of the system for typical perturbations in plasma neutron production rates shows that transients are very fast and that hybrid operational controllability must be based on plasma control as the driver of the system.

Suggestions for Further Work

To accelerate utility interest in the hybrid, its analysis must be relatively complete and realistic. The current work is only a beginning; more efforts to continue improvement of the steady-state model and associated calculations are needed. In addition, the new area of hybrid

dynamics and system interactions requires an accelerated research effort.

The best method for mocking up one-dimensional inhomogeneous hybrid blanket problems is one area in which considerable research is needed. Two possible methods can be used as the basis for determining the equivalent slab geometry for the source problems and associated power calculations.

First, inhomogeneous problems can be based on an equivalent surface source area where blanket fissile volume is conserved in the conversion from the toroidal to the slab system. This basis can be heuristically justified by the fact that fusion neutrons are driving the blanket through a surface so an equivalent surface source should be used to retain equivalence in the most important fusion neutron source. This method was used in the current work for the inhomogeneous source calculations since the neutron source is the driver for production of blanket power.

The alternative method is to base these calculations on an equivalent "volume" where essentially the blanket k_{eff} is conserved. If k_{eff} is the same then the power should be the same given the same current or source of neutrons in the same geometry. If k_{eff} is conserved from one geometry to the other, the surface areas will also need to be conserved or else the fusion source scaled up or down so that the same total number of neutrons are introduced per second. In going to the toroidal volume with lower surface area, a larger surface strength of neutrons is needed so the current should be scaled up to yield the same number of neutrons per second for approximately the same power. A toroidal shell is not exactly the same geometry but it is close in the thicknesses and radii considered

for hybrids. In addition, current results do indicate that the surface

conversion coefficient is extremely dependent on the source entry point

and k_{eff} so the results here may not be predictable.

Another area requiring additional work is the blanket neutronic

analysis. Higher order transport calculations are needed if such quanti-

ties as the tritium and fissile breeding ratios as well as the power

density distributions are to be calculated with the degree of accuracy to

justify utility investment in the Tokamak fusion-fission hybrid device.

One-dimensional, discrete ordinates calculations should be sufficient

but preferably in a P_3-S_8 calculation or even P_3-S_{16} for the inhomogeneous

source calculations for power-producing schemes. Otherwise, the approxi-

mations of the 14 MeV source in one of the quadrature directions may

yield misleading results. Such calculations will require a major commit-

ment of computer resources but are justified by the present results

showing the unexpectedly low worth of 14 MeV neutrons for power pro-

duction. The hybrid can be economically supported because it is not

dependent only on power density. Rather, it can produce fissile or

fusion fuel to offset the capital cost for power production. If such is

the case, then very accurate predictions of breeding ratios will be

needed based on more sophisticated transport theory analysis.

There is considerable room for improvement in the hybrid model.

Although not all aspects of the model were analyzed, it is apparent

that improvements to the model are needed. First, provisions should be

included to allow changing plasma volume with plasma temperature. This

could be incorporated by simply allowing the total number of ions in the

plasma to be the product of the variable ion density and the variable

plasma volume. To be more realistic, this will necessitate including

the magnetic field effects on the volume of the plasma, although the basic global or point-model characteristics can be maintained.

Essentially, the plasma model used for this study utilized density and energy (temperature) conservation equations. The additional requirement is a momentum conservation equation to allow direct incorporation of magnetic field effects on the plasma. Work in this area has indicated a tendency of the plasma to be more stable against perturbations. Such a situation for hybrid plasmas could have far-reaching implications for near-term development of the hybrid concept.

The treatment of plasma volume changes, especially expansions, is an improvement which will allow more realistic analysis of plasma transients as there will be a means within the model for self-stabilization. Beyond this relatively simple improvement, the treatment of spatially-dependent plasmas and even more complex confinement time formulations than the constant value considered in this work is a possibility. Until more information is available from plasma experiments, the latter complication would represent wasted effort, since the constant values for confinement time can be selected over ranges as was the case in this work.

Finally, additional work is needed to develop a multigroup point-model kinetics code for application to the subcritical but power-producing hybrid system. With the development of such a code, the full blanket heat transfer and feedback effects can be incorporated into the time-dependent analysis to obtain conservative but reasonably accurate predictions of hybrid behavior under transient conditions.

When these various extensions have been performed and the results analyzed, the Tokamak hybrid power-producing device will be much closer

to implementation in the electric power grid of this country. The current
work represents only the first step in the transient and stability
analysis required to meet this objective.

APPENDIX A

GLOBAL BLANKET ENERGY MULTIPLICATION

There is considerable confusion in the literature over the adequacy
and applicability of the lumped-parameter equation for the hybrid blan-
ket neutron energy multiplication. The blanket neutron energy deposition
factor is essentially the energy deposited in the hybrid blanket per D-T
fusion reaction occurring in the plasma:

$$Q_B = \frac{G_f}{\bar{\nu}} \left(\frac{k_{eff}}{1-k_{eff}} \right) + E_n + \delta_E \tag{A1}$$

where terms are defined in Chapter 1 following Eq. (16). Some studies
have even neglected the last two terms.[76]

This equation is strictly global in nature; it lacks adequate space
and energy dependence to describe the actual blanket energy deposition
adequately. The formula in Eq. (A1) was derived in several steps assum-
ing a point-model blanket and beginning with the following conservation
equation written for blanket neutrons:

$$
\begin{array}{ll}
\text{Total Number} \\
\text{of Neutrons} \\
\text{in the Blan-} \\
\text{ket per Enter-} \\
\text{ing Fusion} \\
\text{Neutron}
\end{array}
=
\begin{array}{l}
\text{One Fusion Neutron} \\
\text{per Fusion Event}
\end{array}
+
\begin{array}{l}
\text{Fission-Born Neutrons} \\
\text{per Fusion Event}
\end{array}
$$

$$= \quad [\,1\,] \quad + [k_{eff}{\cdot}1 + k_{eff}{\cdot}k_{eff}{\cdot}1 + ...] \tag{A2}$$

$$\text{Number of Neutrons} \quad = \quad 1 \quad + \quad \frac{k_{eff}}{1-k_{eff}} \tag{A3}$$

where the assumption of blanket subcriticality ($k_{eff} < 1$) has been used.

The energy deposition per entering fusion neutron, Q_B, was then derived by multiplying each neutron by its associated energy as follows:

| Energy Deposition per Fusion Reaction | = | Energy of the Fusion Neutron | + | Energy Deposited from Fissions | . (A4) |

The formula for the energy deposition per fusion neutron becomes

$$Q_B = E_n + \frac{G_f}{\bar{\nu}} \left(\frac{k_{eff}}{1-k_{eff}} \right) . \tag{A5}$$

To be more accurate, an extra δ_E-term was added as described in Chapter 3 to account for exothermic reactions caused by neutron absorption so that the relation for the energy deposition per fusion neutron becomes:

$$Q_B = \frac{G_f}{\bar{\nu}} \left(\frac{k_{eff}}{1-k_{eff}} \right) + E_n + \delta_E . \tag{A6}$$

For a typical hybrid blanket and fusion neutron source in which lithium is present for breeding, the exothermic ${}_0^1n({}_3^6Li,{}_2^4He){}_1^3T$ lithium reaction in which 4.8 MeV is released, was used to justify the δ_E-term at about 5.0 MeV.

The reason Eq. (A6) is adequate is now apparent. It is global. No account has been taken of where the fusion or other source of neutrons is introduced into the blanket with respect to position or energy. The derivation assumed that the neutron was introduced into a blanket with effective neutron multiplication factor, k_{eff} near unity. But this assumption is only valid if neutrons are introduced inhomogeneously with the energy spectrum associated with the fission source neutrons used in calculating the blanket k_{eff} value. Neither of these assumptions is true for a fusion neutron surface source or most other sources.

First, the D-T fusion neutron energy is monoenergetic at 14.06 MeV and not a fission spectrum with average energy about 2.0 MeV. Weighting

the calculation of $\bar{\nu}$ to account for the effect of energy dependence in the flux and reaction rate was used as reported in Chapter 5 to account partly for the energy dependence, but only approximately.

Second, the fusion source is introduced very asymmetrically at the vacuum wall. In most hybrid concepts, including the one in this work, neutrons introduced in this poorly multiplying first region separated from the primary thermal lattice have reduced worth. Therefore, the global representation of Eq. (A6) can be expected to overpredict the blanket neutron energy multiplication as demonstrated by the results of Chapter 5.

Estimates of blanket neutron energy multiplication may be obtained using Eq. (A6). However, the results obtained are not reliable unless a space-and energy-dependent calculation has been run to test its adequacy. In such a case, there is less need for the global calculation of Eq. (A6) at any rate despite its frequent application to support hybrid analyses.[64,76,77] The relationship in Eq. (A6) can be useful for a quick estimate of the energy multiplication potential of hybrid blankets where the blanket energy multiplication per source neutron, M_B, is given by

$$M_B = Q_B/E_n \; . \tag{A7}$$

Such estimates are useful for conceptually demonstrating the power potential of hybrids given a fusion source of neutrons. Any great accuracy in the predictions obtained using Eqs. (A6) and (A7) would be strictly fortuitous.

APPENDIX B

HYBRID SYSTEM PHYSICAL CHARACTERISTICS

The Hybrid Blanket Geometric Arrangement and Constituents

The PNL hybrid blanket geometry and constituents were used as the basis for the hybrid blanket analyzed in this work.[64] The basic fissile blanket design was selected as a composite convertor-lattice blanket based on previous work.[55,56,51,64] The characteristics of the blanket design are described here in sufficient detail to indicate applicable sizes, densities, and other input to support blanket and plasma neutronic calculations.

Since the energy-producing portion of the hybrid Tokamak plasma was assumed toroidal for better total power production, the blanket geometry was selected as a toroidal shell; an overall perspective of the hybrid reactor system as a compact torus is depicted in Fig. B1. The chosen model design is based on PNL efforts to optimize the blanket with respect to neutron multiplication and energy production. However, PNL efforts have been directed to spherical mirror plasmas and hence spherical blanket shells versus the toroidal shell used here.[64] The basic regions of the blanket are depicted in Fig. B2 where the regions are shown in physical relation to each other in the following order: the vacuum wall defining the plasma, the inner convertor region, the inner breeder region, the thermal lattice region, the outer convertor region, the graphite reflector, and the composite shield.

TOKAMAK HYBRID

HYBRID PLASMA
VACUUM WALL
INNER CONVERTOR
THERMAL FISSION
OUTER CONVERTOR
REFLECTOR
SHIELD
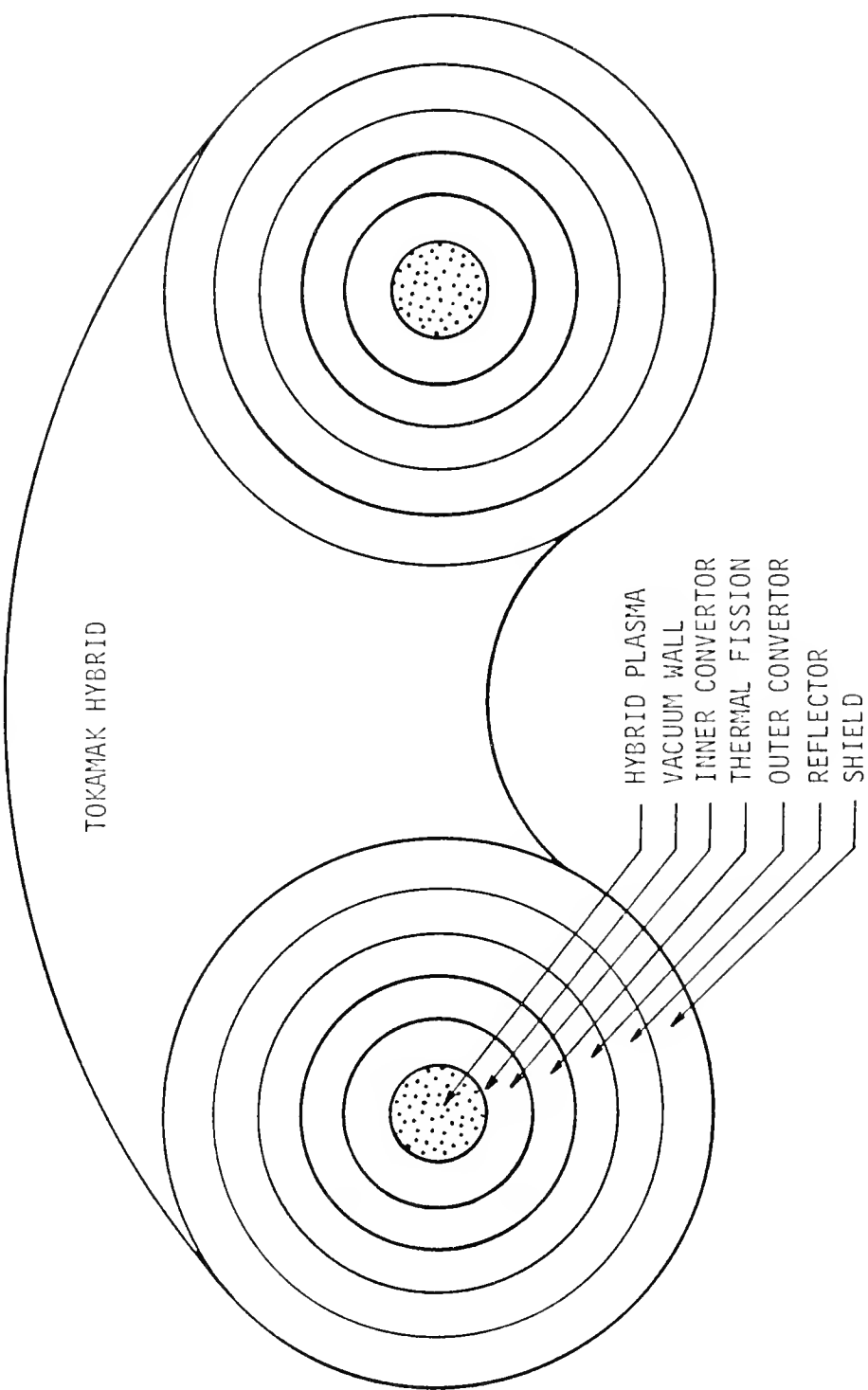
Figure B1. Conceptual Tokamak fusion-fission hybrid reactor system.

- 371 -

VACUUM WALL

INNER CONVERTOR	INNER BREEDER	THERMAL FISSION* LATTICE	OUTER BREEDER	GRAPHITE REFLECTOR	COMPOSITE SHIELD
8.5 cm	1.5 cm	180.0 cm	10.0 cm	30.25 cm	30.0 cm
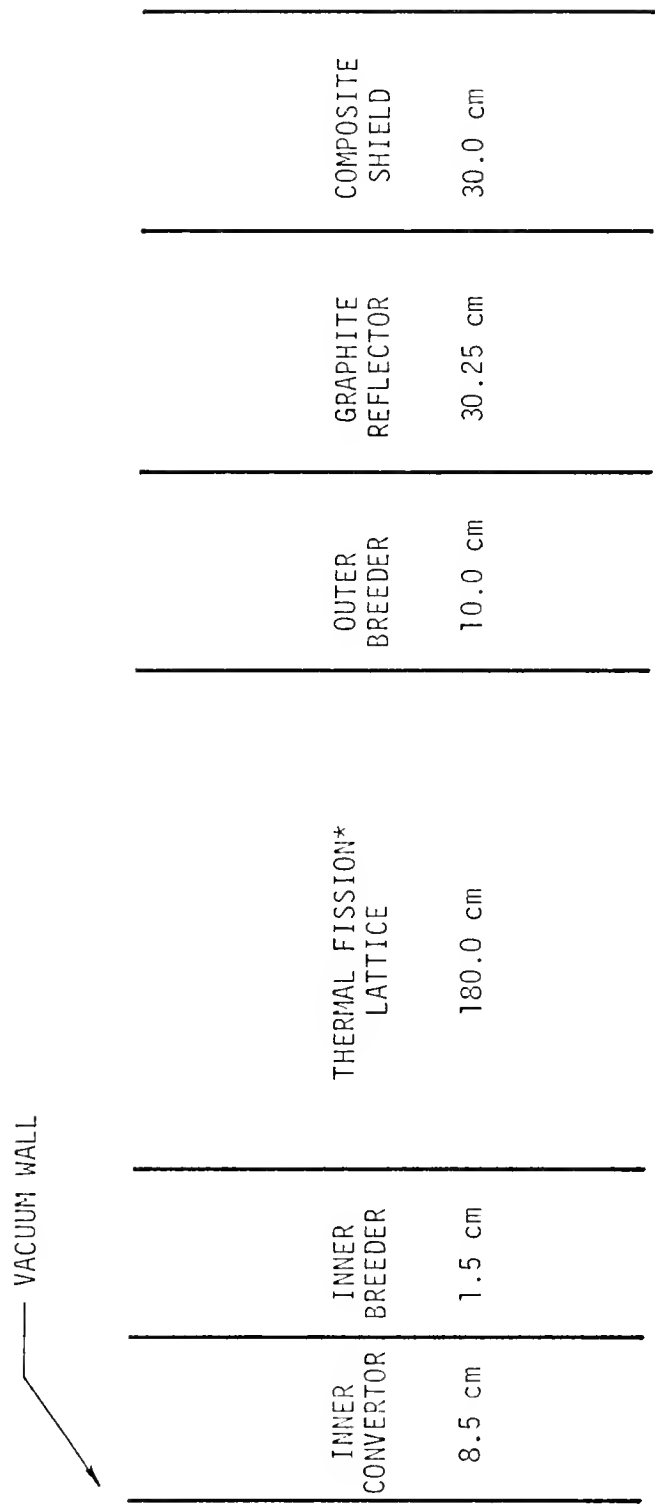
*Regions are not presented to scale.

Figure B2. Overall hybrid blanket slab geometry used in neutronics calculations.

In the hybrid design, the vacuum wall or first wall is the confining boundary for the fusioning plasma. Because the vacuum wall will be subjected to the effects of the 14.06 MeV current of neutrons leaving the plasma, its predicted useful lifetime is an important consideration for fusion and hence hybrid economics and technology. The 8.5 cm thick inner convertor region contains the vacuum wall together with depleted uranium, coolant and structure. The inner convertor region was included in the design to produce fission neutrons efficiently from fusion neutrons but was found to be less efficient than earlier studies have indicated.[1,64] The 1.5 cm thick inner breeder contains natural lithium which was included to breed tritium fuel for the plasma, primarily in the fast neutron inelastic scattering reaction with ^{7}Li.

The 180 cm thick thermal lattice was selected to act as a highly multiplying, neutronically thermalized region in which the majority of the blanket neutron energy multiplication occurs. This is the primary power-producing region and contains the slightly enriched fissile fuel.

The 10 cm outer breeder contains natural lithium which was included to breed tritium. However, since the outer breeder in the design is located external to the thermal lattice, the primary tritium breeding reaction is the slow neutron absorption reaction with ^{6}Li. The 30.25 cm thick graphite reflector region was included to reduce neutron leakage from the thermal lattice and outer breeder regions to enhance neutron multiplication.

Finally, the composite shield region was incorporated to prevent streaming neutrons and other energetic particles, as well as electromagnetic radiation and heat, from reaching the confining magnet system and depositing energy in the magnets. The shield was designed to be about

100 cm thick because a unit of energy entering the supercooled magnets may require as much as three hundred times more energy to be removed at the cryogenic temperatures involved.[30] However, only 30 cm of shield was included for the neutronic calculations in this study. Since the thickness was found to be sufficient to reduce the neutron level over five orders of magnitude, the assumption of a 30 cm shield for neutronics calculations was validated.

As in the PNL design, the power-producing blanket regions, which are 200 cm thick including the outer breeder region, were assumed to be constructed of modules. Each blanket module consists of an equilateral triangular prism as depicted in Fig. B3. In the design a module is made up of many smaller equilateral triangular prisms which constitute the usual unit cells associated with power reactors. A unit cell consists of one fuel element with its coolant and moderator and is the smallest repeating unit in the blanket design.

The fission technology selected for the lattice region of the blanket is a modification of the HTGR fuel lattice.[68,139] The lattice was selected for the PNL hybrid lattice based upon its low neutron absorption, the apparent compatibility of gas coolant with fusion reactor blankets, and the self-shielding properties of the particle fuel.[64] The fuel itself consists of coated spherical UO_2 microparticles extruded into cylindrical columns with 0.635 cm radii and loaded into a graphite matrix containing helium coolant channels with 0.825 cm radii. A detailed description of the unit cell showing fuel rod and coolant channel placement is depicted in the module geometry of Fig. B3. Essentially, the fuel pin separation was fixed at 3.81 cm on a hexagonal pitch with triangular unit cells. The equivalent cylindrical unit cell radii are listed in Table B-I.
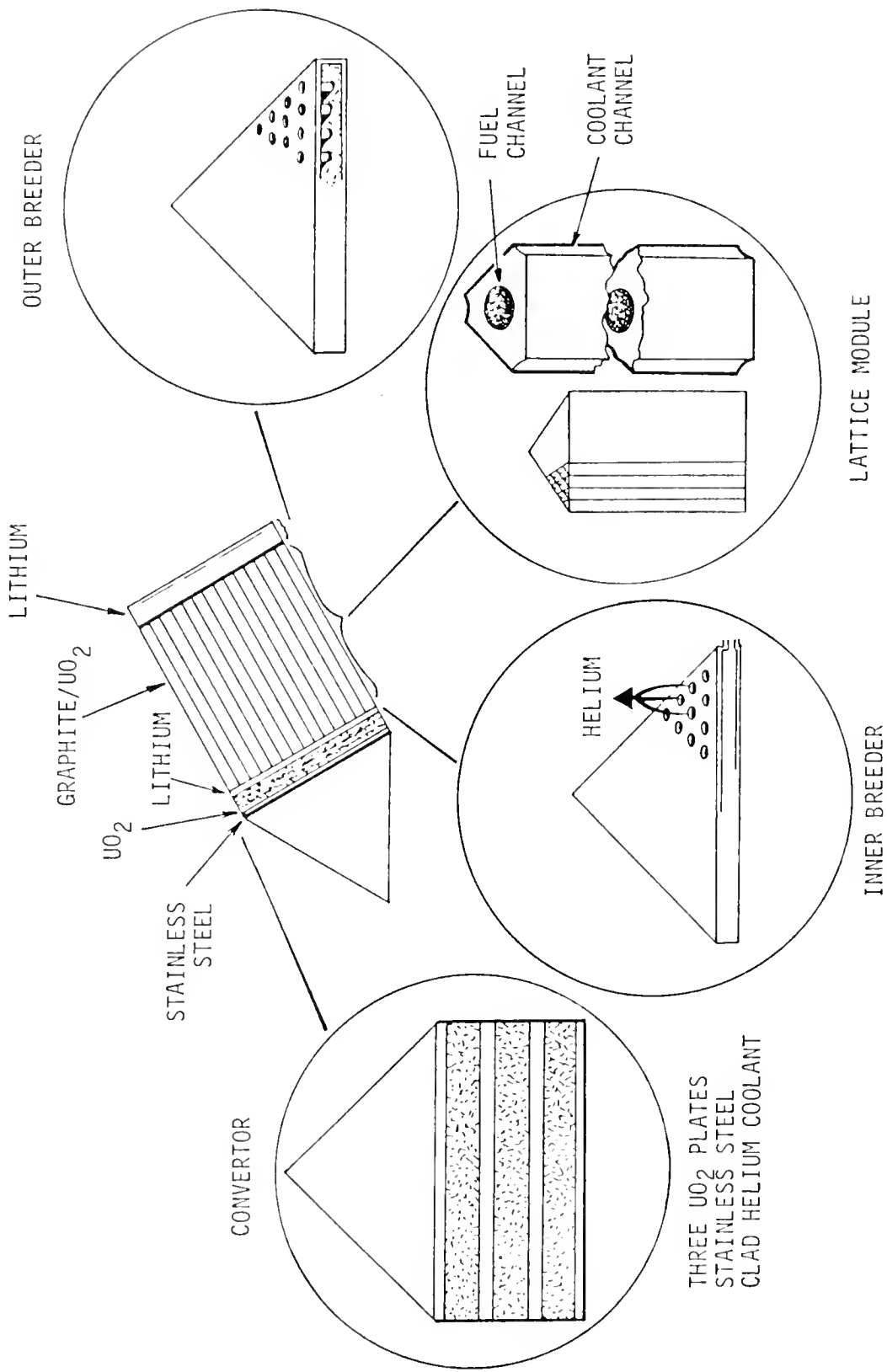
Figure B3.   Selected PNL hybrid blanket module geometry for Tokamak fusion-fission hybrid.

Table B-I

Hybrid Blanket Equivalent Unit Cell Geometry

Unit Cell Region	Region Outer Radius	Unit Cell Volume Fraction
Fuel Column	0.635 cm	0.0672
Graphite	2.38 cm	0.8761
Helium	2.45 cm	0.0567

The actual triangular unit cell is shown to full scale in Fig. B4(a). The equivalent cylindrical unit cell used in neutronic calculations is shown in Fig. B4(b). The geometry summary in Table B-I shows that the cell is primarily graphite so the system is well-moderated. Although the equivalent unit cell differs considerably from a triangle, it was selected as the best available model for input to standard codes for neutronic analysis.

The 1030 μm particle design was also selected in agreement with PNL scoping studies to achieve maximum self-sheilding of the ^{238}U resonances.[64] This is the largest particle size available with current technology. A detailed description of the particles is given in Table B-II. The microspheres were also assumed to fill the fuel column with a 0.60 packing fraction to reduce further the fuel loading per unit cell. All unit cell physical parameters such as number densities were calculated using the descriptions presented here.

The fuel pin averaged nuclide number density for the nuclides represented in the materials included in Table B-II are presented in Table B-III. All densities were assumed temperature independent. These densities were used as the basis for the neutronic calculations presented in Chapter 5.
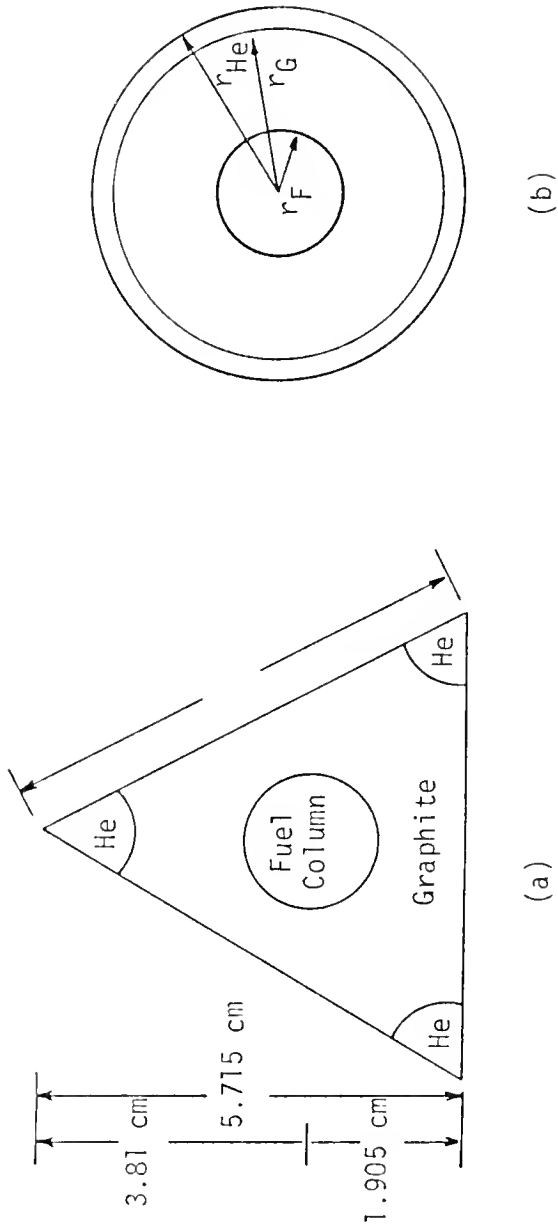
Figure B4. Hybrid thermal fission lattice unit cell: (a) actual full size equilateral triangle unit cell; (b) equivalent cylindrical unit cell with fuel outer radius, r_F, graphite radius, r_G, and helium radius, r_{He}.

Table B-II

Fuel Column Spherical Microparticle Design Parameters

Microregion	Material Content	Microregion Outer Radius (μm)	Material Density (gm/cm^3)
1	UO_2	375	10.5[140]
2	Porous Pyrolitic Carbon	50	1.70[141]
3	High Density Isotopic Carbon	20	2.20[141]
4	SiC*	465	3.217[142]
5	High Density Isotopic Carbon	515	2.20

*The SiC was included for fission product retention.

For the neutron inner convertor, a special fuel design was used. The convertor region is intended to have relatively few fissions but high fissile fuel breeding so a heavy fertile fuel loading is desirable to take advantage of breeding potential. Therefore, a convertor design was selected consisting of alternate plates 2 cm thick of depleted UO_2 (0.2% ^{235}U) clad with 0.1 cm of stainless steel and utilizing low-absorption, 0.8 cm helium coolant gaps. This inner convertor region is depicted in Fig. B5(a) as labeled but not to scale.

A useful hybrid should also be able to breed tritium so a 1 cm thick inner breeder region of natural lithium clad with 0.25 cm of stainless steel was included as shown in Fig. B5(a). The overall geometric arrangement of the inner convertor and inner breeder is shown in Fig. B5(a) for the total 10 cm thickness.

The outer breeder region was also designed with natural lithium for breeding tritium from neutrons leaking from the thermal lattice. The

Table B-III

Temperature-Independent Fuel-Pin-Averaged
Nuclide Number Density Variation
with Enrichment

Enrichment (Weight %)	Nuclide Number Density* (atoms/b-cm)
0.20	$N_{235} = 0.00001099$
	$N_{238} = 0.0054132$
	$N_{0} = 0.01085$
	$N_{Si} = 0.002638$
	$N_{C} = 0.03463$
0.711	$N_{235} = 0.00003906$
	$N_{238} = 0.005370$
1.00	$N_{235} = 0.00005493$
	$N_{238} = 0.005370$
1.20	$N_{235} = 0.00005493$
	$N_{238} = 0.005359$
1.35	$N_{235} = 0.00007416$
	$N_{238} = 0.005351$
1.50	$N_{235} = 0.00008240$
	$N_{238} = 0.005343$

*Note that the number densities of oxygen, N_0, silicon, N_{Si}, and graphite, N_C, remain essentially unchanged for all enrichments of interest in the fusion-fission thermal hybrid blanket; similarly, the number density of ^{238}U as N_{238} does not change appreciably while that of ^{235}U as N_{235} does vary with enrichment as expected.

INNER CONVERTOR WITH INNER BREEDER*

SS	UO$_2$	SS	He	SS	UO$_2$	SS	He	SS	UO$_2$	SS	SS	Li	SS
0.25	2.00	0.10	0.80	0.10	2.00	0.10	0.80	0.10	2.00	0.25	0.25	1.00	0.25

(a)

OUTER BREEDER*

0.25	9.50	0.25
SS	Lithium	SS

(b)

*All region thicknesses are in units of cm.

Figure B5. Geometric arrangement of the (a) inner convertor with inner breeder and (b) outer breeder.

10 cm thick outer breeder was designed with 9.5 cm of lithium clad again with 0.25 cm of stainless steel for structural support as illustrated in Fig. B5(b). The 30 cm graphite reflector region also contains an additional 0.25 cm of stainless steel clad on the inside for structural support.

Finally, a composite shield was included as part of the blanket design required to protect both people and the magnet system. Although about 100 cm of shield are required, the shield neutronic effects were adequately modeled by considering only 30 cm of shield thickness. The shield composition assumed for this work was not considered crucial; structural strength was required so 304L stainless steel was selected; thermal neutron absorption was supplied by boron carbide, B_4C; and moderating ability to promote thermal absorption was assured by including zirconium hydride, ZrH_2. Finally, additional moderation was obtained using graphite, C. The composite shield fractional composition was assumed to be essentially unchanged with temperature as listed in Table B-IV which also contains elemental number densities.

Table B-IV

Hybrid Blanket Shield Composition

Blanket Material	Volume Fraction	Elemental Constituents	Shield-Averaged Nuclide Number Density (atoms/b-cm)
304L SS	0.40	Fe	0.02444
		Cr	0.006824
		Ni	0.00344
		Mn	0.000688
Z_rH_z	0.32	Zr	0.012
		H	0.024
C	0.25	C	0.02215
B_4C	0.03	B	0.003296
		C	0.000824

The only additional data required to define the physical character-
istics of the blanket are the densities of various elements used in the
different regions not yet treated. For the 204L stainless steel, the
number densities were assumed to be independent of temperature for the
iron, nickel, chromium, and manganese nuclides as follows: N_{Fe} = 0.0611
atoms/b-cm, N_{Ni} = 0.0086 atoms/b-cm, N_{Cr} = 0.01706 atoms/b-cm, and N_{Mn} =
0.00172 atoms/b-cm.[143] For the graphite a temperature-independent dens-
ity of 1.7 gm/cm^3 was used which yielded a number density of N_C = 0.08532
atoms/b-cm.

Table B-V

Helium and Natural Lithium Number Density Variation
with Temperature

Temperature ($^\circ$K)	Helium Density* (atoms/b-cm)	Lithium Density** (atoms/b-cm)
290	0.0005164	0.04634
570	0.0002627	0.04328
800	0.0001872	-------
838	0.0001786	-------
900	0.0001664	0.04080
970	0.0001544	0.04024

*All values are for constant 300 psia pressure.
**Lithium atom density values are based on lithium at 92.44% ^{6}Li and 7.56%
^{7}Li.

The only densities which are temperature-dependent are those for
the natural lithium breeding regions and the helium cooland regions.
Helium coolant densities for the 300 psia preliminary design pressure were
calculated from standard tables and supplied sufficient accuracy.[144]

Adequate lithium densities were also obtained from tabular references as a function of temperature.[142] Lithium and helium atom densities are tabulated in Table B-V for those temperatures applicable for the hybrid blanket neutronics calculations.

All number densities for the various blanket neutronics analysis codes were calculated using this basic information and appropriate one dimensional slab geometry. All calculations were also based on a global average blanket temperature.

The Hybrid Plasma Geometry

The remaining geometrical feature of the hybrid system is the plasma size which is needed to establish the plasma fusion neutron source strength and to assure a reasonable system geometry. Essentially, a homogeneous, toroidal-shaped plasma was assumed whose volume, V_p, is given by

$$V_p = \pi r_p^2 \cdot 2\pi R_T \tag{B1}$$

where r_p is the effective plasma radius and R_T is the major radius of the toroidal plasma.

In agreement with fusion power plant design studies, the homogeneous plasma was assumed to extend effectively over 90% of the minor radius of the torus so that

$$r_p = 0.9 \, r_i \tag{B2}$$

where r_i is the minor radius (to the vacuum wall) of the toroidal hybrid device. Next, a safety factor, q_ι, was chosen where the safety factor is defined as follows:

$$q_\iota = R_T/r_i \, . \tag{B3}$$

A safety factor of 3.0 was selected to give good plasma stability as well as space inside the torus for the blanket shield, magnets, coils, structure and wiring associated with the system.

The overall hybrid blanket power density was also factored into geometrical considerations. The blanket power density should be set as high as practicable, but there are restrictions due to the geometry involved and the placement of the driving source of fusion neutrons. The blanket fissile or power-producing volume is limited to the 190 cm of blanket inside the outer lithium convertor region. The volume of the power-producing toroidal blanket shell, V_{BF}, is given by Eq. (B4):

$$V_{BF} = \left[\pi r_o^2 - \pi r_i^2 \right] 2\pi R_T \tag{B4}$$

where r_o is the outer radius from the plasma center to the outer edge of the thermal fission lattice so that

$$r_o = r_i + 190 \text{ cm} . \tag{B5}$$

Previous work on the spherical hybrid system has predicted power densities of about 4.6 W/cm^3.[64] Therefore, a similar quantity was the objective of the toroidal blanket design although much more total power will be possible than in a spherical system with the same plasma radius.

Possible selections for vacuum wall radius and the attendant fissile power-producing blanket volumes are tabulated in Table B-VI. As shown in column 1, the power-producing blanket volume increases geometrically with increasing vacuum wall radius. The consequence of the geometry involved is that large plasmas are forced to have lower power densities but larger total powers. This situation will prevail until very large central station power ratings are needed.

Table B-VI

Effects of Vacuum Wall Radius on Blanket Power
Requirements and Power Density

Vacuum Wall Radius (cm)	Fissile Volume $(\times10^{-9})(cm^3)$	Blanket Power Rating (MWth)	Fissile Blanket Power Density (W/cm^3)
150	0.83	2500	3.02
180	1.11	5000	4.49
200	1.33	5000	3.77
310	1.44	5500	3.82
220	1.56	5500	3.53
220	1.56	6000	3.85
220	1.56	6500	4.17
230	1.68	5500	3.27
230	1.68	6000	3.57
230	1.68	6500	3.86
240	1.81	6500	3.59
250	1.94	6500	3.35
270	2.22	6500	2.93
300	2.67	6500	2.44

In Table B-VI, the cases for the smaller vacuum wall radii indicate
insufficient room for placement of the entire blanket, shield and magnet
system inside the toroidal ring. In order to obtain a power density near
the desired 4.6 W/cm^3, a total power production of 6500 MWth was selected
with the vacuum wall set at r_i = 230 cm. The resultant power density of
3.86 W/cm^3 is reasonably close to the desired value and the 6500 MWth
power rating may be useful in taking advantage of the expected economy of

scale. Larger power ratings will limit the hybrid usefulness for most utility systems, although energy requirements to run magnets and inject particles will need to be considered in any final design.

The attempt was made to maximize the blanket power density since the larger inner convertor blanket power densities of pure fusion machines do not apply so strongly to hybrids. The power is still peaked in the first wall regions but not so sharply because much power is produced in the thermal lattice. To maximize power density, the vacuum wall radius and the major radius of the torus must both be minimized within technical limits. However, space within the center of the torus is proportional to the major radius and must be sufficient to permit magnet placement and cooling along with shielding installation. Since the major radius varies with the vacuum wall radius through the safety factor, it must be large enough to allow such room. This requirement contrasts with the blanket volume design criterion of maximizing power density by minimizing size. Since the two design objectives are contradictory, an engineering tradeoff was made to produce a reasonably attractive hybrid blanket. The reduction of size for such hybrid designs from early pure fusion designs along with the maximized power density are significant. This is most important for utility interest in hybrid implementation.[146]

Although the design power densities are lower than for the PNL hybrid, they apply to toroidal-shaped machines to allow larger power as recommended by recent economic studies.[3] The spherical PNL design is limited; even 5000 MWth is not possible. Few utility companies are interested in the expensive unit capital cost that such a small system output would entail.

Although the hybrid system was predicted to have a power density of about 3.9 W/cm^3, it is only the heat removal rate and the fusion neutron source strength which limit power production from such a thermal fission

hybrid blanket. With such low power densities and reduced 14 MeV neutron wall loadings, a few years operating experience accompanied by fusion technological advances may allow the neutron level from the plasma and the flow of helium coolant to be raised to produce better power densities and more total power from the same basic system.

Wall Loading Considerations

Typical fusion systems are necessarily designed for wall loadings of 1-10 MW/m^2. Such loadings necessitate extreme measures to protect the first wall from 14 MeV neutron bombardment and associated damage. Such damage resulting in frequent first wall replacement with associated power outages is one of the limiting factors on the economics of pure fusion systems.[29,30,33]

For the Tokamak hybrid system considered in this work, the toroidal vacuum wall surface area is given by

$$A_S = 2\pi r_i \cdot 2\pi R_T .$$ (B6)

The steady-state total neutron source is simply

$$Q_p = \frac{n^2 <\sigma v> V_p}{4}$$ (B7)

which is specifically based on meeting the planar source requirements determined from the inhomogeneous, six-group transport theory calculation using XSDRNPM. As presented in Chapter 5, the fusion neutron source requirement was calculated to be 1.336×10^{13} nts/cm^{2}sec entering the blanket through the vacuum wall which yields a wall loading of only 0.30 MW/m^2. This low value means the hybrid reactor may be able to operate for much longer periods of time than pure fusion devices without wall replacement.

If the hybrid is designed as an advanced convertor, or possibly a breeder of fissile fuel, then the system can remain operable for years at a time. The primary obstacle to this extended operation would be reduced blanket power caused by fuel burnup if the system is not breeding, or by buildup of poisons or degradation of other blanket structure if it is breeding. However, if the plasma system is designed to become more reactive with time, then the blanket could have reduced k_{eff} without resorting to lower power outputs or refueling. Conceivably, this sort of hybrid could be designed to run for a number of years without intrusion, since the fuel is not subject to significant damage problems.

APPENDIX C

BURNUP AND SENSITIVITY CONSIDERATIONS
FOR THE HYBRID PLASMA

Comparison of Burnup Effects in Pure Fusion and Hybrid Plasma

Burnup effects on the point-model plasma equations were demonstra-

ted to be negligible based on considerations of how burnup alters the

plasma ion density and energy density (or temperature) equations. Only

the particle density equation is affected directly by the inclusion of

burnup in the plasma model used in this work. The particle (ion) density

equation is repeated here at Eq. (C1):

$$\frac{dn(t)}{dt} = S(t) - \frac{n(t)}{\tau_n} - \frac{\langle\sigma v\rangle_{DT} n^2(t)}{2} \quad . \tag{C1}$$

For direct comparison of burnup (fusion) losses with diffusion losses,

the particle density equation was rewritten in the following form:

$$\frac{dn(t)}{dt} = S(t) - n(t) \left[\frac{1}{\tau_n} + \frac{1}{\tau_F} \right] \tag{C2}$$

where the so-called fusion time or the time constant for confinement

losses by fusion events, τ_F, has been defined as follows:

$$\tau_F = \frac{2}{\langle\sigma v\rangle_{DT} n(t)} \quad . \tag{C3}$$

With the inclusion of plasma ion burnup via the τ_F-term, the effec-

tive equilibrium inverse particle confinement time, $1/\tau_{n_{o_{eff}}}$, was

defined as follows:

$$\frac{1}{\tau_{n_{0_{eff}}}} = \frac{1}{\tau_{n_0}} + \frac{1}{\tau_{F_0}} \tag{C4}$$

to include fusion effects. Typical equilibrium plasma parameters were used to demonstrate that the fusion burnup term (due to $1/\tau_{F_0}$) is negligible with respect to the ordinary diffusion term (due to $1/\tau_{n_0}$) and that effective confinement times remain nearly unchanged, especially for hybrid system plasmas.

For a typical fusion power plant design concept such as UWMAK-III,[30] the appropriate point-model equilibrium conditions are presented in Table C-I. Similar point-model parameters are listed in Table C-I for the hybrid plasma model analyzed in this work. As summarized in Table C-I for the full scale UWMAK-III plasma, the expected design equilibrium conditions show that the incorporation of burnup in the particle equation ($1/\tau_{F_0}$) contributes only about 4.1% increase to the predicted total inverse confinement time. In addition, the effective particle confinement time is only decreased about 3.9% from τ_{n_0} = 3.33 sec to $\tau_{n_{0_{eff}}}$ = 3.20 sec.

For the hybrid reactor case the equilibrium parameters of Table C-I apply for the particular plasma model used to drive the hybrid blanket analyzed for power production in Chapter 5. The calculations summarized in Table C-I indicate the fusion reactivity for the hybrid plasma is less than 20% of that for the point-model UWMAK-III plasma. Consequently, burnup effects are much reduced in the hybrid system. As listed in Table C-I, the incorporation of burnup in the hybrid plasma particle equation contributes only about 1% increase to the total inverse confinement time. More important is the fact that the effective equilibrium confinement

time remains nearly unchanged depending on the particular operational particle confinement time selected for the hybrid model. Therefore, the inclusion of burnup for the hybrid has essentially no effect on the equilibrium condition or on the stability criteria since the effect of burnup is so much reduced from the already small effect in full scale Tokamaks such as UWMAK-III.

Table C-I

Point-Model Comparison of Confinement Times
and Related Plasma Parameters in UWMAK-III
and the Hybrid Plasma

UWMAK-III Model[*]	Hybrid Model
$n_0 = 6.46 \times 10^{13}$ ions/cm^3	$n_0 = 9.56 \times 10^{13}$ ions/cm^3
$T_0 = 18.4$ keV	$T_0 = 8.00$ keV
$\langle\sigma v\rangle_{DT}\big\vert_0 = 3.82\times10^{-16}$ cm^3/sec	$\langle\sigma v\rangle_{DT}\big\vert_0 = 0.618\times10^{-16}$ cm^3/sec
$\tau_{n_0} = 3.33$ sec	3.0 sec $\leq \tau_{n_0} \leq 4.0$ sec
$\tau_{E_0} = 1.66$ sec	1.5 sec $\leq \tau_{E_0} \leq 2.0$ sec
$1/\tau_{F_0} = 0.0123$/sec	$1/\tau_{F_0} = 0.003$/sec
$1/\tau_{n_0} = 0.300$/sec	0.33/sec $\geq 1/\tau_{n_0} \geq 0.25$/sec
$\dfrac{\tau_{n_0}}{\tau_{F_0}} = 0.041$	$0.0089 \leq \dfrac{\tau_{n_0}}{\tau_{F_0}} \leq 0.012$
$\tau_{n_{0_{eff}}} = 3.20$ sec	3.00 sec $\leq \tau_{n_{0_{eff}}} \leq 3.95$ sec

[*]All reactivity data, $\langle\sigma v\rangle_{DT}$, were taken from the standard work by Greene.[113]

Since the inclusion of burnup in the point-model formulation of
the hybrid has no effect on the equilibrium condition or on the stability
criteria, hybrid plasmas must be very nonreactive. The hybrid can have
a lower power density in the plasma as well as in the blanket and yet
compete in producing economical power, because the low power densities
are expected to be augmented by fissile fuel production.

Although the comparisons presented in Table C-I were made between
equilibrium parameters, the small perturbations applicable in the linear-
ized analysis maintain the validity of the comparison. In addition, the
nonlinear transients analyzed for the hybrid were initiated by relatively
small perturbations in an equilibrium state. The resultant temperature
transients were shown to be not very large over the 0-15 seconds of inter-
est for such perturbations. For very large transients over longer time
intervals, other model assumptions such as constant plasma volume break
down anyway, so whether or not the negligible burnup assumption holds
becomes meaningless. The important point demonstrated by the parameters
included in Table C-I is simply that neglecting burnup has little effect
on pure fusion plasma systems and even less on hybrid plasma systems based
on the model presented in Chapter 2.

Fractional Burnup Considerations

Fractional burnup, f_b, has generally been calculated as less than 5%
for typical Tokamak system designs.[29,30] Fractional burnup is defined
as the fraction of all ions fed into the plasma via the source feedrate
which undergoes fusion versus other possible losses such as diffusion.
The formula for the burnup fraction was rearranged as follows using the
particle equation in the steady-state condition:

$$f_b = \frac{n_0^2 <\sigma v>_{DT}\big|_0/2}{\frac{n_0^2 <\sigma v>_{DT}\big|_0}{2} + \frac{n_0}{\tau n_0}} \qquad (C5)$$

which was written in the following form to simplify further reduction:

$$f_b = \frac{1/\tau_{F_0}}{1/\tau_{F_0} + 1/\tau_{n_0}} \qquad . \qquad (C6)$$

As shown in Table C-I, the inverse fusion time is much smaller than the inverse particle confinement time; therefore, the fractional burnup was approximated as follows:

$$f_b \simeq \tau_{n_0}/\tau_{F_0} \qquad (C7)$$

to allow direct comparison of fractional burnup given only the ratio in Eq. (C7). For UWMAK-III the results in Table C-I show only about 4% burnup of injected fuel ions while the hybrid plasma has only about 1% burnup which again demonstrates the reduced reactivity of the equilibrium state of the hybrid plasma.

Sensitivity Analysis for the Neutron Production Rate

In general, the reactivity, $<\sigma v>_{DT}$, is a sharply increasing function of temperature below about 30 keV, which is the temperature regime of interest for Tokamaks and hybrids. Greene's data for the reactivity variation with temperature based on a Maxwellian distribution of ion energies is presented graphically in Fig. C1 to show the strong dependence on temperature.

Since the reactivity is so strongly dependent on temperature, the plasma volumetric neutron production rate,

$$q_p(t) = \frac{n^2(t) \; v_{DT}}{4} \qquad (C8)$$

is also strongly dependent on temperature. This sensitivity means that small fractional perturbations in plasma equilibrium operating temperatures produce much larger fractional perturbations in the neutron production rate. The sensitivity of the neutron production rate to temperature changes was related to the reactivity as follows:

$$\frac{dq_p}{q_p} = \frac{d{<}\sigma v{>}_{DT}}{{<}\sigma v{>}_{DT}} \; . \qquad (C9)$$

Since the sensitivity is specifically concerned with temperature changes, the sensitivity factor, S_{DT} was defined by Eq. (C10):

$$\frac{dq_p}{q_p} = S_{DT}(T) \frac{dt}{T} \qquad (C10)$$

where Eq. (C11) defining the dimensionless D-T sensitivity factor was obtained from Eqs. (C8) and (C7) as follows:

$$S_{DT}(T) = \frac{T}{{<}\sigma v{>}_{DT}} \cdot \frac{d{<}\sigma v{>}_{DT}}{dT} \; . \qquad (C11)$$

Although Greene's reactivity data is presented in Fig. Cl, Gamov's theoretical fit of other experimental D-T reactivity data takes the following form.[25]

$$<\sigma v>_{DT} = \frac{.68 \times 10^{-12}}{T^{2/3}} \; \exp\left[\frac{-19.94}{T^{1/3}}\right] \; . \qquad (C12)$$

For Gamov's analytical fit of the D-T reactivity function, the following temperature-dependent sensitivity factor was obtained:

$$S_{DT}(T) = \frac{6.647}{T^{1/3}} - 2/3 .$$

(C13)

The Gamov sensitivity factor is also presented in Fig. C1 along with the reactivity data for comparison purposes. Note that the sensitivity factor approaches unit as the reactivity curve reaches to peak. When Greene's data plotted in Fig. C1 were used to calculate the derivatives needed to compute $S_{DT}(T)$ in Eq. (C12), the values differed from those calculated from Gamov's analytical fit by less than 8% in the 8.0 keV temperature region applicable for Tokamak hybrid work. These values are also presented in Fig. C1. Both formulations for the sensitivity factor indicate much larger fractional increases in neutron production versus the initiating fractional increase with plasma temperature for hybrids. The sensitivity factor essentially allows a simple equivalence to be made where, given a certain small percent perturbation in the plasma temperatures, the corresponding perturbation in the neutron production rate is predicted to be a factor S_{DT} larger. Such sensitivity analysis is very useful in predicting the neutronic consequences of small temperature variations in fusioning plasmas.
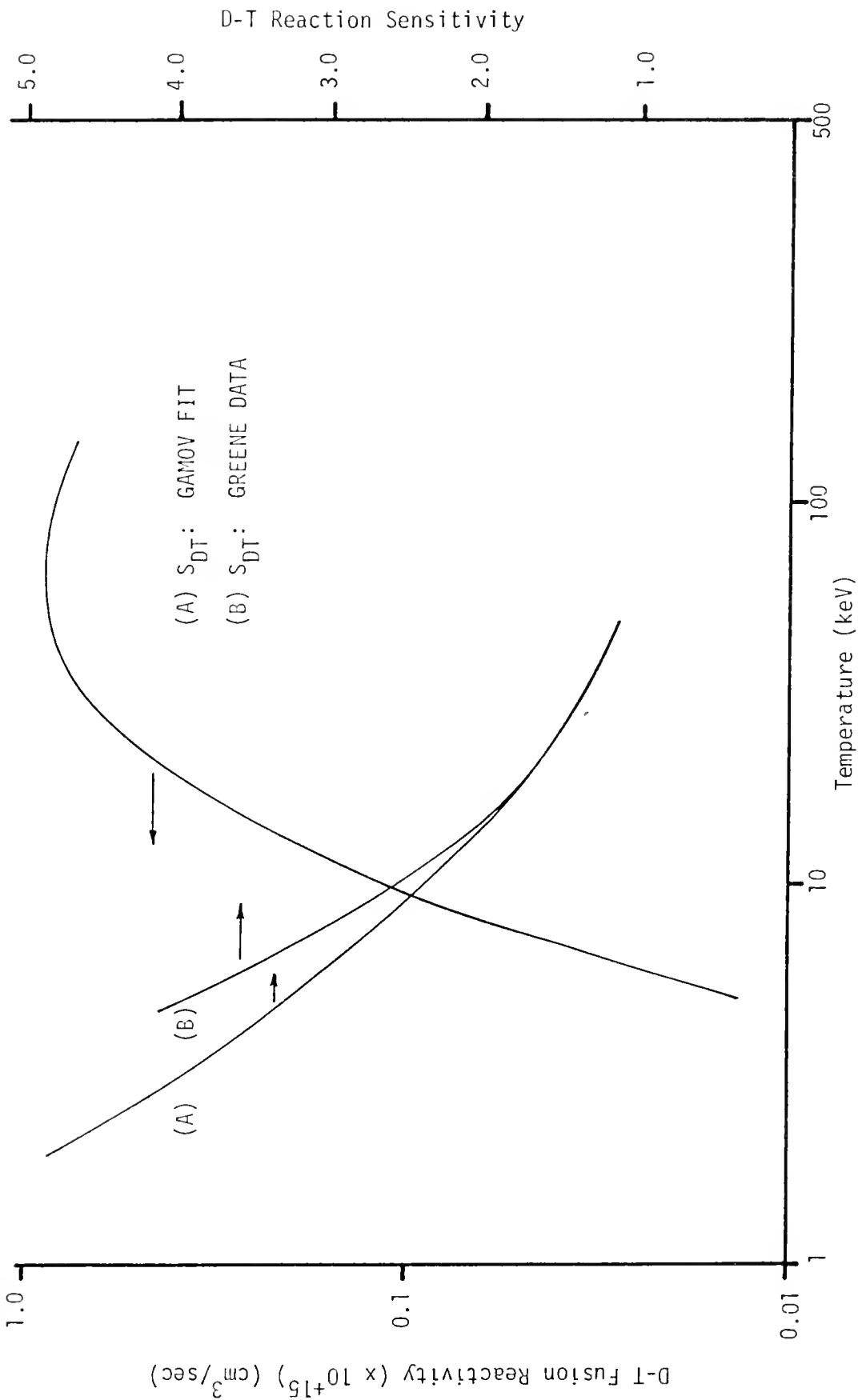
Figure C1. Reactivity and sensitivity variation with temperature for the D-T fusion reaction.

APPENDIX D

COMPUTER CODE DESCRIPTIONS

Description of the CLASSIC2 Program

The CLASSIC2 code[112] calculates the following quantities for a fusioning point-model plasma:

1. Equilibrium conditions (subroutine SSEQ).

2. Temporal development (subroutine NLEQ).

3. Necessary feedback ranges for thermal stability (subroutine FB).

4. Classical control theory characteristics and specifications (subroutine DZTALL).

Equilibrium conditions and time-dependent transient responses are obtained by solving the particle and energy conservation equations given by

$$\frac{dn(t)}{dt} = S(t) + K_s[T_0 - T(t)] - \frac{n^2(t)<\sigma v>_{DT}}{2} - n/\tau_n \tag{D1}$$

$$\frac{d[3n(t)T(t)]}{dt} = [S + K_s(T_0 - T(t)][T_s(t) + K_{T_s}(T_0 - T(t))] \tag{D2}$$
$$+ \frac{n^2(t)<\sigma v>_{DT}Q_\alpha}{4} - b\ n^2(t)T^{1/2}(t) - \frac{n(t)T(t)}{\tau_E}$$

where

$n(t)$ = ion density (ions/cm^3)

$T(t)$ = plasma temperature (keV)

T_0 = derived operating temperature (keV)

$S(t)$ = fuel ion source feedrate (ions/cm^3-sec)

-396-

$T_s(t)$ = injection energy (keV)

K_s = source feedrate feedback gain $\left(\dfrac{1}{cm^3\text{-sec-keV}} \right)$

K_{T_s} = injection energy feedback gain (keV/keV)

$<\sigma v>_{DT}$ = reactivity for the D-T fusion reaction (cm^3/sec)

Q_α = 3520(keV)

b = 3.36 x 10^{-15} ($keV^{1/2}$ cm^3/sec)

and the general confinement model treated by the program is given by

$$\tau_E = \tau_c \, n^\ell T^m \tag{D3}$$

and

$$\tau_n = R \, \tau_E \tag{D4}$$

where τ_E represents the energy confinement time, τ_n represents the par-
ticle confinement time and τ_c, ℓ, m, and R are constants which are
determined by the type of confinement model selected.

The following assumptions are inherent in the formulation of Eqs.
(D1) and (D2):

1. The D-T reaction is the dominant fusion reaction in a homogeneous
   50-50 D-T plasma.

2. All particles exist at the same Maxwell-Boltzmann temperature,
   T, and all particles introduced above T instantaneously slow
   down to T.

3. Bremsstrahlung is the dominant radiative mechanism.

4. Feedback is applied instantaneously.

For the calculation of feedback ranges and classical characteristics
and specifications, the above equations are linearized by the code using
a first-order perturbation expansion about a derived equilibrium point
and Laplace transformed. Transfer functions, $T(s)$, of the following form
are obtained:

$$T(s) = \frac{[s-(-z)]}{s^2+2\xi\omega_n s+\omega_n^2}$$
(D5)

where

A = transfer function gain

-z = location of the zero in the numerator

ξ = system damping

ω_n = undamped natural frequency.

These quantities can all be expressed in terms of the equilibrium

conditions and feedback coefficients. Subroutine FB computes the neces-

sary K_s or K_{T_s}, given the other, to force the roots of the characteristic

equation into the left-hand s-plane. For a specified set of equilibrium

conditions and feedback coefficients, subroutine DZTALL computes the

following:

1. The system damping.

2. Undamped natural frequency.

3. Roots of the characteristic equation.

4. Peak overshoot, time-to-peak, and settling time to 5% for step input perturbations in the source feedrate and injection energy.

5. Bandwidth, resonance peak and resonance frequency.

6. Phase margin.

Description of Blanket Neutronics-Related Codes

The Battelle-Revised-THERMOS Code

The Battelle-Revised-THERMOS (BRT-1)[63] code computes the space-depen-

dent thermal neutron density, flux, and current spectra over the energy

range 0 to 0.683 eV in either slab or cylindrical geometry. The BRT-1

code is restricted to 30 velocity groups, 30 space points, 8 mixtures,

30 isotopes, and the slab or cylindrical geometry. It does, however,

allow hexagonal unit cell arrays. The neutron density is computed from the collision probability form of the integral transport theory matrix equation in which the assumption of isotropy of scattering is used to allow closed form solution. The anisotropic correction is then made to obtain better results, using either a combination of power iteration, overrelaxation, and extrapolation or straight power iteration. The neutron currents are computed from either the gradient of the scalar flux or from the uncollided flux matrix. The flux and current spectra are used to weight point thermal cross sections over an arbitrary thermal energy range for use in multigroup transport or diffusion theory codes.

Features available in the Battelle-Revised-THERMOS code include the white albedo boundary condition, current calculation, transverse buckling, linear anisotropic scattering correction, and smeared-cell punched card output which can be used as region input for a succeeding case. The BRT-1 Code is also capable of treating void regions.

The PHROG Code

The PHROG code[79] is an improved version of the GAM-1 code[120] which generates fast neutron spectra and associated average multigroup neutron corss section data or constants suitable for use in diffusion and transport theory reactor design analysis. The energy-dependent transport equation is solved by a consistent B_1 or P_1 approximation using a 68 fine-group structure to obtain energy-dependent fluxes and currents. The PHROG solution utilizes 68 lethargy groups of cross section, source, and leakage data over an energy range extending from 10 MeV down to 0.414 eV. The computed energy spectrum is then used to collapse the 68-group cross section data into the desired broad group structure using the fluxes and currents as weighting functions.

Resonance integrals can be calculated using the narrow resonance (NR) and the narrow resonance--infinite mass (NRIM) approximations as used in GAM-1[120] or they can be calculated with the Chernick-Nordheim integral treatment incorporated in the RAVEN code.[147] The Dancoff correction is calculated for cylindrical absorber lumps using the method of chord distribution developed by Sauer.[148] The punched output (macroscopic and microscopic averaged cross sections) format can be selected compatible for input to the MONA or CORA diffusion theory codes.

The CORA Code

The CORA code[80] is a few group, one-dimensional neutron diffusion program which solves for either the direct flux in slab, cylindrical, or spherical geometry, or for the adjoint flux. CORA uses the standard Gaussian elimination and backsolution methods for solving the difference equations for the mesh point fluxes in each group and it uses the usual power method or source iteration method with optional Chebyshev acceleration to solve eigenvalue problems.

CORA is limited to 500 mesh points, 50 regions, 40 materials, and 4 energy groups with full downscatter allowance. Some additional useful features include those in the following list.

1. General linear boundary conditions are available of the form:

$$\alpha\phi - \beta J + \gamma = 0, \tag{D6}$$

   for each group and boundary where ϕ is the flux, J is the neutron current and α, β, and γ are coefficients entered by the user. This feature allows a periodic condition that equates boundary fluxes and leakages and also allows surface source modeling.

2. Real (direct) or adjoint (importance function) flux calculations are possible.

3. A generation factor (with a renormalization type of fission source iteration) can be calculated even in the presence of fixed boundary or volume sources.

4. Full downscattering is allowed but no upscatter.

5. Automatic multiple direction buckling iterations can be performed for up to three directions.

6. The code accepts general fixed volume source specifications, allowing separate distributed sources for each group.

7. Available edits include peak-to-average ratios for fluxes, source, and power; also available are neutron balance edits by group and region as well as edits of currents and leakages at all region interfaces.

8. Flexibility is included in the normalization of all edited quantities such as fluxes and sources.

9. CORA has complete "change-case" capability.

10. Efficient solution of fixed source problems with eignevalues near unity is also available.

11. An effective Chebyshev polynomial extrapolation technique is used for accelerating the convergence of problems with dominance ratios near unity.

12. Searches (to a user-specified eignevalue) are available on perpendicular buckling, material poison, region dimensions, or the boundary position between any two regions.

13. Finally, CORA has the capability to store problem input date and solution for later processing by independent programs.

The CORA output consists of program checkpoints, title card edits, optional input data edits, as well as optional iteration covergence edits for fission source iteration data, search iteration data and/or buckling iteration data. Problem solution edits with five different options are available.

The MONA Code

The MONA Code[125] solves for either the real or adjoint flux solutions of the multigroup neutron diffusion equation in one dimension for slab, spherical, or cylindrical geometry. MONA is limited to 260 mesh points, 40 regions, 20 materials, and 26 energy groups. Either homogeneous or inhomogeneous problems can be solved and very general fixed volume sources are allowed.

General inhomogeneous boundary conditions can be specified at either boundary or a periodic condition can be required for slab cases. Any number of groups can be considered thermal (or upscattering) groups. Automatic searches are available on the dimensions of a set of regions, the buckling or poison cross sections of a set of materials, or the boundary between two regions. Average neutron group constants can also be obtained following a problem for sets of coalesced regions or energy groups. This allows efficient use of problem output in other diffusion theory codes such as CORA.

The program employs the usual power iteration method to solve the multigroup problem and for each new fission neutron source the fluxes for each group are obtained in turn. Inner iterations can be performed on the thermal groups alone, with convergence accelerated by a technique forcing an overall neutron balance on each iteration. In each group, the matrix problem posed by the usual set of simultaneous difference equations is solved by Gaussian elimination of the subdiagonal elements of the tri-diagonal matrix.

Data for a complete problem can be written on magnetic tape for use in a subsidiary program. A special option allows a search for the fission neutron source magnitude when a fixed volume source is present which decreases computer time requirements when the generation factor of the reactor is close to unity. The output data can be normalized in various ways, peak-to-average flux and source data is available, and detailed neutron balance data can be obtained by group and by region. The effective "parallel" bucklings corresponding to the computed leakage are also made available for output. The group and region coalescing routine gives average boundary condition constants as well as the average neutron group

constants for each region and group. A Chebyshev polynomial extrapolation technique is available and can be used to accelerate the convergence of the fission neutron source distribution.

MONA is the multigroup version of CORA and the input formats are identical; however, the material group constants and cross sections for MONA are input following the other problem data and are always put on a library tape. The library material data are then mixed to obtain the macroscopic material constants required as input for a given problem.

The XSDRN Code

The XSDRN code[136] is a discrete ordinates, spectral code for the generation of nuclear multigroup constants in the fast, resonance and thermalization energy regions. It combines the features of the one-dimensional anisotropic discrete ordinates ANISN code[58] with the Nordheim integral treatment routines from the GAM-II code.[149] Variable dimensioning is employed to optimize the use of computer core storage space. The XSDRN code calculates an arbitrary number of flux moments for zero- or one-dimensional systems.

The XSDRN code contains three major algorithms. The first is a resonance calculation to provide fine-group parameters; the second algorithm is a neutronics calculation to determine fine-group fluxes; and the third is a multigroup constants calculation to generate parameters for subsequent calculations in XSDRN or in other codes.

In the first type of calculation, XSDRN performs a direct numerical integration of the integral transport equation for the average collision density in media containing a resonance absorber. The XSDRN code uses this calculation in the resolved resonance region along with a rational approximation for the unresolved resonance region to prepare

fine-group constants. These fine-group constants are merged with smooth
data to form a complete fine-group cross section library. The XSDRN code
is written to accept an arbitrary group structure microscopic library with
a P_3 level of elastic scattering as well as inelastic and (n,2n) scatter-
ing matrices, and the desired one-dimensional reaction arrays such as
absorption, fission, and others. The present library at the University of
Florida contains extensive 123 group data extending over the energy scale
from 10^{-4} eV up to nearly 15 MeV.

In the second type of calculation, a forward solution of the one-
dimensional Boltzmann transport equation is performed for slab, cylindrical,
or spherical geometry. This solution is performed in the multigroup dis-
crete ordinates, diffusion, or infinite medium approximation. Several
problem types are provided for, including fixed source, eigenvalue, and
criticality search. The calculational results of such problems provide
space-angle-, and energy-dependent fluxes, as well as region and system
reaction rate distributions.

In the third type of calculation, space- and energy-averaged multi-
group parameters are computed for subsequent use in other calculations.
Extensive cross section libraries are available which can be reduced,
using calculated fine-group fluxes, to arbitrary broad-group structures.
Cell-averaged as well as region-averaged microscopic cross sections are
available for each nuclide in the system. A transport cross section is
computed and edited for each nuclide requested from the library tape.
The multigroup parameters can be output on tape in the correct format
for use with other programs, and the output routines may be easily modi-
fied to provide the desired format for any additional codes.

The flexible dimensioning scheme begun in ANISN and continued in
XSDRN is such that all array dimensions are set for the particular problem

as it is being executed, avoiding the wasted core storage inherent in normal "fixed" dimension programs. Furthermore, if all arrays do not fit in core, XSDRN first tries to gain additional storage by putting cross section data on an input/output (I/O) device; if there is still insufficient space, all fixed source arrays are stored externally; and, finally, the flux moment arrays can be stored externally if necessary. The complete space allocation process is automatic and requires only that the user make I/O devices available.

The theoretical bases of the techniques used in XSDRN involve discrete ordinates transport theory which is adequately described in many references.[150-152] The Nordheim integral treatment is also described in standard references.[135,153]

The AMPX Modular Code System

The AMPX modular code system[81] is designed to produce coupled multigroup neutron-gamma cross section sets. Basic neutron and gamma cross section data for AMPX are obtained from the Evaluated Nuclear Data File (ENDF/B) libraries.[130] Most commonly used operations required to generate and collapse multigroup cross section sets are provided in the system.

The entire AMPX system is flexibly dimensioned: neutron group structures, gamma group structures, and expansion orders to represent anisotropic processes are all arbitrary and limited only by available computer core space, budget, and data accuracy. The basic AMPX system has a variety of features which provide the following capabilities:

1. To generate multigroup neutron cross sections.

2. To generate multigroup gamma cross sections.

3. To generate gamma yields for gamma-producing neutron interactions.

4. To combine neutron cross sections, gamma cross sections, and gamma yields into the final "coupled sets."

5. To perform one-dimensional, discrete ordinates transport or dif-
    fusion theory calculations for neutrons and gammas, and, on
    option, collapse the cross sections to a broad-group structure,
    using the one-dimensional results as weighting functions.

6. To plot cross sections, on option, to facilitate the "evaluation"
    of a particular multigroup set of data.

7. To update and maintain multigroup cross section libraries in such
    a manner as to make it not only easy to combine new data with
    previously processed data, but also to do it in a single pass on
    the computer.

8. To output multigroup cross sections in convenient formats required
    for other codes.

The XLACS Modular Code

The XLACS modular code[131] is a computer program which calculates
weighted multigroup neutron cross sections from ENDF/B data. Essentially,
XLACS serves as the multigroup neutron cross section processing module in
the AMPX system.[81] XLACS is designed to produce full-energy-range neutron
cross section libraries. Provisions are included for treating fast,
resonance, and thermal ENDF/B data in a single calculation. Energy group
structure and expansion orders used to represent differential cross sec-
tions can be arbitrarily specified by the user. Smooth cross sections can
be averaged over an arbitrary user-supplied weighting function or over
any of several built-in weighting functions.

The ENDF/B format is very general, allowing data to be specified in
several ways for practically any nuclear process.[126] A corresponding
generality is required on the part of the processing codes which use the
data. The XLACS program attempts not only to accommodate this generality
but also to allow new processing methods to be easily added as modifica-
tions and improvements in data representation are made.

The XLACS module within the AMPX system is an improved version of the
previous XLACS code.[132] The elastic and inelastic routines have been

upgraded and improved since the original release of the program. The AMPX version of XLACS allows discrete inelastic levels to be treated aniso- tropically to any order, treats all forms of the angular distribution data, supports anisotropic matrices for "continuum" inelastic processes, and is more efficient both timewise and coding-wise than the original version.

The NITAWL Modular Code

The AMPX modular code system is designed to retain as much generality as possible in creating the standard data interfaces, the so-called cross section libraries. The NITAWL modular code[133] is designed to further this scheme of generality. This generality does not directly affect the programming which has to use the data. Because of this generality, many specialized needs are served by the AMPX system. For example, detailed cross section sensitivity analyses require each partial cross section to be retained in full detail and identified in a working library.

The AMPX library formats are quite general and allow any number of processes to be passed. The identification schemes from the Evaluated Nuclear Data Files (ENDF/B) are used where possible. Any scattering process can be represented anisotropically, and some temperature dependence is allowed. Since resonance parameters comprise part of the data, librar- ies tend to be more problem-independent. A transport calculation does not need much of this detail. The NITAWL code module has the responsibility for reading these general formats, for doing resonance self-shielding calculations, and collecting data into working libraries or arrangements of cross section data suitable for input to other codes. In particular, NITAWL can produce working libraries in two forms: first, it can produce output on cards, tape, or disk for ANISN[58], DOT[154], or MORSE;[155] second, it can produce output on tape or disk for the XSDRNPM module[82] which is part of the AMPX system.

Of most importance, NITAWL is specifically designed to process reso-nance nuclides prior to the transport calculation in XSDRNPM. Other AMPX modules pass yields in this case for capture and fission. NITAWL multi-plies the shielded cross section values by these yields to produce self-shielded gamma production matrices. The actual neutron resonance self-shielding calculation generally employs the Nordheim integral treatment, though the narrow resonance and an infinite mass treatment are available as alternate methods.

The XSDRNPM Modular Code

The XSDRNPM module[82] is provided in the AMPX system package for two purposes. First, XSDRNPM provides a one-dimensional transport theory capability for computing reaction rates, eigenvalues, and critical dimen-sions; second, it provides the capability for energy as well as spatial cross section weighting. XSDRNPM is an improved version of the XSDRN code.[136] Improvements include the following nine features:

1. Coupled neutron-gamma calculations can be performed.

2. Any mixture can be presented to an arbitrary order of anisotropy.

3. The adjoint calculation is supported.

4. More efficient data storage methods are used so larger problems can run in less core storage.

5. The resonance calculation is removed and provided within the AMPX system but in the NITAWL module described elsewhere in this appendix. Considerable reduction in the size and time used for typical calculations is allowed by this modular arrangement.

6. Improved thermal flux scaling techniques are employed for better problem convergence.

7. Input specifications are re-ordered with more defaults provided to promote easier use of the XSDRNPM module.

8. Required S_n constants can be calculated for any even order for any of the three standard one-dimensional geometries.

9. Mixture-dependent fission spectra are calculated and used in XSDRNPM, which takes into account all fissionable nuclides in a problem.

The collapsed cross sections from XSDRNPM are written as an AMPX-weighted library which can be used directly by the XSDRNPM module to do transport calculations. These collapsed cross sections can also be output on cards or in a binary format suitable for input to other codes such as ANISN[58], DOT[154] or MORSE.[155]

Four weighting options are provided within XSDRNPM. First, cell weighting is available to generate cross sections consistent with mocking up a cellular configuration as a homogenized region; this means the spatial "disadvantage factors" are taken into account in the cross section weighting.

Second, zone weighting is available where a set of cross sections is produced which is weighted over each material region in which a nuclide occurs.

Third, "region" weighting can be used to produce a single set of cross sections for a nuclide but weighted over a composite spectrum made up of all spectra from zones where the nuclide is present.

Fourth, the "inner" cell weighting option is provided to perform a cell weighting as in the first option but only over the specific regions selected by the input. This option supports a simulated calculation which can include non-zero leakage at the outer boundary of the cell; for example, an explicit cell mock-up can be described within a homogeneous description of a reactor.

The GAKIN II Code

The GAKIN II code[83] is a one-dimensional, multigroup diffusion theory kinetics code. The GAKIN II code solves the time-dependent multigroup

diffusion equations in one spatial dimension (slab, cylindrical, or spherical geometry) using the usual finite difference approximation. Time integration is accomplished using an exponential transformation and semi-implicit differencing. An arbitrary number of space points, regions, and energy groups may be used. Optionally, the effects of time-dependent cross sections, external sources, and xenon poisoning may be included. Time step adjustment can be automatic or established by the user for selected time zones.

The GAKIN II code is a revision of GAKIN[156] which is designed to decrease the storage requirements and running time of the original code. The iterative frequency predictor in GAKIN has been replaced by an explicit scheme; the steady-state initialization calculation has been streamlined; and a large number of programming improvements have been made including an improved and simplified coding format. As a result, GAKIN II is substantially more economical to use than GAKIN. Some GAKIN II limitations include no allowance for region-dependent velocities or neutrons per fission results. In addition, the initial system configuration is artificially forced to be critical and step changes in reactivity must be approximated by the use of multiple time zones.

REFERENCES

1. B.R. Leonard, Jr., "A Review of Fusion-Fission (Hybrid) Concepts," Nucl. Tech., 20, 161 (December 1973).

2. L.M. Lidsky, "Fission-Fusion Systems: Hybrid, Symbiotic, and Augean," Nucl. Fus. 15, 151 (January 1975).

3. F.H. Tenney, C.G. Bethke, W.G. Price, Jr., W.H. Bohlke, R.G. Mills, E.F. Johnson, A.M.M. Todd, C.H. Buchanan, and S.L. Gralnick, A Systems Study of Tokamak Fusion-Fission Reactors, PPPL-1450, Princeton Plasma Physics Laboratory, Princeton, New Jersey (November 1978).

4. E.L. Draper, Jr., and S.J. Gage, "The Fusion-Fission Breeder: Its Potential in a Fuel-Starved Thermal Reactor Economy," Proceedings of Symposium in Technology of Controlled Thermonuclear Fusion Experiments and the Engineering Aspects of Fusion Reactors, Austin, Texas, USAEC Symposium Series 31, CONF-721111, p. 132 (April 1974).

5. J. Graham, Nuclear Report, American Nuclear Society, Washington, D.C., Vol. 1, No. 7 (September 1978).

6. L.M. Lidsky, "Fission-Fusion Symbiosis: General Considerations and a Specific Example," Proceedings of Nuclear Fusion Reactor Conference, Culham Laboratory, England, British Nuclear Energy Society, p. 41 (September 1969).

7. "Fusion Power - An Assessment of Ultimate Potential," Division of Thermonuclear Research, USAEC, Washington, D.C. (February 1973).

8. D. Steiner, "The Nuclear Performance of Fusion Reactor Blankets," Nucl. Appl. and Tech., 9, 83 (July 1970).

9. H. Eubank, R. Goldston, V. Arunasalam, M. Bitter, K. Bol, D. Boyd, N. Bretz, J.P. Bussac, S. Coehn, P. Colestock, S. Davis, D. Dimock, H. Dylla, P. Efthimion, L. Grisham, R. Hawryluk, K. Hill, E. Hinnov, J. Hosea, H. Hsuan, D. Johnson, G. Martin, S. Medley, E. Meservey, N. Sauthoff, G. Schilling, J. Schivell, G. Schmidt, F. Stauffer, L. Stewart, W. Stodiek, R. Stooksberry, J. Strachan, S. Suckewer, H. Takahashi, G. Tait, M. Ulrickson, S. von Goeler, and M. Yamada, PLT Neutral Beam Heating Results, PPPL-1491, Princeton Plasma Physics Laboratory, Princeton, New Jersey (November 1978).

10. L.N. Lontai, "Study of a Thermonuclear Blanket with Fissile Nuclides," Technical Report No. 436, Massachusetts Institute of Technology, Cambridge, Massachusetts (July 1965).

11. United States Nuclear Regulatory Commission, "Nuclear Incident at Three Mile Island," IE Bulletin No. 79-05, Washington, D.C. (April 1979).

12. T.A. Parish and E.L. Draper, Jr., "Neutronic and Photonic Analyses of Simulated Fusion Reactor Blankets Containing Thorium and Natural Uranium," ESL-16, Energy Systems Laboratories Report, University of Texas at Austin (October 1973).

13. L.M. Lidsky, "Fusion-Fission Systems: Classification and Critique," ERDA-4, DCTR Fusion-Fission Energy Systems Review Meeting, Germantown, Maryland, p. 63 (December 1974).

14. W.C. Wolkenhauer, "The Role of a Hybrid (Fusion-Fission) Reactor in a Nuclear Economy," ERDA-4, DCTR Fusion-Fission Energy Systems Review Meeting, Germantown, Maryland, p. 327 (December 1974).

15. R.G. Mills, "The Problem of Control of Thermonuclear Reactors," Proceedings of Symposium on Engineering Problems of Fusion Research, LA-4250, Los Alamos Scientific Laboratory, Los Alamos, New Mexico, p. B1 (April 1969).

16. R.G. Mills, "Control and Ignition of Toroidal Fusion Reactors," Proceedings of Symposium on Thermonuclear Fusion Reactor Design, Lubbock, Texas, USAEC Publication ORO-1171-1, p. 61 (August 1970).

17. R.G. Mills, "Time-Dependent Behavior of Fusion Reactors," Proceedings of Nuclear Fusion Reactor Conference, Culham Laboratory, England, British Nuclear Energy Society, p. 322 (September 1969).

18. M. Ohta, H. Yamato, and S. Mori, "Thermal Instability and Control of Fusion Reactors," Proceedings of Symposium on Plasma Physics and Controlled Thermonuclear Fusion Research, Madison, Wisconsin, IAEA Publication, CONF-710607-132, p. 423 (June 1971).

19. H. Yamato, M. Ohta, and S. Mori, "Numerical Analysis of Thermal Stability in an Inhomogeneous D-T Fusion Plasma," Proceedings of Symposium in Technology of Controlled Thermonuclear Fusion Experiments and Engineering Aspects of Fusion Reactors, Austin, Texas, USAEC Symposium Series 31, CONF-721111, p. 48 (April 1974).

20. H. Yamato, M. Ohta, and S. Mori, "Thermal Stability of a Spatially Non-Uniform Plasma in a D-T Fusion Reactor," Nucl. Fus., 12, 604 (September 1972).

21. M. Ohta, H. Yamato, and S. Mori, "Thermal Instability and Control of Inhomogeneous Plasma in a D-T Fusion Reactor," J. Nucl. Sci. and Tech., 10, 353 (June 1973).

22. W.M. Stacey, Jr., "Operating Regimes of Controlled Thermonuclear Reactors and Stability Against Fundamental-Mode Excursions in Particle Densities and Temperatures," Nucl. Fus. 13, 843 (Decmeber 1973).

23. J.L. Usher and H.D. Campbell, "Thermal Instability for Different Fusion Fuel Cycles," Proceedings of the First Topical Meeting on the Technology of Controlled Nuclear Fusion, San Diego, CONF-740402-P2, Vol. II, p. 301 (April 1974).

24. H.D. Campbell and J.L. Usher, "Thermal Instability and Control for CTR Fuel Cycles," _Trans. Amer. Nucl. Soc._, 21, 45 (June 1975).

25. S. Glasstone and R.H. Lovberg, _Controlled Thermonuclear Reactions_, Van Nostrand Reinhold Co., New York (1960).

26. J.R. Stehn, _Neutron Cross Sections_, BNL-325, Vol. 1, Supplement 2, Brookhaven National Laboratory, Brookhaven, New York (May 1964).

27. J.D. Lee, "Some Neutronic Aspects of a D-T Fusion Reactor," _Proceedings of Symposium on Thermonuclear Fusion Reactor Design_, Lubbock, Texas, USAEC Publication ORO-1171-1, p. 98 (August 1970).

28. A.P. Fraas, _Conceptual Design of the Blanket and Shield Region and Related Systems for a Full Scale Toroidal Fusion Reactor_, ORNL-TM-3096, Oak Ridge National Laboratory, Oak Ridge, Tennessee (May 1973).

29. B.F. Gore and E.S. Murphy, _Current Fusion Power Plant Design Concepts_, BNWL-2013, Battelle Pacific Northwest Laboratories, Richland, Washington (September 1976).

30. Fusion Feasibility Study Group, _UWMAK-III, A Noncircular Tokamak Power Reactor Design_, UWFDM-150, University of Wisconsin, Madison (July 1976).

31. Fusion Engineering Staff, _Conceptual Design Study of a Noncircular Tokamak Demonstration Fusion Power Reactor_, GA-A13992, General Atomic Company, San Diego (November 1976).

32. W.M. Stacey, Jr., Project Manager, _Tokamak Experimental Power Reactor Conceptual Design_, ANL/CTR-76-3, Argonne National Laboratory, Argonne, Illinois (August 1973).

33. D. Steiner, "The Technological Requirements of Power by Fusion," _Nucl. Sci. and Eng._, 58, 107 (October 1975).

34. W.B. Myers, W.M. Wells, and E.H. Canfield, _Tritium Regenration in a D-T Thermonuclear Reactor Blanket_, UCID-4480, Lawrence Radiation Laboratory, Livermore, California (May 1962).

35. A.J. Impink, Jr., "Neutron Economy in Fusion Reactor Blanket Assemblies," _Technical Report 434_, Massachusetts Institute of Technology, Cambridge, Massachusetts (june 1965).

36. W.G. Homeyer, "Thermal and Chemical Aspects of the Thermonuclear Blanket Problem," _Technical Report 435_, Massachusetts Institute of Technology, Cambridge, Massachusetts (June 1965).

37. G.I. Bell, _Neutron Blanket Calculations for Thermonuclear Reactors_, LA-3385, Los Alamos Scientific Laboratory, Los Alamos, New Mexico (August 1965).

38. J.D. Lee, "Tritium Breeding and Energy Generation in Liquid Lithium Blankets," _Proceedings of Nuclear Fusion Reactor Conference_, Culham Laboratory, England, British Nuclear Energy Society, p. 471 (September 1969).

39. D. Steiner, "Neutronic Behavior of Two Fusion Reactor Blanket Designs," Proceedings of Nuclear Fusion Reactor Conference, Culham Laboratory, England, British Nuclear Energy Society, p. 483 (September 1969).

40. S. Blow, V.S. Crocker, and B.O. Wade, "Neutronic Calculations for Blanket Assemblies of a Fusion Reactor," Proceedings of Nuclear Fusion Reactor Conference, Culham Laboratory, England, British Nuclear Energy Society, p. 492 (September 1969).

41. R.W. Werner, B. Meyers, P.B. Mohr, J.D. Lee, and N.C. Christofilos, Preliminary Design Considerations for an Astron Power Reactor System, UCRL-71768, Lawrence Radiation Laboratory, Livermore, California (August 1969).

42. R.W. Werner, "Module Approach to Blanket Design - A Vacuum Wall Free Blanket Using Heat Piper," Proceedings of Nuclear Fusion Reactor Conference, Culham Laboratory, England, British Nuclear Energy Society, p. 536 (September 1969).

43. J.E. Struve and N. Tsoulfanidis, "Two Fusion Reactor Blankets with Vanadium as Structural Material," Nucl. Tech., 21, 201 (March 1974).

44. S. Blow, Editor, "Standard Model for Calculation of Neutronics Codes," Ad Hoc Committee on Fusion Reactor Neutronics Calculations, Proceedings of the International Working Session on Fusion Reactor Technology, Oak Ridge National Laboratory, Oak Ridge, Tennessee, p. 77 (June 1971).

45. J.D. Lee, "Neutronics of Sub-Critical Fast Fission Blankets for D-T Fusion Reactors," Proceedings of Seventh Intersociety Energy Conversion Engineering Conferences, American Chemical Society, San Diego (September 1972).

46. A.P. Fraas, A Diffusion Process for Removing Tritium from the Blanket of a Thermonuclear Reactor, ORNL-TM-2358, Oak Ridge National Laboratory, Oak Ridge, Tennessee (December 1968).

47. D.J. Rose, On the Feasibility of Power by Nuclear Fusion, ORNL-TM-2204, Oak Ridge National Laboratory, Oak Ridge, Tennessee (May 1968).

48. G.R. Hopkins and G. Melese-d'Hospital, "Direct Helium Cooling Cycle for a Fusion Reactor," Proceedings of Nuclear Fusion Reactor Conference, Culham Laboratory, England, British Nuclear Energy Society, p. 522 (September 1969).

49. T. Kammash, Fusion Reactor Physics -- Principles and Technology, Ann Arbor Science Publishers, Inc., Ann Arbor, Michigan, p. 314 (1975).

50. J.D. Lawson, "Some Criteria for a Power Producing Thermonuclear Reactor," Proc. Phys. Soc, 70B, 6 (January 1957).

51. J.W. Weale, H. Goodfellow, M.H. McTaggart, and M.L. Mullender, "Measurements of the Reaction Rate Distribution Produced by a Source of 14 MeV Neutrons at the Center of a Uranium Metal Pile," Reac. Sci. Tech., 14, 91 (May 1961).

52. R.W. Moir, J.D. Lee, and R.J. Burleigh, "Major Features of a Mirror Fusion-Fast Fission Hybrid Reactor," ERDA-4, DCTR Fusion-Fission Energy Systems Review Meeting, Germantown, Maryland, p. 173 (December 1974).

53. J.D. Lee, Neutronics Analysis of a 2500 MWth Fast Fission Natural Uranium Blanket for a DT Fusion Reactor, UCRL-75304, Lawrence Livermore Laboratory, Livermore, California (April 1974).

54. R.W. Moir, "Conceptual Design Considerations for D-T Mirror Reactors with and without a Fission Blanket," Proceedings of the First Topical Meeting on the Technology of Controlled Nuclear Fusion, San Diego, CONF-740402-P2, Vol. II, p. 373 (April 1974).

55. R.W. Moir, J.D. Lee, R.J. Burleigh, W.L. Barr, J.H. Fink, G.W. Hamilton, D.J. Bender, G.A. Carlson, W.L. Dexter, J. Holdren, C.L. Folkers, M.A. Peterson, M.E. Rensink, H.W. Patterson, R.L. Nelson, and C.E. Taylor, Progress on the Conceptual Design of a Mirror Hybrid Fusion-Fission Reactor, UCRL-51797, Lawrence Livermore Laboratory, Livermore, California (June 1975).

56. D.J. Bender, J.N. Doggett, J.D. Lee, and R.W. Moir, Progress on Mirror Fusion-Fission Reactor Designs, UCID-17020, Lawrence Livermore Laboratory, Livermore, California (February 1976).

57. D.J. Bender, "Mirror Hybrid Reactor Studies," Proceedings of the Second Fusion-Fission Energy Systems Review Meeting, Washington, D. C., CONF-771155, p. 99 (July 1978).

58. W.W. Engle, Jr., A Users Manual for ANISN: A One-Dimensional Discrete Ordinates Transport Code with Anisotropic Scattering, Union Carbide Report K-1693, Oak Ridge, Tennessee (March 1967).

59. D. Steiner, Analysis of a Benchmark Calculation of Tritium Breeding in a Fusion Reactor Blanket: The United States Contribution, ORNL-TM-1477, Oak Ridge National Laboratory, Oak Ridge, Tennessee (April 1973).

60. E. Greenspan, A. Schneider, A. Misolovin, D. Gilai, and P. Levin, Natural Uranium Fueled Light Water Moderated Breeding Hybrid Power Reactors, PPPL-1444, Princeton Plasma Physics Laboratory, Princeton, New Jersey (June 1978).

61. B.R. Leonard, Jr., and W.C. Wolkenhauer, "Fusion-Fission Hybrids: A Subcritical Thermal Fission Lattice for a D-T Fusion Reactor," Proceedings of Symposium on Technology of Controlled Thermonuclear Fusion Experiments and the Engineering Aspects of Fusion Reactors, Austin, Texas, USAEC Symposium Series 31, CONF-721111, p. 918 (April 1974).

62. J.L. Carter, HRG3: A Code for Calculating the Slowing-Down Spectrum in the P1 or B1 Approximation, BNWL-1432, Battelle Pacific Northwest Laboratories, Richland, Washington (June 1970).

63. C.L. Bennett and W.L. Purcell, BRT-1, Battelle-Revised-THERMOS, BNWL-1434, Battelle Pacific Northwest Laboratories, Richland Washington, (June 1970).

64. W.C. Wolkenhauer, B.R. Leonard, Jr., A.M. Sutey, and R.W. Moir, Conceptual Design of a Fusion-Fission Hybrid Reactor Based on a Mirror Fusion Reactor with a Subcritical Gas Cooled Fission Blanket, BNWL-SA-4865, Battelle Pacific Northwest Laboratories, Richland, Washington (1974).

65. R.C. Liikala, B.R. Leonard, Jr., W.C. Wolkenhauer, and D.T. Aase, "Review of Battelle-Northwest Technical Studies on Fusion-Fission (Hybrid) Energy Systems," ERDA-4, DCTR Fusion-Fission Energy Systems Review Meeting, Germantown, Maryland, p. 117 (December 1974).

66. W.C. Wolkenhauer, C.W. Stewart, R.W. Werner, and J.D. Lee, Some Safety Considerations of Hybrid Reactors in Comparison with Fission and Fusion Reactors, BNWL-SA-4988, Battelle Pacific Northwest Laboratories, Richland, Washington (1974).

67. V.L. Teofilo, "A Tokamak Demonstration Hybrid Reactor," Proceedings of the Second Fusion-Fission Energy Systems Review Meeting, Washington, D.C., CONF-771155, Vol. II, p. 513 (July 1978).

68. Final Safety Analysis Report for the Fort St. Vrain Nuclear Generating Station, Public Service Company of Colorado, Denver (1969).

69. F. Ribe, T.A. Oliphant, and W.E. Quinn, Feasibility Study of a Pulsed Thermonuclear Reactor, LA-3294-MS, Los Alamos Scientific Laboratory, Los Alamos, New Mexico (April 1965).

70. T.H. Jensen, O. Kofoed-Hansen, and C.F. Wandel, "A Survey of the Energy Balance in a Thermonuclear Reacting Plasma, Containing Deuterium, Tritium, and Reaction Products under Isothermal Pulsed or Steady-State Conditions." Proceedings of the Second United Nations Conference on the Peaceful Uses of Atomic Energy, p. 431, Geneva (October 1958).

71. T.J. Woods, A Study of the Operating Regimes for Proposed Fusion Fuel Cycles, Master's Project, Department of Nuclear Engineering Sciences, University of Florida, Gainesville (June 1974).

72. W. Horton, Jr., and T. Kammash, "Model Tokamak Reactors Limited by Anomalous Diffusion and Synchrotron Radiation," Proceedings of Symposium in Technology of Controlled Thermonuclear Fusion Experiments and the Engineering Aspects of Fusion Reactors, Austin, Texas, USAEC Symposium Series 31, CONF-721111, p. 146 (April 1974).

73. L. Spitzer, Physics of Fully Ionized Gases, Interscience Publishers, Inc., New York (1956).

74. "The Ordeal at Three Mile Island," Nucl. News Special Report, American Nuclear Society, LaGrange Park, Illinois (April 1979).

75. J.J. Duderstadt and L.J. Hamilton, Nuclear Reactor Analysis, p. 67, John Wiley and Sons, New York (1976).

76. W.C. Wolkenhauer and B.R. Leonard, The Nuclear Data Requirements for Fusion-Fission (Hybrid) Reactors, BNWL-SA-4403, Battelle Pacific Northwest Laboratories, Richland, Washington (1972).

77. G.H. Miley, "Energy Balances for Fusion-Fission Hybrids," Proceedings of the Meeting on Fusion-Fission Hybrids, USAEC,COO-2218-25, Washington, D.C. (December 1974).

78. F.F. Chen, Introduction to Plasma Physics, p. 303, Plenum Press, New York (1974).

79. F.J. Wheeler, R.L. Curtis, G.L. Singer, and R.A. Grimesey, PHROG: A Fortran IV Program to Generate Fast Neutron Spectra and Average Multigroup Constants, IN-1435, Idaho Nuclear Corporation, Idaho Falls (April 1971).

80. E.C. Anderson and G.E. Putnam, CORA: A Few Group Diffusion Theory Code for One-Dimensional Reactor Analysis, DIO-17199, Idaho Nuclear Corporation, Idaho Falls (August 1970).

81. N.M. Greene, J.L. Lucius, L.M. Petrie, W.E. Ford, III, J.E. White, and R.Q. Wright, AMPX: A Modular Code System for Generating Coupled Multigroup Neutron-Gamma Libraries from ENDF/B, ORNL-TM-3706, Oak Ridge National Laboratory, Oak Ridge, Tennessee (March 1976).

82. L.M. Petrie and N.M. Greene, "XSDRNPM: AMPX Module with One-Dimensional S_n Capability for Spatial Weighting," AMPX: A Modular Code System for Generating Coupled Multigroup Neutron-Gamma Libraries from ENDF/B, ORNL-TM-3706, Oak Ridge National Laboratory, Oak Ridge, Tennessee (March 1976).

83. K.F. Hansen and J.H. Mason, GAKIN II: A One-Dimensional Multigroup Diffusion Theory Reactor Kinetics Code, COO-2262-3, Massachusetts Institute of Technology, Cambridge, Massachusetts (August 1973).

84. C.C. Baker, P.H. Sager, Jr., and C.R. Harder, Experimental Fusion Power Reactor Conceptual Design Study, Vols. I-III, GA-A14000, General Atomic Company, San Diego (July 1976).

85. E.E. Kintner, "A Survey of the U.S. Magnetic Fusion Program," Proceedings of the 9th Symposium on Fusion Technology, Garmisch-Partenkirchen (FRG), Pergamon Press, New York, p. 225 (1976).

86. E.S. Murphy, Review of Fusion Research Program, BNWL-2011, Battelle Pacific Northwest Laboratories, Richland, Washington (June 1976).

87. E.S. Murphy, "Fusion Power by Magnetic Confinement Program Plan," ERDA-76/110/1, Vol. 1, Washington, D.C. (July 1976).

88. W.C. Gough, "The EPRI Fusion Power Program - Status and Goals," Proceedings of the Second Topical Meeting on the Technology of Controlled Nuclear Fusion, Richland, Washington, CONF-760935-PI, Vol. III, p. 1137 (September 1976).

89. R. Hancox, "The Euratom Fusion Technology Programme," Proceedings of the Second Topical Meeting on the Technology of Controlled Nuclear Fusion, Richland, Washington, CONF-760935-PI, Vol. II, p. 1095 (September 1976).

90. S. Mori, "The Fusion Technology Program in Japan," Proceedings of the Second Topical Meeting on the Technology of Controlled Nuclear Fusion, Richland, Washington, CONF-760935-PI, Vol. II, p. 1105 (September 1976).

91. J.M. Williams, J.W. Beal, and F.W. Coffman, "Development and Technology in the U.S. Magnetic Fusion Power Programs," Proceedings of the Second Topical Meeting on the Technology of Controlled Nuclear Fusion, Richland, Washington, CONF-760935-PI, Vol. III, p. 1075 (September 1976).

92. R.G. Mills, Editor, A Fusion Power Plant, MATT-1050, Princeton Plasma Physics Laboratory, Princeton, New Jersey (June 1974).

93. J.R. Young and B.f. Gore, Reference Commercial Fusion Power Plants, BNWL-2014, Battelle Pacific Northwest Laboratories, Richland, Washington (June 1976).

94. R.G. Mills, Lawson Criteria, MATT-844, Princeton Plasma Physics Laboratory, Princeton, New Jersey (May 1971).

95. I. Maya, Equilibrium Conditions and Critical Temperatures of Thermonuclear Plasmas, Master's Thesis, University of Florida, Gainesville (March 1976).

96. C. Powell and O.J. Hahn, "Energy Balance Instabilities in Fusion Plasmas," Nucl. Fus., 12, 667 (September 1972).

97. I. Maya, Personal Communication (1978).

98. T.N. Edelbaum, P.A. Madden, and R.E. Var, Fusion Reactor Control Study, EPRI-ER-533, First Annual Report Research Project 546-2, Charles Stark Draper Laboratory, Inc., Cambridge, Massachusetts (July 1977).

99. D.L. Hetrick, Dynamics of Nuclear Reactors, Chapter 2, University of Chicago Press, Chicago (1971).

100. W.A. Houlberg, A Review of Plasma Transport Theories for Tokamaks and Experimental Results, IFDM-8, University of Wisconsin, Madison (January 1975).

101. S.E. Attenberger, F.B. Marcus, and D.G. McAlees, Dynamics of Tokamak Plasma Experiments and Reactors, ORNL-TM-5509, Oak Ridge National Laboratory, Oak Ridge, Tennessee (November 1976).

102. S.O. Dean, J.D. Callen, and H.P. Furth, Status and Objectives of Tokamak Systems for Fusion Research, WASH-1295, USAEC, Washington, D.C. (1973).

103. S.S. Medley, Personal Communication (1978).

104. D.L. Hetrick, Dynamics of Nuclear Reactors, Chapter 1, University of Chicago Press, Chicago, Illinois (1971).

105. D.L. Hetrick, Dynamics of Nuclear Reactors, Chapter 8, University of Chicago Press, Chicago, Illinois (1971).

106. G.I. Bell and S. Glasstone, Nuclear Reactor Theory, Chapter 9, Van Nostrand Reinhold Co., New York (1970).

107. General Description of a Boiling Water Reactor, NEDP 20120, Nuclear Energy Division, General Electric Co., San Jose, California (April 1975).

108. G. Masche, Systems Summary of a Westinghouse Pressurized Water Reactor Nuclear Power Plant, Westinghouse Electric Corporation, Pittsburgh, Pennsylvania (1971).

109. E.T. Dugan, Personal Communication (1979).

110. D.L. Hetrick, Dynamics of Nuclear Reactors, Chapter 3, University of Chicago Press, Chicago, Illinois (1971).

111. D.L. Hetrick, Dynamics of Nuclear Reactors, Chapter 5, University of Chicago Press, Chicago, Illinois (1971).

112. I. Maya, "CLASSIC2 - A Computer Code to Simulate Point-Model Fusioning Plasma Equilibrium and Time-Dependent Behavior," Internal Report, Nuclear Engineering Sciences Department, University of Florida, Gainesville (May 1977).

113. S.L. Greene, Jr., Maxwell Averaged Cross Sections for Some Thermonuclear Reactions on Light Isotopes, UCRL-70522, Lawrence Radiation Laboratory, Livermore, California (May 1967).

114. V.V. Arsenin, L.I. Artemenkov, and N.V. Ivanov, Feedback Stabilization of Kink Instability in TO-1 Tokamak, PPL-TRANS-126, Princeton Plasma Physics Laboratory, Princeton, New Jersey (November 1978).

115. C.L. Hoxie, Steady-State and Thermal Stability Analysis of a Two-Energy Component Fusion Plasma, Master's Thesis, University of Florida, Gainesville (March 1978).

116. C.G. O'Farrill and H.D. Campbell, "Preliminary Thermal Stability Study of a Two-Component Fusion Plasma," Trans. Amer. Nucl. Soc., 23, 51 (June 1976).

117. D.L. Jassby, "Neutral-Beam-Driven Tokamak Fusion Reactors," Nucl. Fus., 17, 309 (April 1977).

118. E.T. Dugan, Personal communication (April 1979).

119. G.I. Bell and S. Glasstone, Nuclear Reactor Theory, pp. 164-165, Van Nostrand Reinhold Co., New York (1970).

120. G.D. Joanou and J.S. Dudek, GAM-1: A Consistent P-1 Multigroup Code for the Calculation of Fast Neutron Spectra and Multigroup Constants, GA-1850, General Dynamics Corporation, San Diego (June 1961).

121. E.T. Dugan, Personal Communication (1978).

122. Computer Codes in the Nuclear Industry, NES 617 Class Notes, Nuclear Engineering Sciences Department, University of Florida, Gainesville (Winter 1974).

123. N.J. Diaz, Personal communication (1977).

124. J.R. Lamarsh, Introduction to Nuclear Reactor Theory, p. 448, Addison-Wesley Publishing Company, Inc., Reading, Massachusetts (1966).

125. G.E. Putnam, MONA: A Multigroup One-Dimensional Neutronic Analysis Code, ANCR-1051, Aerojet Nuclear Company, Idaho Falls (March 1972).

126. M.K. Drake, Editor, Data Formats and Procedures for the ENDF Neutron Cross Section Library, BNL-50279, Brookhaven National Laboratory, Brookhaven, New York (October 1970).

127. G.I. Bell and S. Glasstone, Nuclear Reactor Theory, p. 472, Van Nostrand Reinhold Co., New York (1970).

128. J.R. Lamarsh, Introduction to Nuclear Reactor Theory, p. 100, Addison-Wesley Publishing Company, Inc., Reading, Massachusetts (1966).

129. S. Shalev and M.J. Cuttler, "The Energy Distribution of Delayed Fissions," Nucl. Sci. and Eng., 51, 52 (May 1973).

130. D. Garber, C. Dunford, and S. Pearlstein, Data Formats and Procedures for the Evaluated Nuclear Data File, BNL-NCS-50496, (ENDF 102), Brookhaven National Laboratory, Brookhaven, New York (October 1975).

131. J.E. White, N.M. Greene, and J.L. Lucius, "XLACS: A Program to Produce Weighted Multigroup Neutron Cross Sections from ENDF/B," AMPX: A Modular Code System for Generating Coupled Multigroup Neutron-Gamma Libraries from ENDF/B, ORNL-TM-3706, Oak Ridge National Laboratory, Oak Ridge, Tennessee (March 1976).

132. N.M. Greene, J.L. Lucius, J.E. White, R.Q. Wright, C.W. Craven, Jr., and M.L. Tobias, XLACS: A Program to Produce Weighted Multigroup Neutron Cross Sections from ENDF/B, ORNL-TM-3646, Oak Ridge National Laboratory, Oak Ridge, Tennessee (April 1972).

133. L.M. Petrie, N.M. Greene, J.L. Lucius, and J.E. White, "NITAWL: AMPX Module for Resonance Self-Shielding and Working Library Production," AMPX: A Modular Code System for Generating Coupled Multigroup Neutron-Gamma Libraries from ENDF/B, ORNL-TM-3705, Oak Ridge National Laboratory, Oak Ridge, Tennessee (March 1976).

134. N.M. Greene, L.M. Petrie, and R.Q. Wright, "RADE: AMPX Module to Check AMPX Master Cross Section Libraries (AMPX Utility Module)," _AMPX: A Modular Code System for Generating Coupled Multigroup Neutron-Gamma Libraries from ENDF/B_, ORNL-TM-3706, Oak Ridge National Laboratory, Oak Ridge, Tennessee (March 1976).

135. L.W. Nordheim, _A Program of Research and Calculations of Resonance Absorption_ GA-2527, General Dynamics Corporation, San Diego (August 1961).

136. N.M. Greene and C.W. Craven, Jr., _XSDRN: A Discrete Ordinates Spectral Averaging Code_, ORNL-TM-2500, Oak Ridge National Laboratory, Oak Ridge, Tennessee (June 1969).

137. L.M. Petrie, Personal communication (1977).

138. D.L. Hetrick, _Dynamics of Nuclear Reactors_, p. 42, University of Chicago Press, Chicago (1971).

139. R.C. Dahlberg, K. Asmussen, D. Lee, L. Brooks, and R.K. Lane, "HTGR Fuel and Fuel Cycle," _Nucl. Eng. Des._, 26, No. 1, 58 (1974).

140. M.M. El-Wakil, _Nuclear Heat Transport_, p. 79, International Textbook Company, Scranton, Pennsylvania (1971).

141. R.E. Nightingale, _Nuclear Graphite_, Academic Press Inc., New York (1962).

142. R.C. Weast, Editor, _Handbook of Chemistry and Physics_, CRC Press, Cleveland (1974).

143. E.T. Dugan, _Thermal and Fast System Analysis of the Florida SPERT Assembly_, Master's Thesis, University of Florida, Gainesville (March 1972).

144. M.M. El-Wakil, _Nuclear Energy Conversion_, International Textbook Company, Scranton, Pennsylvania (1971).

145. F.F. Chen, _Introduction to Plasma Physics_, p. 290, Plenum Press, New York (1974).

146. T. Kammash, Personal communication (December 1977).

147. F.J. Wheeler, _RAVEN: A Computer Package for Evaluating Resolved and Unresolved Resonance Absorption Including Pin Shadowing_, IDO-17212, Phillips Petroleum Company (February 1967).

148. A. Sauer, "Thermal Utilization in the Square Cell," _J. Nucl. Energy_, 18, No. 2, 425 (1964).

149. G.D. Joanou and J.S. Dudek, _GAM-II. A B_3 Code for the Calculation of Fast-Neutron Spectra and Associated Multigroup Constants_, GA-4265, General Dynamics Corporation, San Diego (September 1963).

150. C.E. Lee, Discrete Ordinates S_n Approximation to Transport Theory, LA-2595, Los Alamos Scientific Laboratory, Los Alamos, New Mexico (June 1962).

151. K.D. Lathrop, DTF-IV, A Fortran IV Program for Solving the Multigroup Transport Equation with Anisotropic Scattering, LA-3373, Los Alamos Scientific Laboratory, Los Alamos, New Mexico (July 1965).

152. B. Carlson, "The Numerical Theory of Neutron Transport," Methods of Computational Physics, Vol. I, Statistical Physics, Academic Press Inc., New York (1963).

153. L.W. Nordheim, "The Theory of Resonance Absorption," Proceedings of Symposia in Applied Mathematics, Vol. XI, p. 48 (1951).

154. F.R. Mynatt, DOT: A Two-Dimensional Discrete Ordinates Transport Code, ORNL K-1694, Oak Ridge National Laboratory, Oak Ridge, Tennessee (June 1967).

155. E.A. Straken, P.N. Stevens, D.C. Irving, and V.R. Cain, The MORSE Code - A Multigroup Neutron and Gamma-Ray Monte Carlo Transport Code, ORNL-4585, Oak Ridge National Laboratory, Oak Ridge, Tennessee (September 1970).

156. K.F. Hansen and S.R. Johnson, GAKIN: A One-Dimensional Multigroup Kinetics Code, GA-7543, General Atomic Corporation, San Diego (August 1967).
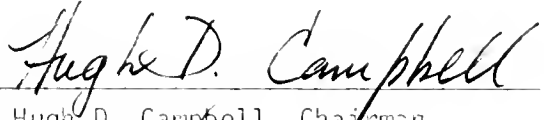
BIOGRAPHICAL SKETCH

William Gerard Vernetson was born in Baltimore, Maryland, on August 14, 1945. He grew up to Halethorpe, Maryland, and graduated from Ascension grade school in June, 1959. He next attended Mount Saint Joseph's High School from which he graduated in 1963 with the Principal's Scholarship to attend Loyola College in Baltimore. After four years majoring in Engineering-Physics at Loyola College, Mr. Vernetson received the Bachelor of Science Degree along with the Excellence in Engineering Medal in June, 1967.

After college, Mr. Vernetson continued his education in the Nuclear Engineering Sciences Department at the University of Florida until drafted into the armed forces in late 1968. After spending one year and 363 days in the army, mostly at Fort Greely in Alaska, Mr. Vernetson returned to the University of Florida where he received his master's degree in June, 1972.

Since that time, Mr. Vernetson has been pursuing the doctorate degree while serving as both a teaching and research assistant in the Department of Nuclear Engineering Sciences. Since January, 1976, Mr. Vernetson has also served as a consultant to the nuclear industry through Florida Nuclear Associates, Inc.
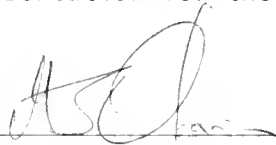
Mr. Vernetson has been happily married to the former Theresa Frances Blankner of Bartow, Florida, since July, 1972.

I certify that I have read this study and that in my opinion it conforms to acceptable standards of scholarly presentation and is fully adequate, in scope and quality, as a dissertation for the degree of Doctor of Philosophy.
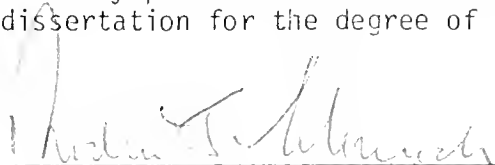
Dr. Hugh D. Campbell, Chairman
Associate Professor of Nuclear
Engineering Sciences

I certify that I have read this study and that in my opinion it conforms to acceptable standards of scholarly presentation and is fully adequate, in scope and quality, as a dissertation for the degree of Doctor of Philosophy.
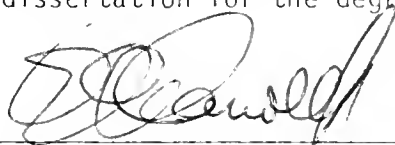
Dr. M.J. Ohanian
Professor of Nuclear Engineering
Sciences, Department Chairman

I certify that I have read this study and that in my opinion it conforms to acceptable standards of scholarly presentation and is fully adequate, in scope and quality, as a dissertation for the degree of Doctor of Philosophy.
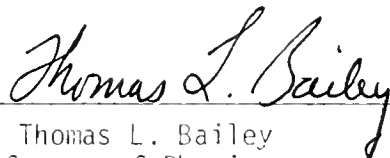
Dr. Richard T. Schneider
Professor of Nuclear Engineering
Sciences

I certify that I have read this study and that in my opinion it conforms to acceptable standards of scholarly presentation and is fully adequate, in scope and quality, as a dissertation for the degree of Doctor of Philosophy.

Dr. Edward E. Carroll
Professor of Nuclear Engineering
    Sciences

I certify that I have read this study and that in my opinion it conforms to acceptable standards of scholarly presentation and is fully adequate, in scope and quality, as a dissertation for the degree of Doctor of Philosophy.

Dr. Thomas L. Bailey
Professor of Physics

This dissertation was submitted to the Graduate Faculty of the College of Engineering and to the Graduate Council, and was accepted as partial fulfillment of the requirements for the degree of Doctor of Philosophy.

June 1979

Dean, College of Engineering

Dean, Graduate School